A Study of the Growth and Hydrogen Production of *Chlamydomonas reinhardtii*

Bojan Tamburic

Imperial College London

Department of Chemical Engineering

Supervised by Dr Klaus Hellgardt and Professor Geoffrey C Maitland

Submitted for the Degree of Doctor of Philosophy

July 2012

Abstract

The green alga *Chlamydomonas reinhardtii* has the ability to produce molecular hydrogen (H_2) through the biophotolysis of water under anaerobic conditions. The aim of this thesis was to improve our understanding of the growth and H_2 production of *Chlamydomonas reinhardtii* in order to develop a continuous and practical biophotolytic H_2 production process.

A novel flat-plate photobioreactor was designed to facilitate green algal growth and H_2 production at the laboratory scale and to measure key process parameters under controlled conditions. Membrane Inlet Mass Spectrometry was developed to measure H_2 production rates *in situ*. In order to achieve effective H_2 production, it was necessary to grow dense and healthy *Chlamydomonas reinhardtii* cultures. Favourable algal growth conditions included a temperature of 25°C, continuous illumination at 5-100 $W \cdot m^{-2}$ and photomixotrophic growth conditions. Optimum photoautotrophic growth was measured at a carbon dioxide concentration of 11%. Photosaturation of *Chlamydomonas reinhardtii* occurred at 273 $W \cdot m^{-2}$ and photoinhibition at 600 $W \cdot m^{-2}$.

A reactor-independent nutrient control technique was developed by optimising the sulphate and acetate concentrations in the *Chlamydomonas reinhardtii* growth medium. It enabled a fully grown algal culture to spontaneously achieve anaerobic H_2 production. A maximum H_2 production rate of 1.52 $mlH_2 \cdot l^{-1} \cdot h^{-1}$ and a H_2 yield of 119.8 $mlH_2 \cdot l^{-1}$ were measured. The sulphur dilution technique proved effective at encouraging cyclic H_2 production, resulting in alternating *Chlamydomonas reinhardtii* recovery and H_2 production stages. *Chlamydomonas reinhardtii* cultures produced H_2 at an average rate as high as 0.4 $mlH_2 \cdot l^{-1} \cdot h^{-1}$ under a series of consecutive 95% dilutions.

These complementary approaches have demonstrated that engineering advances can lead to improvements in the scalability and affordability of biophotolytic H_2 production, giving increased confidence that H_2 can fulfil its potential as a sustainable fuel of the future.

To my parents
Živojin and Slobodanka
and my sister
Tijana

Author Declaration

I declare that the contents of this thesis are my own work except where otherwise acknowledged.

The work was carried out between October 2008 and July 2012 at Imperial College London under the supervision of Dr Klaus Hellgardt and Professor Geoffrey C Maitland.

This thesis is part of the Solar Hydrogen Project, managed by the Energy Futures Lab at Imperial College London, and funded by the UK Engineering and Physical Sciences Research Council (EPSRC) project reference EP/F00270X/1.

Bojan Tamburić

July 2012

Acknowledgements

I would like to start by thanking my supervisors Dr Klaus Hellgardt and Professor Geoffrey C Maitland for their invaluable support and advice throughout the course of this project. Their unique knowledge and vision inspired my interest in green algal hydrogen production in the first place and helped to keep me going when the experiments were not working as planned. I am grateful to Dr Fessehaye Zemichael for his tireless work in setting up the biohydrogen lab, for sharing his extensive knowledge of scientific equipment and procedure, and for being a great friend as well as an indispensable colleague. I would also like to acknowledge the help of Dr Steven Burgess, who was instrumental in helping me understanding the biochemical theory of green algal hydrogen production and also taught me the fundamentals of algal growth and sulphur deprivation procedures. Our interdepartmental collaboration proved to be effective and fruitful.

I would like to thank Paul Crudge from the Department of Chemical Engineering Workshop for helping me with photobioreactor design, constructing our photobioreactors and helping to keep the laboratory in operational condition. I am grateful to Professor Peter J Nixon for allowing me to use his biochemistry laboratory and equipment while providing help and support along the way. I must thank Professor Nigel P Brandon and the Energy Futures Lab staff for their belief in me and for always being there when I needed them. Thank you to everybody else who contributed to this thesis, including: Professor Geoffrey Kelsall, Professor David Stuckey, Dr Stephen Dennison, Patricia Carry, Pongsathorn Dechatiwongse, Leo Tang and Hussein Haji Taha.

I would like to dedicate this thesis to my parents Slobodanka and Živojin, my grandparents, and my sister Tijana, for their unquestionable love and support. I would like to give a special thank you to my girlfriend Sophie Pageon for being my best friend, my editor and my muse. I would also like to thank all of my friends at Imperial College over the years: friends from my Physics undergraduate degree, from the MSc in Sustainable Energy Futures, from the basketball team, from my office, from my research group, as well as everybody else; you know who you are.

Bojan Tamburić

July 2012

List of Publications

Tamburic, B., Zemichael, F.W., Maitland, G.C. & Hellgardt, K. (in preparation) Process and reactor design for biophotolytic H_2 production (working title). *Energy & Environmental Science* (provisional).

Patel, B., **Tamburic, B.**, Zemichael, F.W., Dechatiwongse, P. & Hellgardt, K. (in preparation) Review of algal biofuels (working title). *Algal Research* (provisional).

Tamburic, B., Zemichael, F.W., Maitland, G.C. & Hellgardt, K. (2012) Effect of light regime and phototrophic conditions on growth of the H_2-producing green alga *Chlamydomonas reinhardtii*. *Energy Procedia*. Under review.

Tamburic, B., Zemichael, F.W., Maitland, G.C. & Hellgardt, K. (2012) A novel nutrient control method to deprive green algae of sulphur and initiate spontaneous hydrogen production. *International Journal of Hydrogen Energy*. 37 (11), 8988–9001.

Tamburic, B., Zemichael, F.W., Crudge, P., Maitland, G.C. & Hellgardt, K. (2011) Design of a novel flat-plate photobioreactor system for green algal hydrogen production. *International Journal of Hydrogen Energy*. 36 (11), 6578–6591.

Burgess, S.J., **Tamburic, B.**, Zemichael, F.W., Hellgardt, K. & Nixon, P.J. (2011) Solar-driven hydrogen production in green algae. *Advances in Applied Microbiology*. 75 (1), 71–110.

Tamburic, B., Zemichael, F.W., Maitland, G.C. & Hellgardt, K. (2011) Parameters affecting the growth and hydrogen production of the green alga *Chlamydomonas reinhardtii*. *International Journal of Hydrogen Energy*. 36 (13), 7872–7876.

Table of Contents

Abstract **3**
Author Declaration **7**
Acknowledgements **9**
List of Publications **11**
Table of Contents **13**
List of Figures **19**
List of Tables **25**
Nomenclature **27**
1. General Introduction **33**
2. Algae and Hydrogen for Sustainable Energy **37**
2.1. Introduction 37
2.2. Sustainable Energy 38
2.3. Solar Power and Biofuels 41
2.4. Algae as Biological Factories 45
2.5. Hydrogen as a Fuel 49
2.6. Biohydrogen Production 53
2.6.1. Dark Fermentation *53*
2.6.2. Photofermentation *54*
2.6.3. Biophotolysis *55*
2.6.4. Biological Integration *56*
2.7. Summary 58
3. Biohydrogen Production by *Chlamydomonas reinhardtii* **61**
3.1. Selection of Algal Species: Introduction to *Chlamydomonas reinhardtii* 61
3.2. Biochemistry of Biohydrogen Production 63
3.2.1. Light-harvesting by Photosystem II *63*
3.2.2. Photosynthetic Electron Transport *66*
3.2.3. Hydrogenase Enzyme *72*
3.2.4. Catabolic and Fermentation Pathways *73*
3.3. Induction of Biohydrogen Production 78

3.3.1. Direct Oxygen Removal *78*
3.3.2 Environmental Stimulation *79*
3.3.3. Metabolic Interference *81*
3.3.4 Two-stage Biophotolysis *82*
3.4. Parameters that affect Algal Growth 84
3.4.1. From Algal Cells to Algal Cultures *84*
3.4.2. Algal Strain *85*
3.4.3. Illumination *86*
3.4.4. Phototrophic State *89*
3.4.5. Fluid Dynamics, Temperature and pH *89*
3.5. Parameters that affect Biohydrogen Production 91
3.5.1. From Algal Growth to Biohydrogen Production *91*
3.5.2. Biohydrogen Induction Procedure *93*
3.5.3. Biohydrogen Production Duration *94*
3.5.4. Immobilisation and Genetic Modification *95*
3.6. Photobioreactors 97
3.6.1. Design Principles *97*
3.6.2. Photobioreactor Geometries *98*
3.6.3. Scale-up and Commercialisation *101*
3.7. Summary 107
4. Aim and Objectives **111**
4.1. Aim 111
4.2. Objectives 111
5. Experimental Methods **115**
5.1. Inventories 115
5.1.1. Algal Strains *115*
5.1.2. Photobioreactors *115*
5.1.3. Equipment *116*
5.1.4. Chemicals *116*
5.2. Unit Conversion 122
5.2.1. Light Intensity *122*
5.2.2. Concentration *123*

5.2.3. Algal Growth *123*
5.2.4. Biohydrogen Production *127*
5.3. Photobioreactors 129
5.3.1. Stirred-tank PBRs *129*
5.3.2. Vertical-column PBRs *131*
5.3.3. Tubular PBR *133*
5.3.4. Flat-plate PBRs *136*
5.3.5. Cleaning and Maintenance *138*
5.4. Instrumentation 139
5.4.1. Measuring Instruments and Probes *139*
5.4.2. Calibration *139*
5.5. Medium Preparation 141
5.5.1. TAP *141*
5.5.2. TAP-S *144*
5.5.3. HSM *144*
5.5.4. Customised Media *146*
5.6. Sulphur-deprivation Techniques 149
5.6.1. Centrifugation *149*
5.6.2. Dilution *149*
5.6.3. Nutrient Control *150*
5.7. Analytical Techniques 151
5.7.1. Spectrophotometry *151*
5.7.2. Ion Chromatography *151*
5.7.3. High-Performance Liquid Chromatography *152*
5.7.4. Mass Spectrometry *154*
5.8. Mathematical Models 156
5.8.1. Logistic Growth Model *156*
5.8.2. Aiba Growth Model *157*
6. Results and Discussion **159**
I. Flat-plate PBR Design and Characterisation **159**
I.1. Introduction to PBR Design 159
I.2. Design and Construction 161

I.2.1. Compartmental Design 161
I.2.2. Mixing and Circulation 167
I.2.3. Membrane Inlet Mass Spectrometry (MIMS) 170
I.2.4. Datalogging and Control 175
I.3. Characterisation 177
I.3.1. Light Intensity Distribution 177
I.3.2. Wavelength Modulation 179
I.3.3. Heat Transfer 181
I.4. Operation 187
I.4.1. Calibrations of Probes 187
1.4.2. Dark H_2 Production Experiments 191
I.5. Summary 195
II. Growth of *Chlamydomonas reinhardtii* **199**
II.1. Introduction 199
II.2. Effect of *C. reinhardtii* Strain 201
II.3. Effect of Temperature 206
II.4. Growth under different Light Regimes 211
II.4.1. Growth in TAP 211
*II.4.2. Growth in 5xTAP** 215
II.5. Growth using different Carbon Sources 218
II.5.1. Growth in TAP with CO_2 bubbling 218
II.5.2. Growth in HSM with CO_2 bubbling 224
II.6. Effect of Light Intensity 229
II.6.1. Growth in Sartorius PBR 229
II.6.2. Growth in Flat-plate PBR 234
II.6.3. Growth under High Light Intensity 235
II.7. Summary 239
III. Hydrogen Production by Nutrient Control **241**
III.1. Introduction 241
III.2. Nutrient Uptake Kinetics 242
III.2.1. Acetate Demand 242
III.2.2. Sulphate Demand 246

III.3. Reactor-independent Nutrient Uptake 250
III.3.1. Additional Nutrient Uptake Results 250
III.3.2. Reactor-independent Correlations 255
III.4. H_2 Production at Low Light Intensities 257
III.5. H_2 Production by Centrifugation 261
III.6. H_2 Production by Dilution 266
III.7. H_2 Production by Nutrient Control 268
III.8. Summary 274
IV. Extended Hydrogen Production by Sulphur Re-Addition 277
IV.1. Introduction 277
IV.2. Sulphur Dilution 278
IV.2.1. Sulphur Dilution Experiments 278
IV.2.2. Process Scale-up by Sulphur Dilution 284
IV.3. Sulphur Feed 289
IV.3.1. Sulphur Feed Experiments 289
IV.3.2. Prospects for Continuous H_2 Production by Sulphur Feed 293
IV.4. Summary 297
7. Conclusion and Future Work 299
7.1. Conclusion 299
7.2. Future Work 304
7.2.1. Scale-up 304
7.2.2. Algal Biorefinery 305
7.2.3. Biological Integration 306
7.3. Concluding Remarks 308
References 311

List of Figures

Figure 1.01: Overcoming three of the crucial obstacles to green algal H_2 production 35

Figure 2.01: Schematic diagram of an algal biorefinery 48

Figure 2.02: Schematic diagram of biological integration involving green algae, purple non-sulphur bacteria and dark fermentative bacteria 57

Figure 3.01: Structure and electron transport of photosystem II (PSII) 65

Figure 3.02: Redox potential during photosynthetic electron transport in *C. reinhardtii* 67

Figure 3.03: Photosynthetic electron transport system during oxygenic photosynthesis in C. reinhardtii 70

Figure 3.04: Photosynthetic electron transport system during anaerobic H_2 production in *C. reinhardtii* 71

Figure 3.05: Anaerobic catabolic and fermentative pathways in *C. reinhardtii* 76

Figure 3.06: Photosynthetic, catabolic and fermentative routes to H_2 production in *C. reinhardtii* 77

Figure 5.01: Optical density (OD) calibrations 126

Figure 5.02a: Solar Biofuels Consortium PBR 130

Figure 5.02b: Solar Simulator PBR 130

Figure 5.03: AquaMedic Plankton Light Reactor 132

Figure 5.04a: Sartorius PBR; measurement, sampling and control 134

Figure 5.04b: Sartorius PBR; central vessel, helix and light 134

Figure 5.04c: Sartorius PBR; circulation and mixing 135

Figure 5.04d: Sartorius PBR; light intensity calibration 135

Figure 5.05: Photobioreactor photographs 137

Figure 5.06: Representative ion chromatography (IC) results 153

Figure 5.07: Representative high performance liquid chromatography (HPLC) results 153

Figure 5.08: Representative result of an ion monitoring graph obtained using the mass spectrometer 155

Figure I.01a: Flat-plate PBR; Assembly of the primary and secondary compartments 163

Figure I.01b: Flat-plate PBR dimensions 164

Figure I.01c: Flat-plate PBR; Mixing system features and measuring instruments 165

Figure I.01d: Complete PBR structure with reactor, base, LED array and ancillary equipment 166

Figure I.02: Mixing and circulation in the flat-plate PBR 169

Figure I.03: Design of the Membrane Inlet Mass Spectrometry (MIMS) system 173

Figure I.04: Technical design of the MIMS system 174

Figure I.05: Datalogging & control system architecture 176

Figure I.06: Variations in the spatial light intensity distribution in the flat-plate PBR 178

Figure I.07: Use of the secondary flat-plate PBR compartment for wavelength modulation 180

Figure I.08: Mass transfer in the secondary flat-plate PBR compartment 182

Figure I.09: Heat transfer through the flat-plate PBR compartments 183

Figure I.10a: pH probe calibration 189

Figure I.10b: pO_2 probe calibration 189

Figure I.10c: Photodiode OD calibration 190

Figure I.10d: MIMS calibration 190

Figure I.11: Mutation pathways in *C. reinhardtii* 193

Figure I.12: Dark H_2 production by different *C. reinhardtii* strains 194

Figure I.13: Photographs of the complete and operational dual-compartment flat-plate PBR 196

Figure II.01: Growth curves for the cc124, dum24 and cc406 strains of *C. reinhardtii* in the vertical-column PBR, raw data 202

Figure II.02: Fitting the logistic model parameters r and t_0 using the method of least squares 203

Figure II.03: Logistic model fit to experimental growth data for different *C. reinhardtii* strains 205

Figure II.04: Growth of *C. reinhardtii* cc124 at different temperatures in the Sartorius tubular reactor, raw data 207

Figure II.05: Logistic model fit to experimental data for *C. reinhardtii* cc124 grown at different temperatures 208

Figure II.06: Growth parameter correlations with temperature 210

Figure II.07: Growth of *C. reinhardtii* cc124 in TAP medium under different light regimes in the stirred-tank PBRs, raw data 213

Figure II.08: Logistic model fit to experimental data for *C. reinhardtii* cc124 grown under different light regimes in TAP medium 214

Figure II.09: Growth of *C. reinhardtii* cc124 in 5xTAP* medium under different light regimes in the stirred-tank PBRs, raw data 216

Figure II.10: Logistic model fit to experimental data for *C. reinhardtii* cc124 grown under different light regimes in 5xTAP* medium 217

Figure II.11: Growth of *C. reinhardtii* cc124 in TAP medium bubbled with different CO_2 partial pressures 219

Figure II.12: Logistic model fit to experimental data for *C. reinhardtii* cc124 grown in TAP medium bubbled with different CO_2 partial pressures 222

Figure II.13: Growth parameter correlations with CO_2 feed in TAP 223

Figure II.14: Growth of *C. reinhardtii* cc124 in HSM bubbled with different CO_2 partial pressures 225

Figure II.15: Logistic model fit to experimental data for *C. reinhardtii* cc124 grown in HSM bubbled with different CO_2 partial pressures 227

Figure II.16: Growth parameter correlations with CO_2 feed in HSM 228

Figure II.17: Logistic model fit to experimental data for *C. reinhardtii* cc124 at different light intensities in the Sartorius tubular PBR 232

Figure II.18: Growth parameter correlations with light intensity in the Sartorius tubular PBR 233

Figure II.19: Logistic model fit to experimental data for *C. reinhardtii* cc124 at different light intensities in the ICL flat-plate PBR 234

Figure II.20: Logistic model fit to experimental data for *C. reinhardtii* cc124 at high light intensities under the Solar Simulator 236

Figure II.21: Growth of *C. reinhardtii* cc124 at high light intensities under the Solar Simulator 237

Figure II.22: Growth parameter correlations with light intensity at high light intensities 238

Figure III.01: Reverse logistic model fit to experimental data for *C. reinhardtii* cc124 acetate uptake at different light intensities in the Sartorius tubular PBR 244

Figure III.02: Acetate uptake parameter correlations with light intensity in the Sartorius tubular PBR 245

Figure III.03: Reverse logistic model fit to experimental data for *C. reinhardtii* cc124 sulphate uptake at different light intensities in the Sartorius tubular PBR 248

Figure III.04: Sulphate uptake parameter correlations with light intensity in the Sartorius tubular PBR 249

Figure III.05: Reverse logistic model fit to experimental data for *C. reinhardtii* cc124 acetate and sulphate uptake in the AquaMedic vertical-column PBR 251

Figure III.06: Reverse logistic model fit to experimental data for *C. reinhardtii* cc124 acetate and sulphate uptake in the Solar Biofuels Consortium stirred-tank PBR 252

Figure III.07: Reverse logistic model fit to experimental data for *C. reinhardtii* cc124 acetate and sulphate uptake in the ICL flat-plate PBR 253

Figure III.08: Reactor-independent sulphate and acetate uptake kinetics during *C. reinhardtii* cc124 growth 256

Figure III.09a-d: Growth and H_2 production (measured by injection mass spectrometry) by cc124 *C. reinhardtii* at low light intensities in the Sartorius tubular reactor 258

Figure III.09e-h: Growth and H_2 production (measured by injection mass spectrometry) by cc124 *C. reinhardtii* at low light intensities in the Sartorius tubular reactor 259

Figure III.10: *C. reinhardtii* cc124 WT H_2 production by centrifugation in the ICL flat-plate PBR 262

Figure III.11: *C. reinhardtii* s21 mutant H_2 production by centrifugation in the ICL flat-plate PBR 264

Figure III.12: Comparison of the H_2 production by cc124 and s21 strains of *C. reinhardtii* under centrifugation 265

Figure III.13: *C. reinhardtii* cc124 WT H_2 production by dilution in the ICL flat-plate PBR 267

Figure III.14: *C. reinhardtii* cc124 H_2 production by nutrient control in the ICL flat-plate PBR; 1st experiment 270

Figure III.15: *C. reinhardtii* cc124 H_2 production by nutrient control in the ICL flat-plate PBR; 2nd experiment 272

Figure III.16: Comparison of the H_2 production by the dilution, centrifugation and nutrient control methods of S-deprivation 273

Figure IV.01: H_2 production by *C. reinhardtii* cc124 in the ICL flat-plate PBR following sulphur re-insertion by dilution, 20% and 50% dilutions 280

Figure IV.02: H_2 production by *C. reinhardtii* cc124 in the ICL flat-plate PBR following sulphur re-insertion by dilution, 95% dilution 283

Figure IV.03: Sulphur-re insertion by dilution (20%, 50% and 95%) results extrapolated over a period of 1,000 hours (circa 6 weeks) 286

Figure IV.04: Proposed PBR design for green algal H_2 production scale-up 288

Figure IV.05a-d: Effect of sulphate feed on H_2 production by *C. reinhardtii* cc124 in the ICL flat-plate PBR 291

Figure IV.05e-h: Effect of sulphate feed on H_2 production by *C. reinhardtii* cc124 in the ICL flat-plate PBR 292

Figure IV.06: Assigning a linear fit to the reduction in H_2 production (ΔH_2) associated with the introduction of a sulphate feed 295

Figure IV.07: Relationship between the sulphate feed and the corresponding change in the H_2 production rate 296

List of Tables

Table 3.01: Summary of H_2 production induction procedures 103

Table 3.02: Summary of the parameters that affect *C. reinhardtii* growth 104

Table 3.03: Summary of the parameters that affect *C. reinhardtii* H_2 production 105

Table 3.04: Summary of photobioreactor (PBR) geometries 106

Table 5.01: Algal strain inventory 117

Table 5.02: Photobioreactor inventory 117

Table 5.03: Equipment inventory - photobioreactor peripheries, measuring instruments, laboratory equipment and analytical instruments 118

Table 5.04: Chemical inventory - photobioreactor cleaning & maintenance chemicals, electrode calibration & maintenance chemicals, laboratory gases, medium preparation chemicals, analysis technique chemicals and general laboratory chemicals 120

Table 5.05: Important unit conversions 128

Table 5.06a: TAP salts recipe 143

Table 5.06b: P-solution recipe 143

Table 5.06c: TAP medium recipe 143

Table 5.07a: TAP-S salts recipe 145

Table 5.07b: TAP-S medium recipe 145

Table 5.08: HSM medium recipe 145

Table 5.09a: 5xTAP* medium recipe 147

Table 5.09b: TAP_{12} medium recipe 147

Table 5.10: Concentration of dissolved ion species in various growth media 148

Table 5.11: Sulphur-feed medium recipe 148

Table I.01: Physical properties of water and Perspex 184

Table I.02: Comparison between primary compartment temperature predictions by the Comsol model and experimental data 184

Table III.01: Collection of *C. reinhardtii* cc124 growth and nutrient uptake kinetic parameters in different reactors and under different illumination conditions 254

Nomenclature

ΔG^0	Gibbs free energy
ΔH	decrease in H_2 production rate during sulphur feed
AAT	alanine aminotransferase enzyme
AcDH	acetaldehyde dehydrogenase enzyme
acetyl-P	acetyl phosphate
ACK	acetate kinase enzyme
ADH	alcohol dehydrogenase enzyme
ADP	adenosine diphosphate
algal culture	suspension of algal cells in liquid growth medium
Ar	argon gas
ATP	adenosine triphosphate
ATPase	ATP synthase enzyme
(*aq*)	aqueous solution
C	total quantity of nutrient consumed during logistic growth
$CaCl_2$	calcium chloride
cc124	common *C. reinhardtii* laboratory wild-type strain
cc406	*C. reinhardtii* mutant strain without a cell wall
CCS	carbon capture and sequestration
Chl	chlorophyll molecule
CH_3COO^-	acetate ion
Cl^-	chloride ion
CO_2	carbon dioxide
CoA	coenzyme A
C. reinhardtii	*Chlamydomonas reinhardtii*, unicellular green alga
cyt b_6/f	cytochrome involved in electron transport
DC	direct current
DCMU	3-(3,4-dichlorophenyl)-1,1-dimethyurea
DF	dilution factor
dum24	*C. reinhardtii* mutant strain that accumulates excess starch

FCV	fuel cell vehicle
Fd	ferredoxin
[FeFe]-$h_2$ase	iron-only hydrogenase
[FeS]	iron-sulphur cluster
FNR	ferredoxin/$NADP^+$ reductase enzyme
FTR	ferredoxin/thioredoxin reductase enzyme
GM	genetic modification/ genetically modified
H_2	molecular hydrogen
$h_2$ase	hydrogenase enzyme
H_2O_2	hydrogen peroxide
H-cluster	active site of the iron-only hydrogenase
He	helium gas
HEPES	4-(2-hydroxyethyl)-1-piperazineethanesulfonic acid
HPLC	high performance liquid chromatography
HSM	high-salt growth medium
HVP	high-value product
IC	ion chromatography
ICL	Imperial College London
IR	infra-red light
K	final optical density in logistic growth model
k_s	photosaturation coefficient in Aiba model
k_i	photoinhibition coefficient in Aiba model
KH_2PO_4	potassium phosphate monobasic
K_2HPO_4	potassium phosphate dibasic
LCA	life cycle analysis/assessment
LED	light-emitting diode
LHC	light-harvesting complex
$MgCl_2$	magnesium chloride
$MgSO_4$	magnesium sulphate
MIMS	membrane-inlet mass spectrometry
Mn_4Ca	manganese-calcium water-splitting cluster

MS	mass spectrometer/mass spectrometry
μ_{max}	maximum specific growth rate in the Aiba model
N_2	molecular nitrogen
$NADP^+$	nicotinamide adenosine diphosphate
NADPH	nicotinamide adenosine dinucleotide phosphate
Nda2	NADPH-dehydrogenase enzyme
NH_4^+	ammonium ion
NH_4Cl	ammonium chloride
[NiFe]-$h_2$ase	nickel-iron hydrogenase
NPQR	NADPH-plastoquinone reductase enzyme
O_2	oxygen molecule
OD	optical density
OEC	oxygen-evolving centre
p	p-value coefficient of statistical significance
PAR	photosynthetically active radiation
PBR	photobioreactor
PC	plastocyanin
PDC	pyruvate decarboxylase enzyme
pdc3-KD	*C. reinhardtii* knock-down mutant of the PDC metabolic pathway
PDMS	polydimethylsiloxane polymer membrane
PEM	proton exchange membrane fuel cell
Perspex	polymethyl methacrylate
PFA	perfluoroalkoxy plastic tubing
PFL	pyruvate formate lyase enzyme
PFR	pyruvate ferredoxin reductase enzyme
Pheo	pheophytin molecule
photoautotrophic	growth using CO_2 as the only carbon source
photoheterotrophic	growth using organic substrate as the only carbon source
photomixotrophic	growth using both CO_2 and organic substrate
P_i	inorganic phosphate ion
PO_4^{3-}	phosphate ion

PQ	plastoquinone pool
P-solution	phosphate solution
PSI	photosystem I protein complex
PSII	photosystem II protein complex
PV	photovoltaic
PWM	pulse width modulation
r	specific growth rate in logistic growth model
R	Pearson product-moment correlation coefficient
rpm	rotations per minute
RuBisCO	ribulose-bisphosphate carboxylase enzyme
s21	*C. reinhardtii* potential knock-down mutant of PFL metabolic pathway
-S	without sulphur
S-deprivation	sulphur-deprivation
SO_4^{2-}	sulphate ion
stm6	*C. reinhardtii* GM strain with improved H_2 production
t_0	time of inflection in logistic growth model
TAGs	triglycerides
TAP	tris-acetate phosphate growth medium
TAP-S	sulphur-deplete TAP medium
5xTAP*	customised TAP medium used to investigate *C. reinhardtii* acetate uptake
TAP_{12}	customised TAP medium used for nutrient-controlled H_2 production
Tris	tris-(hydroxymethyl)-aminomethane
UV	ultra-violet light
v/v	volume/volume dilution
WT	wild type
Y_z	tyrosine residue

1. General Introduction

The world is facing an environmental catastrophe on an unprecedented scale. Uncontrolled anthropogenic emissions of carbon dioxide are increasing the global temperature and acidifying the oceans (Stern, 2006). These changes have already resulted in reduced biodiversity (Wijffels & Barbosa, 2010) and, unless addressed effectively, pose a serious threat to our existence as a species. Human carbon dioxide emissions are dominated by the combustion of fossil fuels for energy, implying that climate change is essentially an energy problem. Fossil fuels are not intrinsically dirty or unnatural, as many environmental groups would have us believe (Ricci *et al*., 2010). They are the remnants of ancient microorganisms, which captured solar energy by photosynthesis and stored it within their biomass. However, the combustion of fossil fuels is not sustainable because there is a huge temporal discrepancy between the rapid consumption rate and the sedate geochemical production rate. Our addiction to fossil fuels can be overcome by exploiting photosynthetic processes in rapid real-time now to generate solar fuels independently of the fossil fuel route.

Green algae are a major contributor to the photosynthetic capacity of the biosphere (Hansen *et al*., 2007). Often referred to as pond slime, they actually exhibit vast and complex biodiversity. They have adapted to living in the soil, in fresh water and in salt water, and they consequently inhabit the entire globe. Green algae are therefore affordable, available and flexible; they are an excellent target organism for photosynthetic biofuel production. Green algae are capable of producing multiple fuels, including biodiesel, bioethanol and biochar (Stephens *et al*., 2010a). From a sustainability perspective, the most exciting prospect is their ability to produce molecular hydrogen. Hydrogen is the cleanest possible fuel since its combustion produces only heat energy and pure water. It has the highest energy density per unit mass of any fuel and it can be utilised efficiently in a proton exchange membrane fuel cell. The challenge of sustainable hydrogen production can be addressed using green algae. Green algae produce hydrogen via the process of biophotolysis, which involves the splitting of water by photosynthesis to produce oxygen molecules, protons and electrons, and the subsequent recombination of these protons and electrons by the hydrogenase enzyme to produce molecular hydrogen (Ghirardi *et al*., 2009). Biophotolytic hydrogen production has been demonstrated under anaerobic conditions at the laboratory scale (Melis *et al*., 2000).

More work needs to be carried out in order to improve our understanding of the biophotolysis process. Improved photobioreactors need to be designed to effectively facilitate this process. Genetic engineering of algal cells will probably also be required to enhance hydrogen production. The crucial question that has to be to be answered is whether green algal hydrogen production is scaleable and affordable. Experimental techniques that enable hydrogen production over long time periods, at large scales, under ambient conditions, need to be developed. Green algal hydrogen has the potential to be the sustainable fuel of the future, but the journey towards that noble goal is littered with obstacles. These obstacles include the low photochemical efficiency of the biohydrogen production process (Akkerman *et al*., 2002), the short duration of green algal hydrogen production (Posten & Schaub, 2009), the high cost of commercial photobioreactors (Ugwu *et al*., 2008) and the limited public acceptance of genetically modified organisms (Sheehan *et al*., 1998). Addressing some of these challenges is the aim of this thesis (Figure 1.01).

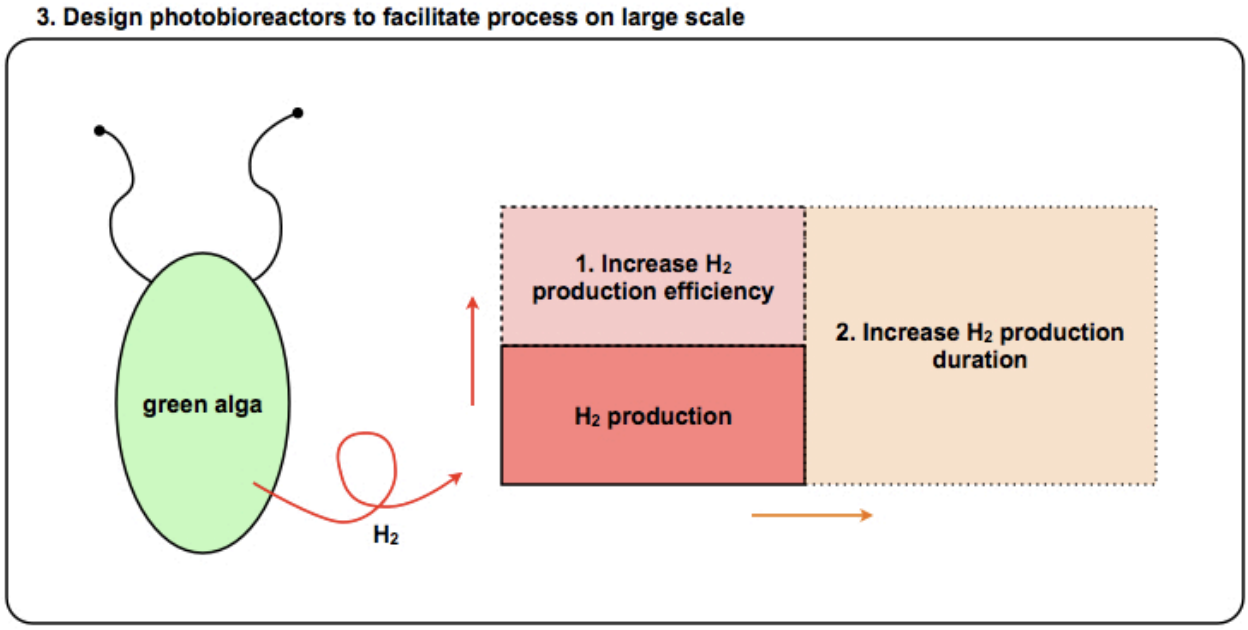


Figure 1.01: Overcoming three of the crucial obstacles to green algal H_2 production

2. Algae and Hydrogen for Sustainable Energy

2.1. Introduction

This chapter will provide an introduction to the global energy challenge and the motivation for producing sustainable energy. The availability and affordability of solar power will be discussed, as will be the benefits and the shortcomings of traditional biofuels. An argument will be made for the utilisation of algae as biological factories and for the development of H_2 as the sustainable fuel of the future. A brief account of the different biohydrogen production processes will be provided.

2.2. Sustainable Energy

In Greek mythology, the Titan Prometheus stole fire from the Gods and gave it to mankind. As punishment for this transgression, he was chained to a rock and destined to suffer an eagle eating his liver for all eternity. While this macabre punishment may not appeal to modern sensibilities, the value of fire to mankind is undeniable. The discovery of fire in the Early Stone Age led to the controlled provision of light and heat, which gave us the means to cook plants and animals, clear land for agriculture and produce tools. Controlled use of fire facilitated the availability of fuel and food that makes our lifestyle so fundamentally different from that of the other great apes. The original combustable fuel was wood, a biofuel (Lewis & Nocera, 2006). It enabled the first civilisations to flourish, powered the furnaces of the Roman Empire and fuelled the Age of Discovery. Then, in 1698, the invention of the first practical steam engine sparked the Industrial Revolution. Biofuels were replaced by fossil fuels, initially coal and later crude oil and natural gas. Fossil fuels had the critical advantage of a significantly higher energy density, as a consequence of having two billion years of accumulated energy reserves on their side (Faunce, 2011). The Industrial Revolution led to improved living standards and exponential population growth, eventually giving way to the modern-day information revolution and globalisation.

Today we live in a world powered by fossil fuels. Global population and energy demand continue to rise rapidly (IEA, 2011). This comes at a time when we have discovered that fossil fuels are not the panacea that they were once believed to be. Proven crude reserves are dwindling and the end of cheap petroleum and diesel is imminent (Blanchette, 2008). Conventional crude oil production peaked at 74 million barrels per day in 2004 and has been in decline since. In addition, the combustion of fossil fuels has released trapped carbon into the atmosphere in the form of carbon dioxide (CO_2), a recognised greenhouse gas (Hansen *et al*., 2007). The great energy challenge of our generation is to secure affordable energy supply while cutting greenhouse gas emissions, a task that may only be accomplished by making the transition to a low-carbon economy based on a sustainable energy mix.

Global population is projected to increase from 6.6 billion in 2008 to 9.2 billion by 2050 (Stephens *et al.*, 2010a). In this time, developing economies will continue to grow, and an ever increasing

number of people will demand access to the living standards available in the developed world: living standards that come with an embedded energy cost. Given current energy consumption trends, the total time-averaged global power consumption is expected to increase from 13 terawatts (TW) in 2000 to as much as 46 TW by 2100 (Kruse *et al.*, 2005a). Under this kind of growth scenario, all proven fossil fuel reserves will be depleted by the end of this century, with transport fuels being the first to go (Stephens *et al*., 2010a). The world therefore needs to develop additional energy resources, which are required on an urgent timescale, and these resources need to be renewable in order to satisfy the energy demands of future generations.

The demand for energy is a basic consequence of modern life. It is difficult to imagine the average UK home without access to electric lights, central heating or even a television. Continuing to supply secure and affordable energy is therefore one of the top priorities for the UK government (DBERR, 2007). With fossil fuel reserves in the North Sea running out, the UK is importing ever-increasing amounts of oil from the Middle East and natural gas from Russia. This dependence on foreign fuels makes the UK more vulnerable to supply disruptions and price fluctuations (DBERR, 2007). Energy security is an issue across the developed world, even in the world's largest economy (US DoE, 2005). There is therefore a strong national incentive to develop local energy resources with the aim of improving the security of energy supply.

CO_2 concentrations in the atmosphere have been increasing exponentially since the dawn of the industrial revolution, contributing towards anthropogenic climate change (Hansen *et al*., 2007). Two thirds of world CO_2 emissions are associated with the way we produce and use energy, a sector that is still dominated by the combustion of fossil fuels (US EPA, 2010). The issue of climate change is therefore an issue of energy use, or more specifically, of fossil fuel use. The present-day CO_2 concentration in the atmosphere is 390 parts per million (ppm), significantly higher than the pre-industrial (historic) level of 280 ppm; the mass of atmospheric CO_2 is also increasing at a rate of 34 gigatonnes of CO_2 per annum ($GtCO_2 \cdot y^{-1}$) (IPCC, 2007). In order to avoid a 2°C global temperature rise, which should prevent the more devastating effects of climate change, the average UK resident would need to reduce their CO_2 emissions from 11 $tCO_2 \cdot y^{-1}$ today to 1 $tCO_2 \cdot y^{-1}$ by 2050 (IPCC, 2007). Similar CO_2 emission reductions would need to be implemented globally. In order to meet its Kyoto protocol targets and fall in line with EU environmental obligations, the UK government has

committed to reducing carbon dioxide emissions by 80% before the year 2050 (DBERR, 2007). Small steps towards reaching this target can be made by improving energy efficiency and decarbonising electricity generation, but a major overhaul of the energy sector will eventually be necessary. This overhaul will almost certainly involve the complete replacement of fossil fuels with alternative low-carbon fuels in the transport sector (Weiss *et al.*, 2000). According to the Stern review on climate change, it would be economically prudent to devote a small percentage of global GDP now to mitigate climate change rather than to pay for the costs of inaction in the future (Stern, 2006). Since the benefits of strong, early action to tackle climate change outweigh the costs, the development of low-carbon, high-efficiency energy technologies is needed on an urgent timescale.

2.3. Solar Power and Biofuels

In summary, solving the energy challenge would require a renewable, locally available, low-carbon energy resource. Ideally, this resource should be available everywhere in the world and it should carry enough power to satisfy the huge global energy demand. In the absence of atomic fusion, the only resource capable of meeting these requirements is solar power. Ultimately, all of our energy comes from the Sun. This energy drives the wind and the ocean currents, the water cycle of evaporation and condensation, and the biological cycle of photosynthesis, life and decay. The power provided by solar irradiation incident on the Earth's surface is close to 120,000 TW, orders of magnitude greater than the total global power consumption of 13 TW (US DoE, 2005). The solar energy incident on the Earth's surface in one hour is roughly equivalent to the entire annual global energy consumption (Melis, 2009). If 0.16% of the Earth's surface could be covered with 10% efficient solar energy converters, it would provide 20 TW of power (US DoE, 2005). Some regions have more access to solar power than others, but even the domestic solar resource of the UK is large enough to make a significant contribution towards satisfying national energy demand (Evans, 2007).

The utilisation of solar power requires three steps: capture, conversion and storage. Solar power utilisation can also be split into three categories based on the primary energy produced: solar electricity, solar thermal and solar fuel. Solar electricity involves the excitation of electrons and holes in a photovoltaic (PV) cell, usually constructed from a semiconductor such as silicon, and the direct conversion of this excitation to electrical energy. Today, PV power is a factor of 5-10 times too expensive to compete with electricity production from fossil fuels, and 25-50 times too expensive to compete as a primary energy source (US DoE, 2010). Solar energy can also be converted to heat energy in solar concentrators, where mirrors are used to focus sunlight collected over a large area onto a heat absorber such as water or molten salts. Solar thermal power requires the construction of large, expensive facilities in Sun Belt countries as well as the construction of an effective power transmission network to centres of high energy demand (DBERR, 2007). A third option is to use the natural process of photosynthesis to fix atmospheric CO_2 into sugars and carbohydrates within plant biomass, and afterwards to convert this biomass into transport fuels such as bioethanol, biodiesel, biomethanol, bio-oil or biohydrogen (Demirbas, 2007; Stephens *et al.,*

2010a). The main problem with solar power, as with all renewable resources, is that the energy is extremely diffuse. Even high-efficiency PV panels installed in the Sun Belt region cannot achieve power densities in excess of 20 $W \cdot m^{-2}$ (US DoE, 2010). This low power density has two major disadvantages: high costs and large surface area requirements. Biofuels generated from traditional energy crops address the former issue at the expense of the latter.

The last decade has seen massive investment in liquid biofuel alternatives to petroleum and diesel, with the US, Brazil and the European Union leading the way (Evans, 2007). Biofuel projects have been funded by policies such as the Renewable Transport Fuel Obligation in the UK, which places a requirement on liquid fossil fuel owners to mix a small percentage of biofuel with their product (Groom *et al.,* 2008). Corn and sugarcane derived bioethanol have been the primary recipients of biofuel grants and subsidies. Not only have these first generation biofuels failed to deliver on CO_2 mitigation targets, they have also contributed to a host of environmental and socio-economic problems. This is because the world today is very different from the biofuel-dominated pre-industrial era: the human population is vast, arable land is limited and energy demand is massive. The low power density of first generation biofuels results in surface area requirements that are impracticable for most European countries. For example, it would be necessary to cover more than one third of the entire UK land area with rape crops to produce enough rape-seed oil to fuel the 30 million personal vehicles on the road today (Chisti, 2008; DBERR, 2007). Even in the US midwest, where arable land is plentiful and growth conditions are good, the use of corn and other agricultural crops to produce biofuels has come under intense scrutiny. The increased cultivation of agricultural biofuels has resulted in a partial coupling of the demand for fuel in the developed world with the demand for food in the developing world. This food vs fuel dilemma exaggerates shortages of both resources and it was partially responsible for the world food price crisis in 2008 that led to widespread malnutrition and starvation, as well as political and social unrest (Pimentel *et al.,* 2009). Developing tropical countries such as Brazil and Indonesia often face a fuel vs forest decision. Clearing primary rainforest to make way for sugarcane plantations not only devastates local biodiversity, it also damages a crucial CO_2 sink (IPCC, 2007). African nations would be better served by using their limited water reserves to feed their respective populations rather than to grow energy crops. Biofuels also require ammonium-based fertilisers produced in the fossil fuel intensive Haber-Bosch process (Searchinger *et al*., 2008). These industrial fertilisers are frequently overused,

triggering soil erosion and deadly algal blooms in river estuaries. Recent wide-scoped life cycle analyses (LCAs) have shown that some first generation biofuels actually increase CO_2 emissions once fertiliser, harvesting, processing and land-use energy costs are taken into account (Searchinger *et al.,* 2008). Even in the cases where biofuels reduce CO_2 emissions, they are not the most cost-effective or the most ethical means of doing so.

Advanced biofuels have been developed to address many of the issues listed in the previous paragraph. They include the large perennial grass *Miscanthus giganteus,* cellulose-based fuels and various waste-to-fuel initiatives (Demirbas, 2007). While less controversial than traditional biofuels and certainly applicable to some niche markets, advanced biofuels remain limited by the same low power density as their predecessors and are unlikely to make more than a small dent in the fossil fuel domination of transport. It is therefore hardly surprising that artificial systems for the production of transport fuels have begun to emerge. Renewable electricity generation (wind, solar photovoltaic or nuclear) could be used to power water electrolysis, producing H_2 for use directly as a fuel or as a reductant to generate more desirable liquid fuels such as methanol (Taylor, 2008). Although renewable electrolysis systems could operate at efficiencies higher than natural photosynthesis, they would be many times more expensive (Perharz *et al.,* 2007). It is therefore more practical to use the renewable electricity directly, although water electrolysis may play an important role as a storage technology for intermittent renewable resources.

Research has also intensified in the area of artificial photosynthesis, with contributions from the fields of synthetic biology, biomimetics, electrochemistry and many others (Blankenship *et al.*, 2011; Hammarström *et al.*, 2011; Lewis & Nocera, 2006; Oh *et al.,* 2004). The problem with this approach is not only that natural photosynthesis is extremely complex, but that many of the proteins and enzymes involved in the processes of light harvesting, water-splitting and CO_2 reduction are already very efficient, having been moulded and perfected by 2.5 billion years of evolutionary selection (Blankenship *et al.*, 2011). Perhaps it is not time to give up on natural photosynthesis just yet. Simple photosynthetic microorganisms such as green algae and cyanobacteria (henceforth referred to as “algae”) do photosynthesis best, but they are only now becoming recognised as a viable biofuel source (Posten & Schaub, 2009). All crude oil ultimately came from algae so it is

certainly plausible that future transport fuels could be obtained from the same source (Schenk *et al*., 2008).

2.4. Algae as Biological Factories

Photosynthesis involves the capture of solar energy by phototrophic organisms and its conversion into chemical energy and biopolymers. It is the basis for almost all life on Earth (Beer *et al.,* 2009). The first stage of the photosynthetic electron transport chain is catalysed by the photosystem II (PSII) protein complex. Pigmented light harvesting molecules within PSII capture solar energy, generating a chlorophyll radical cation and a reduced plastoquinone molecule, the strongest redox pair known in biology (Miyake *et al*., 1999). This electrochemical potential is passed along a series of redox active components to the thylakoid membrane, where the manganese-calcium (Mn_4Ca) cluster oxidises water into oxygen molecules (O_2), protons and electrons (Hallenbeck & Benemann, 2002). Electrons derived from water-splitting eventually create a pH gradient that is responsible for driving the Calvin cycle (Bassham *et al*., 1950). The Calvin cycle, catalysed by the enzyme ribulose-bisphosphate carboxylase (RuBisCO), involves the reduction of atmospheric CO_2 and the subsequent production of carbohydrates such as glucose, sucrose and starch (Darzins *et al*., 2010). When energy is plentiful, surplus starch can be stored in the form of fatty acids, triglycerides (TAGs) or other lipids. In stark contrast to artificial photosynthetic systems (Faunce, 2011; Ham *et al.,* 2010), all the enzymes that carry out natural photosynthesis are non-toxic, they operate at room temperature and pressure and they are based on the most common of elements. These enzymes are difficult to isolate or to biomimic because they are exceptionally unstable, they have very short lifetimes and they only function under a strict set of biological conditions (Brenner, 2006). Such concerns can be overcome by using algae as microbiological factories to create, replicate and repair photosynthetic enzymes, and to eventually produce biofuels (Luiten *et al.,* 2003; Schenk *et al*., 2008; Spolaore *et al*., 2006).

Eukaryotic algae harvest light efficiently because a large percentage of their cell is composed of chlorophyll. Unlike deciduous plants, which lose their leaves in the winter, algae keep their chlorophyll and remain photosynthetically active all year round. Algae do not need to grow roots, leaves, shoots or flowers; all their energy goes into the replication and repair of their photosynthetic apparatus or into reproductive efforts that increase the cell density of the algal culture. Algae are therefore more efficient at converting sunlight into chemical energy than terrestrial plants and require a smaller geographical footprint and less water for cultivation (Beer *et al*., 2009). As a result

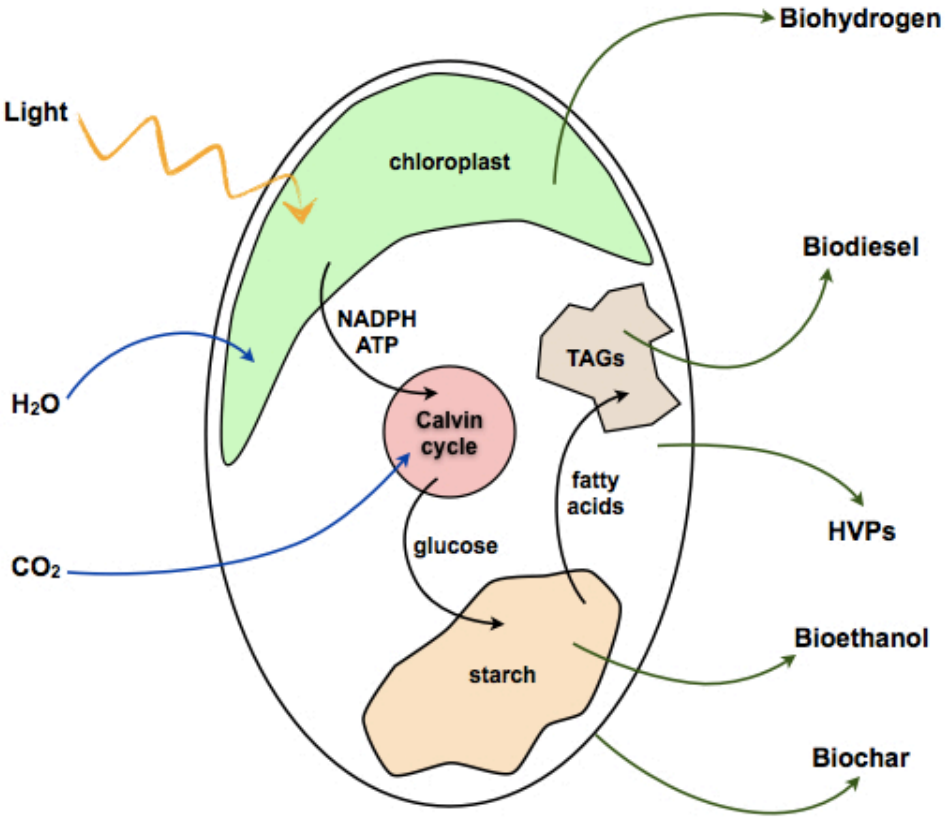
of their high photosynthetic efficiency, algal cultures grow extremely fast. They commonly double their biomass within 24 hours and are capable of doubling times as short as 3.5 hours during the exponential growth phase (Chisti, 2007). Not only do algae grow quickly, but a large proportion of their biomass is usable as fuel. The fuel most commonly associated with algae is biodiesel, which is derived from the lipid fraction of the biomass. On average, lipids constitute approximately 30% of algal biomass (this value can be as high as 80% for some genetically engineered species), compared to 5% of the biomass in the case of palm oil (Chisti, 2008). Algae can produce more biomass per unit time and more biomass per unit area than any other plant.

One of the main advantages of using algae is their massive biodiversity, which makes it possible to select strains for a particular geographical location or a specific purpose (Meuser *et al.,* 2009). Different algal strains have adapted to grow in UK soil, on the surface of the ocean, underneath desert sand, next to hydrothermal vents and in freezing Siberian rivers. There is an optimal algal strain for every location (Sheehan *et al.,* 1998). One potential algal application is to capture the CO_2 emitted by fossil fuel combustion in power stations. To achieve this, it is necessary to select an extremophile with high temperature and low pH tolerance, as well as a very active Calvin cycle (BBSRC, 2010). In some cases, nature simply does not provide the right alga for the job, or the process is not efficient enough to be economically viable. It is in these situations that genetic engineering can come to the rescue. Some model organisms, such as the green alga *Chlamydomonas reinhardtii* and the cyanobacterium *Synechocystis* sp. PCC6803, have had their genomes mapped (Ducat *et al.,* 2011a; Merchant *et al.,* 2007). Since these are relatively simple unicellular organisms, it is possible to create mutants with modified physical or metabolic properties. One promising approach for improving algal biofuel production is to reduce the size of the photosynthetic light-harvesting antennae. Shorter antennae would allow each PSII complex to obtain only the light energy that it needs for water-splitting, rather than wasting energy as heat and fluorescence (Kosourov *et al*., 2011). If successful, this approach would increase algal cell densities and consequently the power density of any biofuels derived from those algal cultures.

Algal biofuel productivity is not dependent on arable land and could therefore be scaled to make a significant contribution to the global demand for fossil fuels without affecting food crops or endangering forested ecosystems (Sheehan *et al*., 1998). This is because many algal strains can be

grown in brackish or saline water. These aquatic systems also happen to contain many of the salts and other nutrients required for algal growth (Borowitzka, 1999). Many different biofuels can be extracted from algae. The most common approach is to process the algal oil fraction into biodiesel or jet fuel. The remaining algal biomass could then be digested or anaerobically fermented to produce biogas (Mussgnug *et al.,* 2010). Although biodiesel production is possible with existing technologies, more energy-efficient and cost-effective techniques are also under development. A new generation of algal biofuels, including hydrogen and isoprene, are released as gaseous products during algal growth, making them much easier to harvest (Hejazi & Wijffels, 2004). These fuels are still in early-phase research: their current production rates are too low for commercial applications, but future rewards could be substantial. Any unusable algal biomass can also be pyrolised to biochar, which can serve as a means of CO_2 sequestration, or as a substitute for coal (Sialve *et al*., 2009). By exploiting these several conversion stages and routes to renewable fuel production, algae offer an almost unique possibility of providing entirely carbon-neutral energy over the entire cradle to grave cycle.

While algal biofuel production may be in its infancy, algal growth for high-value product (HVP) extraction is a mature and very profitable industry. HVP manufacturers typically use the algal protein fraction to obtain valuable commodities such as vitamins, dyes, pharmaceuticals, insecticides and various precursor chemicals (Ducat *et al*., 2011a; Rasala *et al.,* 2010). The success of algal HVPs means that some of the infrastructure required to make algal biofuels a reality already exists. The existing photobioreactor (PBR) models need to be scaled up to a level where they could grab a significant proportion of the vast global biofuels market and beyond. The algal biorefinery concept represents the best approach to the future development of the algal biofuel industry (Chisti, 2007; Skjånes *et al.,* 2007). The idea is not to gear operations exclusively towards a specific end product, but to obtain as many valuable by-products from algae as possible, whether they are vitamins, insecticides, biodiesel, biohydrogen or biochar. This integrated approach would extract the maximum amount of value from a given volume of algae. Figure 2.01 shows how different parts of the cell could be used in an algal biorefinery.



Legend: H_2O - water; CO_2 - carbon dioxide; NADPH - nicotinamide adenosine dinucleotide phosphate; ATP - adenosine triphosphate; TAGs - triglycerides; HVPs - high value products.

Figure 2.01: Schematic diagram of an algal biorefinery

2.5. Hydrogen as a Fuel

Interest in H_2 as a fuel has grown over the last decade with increasing international concern over environmental and security of supply issues involving fossil fuels (Ricci *et al.,* 2010). There is now significant investment in H_2 research and demonstration projects (US DoE, 2008). Nevertheless, H_2 fuel is in the early stage of development and it remains unproven commercially outside some limited applications in the space sector (Ricci *et al.,* 2008). Although the use of H_2 as a fuel is in its relative infancy, over 50 million metric tons of H_2 are produced globally for various chemical purposes from fossil fuel sources by a range of energy- and CO_2-intensive processes, such as the steam reforming of methane and the gasification of coal (US DoE, 2008). H_2 currently has different applications: it is produced and used commercially primarily for the manufacture of ammonia-based fertilisers, as well as for use in petroleum refining, petrochemical manufacturing and glass purification (US DoE, 2008).

Hydrogen is the simplest element on Earth. It readily forms compounds with other elements and is most commonly found in water, hydrocarbons and biomass. Hydrogen gas is a diatomic molecule; under standard temperature and pressure, it exists as a colourless, odourless and tasteless gas, which is lighter than air (Hemmes *et al.,* 1986). Molecular hydrogen is an energy carrier - it has the capacity to store and deliver energy in a usable form. H_2 has the potential to provide safe, clean, secure and affordable energy that can be used to power vehicles, homes, factories and even electronic equipment (US DoE, 2008). H_2 is considered to be the cleanest, lightest and most efficient known fuel (Momirlan & Veziroglu, 1999). It is the cleanest fuel because the combustion of H_2 in air produces only heat energy and water. However, H_2 can only genuinely be called a clean fuel if it is produced by an equally environmentally benign, as well as economical, process. The energy per unit mass of H_2 is 143 $MJ \cdot kg^{-1}$, compared with 46 $MJ \cdot kg^{-1}$ for petrol, making it the lightest available transport fuel (Hemmes *et al*., 1986). On the other hand, hydrogen gas has a very low energy per unit volume, which raises some significant storage challenges. H_2-to-electricity conversion efficiencies in proton exchange membrane (PEM) fuel cells can be as high as 50%, compared with a 20% efficiency of petrol in an internal combustion engine (Barbir, 2005). PEM fuel cells use a platinum catalyst and are consequently uneconomical at present, although there has been significant research and progress in this area recently (US DoE, 2005). Even if all the

technological challenges were to be overcome, H_2 would still need to be accepted by members of the general public, who often associate hydrogen with fire and explosions, particularly with the Hindenburg airship disaster and with the hydrogen bomb (Ricci *et al.,* 2008). A carefully-planned policy of public consultation and education will be required to convince members of the public to accept H_2 as a fuel, as well as to potentially be prepared to pay more for a sustainable H_2 economy.

Whether it was fire, steam power or electricity, the introduction of a new energy carrier has always resulted in periods of economic growth and improved living standards throughout human history. With the advent of steam power in the late eighteenth century, it became possible to construct locomotives, steam ships and traction engines. The introduction of a hydrogen economy would bring about the widespread use of fuel cells in vehicles and other applications (Blanchette, 2008; Meherkotay & Das, 2008). A fuel cell is an electrochemical engine that generates power via the combination of a particular fuel with atmospheric O_2. H_2 can be used in the PEM fuel cell to generate electricity at low temperatures and high efficiencies (Levin, 2004). The only by-products of the PEM fuel cell are water (as steam) and heat, which makes it suitable for vehicles and other portable applications. Fuel cell vehicles (FCVs) are clean and green at the point of use, with no CO_2, nitrous oxide or sulphur oxide emissions. To fully quantify the environmental benefits of H_2-fuelled FCVs, it is necessary to consider the entire well-to-wheel cycle, from production to end use. At present, FCVs store compressed gaseous hydrogen in a fuel tank pressurised to 350-700 bar (US DoE, 2008). This is not an ideal solution because it creates a trade-off between the size and weight of the fuel tank and the range of the vehicle, which needs to be capable of covering 300 miles on a full tank to be competitive with petroleum- and diesel-powered alternatives (Weiss *et al.,* 2000). Alternative H_2 storage technologies are under development and they include cryogenic liquid storage and material storage in metal hydrides, carbon-based structures or other chemical bonds (US DoE, 2008).

Unlike coal, solar power or biomass, H_2 is not an energy source but an energy carrier that must be produced from a particular set of energy sources. The commercialisation of clean H_2 production is a crucial barrier that must be overcome before the hydrogen economy can become a reality. The supply of H_2 is extremely diverse and has no geographical bias; H_2 can be produced by thermal, thermochemical, photolytic and electrolytic processes, and also offers the potential for distributed

generation (US DoE, 2008). Today, most H_2 is produced by thermochemical steam methane reforming at high temperatures in large central facilities (Momirlan & Veziroglu, 1999). The cost of H_2 production by methane reforming is highly sensitive to the price of natural gas, and it is currently in the order of \$3 per kgH_2 (Bartels *et al.,* 2010). Methane reforming releases CO_2 and therefore negates the primary benefit of using H_2 as a fuel; additionally, it is more economical and energy efficient to use the methane directly as a transport fuel rather than to use it to produce H_2. Based on the price of methane reforming, the US Department of Energy has set a price target of \$2.6 per kgH_2 for low-carbon, renewable energy technologies (Amos, 2004). At this price, H_2 would be economically competitive with petroleum, currently priced at approximately \$2-4 per gallon, assuming no taxation of the H_2 fuel (Bartels *et al.,* 2010). For comparison, one kilogram of H_2 is approximately equal to 1 gallon of petroleum, based on the lower heating value content (IEA, 2011).

Decarbonisation of H_2 production could be achieved via the gasification of coal coupled to carbon capture and sequestration or biomass, or by using renewable or nuclear electricity to perform the electrolytic processes of water splitting. H_2 production from the gasification of coal and biomass would cost approximately \$1 per kgH_2 and \$1-3 per kgH_2 respectively (Bartels *et al*., 2010). The clean utilisation of coal would require carbon capture and sequestration (CCS): this is not a proven or commercially available technology and its application would certainly raise the price of H_2 production by coal gasification. The disadvantages of using biomass from traditional energy crops have already been discussed. The price of H_2 production by electrolysis is estimated to be \$7 per kgH_2 for nuclear power and \$6-22 per kgH_2 for renewables, where wind power is the most economical source and solar PV among the least economical sources (James *et al.,* 2009; US DoE, 2009). Electrolysis is expensive because it initially requires the generation of electricity, subsequently followed by the process of water splitting, which is at best 15% efficient (James *et al*., 2009). Once again, having generated the electricity, it would be more practical to use it directly rather than to use it to produce H_2.

As discussed previously, algae are superior to traditional biofuels in terms of their higher biomass production rate, their smaller surface area requirements and their ability to grow on non-arable land. This all equates to more economical biofuel, including biohydrogen, production from algae and

bacteria (Benemann, 1999). Furthermore, certain microorganisms are capable of producing H_2 directly from the cell culture, without the need for energy-intensive drying, processing and gasification (Das & Veziroglu, 2001). There are three routes to direct microbiological biohydrogen production: dark fermentation, photofermentation and biophotolysis.

2.6. Biohydrogen Production

2.6.1. Dark Fermentation

Dark fermentation is carried out most efficiently by purple non-sulphur bacteria, such as *Rhodospirillum* sp. or *Rhodobacter* sp., or by green sulphur bacteria such as *Chlorobium vibrioforme* (Rupprecht *et al.,* 2006). These bacteria are grown on carbohydrate-rich organic substrates, typically glucose or sucrose, in the dark. The organic substrates are degraded by oxidation to provide the building blocks and energy for growth; the use of an organic carbon source for growth is known as heterotrophic growth. This process also produces electrons, which would normally be used to reduce O_2 to water. However, under anaerobic conditions, the electrons are used to drive the process of organic acid, alcohol and H_2 formation by dark fermentation (Hallenbeck & Ghosh, 2009). In the case of glucose fermentation, glucose catabolism initially produces pyruvate. Pyruvate can be oxidised to produce formic acid and acetyl-coenzyme A (acetyl CoA), which can be converted to acetyl phosphate, resulting in the formation of the energy carrier adenosine triphosphate (ATP) and the excretion of acetic acid (Manish & Banerjee, 2008). Pyruvate oxidation requires reduction of the electron carrier ferredoxin (Fd). Reduced Fd is re-oxidised by the nitrogenase or hydrogenase enzymes, which release electrons as H_2 (Nath & Das, 2004).

Dark fermentation redox pathways:

$$\text{pyruvate} + \text{CoA} \rightarrow \text{acetyl-CoA} + \text{formate}$$

$$\text{pyruvate} + \text{CoA} + 2\ Fd_{oxidised} \rightarrow \text{acetyl-CoA} + CO_2 + 2\ Fd_{reduced}$$

$$2\ Fd_{reduced} \rightarrow 2\ Fd_{oxidised} + H_2$$

Dark fermentation reaction:

$$C_6H_{12}O_6\ (\text{glucose}) + 2\ H_2O \rightarrow 2\ CH_3COOH\ (\text{acetate}) + 4\ H_2 + 2\ CO_2$$

The maximum theoretical yield of dark-fermentative H_2 production is 4 $molH_2 \cdot mol^{-1}$ of glucose if all the glucose is completely metabolised to acetate (Das, 2009). In a practical experiment, the substrate conversion is approximately 53% efficient and the H_2 production rate is 1,300-3,000 ml of H_2 per litre of culture per hour ($mlH_2 \cdot l^{-1} \cdot h^{-1}$) (Levin, 2004). Glucose is not the ideal choice of

substrate because it needs to be derived from an energy crop such as sugarcane. Practical and economic dark fermentation would use organic substrates from the food and forestry industry or from sewage sludge (Das, 2009). The main barrier facing the commercialisation of waste-to-H_2 by dark fermentation is the relatively low H_2 yield and the formation of large quantities of side-products, such as acetic, propionic, butyric acids and ethanol (Hallenbeck & Ghosh, 2009). The main concern is therefore one of selection and separation efficiency.

2.6.2. Photofermentation

As well as carrying out dark fermentation, purple non-sulphur bacteria are also capable of carrying out photofermentation in the light, which is sometimes also referred to as anaerobic photosynthesis (Das & Veziroglu, 2001). In this process, the bacteria use a reduced carbon substrate, typically an organic acid such as acetate, together with the light energy captured by their photosystem to produce ATP and high-energy electrons that reduce Fd. Reduced Fd drives H_2 formation via the nitrogenase enzyme (Akkerman *et al.,* 2002). This reaction requires an energy input of 75.2 $kJ \cdot mol^{-1}$, as defined by its Gibbs free energy (ΔG^0).

Photofermentation reaction (purple non-sulphur bacteria):

$$CH_3COOH \text{ (acetate)} + 2\ H_2O \rightarrow 2\ CO_2 + 4\ H_2$$

$$\Delta G^0 = +75.2\ kJ \cdot mol^{-1} \text{ (light energy requirement)}$$

The nitrogenase enzyme is highly sensitive to O_2 and inhibited in the presence of ammonium ions. Photofermentation by purple non-sulphur bacteria must therefore be carried out in closed PBRs, free of N_2 (Akkerman *et al.,* 2002). The process also suffers from low light conversion efficiencies and a high energy demand by the nitrogenase enzyme. Nevertheless, anaerobic photosynthesis has its merits because it can completely convert organic wastes to H_2 and CO_2 (Hallenbeck & Ghosh, 2009). H_2 production rates of 50-180 $mlH_2 \cdot l^{-1} \cdot h^{-1}$ have been documented (Levin, 2004).

An alternative route to photofermentative H_2 production involves the use of nitrogen-fixing cyanobacteria (blue-green algae), such as *Anabaena* sp. PCC 7120 and *Cyanothece* sp. ATCC 51142. *Anabaena* contains a structure called a heterocyst, a walled-off metabolic block within the

cell, which allows it to spatially separate photosynthetic and photofermentative processes (Lopes *et al.,* 2002). The main part of the cell fixes CO_2 to sucrose, which is used to power the nitrogenase enzyme in the heterocyst (Ghirardi *et al.,* 2009). *Cyanothece* does not contain a heterocyst; instead, it separates photosynthesis and photofermentation temporally, fixing CO_2 to glycogen during the day and using this glycogen as an electron donor to the nitrogenase enzyme during the night (Bandyopadhyay *et al.,* 2010). In the absence of molecular nitrogen (N_2), photofermentative cyanobacteria divert all of the fermentative electrons to H_2 production, introducing the stoichiometric H_2 yield by a factor of 4 (Ghirardi *et al.,* 2009). These photofermentative electrons involve the breakup of ATP into adenosine diphosphate (ADP) and an inorganic phosphate ion (P_i), a process that releases energy ($\Delta G^0 = -30.5$ kJ·mol^{-1}).

Photofermentation reactions (cyanobacteria):

In the presence of N_2:

$N_2 + [8\ H^+ + 8\ e^- + 16\ ATP]$ (sucrose/glycogen) $\rightarrow 2\ NH_3$ (ammonia) $+ H_2 + 16\ ADP + 16\ P_i$

In the absence of N_2:

$[8\ H^+ + 8\ e^- + 16\ ATP]$ (sucrose/glycogen) $\rightarrow 4\ H_2 + 16\ ADP + 16\ P_i$

H_2 production rates depend on the quantity of sucrose/glycogen that has been biosynthesised. Photofermentative H_2 production by cyanobacteria could be further increased by feeding the bacteria with an organic substrate such as glucose or glycerol (Bandyopadhyay *et al.,* 2010).

2.6.3. Biophotolysis

Green algae such as *Chlamydomonas reinhardtii* and cyanobacteria such as *Synechocystis* sp. PCC6803 have the ability to produce H_2 from two of nature's most plentiful resources, sunlight and water, by biophotolysis (Benemann, 1997). The PSII protein complex captures sunlight and uses this energy to split water into O_2, protons and electrons. The photosynthetic electrons are transported by Fd and other intermediates to the hydrogenase enzyme, which catalyses the process of proton-electron recombination to produce H_2 (Esper *et al.,* 2006).

Biophotolysis reactions:

Water-splitting:

$2\ H_2O \rightarrow O_2 + 4\ H^+ + 4\ e^-$

Proton-electron recombination:

$4\ H^+ + 4\ e^- \rightarrow 2\ H_2$

Biophotolysis is a completely sustainable H_2 production process. H_2 is produced from water, and it also returns to water once it has been used up as a fuel. Renewable solar power is collected and chemically stored as H_2 by algae. The problem with direct biophotolysis is that the hydrogenase enzyme is inactivated in the presence of O_2 so that the process only works under anoxic or anaerobic conditions (Ghirardi *et al.,* 2009). Since photosynthetic water-splitting constantly evolves O_2, this O_2 needs to be removed as it is being produced. A more detailed description of biophotolytic H_2 production by *Chlamydomonas reinhardtii,* as well as an overview of the techniques used to overcome the O_2 sensitivity of the hydrogenase enzyme, will be discussed in Chapter 3.

2.6.4. Biological Integration

Biological integration involves the combination of different microalgal and cyanobacterial cultures in an integrated system to improve the energy efficiency, economics and the production rate of biohydrogen. The first opportunity involves substrate recycling. The organic acid side-product of dark fermentation could be used as a feed for photofermentation by purple non-sulphur bacteria. CO_2 from dark fermentation could be used together with the ammonia produced by the photofermentation of nitrogen-fixing cyanobacteria to grow photosynthetic green algae, such as *Chlamydomonas reinhardtii* or *Chlorella* (Melis & Melnicki, 2006). Another possibility is to use a fast-growing green alga such as *Chlorella* as the carbohydrate feed for dark fermentation (Skjånes *et al.,* 2007). There is also an opportunity for combining green algae or cyanobacteria with purple non-sulphur bacteria in a single light-harvesting complex. The photosynthetic microorganisms would form the top layer and absorb red light, while the purple bacteria could be placed underneath to harvest the remaining, lower-wavelength photons. Such an arrangement would improve the quantum efficiency of solar energy capture (Ghirardi *et al.,* 2009). The most successful biohydrogen

production approach would likely take advantage of the majority of these biological integration opportunities, as well as utilising high-value chemicals, biomass and other bi-products of H_2 production in a biorefinery approach. Figure 2.02 shows an example of a biologically integrated H_2 production system.

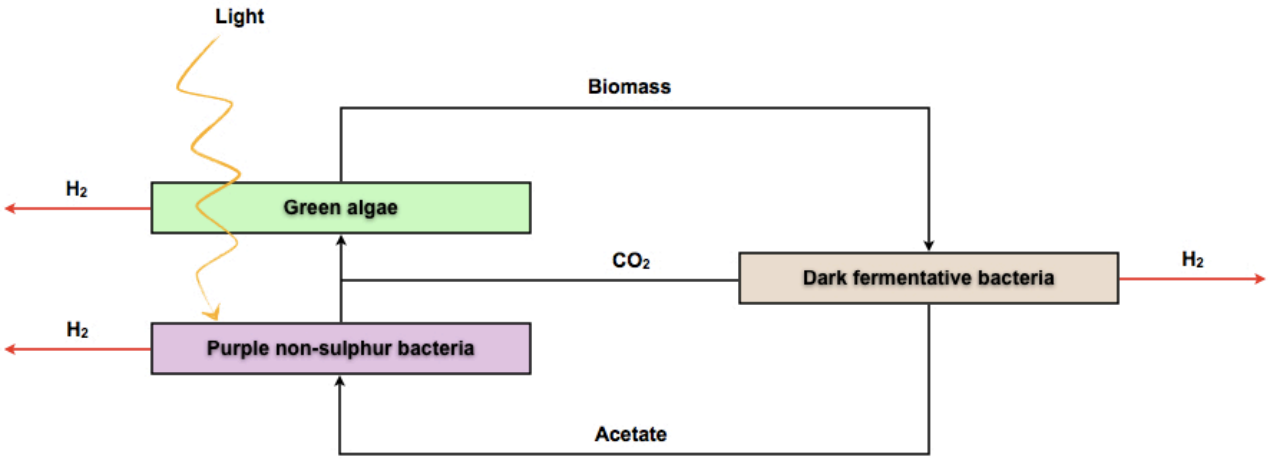


Figure 2.02: Schematic diagram of biological integration involving green algae, purple non-sulphur bacteria and dark fermentative bacteria

2.7. Summary

The world is powered by fossil fuels, but there are signs that their domination is coming to an end. Concerns over rising energy demand, security of supply and greenhouse gas emissions has led to increased interest and investment in sustainable energy technologies. Solar power is the only renewable energy resource large enough to satisfy primary energy demand. Since the generation of solar electricity by PV panels remains prohibitively expensive, there is a large market for solar biofuels, such as corn and sugarcane bioethanol. The low power density and arable land requirements of traditional energy crops has led to the food vs fuel and food vs forest issues, as well as concerns regarding the extent of CO_2 savings achieved with biofuels. Photosynthetic microalgae should be used in place of traditional biofuels. Algae do photosynthesis best; they grow quickly and a large percentage of their biomass is usable as fuel. Algae could produce various HVPs as well as biodiesel, biohydrogen and other fuels in a biorefinery. H_2 is the cleanest, lightest and most efficient available fuel but it remains in the early stage of development and has few commercial applications. A hydrogen economy would require advanced PEM fuel cells, more effective H_2 storage, and sustainable and economical H_2 production. The three routes to direct biohydrogen production are dark fermentation, photofermentation and biophotolysis; they could be biologically integrated to achieve maximum energy efficiency and the best biohydrogen production rates. Biophotolysis has the potential to provide sustainable H_2 from sunlight and water if the O_2 sensitivity of the hydrogenase enzyme could be overcome.

3. Biohydrogen Production by *Chlamydomonas reinhardtii*

3.1. Selection of Algal Species: Introduction to *Chlamydomonas reinhardtii*

Chlamydomonas reinhardtii (*C. reinhardtii*) is a eukaryotic, unicellular green alga commonly found in soil and fresh water. *C. reinhardtii* has a diameter of approximately 10 micrometers, it contains a chloroplast that houses the photosynthetic apparatus, it incorporates multiple mitochondria, and it swims around using two external flagella (cilia) (Grossman *et al.,* 2007). *C. reinhardtii* belongs to the Chlorophytes (green algae), which diverged from the Streptophytes (land plants) over a billion years ago; both of these groups belong to the green plant lineage of Viridiplantae (Merchant *et al.,* 2007; BBSRC, 2010). The laboratory wild type (WT) *C. reinhardtii* strain is used as a model organism for studying chloroplast-based photosynthesis and flagellum structure (Merchant *et al*., 2007). The main advantage of using *C. reinhardtii* is the relatively large size of its chloroplast, which occupies approximately 70% of the cell volume, and enables the alga to efficiently harvest solar energy (Grossman, 2005). This leads to a superior rate of photosynthetic growth and biohydrogen production compared to similar algal species (Meuser *et al.,* 2009). *C. reinhardtii* is consequently a robust organism that can outgrow most competing microalgae and bacteria (Grossman, 2000).

The status of *C. reinhardtii* WT as a model organism has ensured that the alga has been well studied and that its biochemistry is consequently well understood. The *C. reinhardtii* genome (Merchant *et al.,* 2007), its metabolome (Timmins *et al.*, 2009a; Doebbe *et al.*, 2010) and even its transcriptome (Nguyen *et al.*, 2008) have all been successfully mapped. These developments have opened the opportunity to use genetic modification (GM) to improve the photosynthetic growth and H_2 production by *C. reinhardtii*. Since it is relatively simple to carry out nuclear gene cloning and chloroplast transformation on *C. reinhardtii*, the alga has long been described as a photosynthetic yeast (Rochaix, 1995). Recent GM advances have targeted the *C. reinhardtii* light-harvesting antennae (Mussgnug *et al.,* 2007), the D1 protein in PSII (Faraloni & Torzillo, 2010) and the cyclic electron transport apparatus (Kruse *et al.,* 2005b).

This chapter will explore the biochemistry of biohydrogen production, covering both the photolytic and fermentative routes. It will describe the historic and present day methods used to overcome the O_2 sensitivity of the hydrogenase enzyme ($h_2$ase) and induce H_2 production. The parameters that affect the photosynthetic growth and H_2 production of *C. reinhardtii* will be described and analysed. This will include the rationale behind choosing the particular *C. reinhardtii* strain that was used in this thesis. The photobioreactor (PBR) design challenges and geometries will be reviewed. Finally, the issues surrounding the process design, scale-up, costs and efficiencies of biohydrogen production by *C. reinhardtii* will be discussed.

3.2. Biochemistry of Biohydrogen Production

3.2.1. Light-harvesting by Photosystem II

Green algae such as *C. reinhardtii* are photoautotrophic microorganisms: they can grow using sunlight and CO_2 without requiring an organic source of carbon (Greenbaum, 1988). They achieve this by carrying out oxygenic photosynthesis.

Oxygenic photosynthesis:

$$6\ CO_2 + 6\ H_2O \rightarrow C_6H_{12}O_6\ (\text{glucose}) + 6\ O_2$$

The light-harvesting photosystems and most of the photosynthetic electron transport chain involved in this reaction are located within the thylakoid membrane, in the chloroplast of *C. reinhardtii* (Ferreira *et al.,* 2004). Photosynthesis starts with light-absorption by pigmented chlorophyll molecules (Chl), which are grouped into light-harvesting complex (LHC) proteins. LHC proteins arrange themselves into extensive and environmentally-adaptable light-harvesting antennae, which are bound to two multi-membrane protein complexes: photosystem I (PSI) and PSII. The photosystem and the antennae form a rectangular-shaped supercomplex. PSII is located within the grana (stacked thylakoid membrane), while PSI is located within the stromal lamellae (unstacked thylakoid membrane) (Zhang *et al.,* 2002). The main reason for this spatial separation is to prevent the uncontrolled exchange of excitation energy between the photosystems, since the kinetics of PSI are much faster than those of PSII (Kruse *et al.,* 2005a). Light energy absorbed in the LHC is transferred to the reaction centre pigments of PSI and PSII, where charge separation takes place.

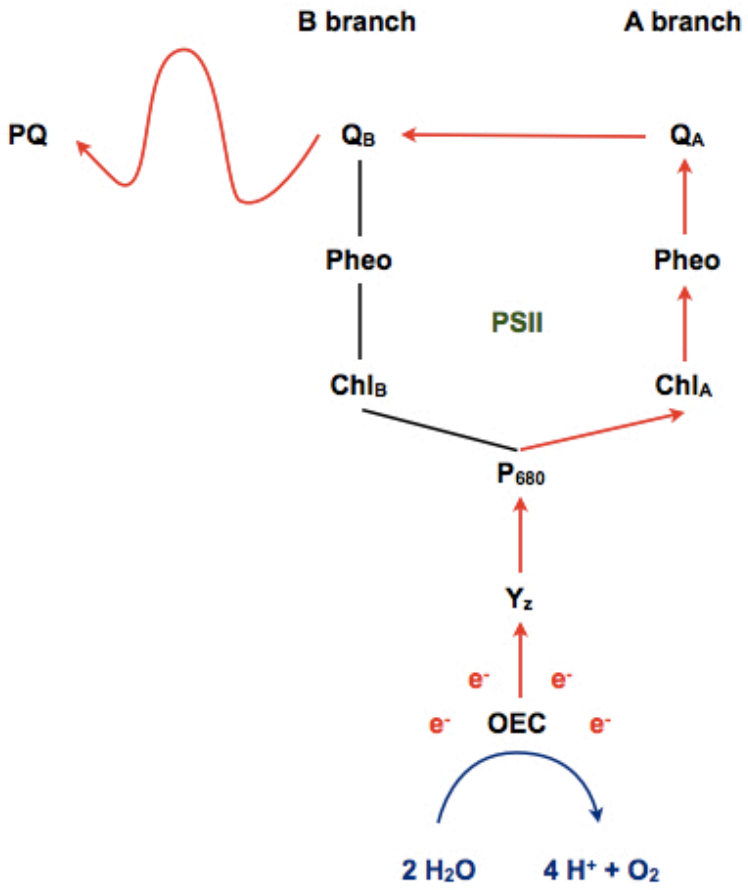
The quantity and composition of LHC proteins depends strongly on the light environment (Kruse *et al.,* 2005a). This flexibility is made possible by at least 20 nuclear genes that encode peripheral antennae proteins (Merchant *et al.,* 2007). Light is essential for photosynthesis but also damaging in large quantities because it results in the formation of toxic oxygenic species. Light input to the photosystems is therefore carefully controlled by the xanthophyll cycle fluorescence and by state transitions between the photosystems (Kruse *et al*., 2005a). The xanthophyll cycle involves the dissipation of excess light energy as heat by a process also known as chlorophyll fluorescence.

Fluorescence is therefore a good way of measuring photosynthetic efficiency; high fluorescence implies low efficiency (Greenbaum, 1988). Under optimal illumination conditions, light capture is limited only by the quantum efficiency of photosynthetically active radiation (PAR). *C. reinhardtii* absorbs light in the 400-700 nm wavelength range, so the light-harvesting process is at best 45% efficient (Melis, 2009). Approximately two thirds of the absorbed energy is lost in the solar-to-chemical energy conversion by the photosystems, giving a maximum photosynthetic efficiency of 30%. *C. reinhardtii* also has the ability to move the majority of LHC proteins between PSI and PSII in a process known as state transition (Kruse *et al.,* 2005a). Under low illumination, LHC proteins migrate from PSI to PSII to increase the rate of water oxidation, while under high illumination, LHC proteins migrate the other way to reduce the formation of toxic species. State transition also plays a role in regulating linear and cyclic electron flow (Kruse *et al.,* 2005b).

PSI is associated with the pigment P_{700}, a chlorophyll heterodimer. Excitation energy generates the P_{700}^{+} free radical with a redox potential of +0.43 V (Ghirardi *et al.,* 2009). This is not enough to split water, but PSI is involved further downstream in the photosynthetic electron transport chain. PSII catalyses water-splitting and the first step of the photosynthetic electron transport chain. PSII is centred around the pigment P_{680}, a chlorophyll dimer that is tightly bound by D1 and D2, the two major proteins of the reaction centre (Hemschemeier *et al.,* 2008). PSII then splits into two branches: A and B. Two chlorophyll monomers (Chl_A and Chl_B) are located in close proximity to P_{680}, on branches A and B respectively. They are followed by two pheophytin (Pheo) molecules and eventually two plastoquinone molecules (Q_A and Q_B) (Rochaix, 2011). The excitation energy provided by the LHC generates the P_{680}^{+} free radical, the strongest oxidant known in Biology, with a redox potential of +1.12 to +1.27 V (Ghirardi *et al.,* 2009). The corresponding reductive potential is passed down the A branch of PSII, via Chl_A and Pheo (-0.75 to -0.35 V), to Q_A (-0.13 to -0.03 V). This rapid charge transfer, which takes place in less than 300 picoseconds, is designed to prevent the oxidising and reducing sides of PSII from recombining (Ghirardi *et al.,* 2009). The structure and electron transport of PSII are shown in Figure 3.01.

PSII can be completely inactivated by the inhibitor 3-(3,4-dichlorophenyl)-1,1-dimethyurea (DCMU). DCMU has been used to study the photosynthetic electron transport and the limiting steps of photosynthesis (Cournac *et al.,* 2002; Hemschemeier *et al.,* 2008). Like most enzymes, PSII is

extremely unstable and requires constant maintenance and repair by *C. reinhardtii*. The D1 protein that binds P_{680}^{+} has a particularly high turnover and the biosynthesis of D1 requires a steady supply of sulphur (Lardans *et al.,* 1998, Nixon *et al.,* 2010).



Legend: PQ - plastoquinone pool; Q_A/Q_B - plastoquinone molecules; Pheo - pheophytin molecule; Chl_A/Chl_B - chlorophyll molecules; P_{680} - chlorophyll dimer; Yz - tyrosine residue; OEC - oxygen-evolving centre; H_2O - water; O_2 - oxygen molecule.

Figure 3.01: Structure and electron transport of photosystem II (PSII)

3.2.2. Photosynthetic Electron Transport

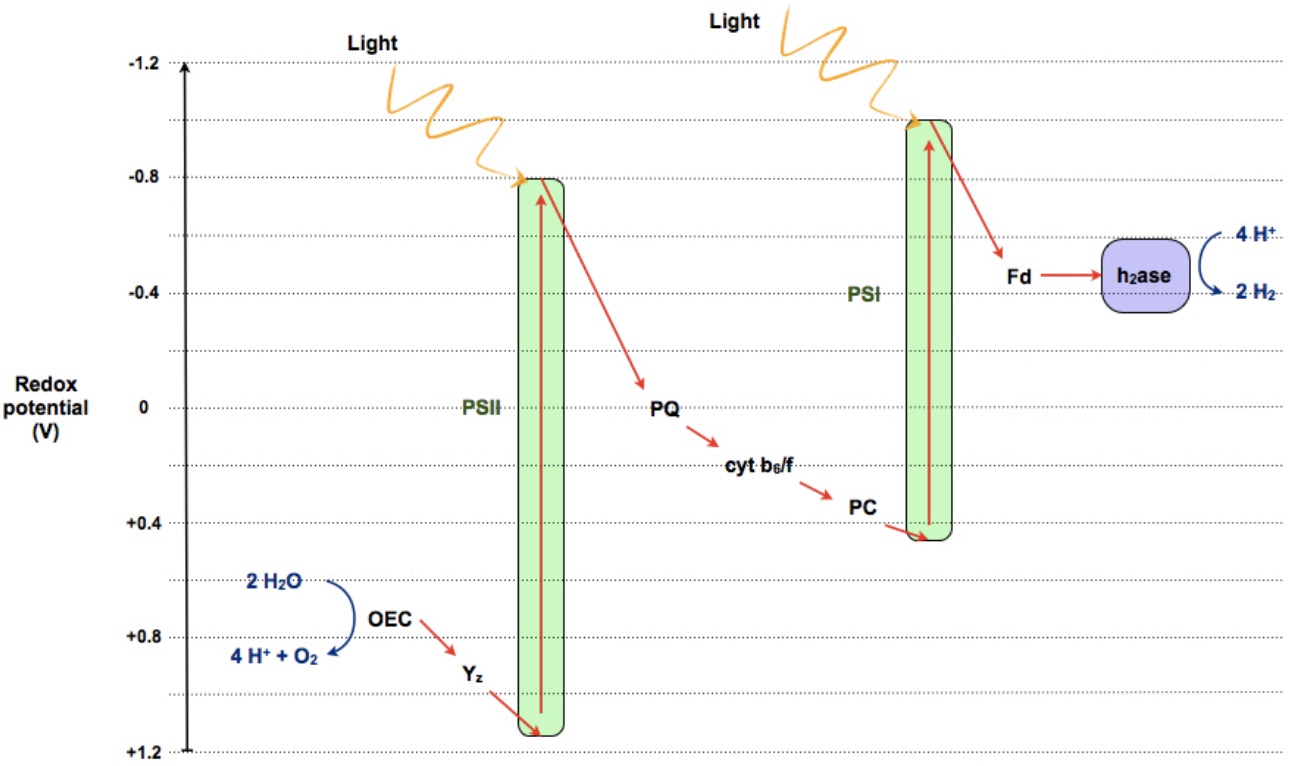
Light-triggered charge separation by PSII generates a highly-oxidising P_{680}^+ free radical and a reduced Q_A plastoquinone. P_{680}^+ extracts electrons from the tyrosine residue (Y_z) (+0.97 V), located nearby in the lumen of *C. reinhardtii* (Ghirardi *et al.,* 2009). The oxidised Y_z activates the oxygen-evolving centre (OEC). The exact structure and functionality of the OEC is still under investigation, but it is understood that the OEC accumulates four successive positive charges following each PSII charge-separation event (Esper *et al.,* 2006). This charge becomes localised in the Mn_4Ca cluster, which splits water by biophotolysis into O_2, protons and electrons (Esquivel *et al.,* 2011).

Biophotolytic water-splitting:

$$2\ H_2O \rightarrow O_2 + 4\ H^+ + 4\ e^-$$

O_2 diffuses out of the thylakoid membrane, out of the cell, and into the atmosphere. The proton gradient drives ATP production by the enzyme ATP synthase (ATPase) (Esper *et al*., 2006). The negative charge is passed down PSII to reduce the Q_A plastoquinone. In the next step of the photosynthetic electron transport chain, Q_A passes its charge to Q_B (+0.03 V), initially located on the B branch of PSII. Once doubly reduced, Q_B leaves PSII and diffuses through the thylakoid membrane before docking and reducing electron acceptors at the cytochrome b_6/f (cyt b_6/f) complex (Hemschemeier & Happe, 2011). While defusing freely through the membrane, Q_B is said to be in the plastoquinone pool (PQ). PQ can accept electrons from cyclic electron transport and from catabolic processes as well as from PSII (Hemschemeier & Happe, 2005). The redox state of PQ is understood to play a critical role in the light response of LHC proteins, namely in the processes of chlorophyll fluorescence and state transitions. For example, a depleted PQ pool implies reduced water-splitting activity, encouraging the state transition of LHC proteins from PSI to PSII (Nguyen *et al*., 2008). The cyt b_6/f complex donates electrons to PSI via a lumen-soluble plastocyanin (PC) molecule (+0.38 V) (Ghirardi *et al*., 2009). PSI catalyses a secondary stage of light-driven electron excitation, which is eventually used to reduce ferredoxin (-0.45 to -0.40 V). Ferredoxin (Fd) is a soluble protein that contains a two-iron-two-sulphur cluster [2Fe2S] (Yacoby *et al.,* 2011). It diffuses out of the thylakoid membrane and into the stroma, where it acts as an electron donor to a number of different enzymes (Happe & Kaminski, 2002). It plays a critical role in H_2 production,

biosynthesis, protein repair and cyclic electron transport (Yacoby *et al.,* 2011). The redox potential during photosynthetic electron transport is shown in Figure 3.02.



Legend: H_2O - water; O_2 - oxygen molecule; OEC - oxygen-evolving centre; Y_z - tyrosine residue; PSII - photosystem II; PQ - plastoquinone pool; cyt b_6/f - cytochrome b_6/f; PC - plastocyanin; PSI - photosystem I; Fd - ferredoxin; $h_2$ase - hydrogenase enzyme; H_2 - molecular hydrogen.

Figure 3.02: Redox potential during photosynthetic electron transport in *C. reinhardtii*

Under standard photosynthetic growth conditions, involving linear electron transport, Fd donates electrons to the ferredoxin/$NADP^+$ reductase enzyme (FNR). FNR catalyses the reduction of nicotinamide adenosine diphosphate ($NADP^+$) to NADPH (Melis & Happe, 2004). NADPH and ATP provide the energy required to drive the Calvin cycle, which involves the multi-stage cyclic reduction of CO_2 by the enzyme RuBisCO (Boyle & Morgan, 2009). The primary product of the Calvin cycle is glucose, which is later converted to the polysaccharide called starch, the carbohydrate store of the *C. reinhardtii* cell (Jorquera *et al.,* 2008). When *C. reinhardtii* is placed under an extracellular stress condition, as in the case of nutrient deprivation or photoinhibition, the alga produces additional ATP for use as an energy source (Melis, 2007). Additional ATP production requires an increased proton gradient across the thylakoid membrane, which is achieved by cyclic electron transport (Iwai *et al.,* 2010). In cyclic electron transport, Fd once again donates photosynthetic electrons to FNR, which reduces $NADP^+$ to NADPH. In this case however, NADPH donates electrons back into PQ via the NADPH-dehydrogenase enzyme (Nda2) (Melis & Happe, 2004). These cyclic electrons flow back to Fd via PSI, creating an additional proton gradient (Antal *et al.,* 2009). This process may be repeated until enough ATP has been produced to overcome the environmental stress factor, at which point biosynthesis via the Calvin cycle can resume. Linear and cyclic electron transport pathways during oxygenic photosynthesis are shown in Figure 3.03.

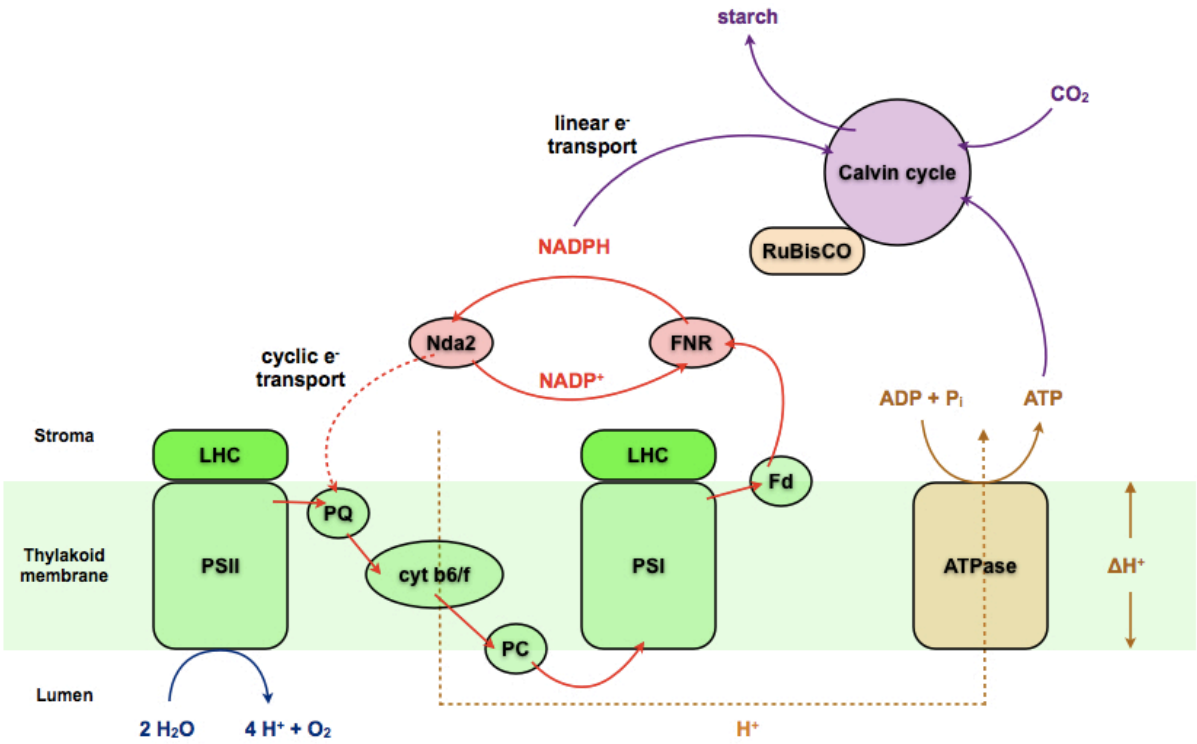
Under anaerobic conditions, oxygenic respiration is no longer possible, so *C. reinhardtii* generates its energy via the anaerobic photosynthesis of ATP and the catabolic glycolysis of starch to pyruvate and the subsequent fermentation of pyruvate (Winkler *et al*., 2009). The activity of the energy-intensive Calvin cycle reduces dramatically, creating the requirement for an additional electron sink for reduced Fd (Redding *et al.,* 1999). The $h_2$ase enzyme becomes activated under anaerobic conditions to act as this electron sink. Fd donates electrons to the $h_2$ase enzyme, which catalyses the process of proton-electron recombination to produce H_2 (Ducat *et al.,* 2011b).

Anaerobic H_2 production:

$$4\ H^+ + 4\ e^- \rightarrow 2\ H_2$$

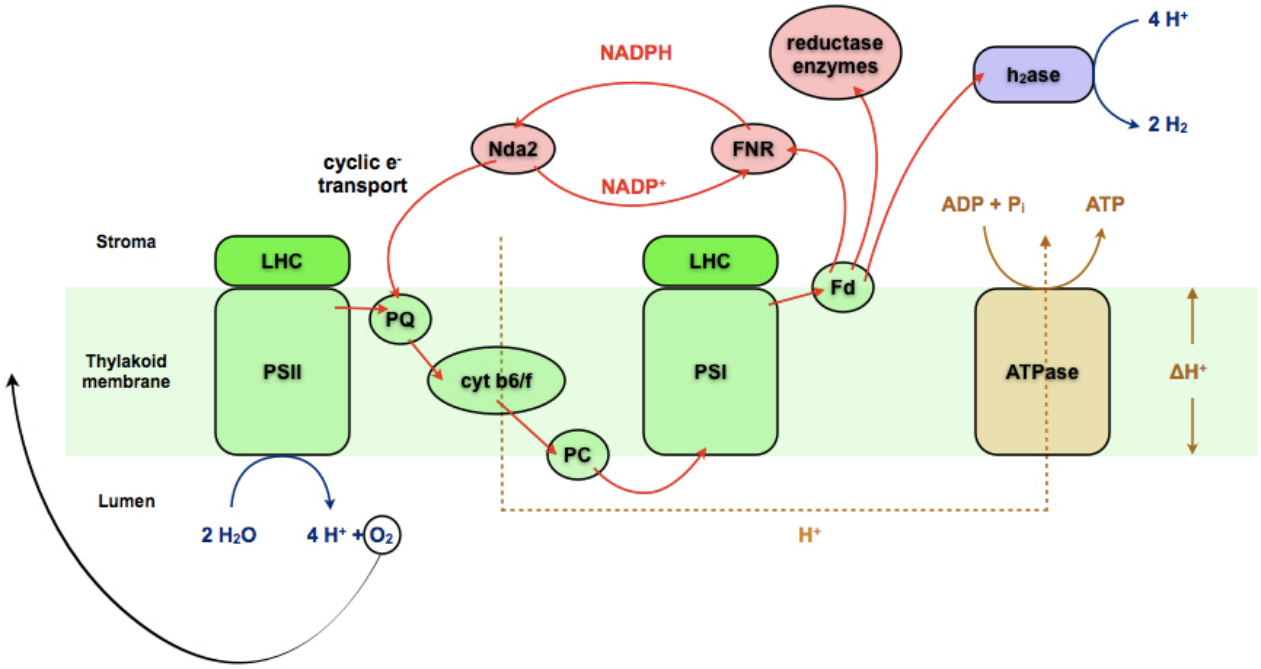
The $h_2$ase enzyme does not have a monopoly on the supply of electrons from Fd. It must compete with FNR, which facilitates the increasingly active cyclic electron transport that produces additional

ATP (Antal *et al.,* 2009; Marín-Navarro *et al.,* 2010). It also typically competes with ferredoxin/ thioredoxin reductase (FTR), nitrate reductase, sulphate reductase and glutamate reductase (Boyle & Morgan, 2009; Dasgupta *et al.,* 2010). These enzymes are activated under nutrient stress conditions: FTR regulates CO_2 fixation under anaerobic conditions, while the sulphate, nitrate and glutamate reductase enzymes respond to a shortage in the corresponding nutrient (Peltier *et al*., 2010). The photosynthetic electron transport system during anaerobic H_2 production is shown in Figure 3.04. As an additional complication, PQ and Fd also receive additional electrons during anaerobic conditions via catabolic and fermentative processes respectively (Burgess *et al*., 2011). It has been estimated that the h$_2$ase enzyme has the capacity to accept approximately one third of photosynthetic electrons, giving a maximum theoretical photochemical efficiency of 10-13% for biophotolytic H_2 production by *C. reinhardtii* (Kruse *et al*., 2005b). Photochemical efficiency is the efficiency of converting a solar photon, incident on the *C. reinhardtii* cell, into stored chemical energy in the H_2 molecule (Winkler *et al.,* 2009). The best *C. reinhardtii* strains are approximately 2% efficient, leaving plenty of space for improvement through GM methods and process optimisation (Kruse & Hankamer, 2010).



Legend: H_2O - water; O_2 - oxygen molecule; PSII - photosystem II; LHC - light-harvesting complex; PQ - plastoquinone pool; cyt b_6/f - cytochrome b_6/f; PC - plastocyanin; PSI - photosystem I; Fd - ferredoxin; FNR - ferredoxin/$NADP^+$ reductase enzyme; NADP+ - nicotinamide adenosine diphosphate; NADPH - nicotinamide adenosine dinucleotide phosphate; Nda2 - NADPH-dehydrogenase enzyme; RuBisCO - ribulose-bisphosphate carboxylase enzyme; CO_2 - carbon dioxide; ADP - adenosine diphosphate; P_i - inorganic phosphate ion; ATP - adenosine triphosphate; ATPase - ATP synthase enzyme.

Figure 3.03: Photosynthetic electron transport system during oxygenic photosynthesis in *C. reinhardtii*



Legend: H_2O - water; O_2 - oxygen molecule; PSII - photosystem II; LHC - light-harvesting complex; PQ - plastoquinone pool; cyt b_6/f - cytochrome b_6/f; PC - plastocyanin; PSI - photosystem I; Fd - ferredoxin; FNR - ferredoxin/$NADP^+$ reductase enzyme; NADP+ - nicotinamide adenosine diphosphate; NADPH - nicotinamide adenosine dinucleotide phosphate; Nda2 - NADPH-dehydrogenase enzyme; h2ase - hydrogenase enzyme; H_2 - molecular hydrogen; ADP - adenosine diphosphate; P_i - inorganic phosphate ion; ATP - adenosine triphosphate; ATPase - ATP synthase enzyme.

Figure 3.04: Photosynthetic electron transport system during anaerobic H_2 production in *C. reinhardtii*

3.2.3. Hydrogenase Enzyme

Hydrogenase enzymes catalyse the process of proton-electron recombination, which serves as an important electron sink for various microorganisms in anaerobic environments. Certain species, such as the cyanobacterium *Ralstonia eutrophus*, are also capable of running the h$_2$ase in reverse in order to use H_2 as a source of energy (Cracknell *et al.,* 2008). There are two main classes of h$_2$ase: the iron-only [FeFe]-h$_2$ase and the nickel-iron [NiFe]-h$_2$ase, named after the metals that are present at the active site during H_2 production. All h$_2$ase enzymes contain one or more [FeS] clusters to store and transport electrons, as well as the diatomic CO and CN^- ligands, which stabilise metals in low oxidation states (Armstrong, 2005). These ligands give a strong and distinctive infrared absorption band that is sensitive to the electronic structure of the adjacent metal atoms, and therefore provide an excellent way of monitoring reactions at the active site (Armstrong, 2004). No [NiFe]-h$_2$ase has yet been found in eukaryotic microorganisms, while prokaryotic microorganisms tend to have a combination of both [NiFe]- and [FeFe]-h$_2$ase (Ghirardi *et al.*, 2009). *C. reinhardtii* is a eukaryote that contains an [FeFe]-h$_2$ase.

The *C. reinhardtii* [FeFe]-h$_2$ase has a molecular weight of approximately 53.1 kilodaltons (Happe & Kaminski, 2002). The active site is known as the H-cluster and contains a total of six iron atoms. It consists of a [4Fe4S] cluster, which is connected to a [2Fe2S] cluster stabilised by CO and CN^- ligands and by a dithiolate bridge between the two sulphur atoms (Peters, 1999). The [4Fe4S] cluster accepts electrons from Fd and delivers them to the [2Fe2S] cluster, where the distal iron atom becomes doubly-reduced to Fe^{2-}. A proton binds to Fe^{2-}, becoming doubly-reduced to a hydride ion. In the meantime, a different proton is held captive by the active site through a mechanism that is not yet fully understood. The hydride ion and the captive proton combine at the active site to produce H_2 (Armstrong, 2004). The [FeFe]-h$_2$ase has a very high turnover rate of 6000-9000 enzyme units per second (Ghirardi *et al.*, 2009). Its activity is also highly sensitive to the presence of O_2.

Oxygen gas diffuses from the solvent to the active site, oxidising the H-cluster and inactivating the h$_2$ase enzyme (Lee & Greenbaum, 2003). Diffusion through the h$_2$ase enzyme is governed by the molecular interactions between O_2 and proteins. It has been shown that the protein structure of

h2ase limits O_2 diffusion to a single pathway, offering a measure of protection to the active site and enabling the enzyme to function under highly anoxic as well as anaerobic conditions (Cohen *et al*., 2005). Under aerobic conditions, the enzyme becomes irreversibly inactivated and ceases to be expressed by the *C. reinhardtii* cell (Happe & Kaminski, 2002). Once anaerobic conditions are re-established, traces of h2ase expression are observable within twenty minutes, but an entire day is required to establish maximal h2ase expression and consequently to measure maximum H_2 production rates (Forestier *et al.,* 2003).

3.2.4. Catabolic and Fermentation Pathways

The photosynthetic energy carried by ATP and NADPH is used in the Calvin cycle to reduce atmospheric CO_2 into glucose and other sugars, which are then stored as starch (Marín-Navarro *et al.,* 2010). Starch is the main carbohydrate store of *C. reinhardtii* cells and it has multiple metabolic roles. Its primary role is to facilitate aerobic respiration, effectively the inverse of photosynthesis, since it involves the oxidation of glucose to release energy. This energy makes possible the basic physiological functions of survival, growth, reproduction and motivity (Melis, 2002).

Aerobic respiration:

$$6\ O_2 + C_6H_{12}O_6\ (\text{glucose}) \rightarrow 6\ CO_2 + 6\ H_2O$$

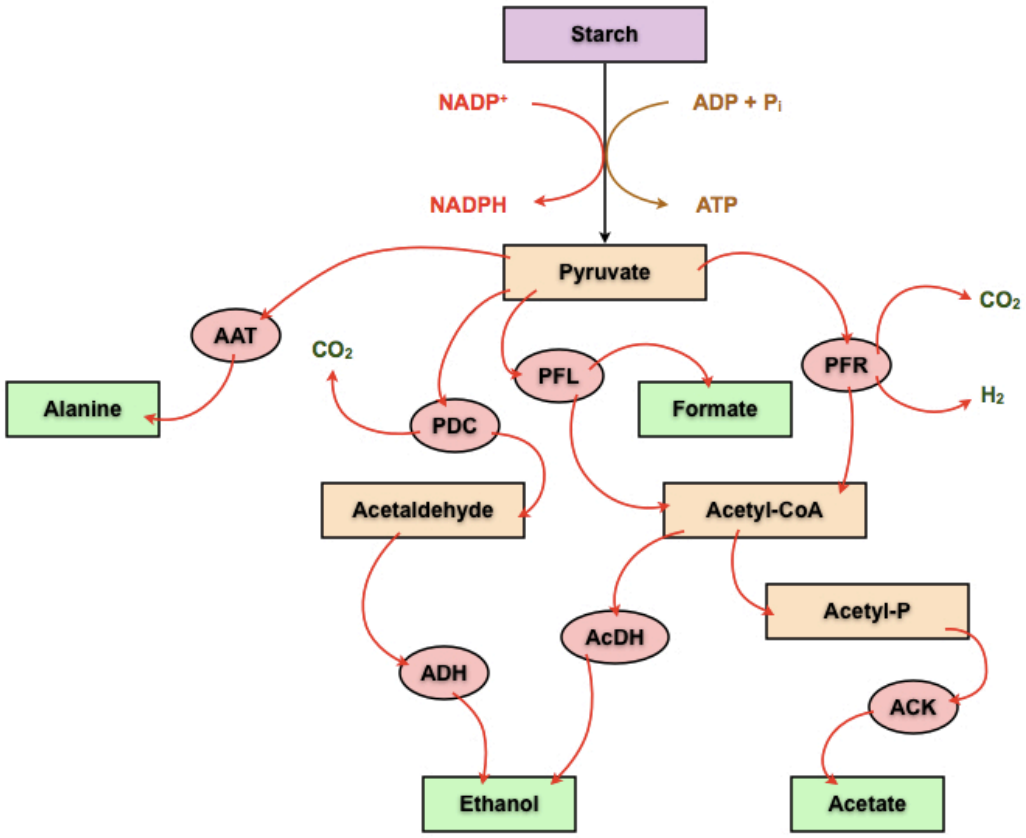
Starch can also be broken down to pyruvate by the catabolic process of glycolysis. Pyruvate is an intermediate for many fermentative reactions. During the day, under aerobic conditions, *C. reinhardtii* carries out photofermentative reactions (Spalding, 2008). Photofermentation produces the amino acid alanine, used for the biosynthesis and repair of proteins (Grossman *et al.,* 2011). It synthesises pigmented Chl and carotenoid molecules that arrange themselves into LHC proteins and photosystems. It produces steroids that include various hormones and vitamins. It can be used to store energy in the long-term in the form of fatty acids, which are later biosynthesised further into TAGs and other lipids (Chisti, 2007). Photofermentation is also known as photoautotrophic biosynthesis because it utilises atmospheric CO_2 as the only carbon source. It is equally possible to grow *C. reinhardtii* on an organic substrate: this is known as photoheterotrophic growth. *C. reinhardtii* grows particularly well on a source of acetate or glucose (Barbosa *et al*., 2001;

Hallenbeck & Benemann, 2002), but more complex substrates such as olive mill wastewater are also usable (Faraloni *et al*., 2011). Unless controlled by experiment, *C. reinhardtii* normally grows under photomixotrophic conditions: it uses both CO_2 and organic substrate as carbon sources for biosynthesis (Kosourov *et al.,* 2007).

Aerobic respiration and photofermentation stop under anaerobic conditions, activating a different set of fermentative pathways (Chochois *et al.,* 2009). Only the production of alanine for protein repair by the enzyme alanine aminotransferase (AAT) remains active under both aerobic and anaerobic conditions (Doebbe *et al*., 2010). Anaerobic fermentation processes are normally referred to as dark fermentation because dark conditions switch off photosynthetic O_2 production. Anaerobic fermentation is always initiated by the catabolism of starch to pyruvate. The enzyme pyruvate decarboxylase (PDC) can convert pyruvate to another intermediate, acetaldehyde, releasing CO_2. Acetaldehyde is then reduced to ethanol by the alcohol dehydrogenase enzyme (ADH) (Chochois *et al.,* 2010). Another set of anaerobic fermentative pathways involve the intermediate acetyl-CoA. Acetyl-CoA can be produced from pyruvate by pyruvate formate lyase (PFL), which releases formate as a by-product. Alternatively, acetyl-CoA is produced by pyruvate ferredoxin reductase (PFR), which releases CO_2 as a by-product and also donates electrons to Fd, resulting in H_2 production by the h2ase enzyme (Burgess *et al.,* 2011). Acetyl-CoA can be converted to ethanol by the acetaldehyde/alcohol dehydrogenase enzyme (AcDH). Any acetyl-CoA that has not been converted to ethanol forms acetyl phosphate (acetyl-P), which can be converted to acetate by acetate kinase (ACK) (Grossman *et al.,* 2011). In summary, anaerobic fermentation pathways involve a number of enzymes and intermediates, and the final products are alanine, ethanol, formate, acetate, CO_2 and H_2 (Figure 3.05) (Doebbe *et al.,* 2010).

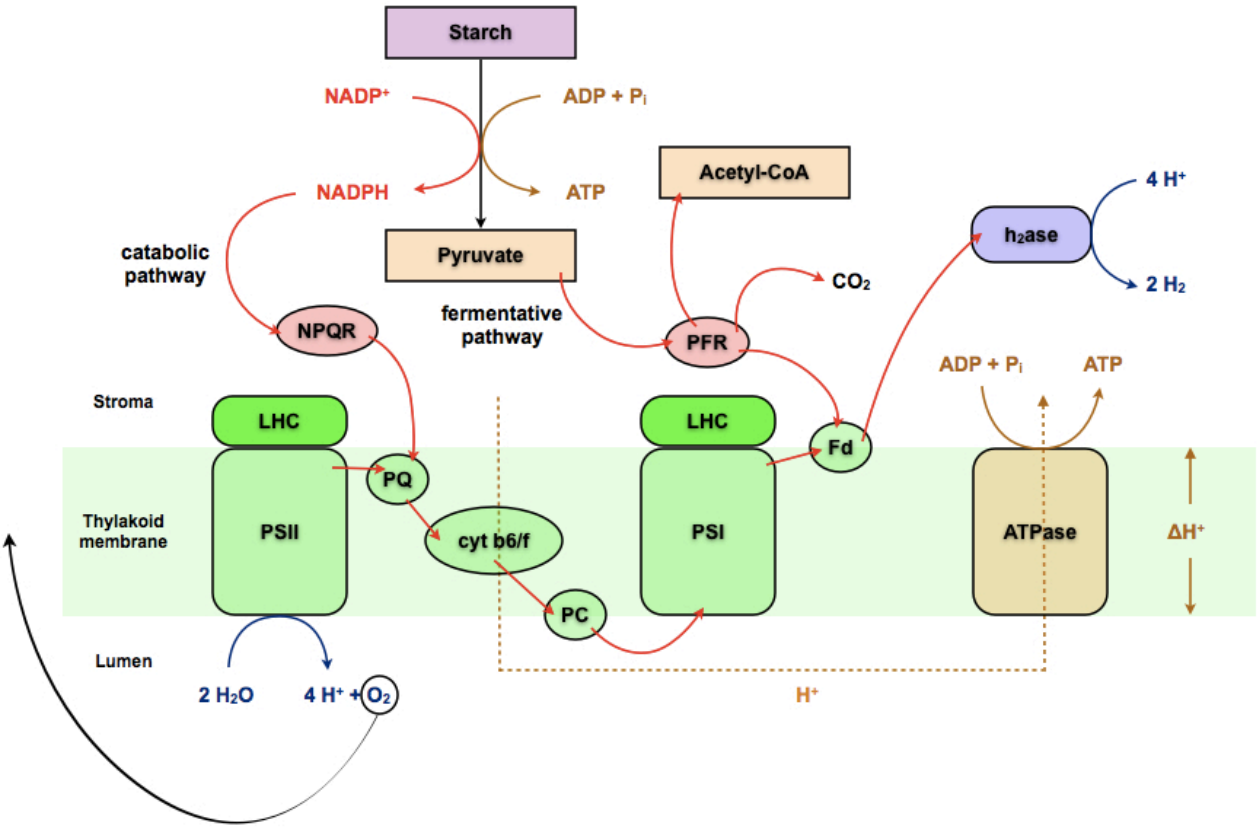
C. reinhardtii can produce H_2 by the biophotolysis of water or through the breakdown of starch. Both processes are only possible under anaerobic conditions due to the extreme O_2 sensitivity of the h2ase enzyme. Biophotolytic electrons arrive at the h2ase enzyme via the linear photosynthetic electron pathway that includes PSII, PQ, cyt b_6/f, PC, PSI and Fd. Starch breakdown can contribute to H_2 production via catabolic and fermentative electron pathways (Chochois *et al*., 2009). Catabolic electrons are produced during the glycolysis of starch to pyruvate. This process produces energy in the form of ATP and simultaneously reduces $NADP^+$ to NADPH. Catabolic NADPH

molecules can deposit their electrons into the PQ pool by the action of the NADPH-plastoquinone reductase enzyme (NPQR). These electrons follow the cyclic electron transport route through PSI and Fd to $h_2$ase, increasing the proton gradient across the thylakoid membrane and therefore increasing the activity of ATPase (Chochois *et al*., 2010). Fermentative electrons are produced during the anaerobic fermentation of pyruvate to acetyl-CoA along the PFR pathway. PFR directly reduces Fd, which is re-oxidised by H_2 production at the $h_2$ase enzyme active site (Grossman *et al.,* 2011). Photosynthetic, catabolic and fermentative pathways to anaerobic H_2 production are shown in Figure 3.06. There is still some debate regarding the exact percentage contribution of each electron pathway to H_2 production by *C. reinhardtii*. The consensus is that the majority of electrons arrive via the biophotolytic pathway, but that this depends on a number of factors, including the activity of PSII, the redox level of PQ and the starch content of the cells (Hemschemeier *et al*., 2009; Eroglu & Melis, 2011). It has been possible to create GM *C. reinhardtii* strains with improved H_2 production rates by improving the light-harvesting by LHC proteins, by knocking-down competing Fd targets and undesirable fermentative pathways and even by re-wiring the electron transport chain (Grossman *et al*., 2007; Timmins *et al.,* 2009b).



Legend: NADP+ - nicotinamide adenosine diphosphate; NADPH - nicotinamide adenosine dinucleotide phosphate; ADP - adenosine diphosphate; P_i - inorganic phosphate ion; ATP - adenosine triphosphate; CO_2 - carbon dioxide; H_2 - molecular hydrogen; AAT - alanine aminotransferase enzyme; PDC - pyruvate decarboxylase enzyme; PFL - pyruvate formate lyase enzyme; PFR - pyruvate ferredoxin reductase enzyme; ADH - alcohol dehydrogenase enzyme; AcDH - acetaldehyde dehydrogenase enzyme; ACK - acetate kinase enzyme.

Figure 3.05: Anaerobic catabolic and fermentative pathways in *C. reinhardtii*



Legend: H_2O - water; O_2 - oxygen molecule; PSII - photosystem II; LHC - light-harvesting complex; PQ - plastoquinone pool; cyt b_6/f - cytochrome b_6/f; PC - plastocyanin; PSI - photosystem I; Fd - ferredoxin; PFR - pyruvate ferredoxin reductase enzyme; NADP+ - nicotinamide adenosine diphosphate; NADPH - nicotinamide adenosine dinucleotide phosphate; ADP - adenosine diphosphate; P_i - inorganic phosphate ion; ATP - adenosine triphosphate; ATPase - ATP synthase enzyme; NPQR - NADPH-plastoquinone reductase enzyme; CO_2 - carbon dioxide; $h_2$ase - hydrogenase enzyme; H_2 - molecular hydrogen.

Figure 3.06: Photosynthetic, catabolic and fermentative routes to H_2 production in *C. reinhardtii*

3.3. Induction of Biohydrogen Production

3.3.1. Direct Oxygen Removal

C. reinhardtii has the capacity to produce sustainable H_2 from sunlight and water by biophotolysis. This process is inhibited by the extreme O_2 sensitivity of the h2ase enzyme, so that anaerobic conditions are required for H_2 production. There are two options for establishing anaerobic conditions: the first is to stop O_2 production completely and the second is to remove all photosynthetic O_2 as it is being produced. Hans Gaffron developed the original H_2 production methodology as far back as 1939 (Gaffron, 1939). Since then, a number of different techniques have been developed, investigated, dismissed, discussed and propagated (Melis & Happe, 2004). These techniques can be classified according to the approach that was used. The brute force approach involves the direct and immediate removal of O_2 by purging or absorption. A more subtle approach is to get the algae to respond to an environmental stimulus, such as a change in the illumination conditions. The most scientifically rigorous, as well as the most effective, approach is to interfere with *C. reinhardtii* metabolism by using chemical inhibitors or by nutrient deprivation.

One way of directly removing O_2 as it is being produced is to continuously purge the liquid algal culture with an inert gas, such as helium, argon or nitrogen (N_2 is an inert gas because green algae are only capable of using fixed nitrogen in the form of ammonia) (Weaver *et al*., 1980). A helium purge is the most effective since it is the smallest molecule and therefore most easily permeates the algal culture and expels the more massive O_2 molecule (Greenbaum, 1988). However, argon and nitrogen purging is more common because these gasses are less expensive (Benemann, 1999). Inert gas purging faces three major challenges: the cost of the inert gas supply, the cost of pumping that gas through the algal culture, and the difficulty of separating O_2 from the outlet stream. These challenges are intrinsically related because a failure to remove almost all of the purged O_2 from the outlet stream means that the outlet gas cannot be cycled back through the culture, and hence necessitates the purchase of additional inert gas (Brand *et al*., 1989). Once anaerobic conditions have been established and H_2 production has been initiated, it is also necessary to remove the H_2 product from the outlet gas stream, so that a membrane gas separation system is definitely necessary. Although H_2 production by inert gas purging has been successfully carried out and

investigated in the laboratory, this process is neither economic, nor energetically efficient, nor scaleable (Benemann, 1999).

An alternative brute force technique for removing O_2 as it is being generated is to use oxygen absorbers or scavengers (Benemann, 1997). Commercial oxygen absorbers are commonly used in the food industry and consist of a mixture of iron, salt and moisture. The salty iron readily absorbs O_2, producing iron oxide (rust). Commercial O_2 absorbers are impractical because a large quantity of iron is required, and iron is toxic to *C. reinhardtii* in that quantity (Skjånes *et al*., 2008). It is possible to extract a reversible, aggressive, biological oxygen scavenger from the algae themselves. It is called plastoquinol, the doubly-reduced form of the plastoquinone molecule. At the moment, the extraction of plastoquinol is extremely expensive and only possible in small quantities (Brenner, 2006). The most promising oxygen scavenger appears to be glucose. The enzyme glucose oxidase is capable of utilising glucose from the substrate and combining it with atmospheric O_2 to facilitate *C. reinhardtii* respiration (Peters, 1999). Providing additional glucose should therefore increase O_2 consumption by respiration. In practise, this technique is very hit-and-miss because the glucose feed does not regulate the respiration rate on its own, but rather forms a small part of a larger puzzle (Hallenbeck & Benemann, 2002). To date, no practical, reliable or economic oxygen absorber or scavenger has been developed to facilitate direct biophotolysis in *C. reinhardtii* (Benemann, 1999).

3.3.2 Environmental Stimulation

The use of an appropriate environmental stimulus is a more practical and less invasive method of inducing H_2 production in *C. reinhardtii*. Since photosynthetic O_2 production requires light energy, the stimulus in question normally relates to the light availability or light intensity of the system. H_2 production by *C. reinhardtii* has historically been initiated by dark incubation (Gaffron, 1939; Gaffron & Rubin, 1942). The process of dark incubation begins when a fully grown algal culture is sealed shut and placed in complete darkness. Photosynthesis quickly shuts down and any remaining O_2 is used up by respiration. In a variation of this technique, the culture may be purged briefly with inert gas to ensure that the environment is fully anaerobic (Healey, 1970; Ben-Amotz *et al*., 1975). H_2ase enzyme expression is activated under anaerobic conditions, and the maximum expression level is attained after approximately one day. Catabolic and fermentative pathways are activated in

the dark, resulting in low rates of PSII-independent H_2 production (Mus *et al.,* 2007). Following this incubation period, the sealed culture is returned to the light. PSII activity commences, but the culture is initially so oxygen-hungry that all of the O_2 produced by photosynthesis is immediately used up. H_2 production, now bolstered by the activation of the photosynthetic electron pathway, continues under these anoxic conditions (Brand *et al*., 1989). Eventually, enough O_2 is produced to flood the system, inactivating the h2ase enzyme and terminating H_2 production. The rate and duration of H_2 production depends on the initial expression of the h2ase enzyme, which is itself governed by the duration of the dark incubation period. In other words, there is a trade-off between the H_2 yield and the amount of time required to initiate H_2 production. Dark incubation periods of 0.3-24.0 hours have been investigated in the literature, giving H_2 production rates of 0.02-0.34 $mlH_2 \cdot l^{-1} \cdot h^{-1}$ for WT *C. reinhardtii* (Ben-Amotz *et al*., 1975; Brand *et al*., 1989). H_2 production in the light normally lasts only a few minutes, up to a maximum of 20 minutes for complete h2ase expression, which requires almost 24 hours of dark incubation (Gaffron & Rubin, 1942), or 4 hours of dark incubation combined with an inert gas purge (Healey, 1970). Although the process of dark incubation has played a significant historical role in improving the understanding of biophotolytic H_2 production, it has no practical application outside the laboratory.

C. reinhardtii has adapted to grow most efficiently under the moderate solar irradiation available in a country like the UK (Sheehan *et al*., 1998), where the daytime irradiation varies between 40 and 100 $W \cdot m^{-2}$, depending on the time of day and the season (DBERR, 2007). Under higher light intensities, LHC proteins are no longer able to utilise all of the incident photons, resulting in energy losses by xanthophyll cycle florescence and other mechanisms (Kruse *et al*., 2005a). Under lower light intensities, the rate of photosynthesis drops, an effect that can be used to initiate H_2 production during *C. reinhardtii* growth. H_2 production at low illumination is initiated by sealing a growing culture of *C. reinhardtii* and reducing the irradiation to approximately one quarter of the optimal value (approximately 10-20 $W \cdot m^{-2}$, depending on the cell density of the culture) (Degrenne *et al*., 2011). The rate of photosynthetic O_2 production drops below the rate of O_2 consumption by respiration, so that an anoxic environment is established. H_2 production rates of 1.44 $mlH_2 \cdot l^{-1} \cdot h^{-1}$ for WT *C. reinhardtii* have recently been observed using the low illumination technique (Degrenne *et al*., 2011). Unfortunately, H_2 production by low illumination is ultimately a self-defeating prospect. Using low illumination reduces the number of photosynthetic electrons flowing to the h2ase

enzyme, meaning that the maximal photosynthetic H_2 yield can never be attained. The production of H_2 during algal growth also reduces the biosynthesis of starch, TAGs and HVPs, reducing the overall value of the algal biomass (Degrenne *et al*., 2011).

C. reinhardtii cells are known to experience significant photoinhibition at light intensities higher than 200 $W \cdot m^{-2}$ (Li *et al*., 2009). In fact, it has been shown that exposure to a light intensity of approximately 500 $W \cdot m^{-2}$ over a period of 15-90 minutes produces a light shock that temporarily disables PSII and initiates H_2 production (Markov *et al*., 2006). This H_2 production by light shock lasts for approximately 1 hour, with a maximum production rate of 1.76 $ml H_2 \cdot l^{-1} \cdot h^{-1}$ in WT *C. reinhardtii* (Markov *et al*., 2006). H_2 production by light shock is a technique that would be difficult to replicate outside the laboratory. Extremely high light intensities have also been shown to cause permanent structural damage to PSII; this can be deduced from the decrease in the O_2 production rate and the decrease in *C. reinhardtii* growth rate following the light shock procedure. Other environmental stimuli that would also initiate H_2 production but irreversibly disable PSII include the alkaline treatment of *C. reinhardtii* cells and the excess heating of the algal culture (Markov *et al.,* 2006).

3.3.3. Metabolic Interference

The most promising way to induce H_2 production in *C. reinhardtii* is by interference with the algal metabolism. In its simplest form, this involves the inactivation of PSII using an inhibitor, most commonly DCMU. The use of DCMU produces a similar effect to that of dark incubation, resulting in anaerobic conditions and H_2 production via the PSII-independent pathways (Bamberger *et al*., 1982). DCMU has been used to induce H_2 production historically (Healey, 1970; Bamberger *et al*., 1982), to measure the limiting steps of H_2 production (Cournac *et al.,* 2002) and to investigate the contribution of different electron transport pathways to H_2 production (Hemschemeier *et al.,* 2008; Antal *et al*., 2009). A less expensive and more effective way of modifying PSII activity is through the use of nutrient deprivation techniques.

PSII activity could be shut-down completely by denying *C. reinhardtii* access to a source of manganese ions (Makarova *et al*., 2007). Manganese forms a critical part of the Mn_4Ca oxygen-

evolving centre (OEC), which splits water into oxygen molecules, protons and electrons. An alternative approach is to deny *C. reinhardtii* access to sulphur, which is critical for the biosynthesis of the D1 protein that binds the P_{680} redox centre of PSII. Sulphur is assimilated by the cell in the form of the sulphate ion (SO_4^{2-}); sulphate esters and sulphonates are common in the soil but difficult for the algae to exploit (Pootakham *et al.,* 2010). When *C. reinhardtii* is starved of sulphur, it stops dividing, increases the accumulation of starch and produces SO_4^{2-} scavenging enzymes (Yildiz *et al*., 1994). The rate of photosynthetic O_2 evolution reduces by 75% within 24 hours of sulphur deprivation, an anoxic environment is established and H_2 production is induced (Wykoff *et al*., 1998). H_2 production can also be induced by nitrogen deprivation. Nitrogen deprivation is known to increase the production of starch and lipids in *C. reinhardtii* cells, and it has been used frequently to increase biodiesel yields (Chisti, 2007; Siaut *et al.,* 2011). In theory, the increased starch reserves should increase H_2 production by catabolic and fermentative pathways; in practise, nitrogen deprivation requires 48 hours to reduce PSII activity, by that time it also damages the cyt b_6/f complex, so that actual H_2 production is minimal (Phillips *et al.,* 2011a).

3.3.4 Two-stage Biophotolysis

One of the most important discoveries in the field of green algal H_2 production was made by Melis and co-workers in 2000. Using the model green alga *C. reinhardtii*, they established that sulphur deprivation (S-deprivation) results in a reversible decline in the rate of oxygenic photosynthesis without affecting the rate of mitochondrial respiration (Melis, 2000). In the absence of sulphur, PSII proteins are unable to repair their genetic structure and the photosynthetic oxygen production eventually slows down to 10% of its initial rate (Ghirardi *et al.,* 1997; Ghirardi et al., 2000). This discovery resulted in the creation of the two-stage biophotolysis process. In the first stage, the algae are grown photosynthetically until they reach a density of 3-6 million cells per ml of algal culture (Melis, 2000). All sulphur in the system is then removed by replacing the algal growth medium using centrifugation, dilution or microfiltration techniques (Melis & Happe, 2004). After approximately 24 hours of S-deprivation, the rate of photosynthesis drops below the rate of respiration (Zhang & Melis, 2002). The algal culture becomes anaerobic within 20 minutes of this event, despite the fact that it is maintained at constant illumination (Hemschemeier *et al*., 2008). The $h_2$ase enzyme is activated and the algae enter a stage of biophotolytic H_2 production.

The sustained production of H_2 can be observed for approximately 60-120 hours after imposing anaerobic conditions on the *C. reinhardtii* culture (Kosourov *et al.*, 2002). After this period, the algae are no longer able to produce enough energy to maintain their cellular functions and they eventually die (Gonzáles-Ballester *et al.,* 2010). The H_2 photoproduction process is strongly light-dependent, with production rates of 2.05 $mlH_2 \cdot l^{-1} \cdot h^{-1}$ of culture observed for WT *C. reinhardtii* at high light intensities (Melis, 2002). Most of the electrons required for H_2 production are therefore believed to come from the residual PSII water-splitting activity. During the H_2 production phase, reductions in the algal starch and glucose concentrations have also been observed, suggesting that some of the electrons also come from catabolic and fermentative processes within the algal cells (Tsygankov *et al*., 2006; Faraloni *et al.,* 2011). It is therefore important to grow dense algal cultures with large starch reserves that will donate electrons by PSII-independent pathways, while also optimising light intensity and light penetration through the culture to maximise photosynthetic electron production.

Two-stage biophotolysis by S-deprivation is the only fully controllable and reproducible technique for inducing H_2 production in *C. reinhardtii* (Melis & Happe, 2004). Since the growth and H_2 production stages are split both spatially and temporally, it is possible to optimise biomass synthesis and H_2 production individually. Two-stage biophotolysis results in sustained H_2 production over several days at the highest observed H_2 production rates. Although S-deprivation eventually results in *C. reinhardtii* cell death, the PSII damage is reversible, and aerobic photosynthetic growth can be re-established by re-inserting sulphur following the H_2 production stage (Kim *et al.,* 2010).

3.4. Parameters that affect Algal Growth

3.4.1. From Algal Cells to Algal Cultures

When considering the parameters that affect *C. reinhardtii* growth, it is important to differentiate the growth requirements of individual algal cells from those of entire algal cultures. An algal cell grows by carrying out oxygenic photosynthesis and using this energy to fix carbon into glucose, starch, lipids, and other hydrocarbons (Esper *et al.,* 2006). This process increases the cellular mass until the cell is ready to reproduce by multi-stage meiosis, generating 4-8 daughter cells, which proceed to synthesise biomass for themselves (Rochaix, 1995). It is relatively simple to satisfy the growth requirements of an isolated *C. reinhardtii* cell. It needs to receive just enough light to satisfy the charge-transfer requirements of both photosystems, so that enough photosynthetic electrons are produced to efficiently run the Calvin Cycle and to facilitate subsequent biomass synthesis (Hankamer *et al.,* 2007). Light intensities above this photosaturation limit result in energy dissipation by fluorescense, while extremely high light intensities lead to photoinhibition and can potentially damage the light-harvesting mechanism (Li *et al.,* 2009). The *C. reinhardtii* cell must be suspended in water, or another aqueous solution, in order to carry out the water-splitting element of photosynthesis. The aqueous solution in question should contain sources of carbon, nitrogen, sulphur and phosphorus, as well as a number of trace metals, including iron and manganese, for optimal growth (Wijffels & Barbosa, 2010). The temperature and pH need to remain close to room temperature and neutral pH, respectively, so that the *C. reinhardtii* cells are not damaged (Kruse *et al.,* 2005a).

A culture of *C. reinhardtii* consists of millions of *C. reinhardtii* cells, all suspended in a common aqueous broth. Since *C. reinhardtii* are microscopic unicellular organisms, cultivating them in cultures is the only way of achieving usable biofuel yields. An algal culture is said to grow as its cell density increases. Satisfying the growth requirements of algal cultures is more complicated, because the individual cells now interact with each other, as well as with the external environment (Posten, 2009). The most evident example of this is the relationship between culture growth and illumination. For individual cells, the light intensity incident on that cell governs its growth rate. This is also true for algal cultures at low cell densities, but as the cell density increases, the cells

closer to the source of illumination begin to shade those behind them (Degrenne *et al*., 2011). This shading effect not only places a saturation limit on the total cell density of a given culture, it can result in localised cell death and culture fouling (Carvalho *et al.,* 2006). Culture growth can also be inhibited by local gas transfer, temperature and pH gradients (Bosma *et al*., 2007; Morweiser *et al*., 2010). Appropriate culture mixing through the careful control of fluid dynamics is therefore an important factor in growing dense and healthy *C. reinhardtii* cultures (Barbosa *et al*., 2004). A well-mixed *C. reinhardtii* culture will normally follow the standard logistic (sigmoid) population growth model (Molina Grima *et al.,* 1999; Lemesle & Mailleret, 2004). The culture will grow with a specific growth rate (often expressed as a doubling-time in biology) up to a maximum cell density. The maximum cell density is typically defined by the effective light intensity; it may also be governed by nutrient availability in the case of a nutrient-limited environment (Kooijman *et al.,* 1983). The parameters that affect the specific growth rate of algal cultures include the algal strain, illumination, phototrophic state, fluid dynamics, temperature and pH (Sheehan *et al.,* 1998; Janssen *et al.,* 2000a; Kosourov *et al*., 2007).

3.4.2. Algal Strain

Green algae have incredible biodiversity, with approximately 7,000 documented species, from the tiny marine Prasinophytes, such as *Ostreococcus*, via the sea lettuce Ulvophytes, to Chlorophytes such as *C. reinhardtii* (Sheehan *et al.,* 1998). There are also multiple different strains of *C. reinhardtii* in existence. In the wild, *C. reinhardtii* adapts to the local climate and nutrient availability, so that an optimal strain could be identified for any natural habitat. Some of these strains have been extracted and cultivated on petri dishes: these are known as laboratory wild-type (WT) strains. *C. reinhardtii* is a unicellular organism that acquires genetic mutations at a rapid rate so that no two laboratory WT strains are identical, even if they originated from the same source. The most commonly used WT *C. reinhardtii* strain is cc124, although the use of cc125 and cc1690 for H_2 production has also been documented (Davies *et al.,* 1994; Siaut *et al*., 2011). The choice of algal strain is the single most important parameter affecting algal growth, since each strain is associated with its own optimal set of growth conditions.

C. reinhardtii WT strains can acquire mutations that affect their physiological or metabolic properties. An example of the former is the cc406 mutant strain, which lacks a cell wall, a mutation that makes the cells more difficult to grow but easier to genetically modify (Doebbe *et al.,* 2010). The dum24 mutant strain has modified metabolic properties: it accumulates additional starch at the expense of a slower growth rate (Tamburic *et al.,* 2011a). In the event that no naturally-occurring *C. reinhardtii* strain exhibits a particular desired property, it is possible to use GM approaches to engineer a strain that does (Merchant *et al.,* 2007).

It is relatively simple to grow the vast majority of WT and mutant *C. reinhardtii* strains, although difficult to fully optimise their growth conditions. Frequently, the main challenge is to maintain a healthy algal monoculture devoid of contamination. Avoiding contamination is the only way to ensure that experimental results really do represent the specific algal strain under investigation. The problem is that the growth medium used to cultivate *C. reinhardtii* cultures also provides an excellent habitat for many other species of algae and bacteria, as well as microalgal-grazing zooplankton and fungi (Mahan *et al.,* 2005). At the petri dish level, different algal and bacterial strains frequently end up sharing the same plate, so that the desired algal strain needs to be extracted and re-threaded approximately once a month (Sheehan *et al.,* 1998). At the laboratory photobioreactor scale, the main challenge is keeping out fungal spores, which can be achieved by using a combination of air filters and fungicides. At larger scales, the use of sterilised enclosed photobioreactors increases the probability of avoiding disastrous contamination and predation (Janssen *et al*., 2000b). Enclosed large-scale PBRs could be economically viable, provided that sufficient financial prudence is applied when selecting reactor materials, mixing equipment and temperature control systems.

3.4.3. Illumination

Algal growth is impossible without illumination, so it is not surprising that illumination is the most important environmental parameter that affects algal growth (Kosourov *et al*., 2002). Providing appropriate illumination requires an understanding of all its constituent elements: wavelength, light intensity, light path (light penetration), light mixing (light diffusion), light regime (light-dark cycle), photosaturation and photoinhibition. The photosystems of *C. reinhardtii* are only capable of

absorbing illumination within a specific wavelength range, known as the photosynthetically active radiation (PAR). Infrared illumination tends to have a positive effect on algal growth by heating up the culture, while high-frequency photons have the potential to damage algal cells (Uyar *et al*., 2007). Light intensity is a measure of the photon flux density incident on an algal culture. As a general rule, an increase in the light intensity increases the growth rate (Barbosa *et al*., 2003a). Algal cells within an algal culture do not all receive access to the same light intensity. The distance that light can penetrate into an algal culture is known as the light path, and it is a function of the cell density of that culture (Janssen *et al*., 2000a). Light mixing defines whether the culture is mixed well enough that all algal cells have access to sufficient illumination (Molina Grima *et al.,* 1999). It is possible to define an average (or effective) light intensity for a well-mixed culture (Molina Grima *et al.,* 2000). In the wild, *C. reinhardtii* experience a diurnal light-dark cycle; the algae are well adapted to deal with changes in the light regime. It is possible to reproduce and test various light regimes in the laboratory, from diurnal cycles, to more rapid light-dark cycling (Posten, 2009). Photosaturation of an algal culture occurs once the effective light intensity is sufficient to satisfy the growth requirements of that culture. Raising the light intensity above the photosaturation limit reduces the photosynthetic efficiency of the *C. reinhardtii* cells. Raising the light intensity even further can lead to photoinhibition and eventually to irreversible damage of the photosynthetic mechanism (Bosma *et al*., 2007).

PSI and PSII are biologically optimised to absorb solar radiation, with known absorption maxima at 645 nm and 663 nm (Kosourov *et al.*, 2002). There has been little attempt to optimise wavelength in the literature, with most authors opting to use cool-white light. It is accepted that wavelength in the 400-700 nm range is essential for photosynthesis, while near-infrared light (750-950 nm) also appears to play a role in the production of H_2 (Uyar *et al*., 2007). It can be argued that wavelength optimisation is of no practical importance, since a commercial green algal H_2 production system would need to be capable of operating at ambient conditions (Amos, 2004). On the other hand, it would be advantageous to investigate the benefits of selective wavelength to determine if solar filters could positively influence algal growth.

A number of studies have attempted to optimise the light intensity required for *C. reinhardtii* growth and biophotolytic H_2 production (Laurinavichene *et al*., 2004; Tsygankov *et al*., 2006;

Morweiser *et al.,* 2010; Tamburic *et al.,* 2011a). Laurinavichene and co-workers have shown that optimal H_2 production is obtained when algae are grown at relatively low light intensities of 30-40 micro Einsteins per metre per second ($\mu E \cdot m^{-2} \cdot s^{-1}$) of PAR, circa 6-8 $W \cdot m^{-2}$ (Laurinavichene *et al*., 2004). A higher light intensity in the growth phase would result in increased photosynthetic O_2 production, making it more difficult to impose anaerobic conditions by S-deprivation. A recent study by Morweiser and colleagues shows that increasing light intensities up to 80 $\mu E \cdot m^{-2} \cdot s^{-1}$ results in a linear increase in the specific growth rate of *C. reinhardtii*. Increasing light intensity beyond 80 $\mu E \cdot m^{-2} \cdot s^{-1}$ and all the way to 400 $\mu E \cdot m^{-2} \cdot s^{-1}$ continues to increase the specific growth rate, but the rate of return on the light energy invested is greatly diminished (Morweiser *et al*., 2010).

The different experiments do not result in the same optimised light intensity because all the authors use different photobioreactors (PBRs) to investigate the algal growth rate. Each PBR has its own particular light mixing pattern, which is determined by the fluid dynamics of that reactor (Molina Grima *et al*., 1999). Another important factor is the geometry of the PBR, and in particular its surface-to-volume ratio (Janssen *et al*., 2000a). A large surface-to-volume ratio implies that more algal cells have access to the direct unattenuated light intensity available at the surface of the reactor and are therefore more likely to grow effectively. On the other hand, a small surface-to-volume ratio enables more algal cells to be cultivated within the same surface area, resulting in better biofuel yield, provided that there is sufficient light mixing to ensure that all algal cells have access to illumination (Carvalho *et al*., 2006). There is therefore a trade-off between the surface area requirements of an algal PBR and the energy requirements of algal mixing (Amos, 2004).

The effect of light-dark cycles on *C. reinhardtii* growth (Janssen *et al*., 2000a) and biohydrogen production (Oncel & Vardar Sukan, 2010) has been investigated. *C. reinhardtii* cells are known to suspend their photosynthetic growth mechanism during the night, focusing instead on generating the energy required for their survival (Scoma *et al*., 2011). Although the hydrogenase enzyme can be expressed under anoxic conditions in the dark, the resulting H_2 production utilises fermentative and catabolic rather than biophotolytic electrons. Janssen and co-workers investigated the effect of short light-dark cycles, between 6.1 and 24.3 seconds, on algal growth. They discovered that the biomass yield, photosynthetic activity and photochemical yield all reduced by 30-50% compared to

the results under constant illumination (Janssen *et al*., 2000a). These studies on light regime demonstrate that biomass and H_2 yields in outdoor photobioreactors will never match the results observed in laboratory settings with constant illumination (Scoma *et al*., 2011).

C. reinhardtii photosaturation begins to occur at light intensities of approximately 70-80 Wm^{-2} (Bosma *et al.,* 2007; Morweiser *et al*., 2010), while significant photoinhibition has been observed for light intensities higher than 200 $W \cdot m^{-2}$ (Li *et al*., 2009). Photosaturation and photoinhibition light intensities depend on the cell density of the culture, the light mixing and the photobioreactor surface-to-volume ratio.

3.4.4. Phototrophic State

A phototroph is an organism that carries out photosynthesis to acquire the energy needed for growth. *C. reinhardtii* cultures have traditionally been grown photoheterotrophically (Zhang & Chen, 1999; Melis *et al.*, 2000). This means that they were supplied with an organic substrate, most commonly acetate, which then provides the carbon needed for algal growth and development (Chen & Johns, 1994). *C. reinhardtii* is also capable of photoautotrophic growth: it is an organism that can use light energy to produce complex organic compounds from simple inorganic molecules. Photoautotrophic growth allows the substitution of acetate with much cheaper nutrients such as sodium bicarbonate or even CO_2 (Kosourov *et al*., 2007). Unfortunately, photoautotrophic growth under atmospheric CO_2 concentrations is approximately three times slower than photoheterotrophic growth (Hallenbeck & Benemann, 2002). The photoautotrophic growth rate may be increased by CO_2 enrichment up to a gas fraction of 5-10% (Schenk *et al*., 2008).

3.4.5. Fluid Dynamics, Temperature and pH

It is essential to mix the algal culture in order to prevent individual algal cells from agglomerating in clusters or drifting to the bottom of the photobioreactor, where they would have insufficient access to light and mineral nutrients (Morweiser *et al.,* 2010). The understanding of the fluid dynamics within a particular reactor geometry is a prerequisite to establishing good light mixing within the algal culture (Zhang, 2011). Controlling the fluid dynamics also reduces the probability

of forming local O_2 gradients that inhibit *C. reinhardtii* growth (Chisti & Jauregui Haza, 2002). Depending on the reactor design, mixing may be provided by a magnetic stirrer bar, a circulation pump or a gas-lift system (Hankamer *et al*., 2007). It is essential to avoid high extensional and shear stress on algal cells during mixing, as this may also be a cause of cell death (Barbosa *et al.,* 2004). Barbosa and colleagues measured that superficial gas velocities exceeding 0.03 $m \cdot s^{-1}$ result in significant *C. reinhardtii* death rates.

C. reinhardtii cultures grow well at temperatures in the range of 20-28°C (Benemann, 1997). An increase in the temperature within this optimal temperature range results in only a small increase in the algal growth rate. The growth rate decreases exponentially at temperatures below 20°C, with rapid cell death occurring as the temperature approaches freezing. Temperatures in excess of 28°C also have the potential to damage *C. reinhardtii* cells, meaning that all outdoor photobioreactors must incorporate a temperature control system (Kunjapur & Eldridge, 2010). A recent study has shown that the temperature sensitivity of *C. reinhardtii* increases under nutrient-deprived conditions (Schmollinger *et al.,* 2010).

C. reinhardtii is typically grown at a pH of 7.0-7.2 (Kim *et al.,* 2010). Kosourov and co-workers have established that the optimal pH for algal growth and H_2 production is actually in the region of pH 7.7 (Kosourov *et al.,* 2003). The pH effect on algal growth is very small not only because the algal growth medium tends to be heavily buffered, but also because the algal cells are capable of carrying out their own buffering processes (Hahn *et al.,* 2007). A significant decrease in algal growth rates is only observed when the pH is brought outside the 6.5-8.2 range (Kosourov *et al.*, 2003).

3.5. Parameters that affect Biohydrogen Production

3.5.1. From Algal Growth to Biohydrogen Production

There are at least five ways to increase the H_2 production rate and/or yield from a particular *C. reinhardtii* culture: increase the algal growth rate and the cell density, increase the number of cells effectively producing H_2, optimise the induction of H_2 production, increase the H_2 production duration, and increase electron flow to the $h_2$ase enzyme (Eroglu & Melis, 2011). The growth rate and the cell density may be increased by applying the lessons learned from the previous section on the parameters that affect algal growth (Janssen *et al*., 2000b; Kosourov *et al*., 2007). The accumulation of additional biomass during the growth phase of *C. reinhardtii* results in an increase in the H_2 yield. The primary reason for this is that a higher concentration of cells per unit volume is achieved. More cells imply more PSII reaction centres and therefore more H_2 production, assuming that the additional cells have sufficient access to illumination (Demirbas, 2007). In order to produce H_2 effectively, *C. reinhardtii* cells require the appropriate light intensity, light regime, nutrients, pH, temperature and culture mixing (Jo *et al*., 2006; Park & Moon, 2007). These requirements are similar to those for algal growth, which is not a surprise since both processes rely on the same photosynthetic mechanism (Giannelli *et al*., 2009). As discussed previously, H_2 production can be induced in different ways: some are better than others. H_2 production by S-deprivation lasts no more than 120 hours before the *C. reinhardtii* culture begins to die (Kosourov *et al*., 2002). Extending the H_2 production duration is critical for improving H_2 yield and for economically scaling up the process (Amos, 2004). The most direct way of improving H_2 production is to genetically engineer mutant strains or immobilised enzymes that are more efficient than WT *C. reinhardtii* (Burgess *et al.,* 2011; Phillips *et al*., 2011).

As discussed in the algal growth section, the optimal pH for H_2 production is approximately 7.7 (Kosourov *et al*., 2003) and the appropriate temperature range is 20-28°C (Benemann, 1997). The photosynthetic apparatus of the green algae is assumed to be optimised for wavelengths of the solar radiation spectrum, while the optimal light intensity is approximately 10 $W \cdot m^{-2}$, but may be further optimised for various stages of the process (Morweiser *et al*., 2010). Mixing is required so that all algal cells receive access to sufficient mineral nutrients and illumination.

A detailed study conducted by Tsygankov and co-workers reported that the optimal light intensities for H_2 production are 25 $\mu E \cdot m^{-2} \cdot s^{-1}$ PAR in the growth phase, 110 $\mu E \cdot m^{-2} \cdot s^{-1}$ PAR during the early S-deprivation and O_2 consumption phases, and 20 $\mu E \cdot m^{-2} \cdot s^{-1}$ PAR thereafter (Tsygankov *et al*., 2006). The total volume of H_2 collected under this variable light intensity (56.4±16.7 $ml H_2 \cdot l^{-1}$) was much greater than that at consistently high light intensity (4.4±4.7 $ml H_2 \cdot l^{-1}$) or at consistently low light intensity of 25 $\mu E \cdot m^{-2} \cdot s^{-1}$ (7.3±10.4 $ml H_2 \cdot l^{-1}$). It is advantageous to provide a higher light intensity at the early S-deprivation phase because this encourages starch formation, which is later involved in the catabolic and fermentative H_2 production pathways (Tsygankov *et al.*, 2006). Oncel and Vardar Sukan investigated the effect of various long (for example 12h:12h) and medium (for example 30min:30min) light-dark cycles on the H_2 production by *C. reinhardtii*. They collected approximately twice as much H_2 under constant illumination (175-210 $ml H_2 \cdot l^{-1}$) as they did under either long light-dark cycles (92-125 $ml H_2 \cdot l^{-1}$) or medium light-dark cycles (90-114 $ml H_2 \cdot l^{-1}$) (Oncel & Vardar Sukan, 2011).

A study conducted by Kosourov and colleagues revealed that H_2 production is optimised when *C. reinhardtii* are grown under photomixotrophic (acetate and CO_2) conditions. The photomixotrophic H_2 yield (113 $ml H_2 \cdot l^{-1}$) was significantly greater than either the photoheterotrophic yield (24 $ml H_2 \cdot l^{-1}$) or the photoautotrophic yield (30 $ml H_2 \cdot l^{-1}$) (Kosourov *et al*., 2007). In this scenario, the algae use acetate as the primary carbon source but also obtain photosynthetic electrons from the CO_2 that is being bubbled through the reactor. The maximum H_2 production rates were 6.9 $ml H_2 \cdot l^{-1} \cdot h^{-1}$, 4.0 $ml H_2 \cdot l^{-1} \cdot h^{-1}$ and 2.8 $ml H_2 \cdot l^{-1} \cdot h^{-1}$ in photomixotrophic, photoheterotrophic and photoautotrophic cultures, respectively (Kosourov *et al*., 2007). The low efficiency of H_2 production under photoautotrophic conditions is attributed to the need of algae to start respiring starch earlier, during the oxygen consumption phase (Vijayaraghavan *et al*., 2009). Utilisation of acetate as the main carbon source allows the cells to accumulate extra starch (Degrenne *et al*., 2010). Using photoautotrophic *C. reinhardtii* growth opens the possibility to sequester CO_2 in algal biomass as a part of the biophotolytic H_2 production process (Torri *et al.*, 2011).

3.5.2. Biohydrogen Induction Procedure

As previously discussed, biohydrogen production may be induced by direct oxygen removal, environmental stimulation or metabolic interference. The choice of induction procedure has a strong influence on H_2 production rates by WT *C. reinhardtii*. Dark incubation gives H_2 production rates of 0.02-0.34 $mlH_2 \cdot l^{-1} \cdot h^{-1}$ (Brand *et al*., 1989). H_2 production rates of 1.44 $mlH_2 \cdot l^{-1} \cdot h^{-1}$ have been observed using the low illumination technique (Degrenne *et al*., 2011). H_2 production by light shock has a maximum production rate of 1.76 $mlH_2 \cdot l^{-1} \cdot h^{-1}$ (Markov *et al*., 2006). The two-stage biophotolysis process induced by S-deprivation gives H_2 production rates of 2.05 $mlH_2 \cdot l^{-1} \cdot h^{-1}$ and exhibits by far the longest H_2 production duration (Melis, 2002).

Carrying out complete and efficient S-deprivation is a prerequisite for attaining the optimal H_2 production rate and yield. S-deprivation can be carried out by centrifugation, microfiltration or dilution procedures. The centrifugation and microfiltration procedures are based around exchanging the growth medium of a fully-grown *C. reinhardtii* culture (Melis *et al*., 2000). The culture is considered to be fully grown once it reaches a cell density of 14-24 micrograms of chlorophyll per millilitre of culture (14-24 $\mu gChl \cdot ml^{-1}$) (Tolstygina *et al*., 2009). In the centrifugation procedure, these cells are spun down at 3,000 rpm until they form a solid pellet at the bottom of the centrifugation vessel. The cells are then washed and re-suspended in a sulphur-deplete medium (Laurinavichene *et al*., 2004). Approximately 20% of the cells are lost during the centrifugation process, giving sulphur-deprived algal concentrations of 14-16 $\mu gChl \cdot ml^{-1}$ (Tsygankov *et al.,* 2002; Kosourov et al., 2007). This medium exchange could alternatively be carried out by cross-flow microfiltration (Rossignol *et al*., 1999). A surface or bulk filter with a pore diameter of circa 5 micrometers is required (Morineau-Thomas *et al*., 2002). *C. reinhardtii* cells may also be bound to solid support particles such as silica to improve the filtration efficiency (Hahn et al., 2007). Algal microfiltration techniques are still under development and they are considered a crucial step towards commercial algal biofuel production (Holdich *et al.,* 2004).

The dilution method of sulphur deprivation is a procedure well suited to laboratory scale H_2 production. A small volume of growing *C. reinhardtii* culture is diluted in a sulphur-limited medium. The algae continue to photosynthesise and grow as long as they have access to sulphur.

Once the sulphur runs out, the algae use up all O_2 in the system by respiration and eventually enter the phase of anaerobic H_2 production. The main disadvantage of the dilution method is that it takes a number of days before the culture becomes anaerobic and the subsequent H_2 yield is relatively low (Laurinavichene *et al*., 2002). The H_2 yield by dilution is lower than the H_2 yield by centrifugation because the starting cell density is lower. Laurinavichene and co-workers measured dilution H_2 yields of 40-110 $mlH_2 \cdot l^{-1}$ of algal culture, compared with 180 $mlH_2 \cdot l^{-1}$ for centrifugation (Laurinavichene *et al*., 2002). It should be possible to optimise the dilution procedure so that it is just as effective as centrifugation by carefully controlling the sulphur levels within the algal culture (Yildiz *et al*., 1994). Dilution eliminates the need for a difficult and energy-intensive medium separation procedure and it is easy to scale- up.

3.5.3. Biohydrogen Production Duration

After a maximum of 120 hours of H_2 production in sulphur-deprived algal cultures, the algae are no longer able to generate enough energy through the production of ATP, resulting in gradual cell death (Kosourov *et al.,* 2002). This is a major issue for process scale-up, because it results in a continual demand for fresh algal stocks and makes it difficult to develop a continuous process (Antal *et al*., 2003). It is possible to use sulphur re-insertion techniques to prolong algal lifetime from approximately a week to 20-120 days (Laurinavichene *et al*., 2006; Oncel & Vardar Sukan, 2009; Kim *et al.,* 2010). One method of prolonging algal lifetime is to provide the culture with a constant flow of TAP medium containing micromolar sulphate concentrations. Another possibility is to develop a continuous process by cycling algal cells between sulphur-rich and sulphur-deplete conditions. Algal lifetime may be compared to sulphur starvation time to determine the optimal multi-batch process of H_2 production.

Laurinavichene and co-workers were able to switch immobilised *C. reinhardtii* cells between a sulphur-rich and a sulphur-deplete environment over a period of 30 days, producing a total H_2 yield of 320 $mlH_2 \cdot l^{-1}$ with a maximum production rate of 1.75 $mlH_2 \cdot l^{-1} \cdot h^{-1}$ (Laurinavichene *et al*., 2006). Oncel and Vardar-Sukan developed a semi-continuous process regime featuring a micromolar sulphur feed. They were able to extend lifetime to 120 days, producing 1,100 $mlH_2 \cdot l^{-1}$ at a maximum production rate of 0.83 $mlH_2 \cdot l^{-1} \cdot h^{-1}$ (Oncel & Vardar Sukan, 2009). Kim and co-workers

cycled *C. reinhardtii* between sulphur-rich and sulphur-deplete environments over a period of 20 days, with a longer frequency of 5 days per cycle. Their initial cycle produced 250 $mlH_2 \cdot l^{-1}$ and the H_2 yield decreased slightly with every subsequent cycle, for a total H_2 yield of 790 $mlH_2 \cdot l^{-1}$ (Kim *et al*., 2010).

3.5.4. Immobilisation and Genetic Modification

Immobilisation and genetic modification (GM) techniques have been used to increase the cell density of *C. reinhardtii* cultures and to increase the flow of electrons to the $h_2$ase enzyme within individual *C. reinhardtii* cells (Melis, 2009). Increasing the cell density increases the number of reaction centres that have the potential to produce H_2 under anaerobic conditions (Horner & Wolinsky, 2002). Kosourov & Seibert successfully immobilised the cc124 strain in a thin (<400 μm) alginate layer that was extracted from brown seaweed (Kosourov & Seibert, 2009). They were able to achieve cell densities of 2,000 $\mu gChl \cdot ml^{-1}$ of alginate matrix, a factor of 100 times thicker than a typical *C. reinhardtii* culture. The immobilised cells produced H_2 at approximately five times the normal rate, giving a photochemical conversion efficiency of 1% (Kosourov & Seibert, 2009). *C. reinhardtii* cells immobilised in matrices of single-cell thickness would theoretically give the highest photochemical efficiency, but the surface area requirement of such a system renders it completely impractical (Dasgupta *et al*., 2010). The ideal scenario would involve multiple immobilised layers of densely packed *C. reinhardtii*; such an approach requires a reduction in the chlorophyll content (the 'greenness') of individual cells, reducing the shading effect and allowing all the layers to have sufficient access to illumination (Kosourov *et al.,* 2011). This can be achieved by using GM to truncate the algal light-harvesting antennae, reducing the number of pigmented molecules in order to make the cells less green (Melis, 2009). WT *C. reinhardtii* cells use their large antennae to shield themselves from photoinhibition by excess irradiation and to shade competing cells in order to gain an evolutionary advantage; these properties are no longer desired in a controlled PBR environment. Truncating the light-harvesting antenna allows the cells to work more efficiently at higher light intensities, improving the overall efficiency of biohydrogen production (Melis, 2009).

An alternative approach involves the extraction and immobilisation of individual *C. reinhardtii* h2ase enzymes on gold electrodes (Krassen *et al*., 2009). Such a process is prohibitively expensive, but it does give an insight into the kinetics, structure, function and limitations of the [FeFe]-h2ase enzyme (Armstrong, 2005). It raises the possibility of chemically synthesising more practical and economical H_2 production catalysts based on the h2ase enzyme by biomimicry techniques (Lewis & Nocera, 2006).

H_2 evolution competes for electrons with other reductive pathways, including the cyclic electron flow and the assimilation of CO_2 to produce organic acids, ethanol and other fermentation products (Levin *et al*., 2004). To demonstrate the effect of alternative metabolic pathways on H_2 production, it is possible to conduct experiments that inhibit the PSII reaction centre or control the pH of the substrate. Blocking PSII activity inhibits about 80% of the H_2 photoproduction, showing that the majority of electrons originate from the photolytic water-splitting reaction (Makarova *et al.,* 2007). Allowing the substrate to become acidic increases the assimilation of CO_2 and reduces the production of H_2 (Kosourov *et al.*, 2003). It is possible to use genetic engineering to knock-down undesirable metabolic pathways and re-direct additional electrons to the h2ase enzyme, hence improving H_2 production (Doebbe *et al*., 2007).

GM has been used to engineer the stm6 strain, which increases H_2 production by reducing cyclic electron transport in *C. reinhardtii* (Kruse *et al.*, 2005b). The stm6 strain has also had its light-harvesting antennae truncated to produce stm6glc4t7, a strain with improved light-harvesting properties at high light intensities (Beckmann J. *et al*., 2009). Kruse and colleagues report 20-30% faster growth rates at high light intensity (800 $\mu E \cdot m^{-2} \cdot s^{-1}$) and a 50% increase in H_2 production rates using this mutant. H_2 yields of 400-600 $ml H_2 \cdot l^{-1}$ have been measured, with a maximum H_2 production rate of 8 $ml H_2 \cdot l^{-1} \cdot h^{-1}$ (Kruse & Hankamer, 2010). D1 protein mutants have been used to progressively impair the activity of PSII without the need for S-deprivation (Makarova *et al.,* 2007; Torzillo *et al*., 2009). Fermentation mutants have been used to increase the flow of fermentative electrons to the h2ase enzyme by knocking-down competing fermentative pathways (Burgess *et al.,* 2011).

3.6. Photobioreactors

3.6.1. Design Principles

The development of efficient, economic, scaled-up photobioreactor (PBR) systems is required to facilitate the photosynthetic growth and biophotolytic H_2 production by *C. reinhardtii*. (Giannelli *et al*., 2009; Morweiser *et al*., 2010; Posten, 2009). Inexpensive open systems such as natural ponds, circular ponds with a rotating arm for stirring, and raceway ponds have already been used for commercial growth of algal biomass, in particular of the green algae *Chlorella* and *Dunaliella*, grown for the pigmenting agent astaxanthin and β-carotene, respectively (Akkerman *et al*., 2002). The disadvantages of such outdoor systems include a lack of control of temperature and fluid dynamics, poor mass transfer and gas exchange within the algal culture, and a strong possibility of contamination, predation and evaporative losses (Carvalho *et al*., 2006). Additionally, there is significant public concern about genetically manipulated algal strains, particularly if biomass cultivation is open to the environment. Open systems are definitely not a suitable choice for the biophotolytic H_2 production process due to the need to efficiently harvest a highly mobile and diffusive gaseous molecule.

Enclosed PBR systems feature more reproducible cultivation conditions, with better heat and mass transfer control. This increases biomass yield and H_2 yield, resulting in better product quality as well as providing an opportunity for more flexible technical design (Pulz, 2001). Enclosed PBRs can enable algal cultivation in arid regions, hence ensuring that algae do not need to compete for land area with food crops, while also opening new economic possibilities in desert countries (Ugwu *et al*., 2008). The main drawbacks of enclosed PBR systems are their high capital and operating costs (Melis, 2002).

A PBR is best described as a complex, multiphase system, consisting of the gaseous H_2 product, the liquid growth medium, and the solid algal cells, as well as the superimposed light radiation field (Borowitzka, 1999; Posten, 2009). The PBR geometry affects the relationship between these components and determines the effectiveness of the reactor, which can be measured in terms of the *C. reinhardtii* biomass yield and the biophotolytic H_2 yield. To achieve optimal biomass yield, the

PBR should be operated at appropriate illumination conditions, with an optimal surface-to-volume ratio and light–dark cycle, and with sufficient gaseous mass transfer through the algal culture (Posten, 2009). Both the intensity and wavelength of light incident on the PBR are equally important, along with the parameters that influence the light penetration and light mixing in the system (Tsygankov, 2001).

The efficiency of the two-stage biophotolysis process is also dependent on many variables that may be influenced by PBR design, including the light intensity distribution, pH, temperature, media composition and substrate feed rates (Hankamer *et al*., 2007). Since H_2 production is light-limited, the photobioreactor must have a high surface-to-volume ratio, so that the majority of algal cells have access to PAR. The low photochemical efficiencies of the H_2 production process imply that it is necessary to diffuse the light throughout the culture, which can be achieved by high culture mixing rates (Akkerman *et al*., 2002). The PBR must provide the capacity to control flow rates and to measure *C. reinhardtii* cell density, as well as the dissolved oxygen, carbon dioxide, sulphur and hydrogen concentrations. It is also advantageous to be able to monitor other fermentation products such as formate and ethanol (Melis, 2002).

The PBR geometries previously considered in the literature are the stirred-tank reactor (often with internal illumination), the vertical-column reactor, the horizontal tubular reactor, and the flat-plate reactor (Akkerman *et al*., 2002; Borowitzka, 1999; Carvalho *et al*., 2006; Dasgupta *et al*., 2010; Melis, 2002; Posten, 2009; Pulz, 2001; Tamburic *et al*., 2011b; Ugwu *et al*., 2008).

3.6.2. Photobioreactor Geometries

Stirred-tank fermenter-type reactors have regularly been used to conduct laboratory-scale measurements of biophotolytic H_2 production (Melis *et al.,* 2000; Janssen *et al.,* 2003; Berberoglu *et al*., 2007). In their simplest form, stirred-tank PBRs may be constructed by modifying common laboratory glass flasks, which partially explains their widespread use. Unfortunately, these reactors are characterised by a high degree of back-mixing and poor light penetration through the culture (Pulz, 2001; Cornet & Dussap, 2009). Culture mixing is typically provided by means of a mechanical stirrer, which becomes a major source of energy consumption at large operational

volumes (Chisti & Jauregui-Haza, 2002). Mechanical mixing also generates high extensional stress on the algal cells, resulting in substantial cell death (Rosello-Sastre *et al.,* 2007). The possibility of providing internal illumination to stirred-tank systems through the use of optical fibres has been explored as a means of increasing their functionality, but this approach would be difficult to implement for large-scale reactors (Chen *et al.,* 2008; Fouchard *et al*., 2008).

Vertical-column reactors used for this application are simple systems consisting of a polyethylene or glass tube, agitated by means of an air-lift loop or a bubble column (Miron-Sanchez *et al.,* 2000; Xu *et al.,* 2002). They are compact, low cost, easy to operate, and therefore frequently used for domestic (and laboratory) microalgal and plankton growth (Uyar *et al*., 2007). Due to the reactor orientation, artificial lighting is important; a high degree of turbulence is also required to produce sufficient light diffusion and light-dark cycling of the culture (Barbosa *et al.,* 2003b; Skjånes *et al*., 2007). The main advantages of vertical-column reactors are the high mass transfer rates and good culture mixing with low shear stress on the algae (Lehr & Posten, 2009). The main limitation is the relatively small surface-to-volume ratio compared with the flat-plate or stirred-tank reactors (Perner-Nochta & Posten, 2007). Other drawbacks include the variable light penetration through the algal culture, the need for sophisticated construction materials to keep the reactor H_2 leak-free, and the decrease in illumination surface area upon scale-up (Uyar *et al*., 2007).

Tubular PBRs consist of straight, coiled, or looped transparent tubing laid out in a specific geometric arrangement that is designed to maximise light capture (Xu et al., 2002). They come in multiple reactor geometries including horizontal, helical, conical, and α-shape and can be made from a wide variety of materials ranging from glass capillaries to plastic bags (Janssen *et al*., 2000b; Kunjapur & Eldridge, 2010). Tubular reactors are widely available because of the ease of manufacture, process scale-up, and suitability for outdoor use due to their large illumination surface area (Bosma *et al.,* 2007; Scoma *et al.,* 2011). Large illumination surface areas are obtained by using thin tubes with a diameter of no more than 10 cm and illuminating the reactor from multiple directions (Molina Grima *et al.,* 2000). Horizontal tubular plastic bag reactors have achieved commercial success for the cultivation of *Chlorella* (Ugwu et al., 2008). Helical designs enclosing a central light source usually aim to attain high surface-to-volume ratios, while conical and α-shape geometries create a better angle relative to the direction of sunlight, but have so far proven difficult

to scale up (Akkerman *et al*., 2002). The main disadvantage of tubular reactors is their poor axial mass transfer; long reactors are characterised by significant gas gradients that occur axially along the tubes (Molina Grima *et al.,* 1999; Xu et al., 2002). Tubular reactors are scaled up by the incorporation of additional sections via manifolds (Borowitzka, 1999). However, each additional link increases the possibility of H_2 diffusive losses and the requirement for a H_2-tight reactor also reduces the number of potential tubular reactor materials (Molina Grima *et al*., 1999).

The main advantages of the flat-plate reactor are its large surface-to-volume ratio, its operational flexibility and its suitability for outdoor applications. A flat-plate reactor typically features a rectangular compartment with a depth of 1-5 cm, depending on the quality of light mixing in the system (Nedbal *et al.,* 2008; Skjånes *et al*. 2008). The height and width may be scaled up to a practical limit of 2-3 m (Borowitzka, 1999). Flat-plate reactors may be run in both batch and continuous modes and therefore provide operational flexibility (Sierra *et al.,* 2008). Artificially illuminated flat-plate reactors are normally vertical and the irradiation is incident on one of the large reactor surfaces, while outdoor flat-plate reactors tend to be tilted at an angle corresponding to the mean solar irradiation angle (Akkerman *et al*., 2002). The reactor region adjacent to the illuminated surface is known as the photic zone (Perner-Nochta & Posten, 2007). Within the photic zone, light saturation of the algal culture may result in photoinhibition of the cells (Skjånes *et al*., 2008). Light intensity decreases exponentially away from the photic zone, with a limiting light path of 0.8 mm for a fully grown culture of *C. reinhardtii* (Janssen et al., 2003). These light gradients may be minimised, and the light-dark cycles experienced by algal cells may be controlled, by introducing effective mixing into the system (Janssen *et al,* 200b). Since the space between flat-plate reactor panels is restricted, the gaseous mass transfer rates tend to be low, which reduces the clearance efficiency of the dissolved oxygen produced by photosynthesis (Molina Grima *et al*., 2000). Gas-lift mixing is therefore required to achieve commercially-viable algal biomass production rates. Other limitations for flat-plate reactors include the difficulty in controlling culture temperature and the requirement for multiple compartments and support materials when scaling up the reactors (Molina Grima *et al*., 2000).

3.6.3. Scale-up and Commercialisation

The stirred-tank, vertical-column and flat-plate PBR geometries may be scaled up by repeating multiple PBR units or by increasing the size of the individual units. The tubular flow PBR capacity may be increased by connecting additional tubes via manifolds (Borowitzka, 1999). Large-scale PBRs need to be operated outdoors, under solar illumination. Scale-up requires the development of a continuous and fully automated H_2 production process. This can be achieved either by finding an efficient way of filtering *C. reinhardtii* cultures in order to exchange the growth medium between photosynthetic growth and H_2 production stages, or by extending algal lifetime during anaerobic H_2 production (Amos, 2004). A strategy for cycling cultures between sulphur-deplete and sulphur-rich media, perhaps by immobilising the cells on silica particles, needs to be developed in order to extend algal lifetime (Laurinavichene *et al.,* 2006). Scaling-up decreases H_2 production costs due to the effect of economies of scale and by reducing the number of measuring instruments required, but it introduces new challenges relating to the fluid dynamics, maintenance and the H_2 product extraction (Cournac *et al*., 2002). Algal cells in large-scale outdoor PBRs are more likely to be exposed to high shear stress, high temperature gradients, photoinhibitive light intensities and long light-dark cycles. The cells therefore need to be stable, robust and resistant to contamination and fouling (Wijffels & Barbosa, 2010), which are properties that may be improved by genetic engineering.

The two most important parameters that will determine the commercial potential of large-scale PBRs are the surface area requirement and the cost per unit of H_2 produced (Wijffels & Barbosa, 2010). The ultimate aim of any area-efficient PBR is to deliver all incident sunlight to *C. reinhardtii* cells at a light intensity that will be usable for algal growth and H_2 production. A good example of an area-efficient PBR is the Green Solar Collector, which uses light-tracking fresnel lenses to focus sunlight and deliver it to the algal culture via a series of light guides (Zijffers *et al*., 2008). Since no commercial H_2 production facility currently exists, biohydrogen cost estimates are extremely varied and uncertain. An early analysis conducted by the National Renewable Energy Laboratory estimates the cost of H_2 production by *C. reinhardtii* at \$0.57-\$13.53 per kg of H_2 produced ($kg^{-1}H_2$), depending upon where the system boundaries are defined (Amos, 2004). A more recent review suggests that the best estimate of the cost of H_2 production is \$1.37 $kg^{-1}H_2$ (Melis, 2007). This

result assumes a higher H_2 production efficiency than is currently achievable in outdoor PBRs. A more realistic cost estimate comes from Norsker and co-workers, who estimate the cost of algal growth at circa \$8 kg^{-1}biomass in tubular reactors and \$11 kg^{-1}biomass in flat-plate reactors (Norsker *et al*., 2011); the cost would be approximately double for H_2 production, i.e. \$16-22 $kg^{-1}H_2$.

One kilogram of H_2 is the energetic equivalent of a gallon of gasoline, which is trading at around \$4 in early 2012, including all taxes and charges. Photobiological H_2 is pure enough (94-98%) to use directly in a hydrogen fuel cell (Tsygankov *et al*., 2006). This highlights the potential of green algal H_2 production, as well as the need to improve efficiencies if the product is to become commercially competitive. The theoretical photochemical efficiency of biophotolytic H_2 production is 10-13% (Akkerman *et al*., 2002). Photochemical efficiencies approaching this value are only observed at low artificial light intensities, with associated low H_2 production rates. Among experiments that attempt to maximise H_2 production, the highest reported photochemical efficiency is 2% (Melis, 2007). The photochemical efficiency of green algal H_2 production needs to be increased by at least a factor of 3 if the process is to become competitive with solar energy harvesting by photovoltaics or the rapid growth of algal biomass for the purposes of organic oil extraction and electricity generation (US Department of Energy, 2005).

The benefits of the two-stage biophotolysis process extend beyond the H_2 product. High-value products could be extracted from algal biomass or 'milked' from the growing *C. reinhardtii* culture (Hejazi & Wijffels, 2008). The residual algal biomass may be dried and burnt to generate electricity or pressed to extract biodiesel (Putt, 2007). It may also be possible to use green algal residues in combination with cyanobacteria and dark-fermentation bacteria to produce a higher molar yield of H_2 or to produce biogas (Taylor, 2008). These integrated biorefinery approaches improve the overall value of the biophotolysis process, while at the same time increasing the requirement for an intelligent and efficient PBR design. It is clear that PBR development will play a major role in determining the commercial viability of green algal H_2 production (Stephens *et al.,* 2010a).

Table 3.01: Summary of H_2 production induction procedures

Procedure name	How does it work?	Disadvantages
Inert gas purge (N_2, Ar or He)	mechanical O_2 removal	expensive gas separation required
O_2 scavenger (salty iron, plastoquinol or glucose)	chemical O_2 absorption	toxic expensive unreliable
Dark incubation	O_2 consumed by respiration	low H_2 production rate short H_2 production duration
Low light intensity (<20 $W \cdot m^{-2}$)	O_2 consumed by respiration	low H_2 yield reduced biomass yield unreliable
Light shock (~500 $W \cdot m^{-2}$)	(temporary) PSII inactivation	short H_2 production duration partially irreversible
DCMU	PSII inactivation	low H_2 production rate irreversible
Mn-deprivation	PSII inactivation	low H_2 production rate irreversible
N-deprivation	partial PSII inactivation	damage to electron transport pathway
S-deprivation	partial PSII inactivation	-

Table 3.02: Summary of the parameters that affect *C. reinhardtii* growth

Parameter	Description	Comments
Algal strain	WT: cc124, cc125, cc1690 cc406 mutant - no cell wall dum24 mutant - more starch accumulation	choose appropriate strain for given situation
Contamination	foreign algae & bacteria fungi zooplankton	use sterilised vessels, air filters and fungicides
Wavelength	400-700 nm PAR 750-950 nm near infrared	use cool white light
Light intensity	5-80 $W \cdot m^{-2}$	increasing light intensity increases growth rate
Photosaturation	80-200 $W \cdot m^{-2}$	increasing light intensity has little effect on growth rate
Photoinhibition	>200 $W \cdot m^{-2}$	increasing light intensity inhibits growth rate
Nutrients	usable source of carbon, nitrogen, sulphur, phosphorus and trace metals	
Phototrophic state	photoautotrophic: CO_2 only C-source photoheterotrophic: acetate only C-source photomixotrophic: CO_2 & acetate	photomixotrophic best growth photoautotrophic best value
Fluid dynamics	magnetic stirrer bar circulation pump gas-lift system	improve light mixing reduce light-dark cycles eliminate O_2, T & pH gradients
Temperature	20-28°C	
pH	6.5-8.2	7.7 optimum

Table 3.03: Summary of the parameters that affect *C. reinhardtii* H_2 production

Parameter	Description	Comments
Cell density	fully grown: 14-24 μgChl·ml^{-1} number of PSII reaction centres amount of starch reserves	may be increased by immobilisation and antennae mutants
Light intensity	~10 W·m^{-2} 50 W·m^{-2} during S-deprivation	high light intensity during S-deprivation increases starch accumulation
Light-dark cycle	constant illumination: ~200 mlH_2·l^{-1} light-dark cycles: ~100 mlH_2·l^{-1}	minimise light-dark cycles with good light mixing
Phototrophic state	photomixotrophic: ~110 mlH_2·l^{-1} photoautotrophic: ~30 mlH_2·l^{-1}	photoautotrophic H_2 production more economical
Induction procedure	S-deprivation superior centrifugation: ~180 mlH_2·l^{-1} dilution: ~40-110 mlH_2·l^{-1}	dilution procedure easier to implement and scale up
Sulphur re-addition	use to extend H_2 production duration 7 days → 20-120 days	cycle cells between S-rich and S-deprived media or apply micromolar S-feed
Genetic modification	stm6: inhibited cyclic electron transport stm6glc4t7: truncated antennae fermentation knock-down mutants	WT: 2 mlH_2·l^{-1}·h^{-1} stm6glc4t7: 8 mlH_2·l^{-1}·h^{-1}
Temperature	20-28°C	
pH	6.5-8.2	7.7 optimum

Table 3.04: Summary of photobioreactor (PBR) geometries

PBR geometry	Advantages	Disadvantages
Stirred-tank	common laboratory use easy and inexpensive to construct	high degree of back-mixing poor light penetration energy-intensive mixing high shear stress difficult to scale up
Vertical-column	used for domestic algal growth compact and low cost easy to operate high mass transfer rates good culture mixing low shear stress	usually require artificial light require high degree of turbulence small surface-to-volume ratio variable light penetration difficult to keep leak-free illumination area reduced on scale-up
Tubular	used for commercial *Chlorella* growth easy to manufacture available in multiple arrangements large illumination surface area easy to scale up suitable for outdoor use	poor axial mass transfer development of gas gradients difficult to keep leak-free
Flat-plate	operational flexibility highest surface-to-volume ratio suitable for outdoor use	low gaseous mass transfer difficult light mixing environment difficult temperature control expensive to scale up

3.7. Summary

C. reinhardtii is a model green alga capable of producing H_2 under anaerobic conditions by biophotolysis. Light energy is captured by light-harvesting proteins in PSII and used to spilt water into O_2, protons and electrons. These photosynthetic electrons are transported, via the plastoquinone pool and PSI, to ferredoxin. During photosynthetic growth, ferredoxin donates its electrons to NADPH or cycles them back to the plastoquinone pool to facilitate ATP synthesis. NADPH and ATP are used to run the Calvin Cycle, which involves the fixation of CO_2 to starch, a prerequisite for all further biosynthesis. Under anaerobic conditions, ferredoxin also donates its electrons to the [FeFe]-h$_2$ase enzyme. The h$_2$ase enzyme catalyses the process of proton-electron recombination to produce H_2. In addition to the photosynthetic pathway, the h$_2$ase enzyme also receives electrons from the catabolic breakup of starch and from the fermentation of pyruvate.

The h$_2$ase enzyme is extremely oxygen-sensitive, yet the algae constantly produce O_2 by photosynthesis; this presents a major challenge for the induction of H_2 production. The solution is to remove the O_2 as it is being produced, creating a highly anoxic environment. This can be achieved by purging the *C. reinhardtii* culture with an inert gas, by using an oxygen scavenger, or by subjecting the algae to a period of dark incubation or to a low light intensity. However, the best method for inducing H_2 production is two-stage biophotolysis by sulphur deprivation. S-deprivation reversibly reduces the activity of PSII without affecting the rate of respiration. The rate of photosynthetic O_2 production drops below the level of respirative O_2 consumption, resulting in a net consumption of O_2. The algae metabolically bring themselves into a state of anoxic H_2 production. The H_2 production rate by WT *C. reinhardtii* by two-stage biophotolysis is circa 2 $mlH_2 \cdot l^{-1} \cdot h^{-1}$. H_2 induction techniques are summarised in Table 3.01.

For a *C. reinhardtii* cell to grow, it requires access to illumination, water and nutrients, including usable sources of carbon, nitrogen, sulphur, phosphorus and trace metals. Room temperature and neutral pH are suitable for growth. An algal culture consists of millions of algal cells, which interact with each other as well as with their environment. Algal cultures follow the logistic population growth model, where the cell density increases at a specific growth rate until illumination or nutrient availability become limited and the cell density reaches a saturation value. The growth of

algal cultures is strongly influenced by various aspects of illumination including: wavelength, light intensity, light mixing, light regime, photosaturation and photoinhibition. Careful control of fluid dynamics is required to ensure good nutrient, gas and light mixing in the culture, and to protect individual cells from photoinhibition and long light-dark cycles. The phototrophic state plays a role in the growth rate and growth economics of *C. reinhardtii* cultures. Parameters that affect algal growth are summarised in Table 3.02.

To increase the rate of biophotolytic H_2 production by *C. reinhardtii*, it is necessary to increase the algal growth rate and the cell density, increase the number of cells producing H_2 efficiently, optimise H_2 induction, increase H_2 duration or increase electron flow to the $h_2$ase enzyme. A high algal growth rate and efficient H_2 production can be achieved by optimising environmental parameters, such as the light intensity, light mixing and phototrophic state. S-deprivation may be achieved by centrifugation, microfiltration or dilution procedures, which all have their limitations. The duration of H_2 production needs to be extended beyond one week if the process is ever to become commercially viable. Various immobilisation, medium exchange and nutrient feed techniques have been implemented to improve the S-deprivation procedure and increase H_2 production duration, but there is no clear winner as yet. Genetic modification of *C. reinhardtii* has been used to increase electron flow to the $h_2$ase enzyme by truncating light-harvesting antennae, reducing cycling electron flow, and knocking down competing fermentative pathways. Parameters that affect H_2 production are summarised in Table 3.03.

The development of efficient, economic and scaled-up photobioreactors is required to facilitate green algal H_2 production. An enclosed PBR is required to provide more reproducible cultivation conditions, better heat and mass transfer, and harvesting of the H_2 product. PBR design must take into account all the elements of a complex multi-phase system, which includes the gaseous H_2 product, the liquid algal growth medium, the solid algal cells, and the superimposed light radiation field. The effectiveness of the PBR can be measured in terms of the *C. reinhardtii* biomass yield and the biophotolytic H_2 yield. The PBRs that have been considered for H_2 production are the stirred-tank reactor, the vertical-column reactor, the tubular reactor and the flat-plate reactor. The benefits and limitations of different PBR geometries have been summarised in Table 3.04. Scaling up requires the development of a continuous and fully-automated H_2 production process, which is not

currently available. It introduces new challenges relating to the fluid dynamics, maintenance and H_2 extraction from the reactor. The two most important parameters that will determine the value of large-scale PBRs are the surface area requirement and the cost per unit of H_2 produced. Biophotolytic H_2 production is currently too expensive to compete commercially, primarily due to the low photochemical efficiency of the process. Improvements in the photochemical efficiency of biophotolysis and the extraction of high-value by-products in a biorefinery approach are required to make green algal H_2 production a reality.

4. Aim and Objectives

4.1. Aim

The green alga *C. reinhardtii* has the capacity to produce renewable H_2 fuel from two of nature's most plentiful resources, sunlight and water. The aim of this thesis is to improve our understanding of the growth and H_2 production of *C. reinhardtii* in order to develop a continuous, practical and scaleable biophotolytic H_2 production process, as well as to evaluate the potential of this technology as a sustainable source of H_2. This aim will be achieved by addressing the following four objectives.

4.2. Objectives

Objective I: Design novel flat-plate PBR (Chapter I)

The first objective is to design a novel flat-plate PBR specifically to facilitate green algal growth and H_2 production at the laboratory scale, and to enable quick measurement of the key process parameters under carefully controlled conditions. The illumination, temperature and fluid dynamics within this PBR will be fully controllable. The PBR will be equipped with instruments that measure the pH, pO_2 and OD of the algal culture. A continuous and reliable *in situ* H_2 measurement technique will be developed and tested. Once built and commissioned, the flat-plate PBR will be used to measure *C. reinhardtii* growth and H_2 production, contributing towards the other objectives of this thesis.

Objective II: Evaluate algal growth kinetics (Chapter II)

In order to achieve effective H_2 production, it is necessary to grow dense and healthy *C. reinhardtii* cultures. The second objective is to evaluate the effect of *C. reinhardtii* strain, temperature, light regime, carbon source, and light intensity on algal growth. Kinetic parameters, such as the specific growth rate and the final cell density, will be obtained from experimental growth measurements.

Correlations between algal growth rates and variations in the cultivation conditions will be determined using a mathematical growth model.

Objective III: Develop nutrient control technique (Chapter III)

H_2 production by *C. reinhardtii* is normally initiated by sulphur-deprivation, but current sulphur-deprivation techniques are time- and energy-consuming, inefficient, and difficult to scale up. The third objective is to achieve H_2 production by controlling the nutrient composition of the algal growth medium. To achieve this, sulphate and acetate consumption rates will be measured and the appropriate kinetic parameters will be extracted. A reactor-independent relationship between algal growth rates and nutrient uptake rates will be determined. The initial composition of the algal medium will then be optimised so that a fully-grown algal culture spontaneously enters a state of anaerobic H_2 production. H_2 production rates and yields by nutrient control will be compared to the results obtained by the established centrifugation and dilution procedures during experiments carried out as part of this thesis, as well as to the values recorded in the literature.

Objective IV: Extend H_2 production by sulphur re-addition (Chapter IV)

Anaerobic *C. reinhardtii* cultures ultimately fail to produce enough energy to satisfy their metabolic requirements and die. The fourth and final objective is to extend H_2 production duration by sulphur re-insertion. *C. reinhardtii* cultures will be cycled between growth and H_2 production stages using the nutrient control technique. The duration of these aerobic:anaerobic cycles will be optimised. The alternative approach of applying a small but continuous sulphur feed to an anaerobic algal culture will also be attempted. These investigations are targeted at understanding the process sufficiently at a mechanistic level to enable a more systematic study of the extent to which it can be scaled up to a range of process sizes.

5. Experimental Methods

5.1. Inventories

In this section all the equipment and materials used during this research are summarised and specified.

5.1.1. Algal Strains

Professor Peter Nixon's group in the Biology department at Imperial College London (ICL) cultivates various *C. reinhardtii* strains on agar plates and stores them in liquid nitrogen. Five of these strains were used during this thesis: cc124, cc406, dum24, pdc3-KD and s21. The laboratory wild-type cc124 strain was used in the majority of experiments. The natural mutants cc406 and dum24 were used to compare the growth kinetics between different *C. reinhardtii* strains. The knock-down mutant pdc3-KD was used to test a novel H_2 measurement setup. The candidate knock-down mutant s21 was tested for H_2 production alongside cc124 to determine the validity of its mutation. A summary of the different algal strains is given in Table 5.01.

5.1.2. Photobioreactors

Four different photobioreactor (PBR) geometries were used in this study: stirred-tank, vertical-column, tubular and flat-plate. Stirred-tank reactors included the Solar Biofuels Consortium 250 ml conical flask PBRs and the Solar Simulator "storage jar" PBR. A number of commercial vertical-column PBRs from AquaMedic were used to cultivate *C. reinhardtii* cultures. The Sartorius tubular PBR was primarily used to investigate *C. reinhardtii* growth kinetics. The ICL Chemical Engineering flat-plate PBRs were designed and used to conduct H_2 production experiments. Table 5.02 shows the full PBR inventory.

5.1.3. Equipment

A list of the important pieces of equipment (and their manufacturers) used during this thesis is given in Table 5.03. It includes PBR peripheries, such as the compressed air pump, LED array and Sartorius control tower. All measuring instruments, including the pH, pO_2 and OD probes, are also taken into consideration. General laboratory equipment, such as the toolbox, centrifuges, rig construction equipment and sterilisation equipment, are listed. Finally, large analytical instruments, including the spectrophotometer and the mass spectrometer, are also catalogued.

5.1.4. Chemicals

The chemicals and chemical suppliers used during this thesis are listed in Table 5.04. This includes PBR cleaning and biowaste disposal chemicals, such as Trigene solution and Virkon tablets. Electrode calibration and maintenance chemicals, incorporating pH electrode buffer solutions and pO_2 probe electrolytes, are catalogued. The various gases used for calibration, purging and as carrier gases for mass spectrometry are listed. All the chemicals used in algal growth medium preparation are indexed, as are the chemicals required for ion chromatography and high performance liquid chromatography analysis techniques. Finally, general laboratory chemicals, such as acetone, hydrochloric acid and sodium hydroxide are also listed.

Table 5.01: Algal strain inventory

Algal strain name	Description
cc124	*C. reinhardtii* common laboratory wild-type strain
cc406	*C. reinhardtii* natural mutant strain without a cell wall
dum24	*C. reinhardtii* natural mutant strain that accumulates excess starch
pdc3-KD	*C. reinhardtii* knock-down mutant of the PDC metabolic pathway
s21	*C. reinhardtii* potential knock-down mutant of PFL metabolic pathway

Table 5.02: Photobioreactor inventory

Geometry	Name	Description	Units
Stirred-tank	Solar Biofuels Consortium PBR	250 ml conical flask	10
Stirred-tank	Solar Simulator PBR	2 litre storage jar	1
Vertical-column	AquaMedic Plankton Light Reactor	1.5 litre vertical tube	6
Tubular	Sartorius Biostat PBR 2S	2 litre helix, 1 litre central vessel	1
Flat-plate	ICL Chemical Engineering PBR	1 litre vertical compartment	2

Table 5.03: Equipment inventory - photobioreactor peripheries, measuring instruments, laboratory equipment and analytical instruments

Equipment (manufacturer)	Application
Fluorescent array (Abalab)	Illumination, Solar Biofuels Consortium PBR
Mechanical shaker (Abalab)	Mixing, Solar Biofuels Consortium PBR
Solar Simulator (LOT)	Illumination, Solar Simulator PBR
Magnetic plate (Clifton)	Mixing, Solar Simulator PBR
Datalogging unit (Consort)	Datalogging, Solar Simulator PBR
Fluorescent tube (AquaMedic)	Illumination, AquaMedic PBR
Compressed air pump (AquaMedic)	Mixing, AquaMedic PBR
Circular fluorescent array (Sartorius)	Illumination, Sartorius PBR
Peristaltic pump (Ismatec)	Mixing, Sartorius PBR
Control tower (Sartorius)	Control & datalogging, Sartorius PBR
LED array (LED Wholesalers)	Illumination, ICL Chemical Engineering PBR
Diaphragm pumps (KNF Neuberger)	Mixing, ICL Chemical Engineering PBR
Compact RIO (National Instruments)	Control & datalogging, ICL Chemical Engineering PBR
Syringe pump (Chemyx)	Sulphate feed, ICL Chemical Engineering PBR
Pt100 thermocouple (Sartorius)	Temperature measurement, Sartorius PBR
Fundalux OD probe (Sartorius)	OD measurement, Sartorius PBR
Easyferm pH electrode (Hamilton)	pH measurement, Sartorius PBR
Oxyferm pO_2 electrode (Hamilton)	pO_2 measurement, Sartorius PBR
K-type thermocouple (RS Components)	Temperature measurement, ICL Chemical Engineering PBR Temperature measurement, Solar Simulator PBR
Photodiode (RS Components)	OD measurement, ICL Chemical Engineering PBR
SP10T pH electrode (Consort)	pH measurement, ICL Chemical Engineering PBR pH measurement, Solar Simulator PBR
SZ10T pO_2 electrode (Consort)	pO_2 measurement, ICL Chemical Engineering PBR pO_2 measurement, Solar Simulator PBR
Laptop computers (Toshiba; Acer; HP)	Datalogging & control
Centrifuge (Beckman)	S-deprivation by centrifugation
Mini-centrifuge (MSE)	Sample analysis

Equipment (manufacturer)	Application
Microscope (Medilux)	Cell count
Mass flow controller (Porter)	Gas flow control
Pipetteman classic (Gilson)	Medium preparation; Titration
Balance (Mettler Toledo)	Medium preparation
Water deioniser (Elga)	Medium preparation
Glassware (VWR)	Medium preparation; Sterilisation
Autoclave (LTE Scientific)	Sterilisation
Laminar flow hood (Microflow)	Sterilisation
Toolbox (Draper)	Rig construction
Stainless steel fittings (Swagelok)	Rig construction
Spectrophotometer (Perkin-Elmer)	OD measurement
Compact IC Plus (Metrohm)	Sulphate concentration measurement
HPLC Series 1050 (Hewlett Packard)	Acetate concentration measurement
Vacuum Prisma MS (Pfeiffer)	H_2 measurement

Table 5.04: Chemical inventory - photobioreactor cleaning & maintenance chemicals, electrode calibration & maintenance chemicals, laboratory gases, medium preparation chemicals, analysis technique chemicals and general laboratory chemicals

Chemical (supplier)	Application
Bleach (Domestos)	Cleaning, all PBRs
Trigene (Medichem)	Cleaning, all PBRs
H_2O_2 (Sigma-Aldrich)	Cleaning, Sartorius PBR
Virkon (Fisher Scientific)	Biowaste disposal
pH buffer solutions (Hamilton)	pH electrode calibration
Oxylyte electrolyte (Hamilton)	pO_2 electrode maintenance
pO_2 electrolyte (Consort)	pO_2 electrode maintenance
Ar (BOC)	MS carrier gas (injection MS)
He (BOC)	MS carrier gas (MIMS)
N_2 (BOC)	Purge gas
O_2 (BOC)	pO_2 electrode calibration
Air (BOC)	pO_2 electrode calibration Photoautotrophic growth experiments
20% CO_2 in air (BOC)	Photoautotrophic growth experiments
NH_4Cl (Sigma-Aldrich)	TAP salts; TAP-S salts
$MgSO_4$ (Sigma-Aldrich)	TAP salts; sulphur-feed
$MgCl_2$ (Sigma-Aldrich)	TAP-S salts
$CaCl_2$ (Sigma-Aldrich)	TAP salts; TAP-S salts
KH_2PO_4 (Sigma-Aldrich)	P-solution
K_2HPO_4 (Sigma-Aldrich)	P-solution
Tris (Melford)	TAP; TAP-S; 5xTAP*; TAP_{12}
Acetic acid (Sigma-Aldrich)	TAP; TAP-S; 5xTAP*; TAP_{12}; sulphur-feed HPLC calibration
HEPES (Sigma-Aldrich)	sulphur-feed
Hutner's trace elements (ICL)	TAP; HSM; 5xTAP*
Hutner's trace elements -S (ICL)	TAP-S; TAP_{12}
Sodium carbonate (Merck)	IC liquid phase

Chemical (supplier)	Application
Sodium bicarbonate (Merck)	IC liquid phase
Sulphuric acid (Merck)	IC liquid phase; HPLC liquid phase
Anion multi-element standards (Merck)	IC calibration
Acetone (Sigma-Aldrich)	Chl measurements
70% ethanol (Sigma-Aldrich)	Sterilisation
Acrylic polish (Xerapol)	ICL Chemical Engineering PBR maintenance
Sodium hydroxide (Sigma-Aldrich)	pH titration
Hydrochloric acid (Sigma-Aldrich)	pH titration
Carbendazim (Sigma-Aldrich)	Fungicide

5.2. Unit Conversion

During this research a number of different units and conversion factors have been used to quantify some key variables. This section summarises the measures used and how they are inter-related.

5.2.1. Light Intensity

Light intensity is one of the most important parameters that affect *C. reinhardtii* growth and H_2 production. Photosynthetically active radiation (PAR) units and SI units ($W \cdot m^{-2}$) are both commonly used to measure light intensity in the field of green algal research (Molina Grima *et al*., 1999). Photosynthetically active radiation (PAR) is a unit commonly used in biology to measure the solar irradiance in the 400-700 nm wavelength range, the region of the solar spectrum harvested by photosynthesis. It is given in units of microEinstein per square metre per second, where one Einstein is the energy carried by one mole of photons. It is possible to calculate the energy carried by a single photon using Equation 5.01.

$$E_v = \frac{hc}{\lambda} \qquad \textit{Equation 5.01}$$

In Equation 5.01, h is the Planck's constant, c is the speed of light and λ is the wavelength of the photon. Given a mean PAR wavelength of 550 nm, the photon would have an energy of $3.6 \cdot 10^{-19}$ J. The energy of one mole of such photons, known as one Einstein, is calculated by multiplying the energy of a single photon by Avogadro's number, N_A, as shown in Equation 5.02.

$$E = E_v \cdot N_A = 216{,}000\ J \qquad \textit{Equation 5.02}$$

Therefore, the power carried by one micro Einstein of photons per second is $0.216\ J \cdot s^{-1}$, and the corresponding surface irradiance is $0.216\ W \cdot m^{-2}$.

$$1\ \mu E \cdot m^{-2} \cdot s^{-1} = 0.216\ W \cdot m^{-2} \qquad \textit{Equation 5.03}$$

Equation 5.03 is only true if all the photons have a wavelength of exactly 550 nm. Since this is normally not the case, an approximate SI value is obtained by dividing the PAR value by 5.

5.2.2. Concentration

There are many different ways of expressing concentration. The SI unit is the mole per decimetre cubed ($mol \cdot dm^{-3}$), which is the equivalent of a mole per litre ($mol \cdot l^{-1}$) of an aqueous solution, or a millimolar (mM) molarity. Measurements of small concentrations of the aqueous ions of sulphate (SO_4^{2-}), acetate (CH_3COO^-), ammonium (NH^{4+}) and phosphate (PO_4^{3-}) were necessary to achieve the objectives of this thesis. These ions were incorporated into the algal growth medium by dissolving a small mass of the appropriate salt, for example magnesium sulphate in the case of SO_4^{2-}. It is therefore useful to express their concentrations in terms of the milligrams of dissolved ion per litre of growth medium ($mg \cdot l^{-1}$), which is also the equivalent of one part per million (ppm). In the case of SO_4^{2-}, with a molar mass of 96 $g \cdot mol^{-1}$, this unit conversion is given in Equation 5.04.

$$1\ mM(SO_4^{2-}) = 0.096\ mg(SO_4^{2-}) \cdot l^{-1} \qquad \textit{Equation 5.04}$$

The remaining dissolved ion concentration conversions are shown in Table 5.05, together with all the other relevant unit conversions. Another important concentration measurement was that of dissolved oxygen content (pO_2), which indicates whether the *C. reinhardtii* culture is aerobic or anaerobic. Dissolved oxygen is normally measured as a percentage of saturation (%): 0% for an anaerobic culture, 21% for an aerated culture and 100% for an O_2-saturated culture. Under standard ambient temperature and pressure (25°C, 1 bar), O_2-saturated fresh water contains 8.3 $mg \cdot l^{-1}$ of O_2 (Sander, 1999). This relationship has been expressed in Equation 5.05.

$$1\ mg \cdot l^{-1}\ O_2 = 12\%\ O_2\ saturation \qquad \textit{Equation 5.05}$$

5.2.3. Algal Growth

The light-scattering properties of *C. reinhardtii* cells have been used to measure the chlorophyll (Chl) concentration and the optical density (OD) of the algal culture. The chlorophyll (Chl) concentration was quantified using the classical method developed by Arnon (Arnon, 1949). A small sample of culture (10-20 ml) was removed under sterile conditions. A few microlitres (typically 200 µl) were extracted from this sample using a pipette and diluted in 80% acetone – this

gives a dilution factor (DF) of 5. The solution was placed in a mini-centrifuge and spun at 13,000 rotations per minute (rpm) for 5 minutes. At the end of this procedure, a white pellet of algal cells formed, indicating that all Chl had dissolved. A spectrophotometer was then used to measure the light absorbance of the Chl sample at the photosynthetically active wavelengths of 645 nm (OD_{645}) and 663 nm (OD_{663}). It is possible to calculate the Chl content from these absorbance measurements using Equations 5.06-5.08 (Arnon, 1949).

$$Chl\ a\ (\mu g \cdot ml^{-1}) = (12.7 \cdot OD_{663} - 2.69 \cdot OD_{645}) \cdot DF \qquad \textit{Equation 5.06}$$

$$Chl\ b\ (\mu g \cdot ml^{-1}) = (22.9 \cdot OD_{645} - 4.68 \cdot OD_{663}) \cdot DF \qquad \textit{Equation 5.07}$$

$$Total\ Chl\ (\mu g \cdot ml^{-1}) = (20.2 \cdot OD_{645} + 8.02 \cdot OD_{663}) \cdot DF \qquad \textit{Equation 5.08}$$

The Chl concentration units ($\mu g \cdot ml^{-1}$) are in fact identical to nutrient concentration units ($mg \cdot l^{-1}$). The main advantage of using Chl content as a measure of algal growth is that the results show a strong correlation with the health of the *C. reinhardtii* culture (Markov *et al*., 2006). Any sign of contamination or malnutrition can quickly be detected and steps can be taken to prevent further fouling of the culture (Siaut *et al*., 2011). On the other hand, Chl measurements are time-consuming and cannot be carried out *in situ*. No two algal cells are the same, nor will they have the same Chl concentration; there are strong variations in Chl concentration between algal cultures and even within a single culture. This implies that specific Chl concentration targets are difficult to reproduce and H_2 production measurements are therefore often specified per unit of Chl (Tsygankov *et al*., 2002; Melis & Melnicki, 2006).

OD is a direct measure of the algal cell density. An OD probe consists of a light emitting diode (LED) and a photodetector, located a short distance apart (an OD probe with an optical path length of 10 mm was used in the Sartorius tubular PBR). Light scattering caused by algal cells reduces the photocurrent in the probe and generates an OD measurement in absorbance units (AU). The LED emits light in the near infra-red (IR) region of the spectrum (840-910 nm) to avoid interference from the photosynthetic Chl absorption peaks. In the absence of an OD probe, a spectrophotometer was used to measure OD. In this case, a small sample of *C. reinhardtii* was extracted and analysed under the appropriate wavelength: at 663 nm to capture the *C. reinhardtii* absorption maximum or at 875 nm to avoid photosynthetic absorption peak interference. OD measurements were much

quicker and simpler to carry out than Chl concentration measurements. More importantly, it was also possible to carry out OD measurements continuously and *in situ*, using OD probes that were readily available on the market (Akkerman *et al.*, 2002). OD is therefore a better choice for measuring algal growth in PBRs, particularly in light of the need to scale up and automate the H_2 production process. The main disadvantage of OD measurements is that they do not discriminate between green *C. reinhardtii* cells, dead cells, contaminants or impurities and hence may not be fully representative of the cell density of the *C. reinhardtii* culture (Melis & Melnicki, 2006). Since OD measurements are carried out at sub-micrometer wavelengths, the majority of light scattering actually takes place off the organelles of *C. reinhardtii* cells (the cell diameter is 5-10 μm). This leads to OD measurement errors during the exponential phase of algal growth; *C. reinhardtii* daughter cells are smaller and have less developed organelles than the mature cells and are therefore less likely to register in the OD measurements (Posten & Schaub, 2009).

For the purpose of this thesis, a correlation has been established between OD measurements at 663 nm and at 875 nm and the corresponding Chl concentration, calculated from Equation 5.08 (Figure 5.01a & 5.01c). These correlations enable a quick calculation of the Chl content without the need to continuously implement Arnon's method; the relationships are given in Equation 5.09 & 5.10.

$$OD_{663}\ (mg \cdot l^{-1}\ Chl) = 17.9 \cdot OD_{663}\ (AU) \qquad \textit{Equation 5.09}$$

$$OD_{875}\ (mg \cdot l^{-1}\ Chl) = 28.0 \cdot OD_{875}\ (AU) \qquad \textit{Equation 5.10}$$

The OD measurements have also been correlated to a *C. reinhardtii* cell count carried out using a microscope (Figure 5.01b & 5.01d). The cell count involves manually counting the number of cells in a small square and multiplying this value by 250,000. It should therefore be used only as a very rough approximation of the cell density. Cell counts can be calculated using Equation 5.11 & 5.12.

$$OD_{663}\ (cells) = 2.6 \cdot 10^{7} \cdot OD_{663}\ (AU) \qquad \textit{Equation 5.11}$$

$$OD_{875}\ (cells) = 4.2 \cdot 10^{7} \cdot OD_{875}\ (AU) \qquad \textit{Equation 5.12}$$

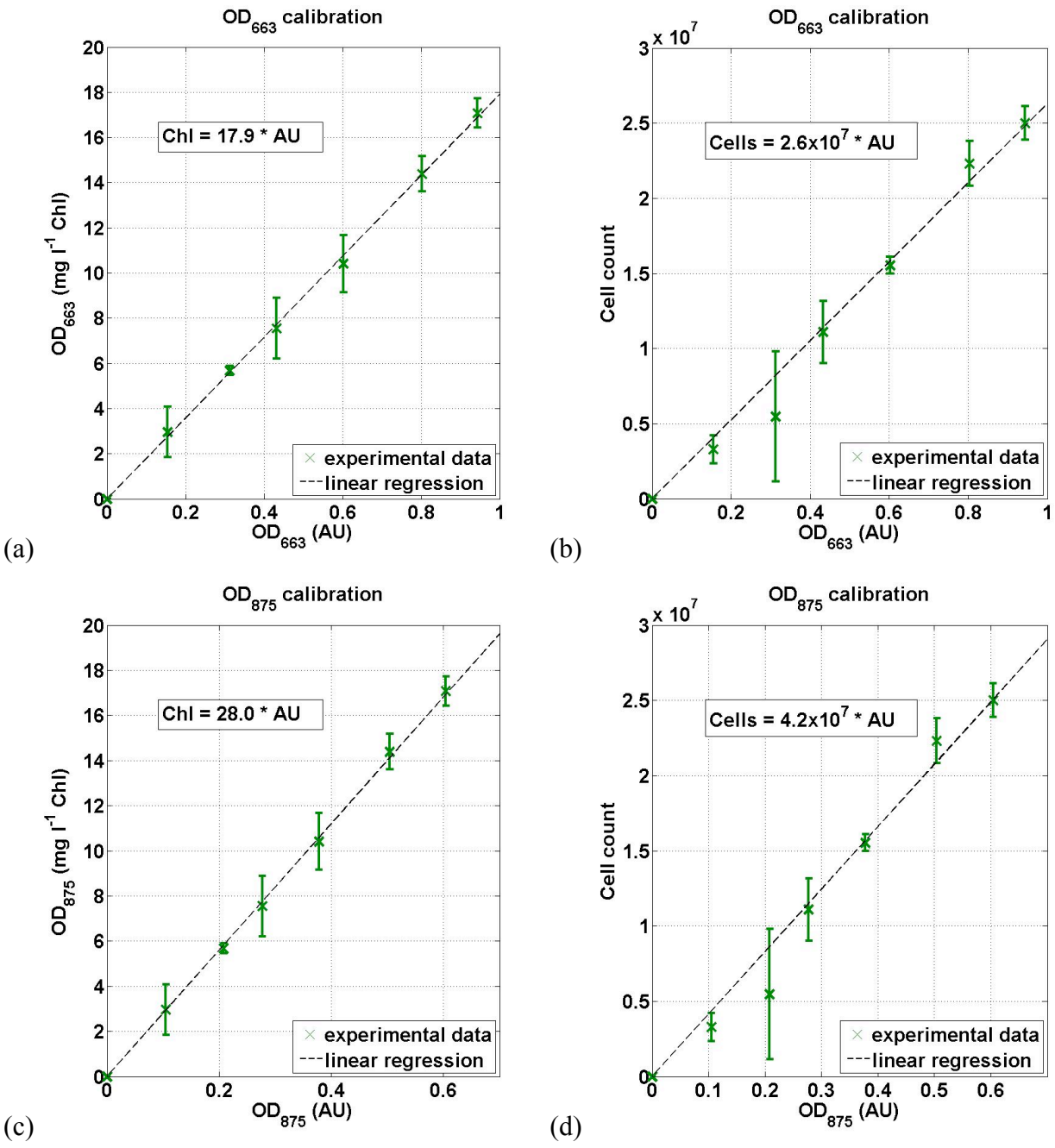


Figure 5.01: Optical density (OD) calibrations

(a) Relationship between OD and Chl content at 663 nm

(b) Relationship between OD and Cell count at 663 nm

(c) Relationship between OD and Chl content at 875 nm

(d) Relationship between OD and Cell count at 875 nm

5.2.4. Biohydrogen Production

Biohydrogen production can be expressed in terms of a production yield ($mlH_2 \cdot l^{-1}$), a production rate ($mlH_2 \cdot l^{-1} \cdot h^{-1}$) or a photochemical efficiency (%). Given that H_2 has a molecular mass of 2 Daltons and a density of 0.089 $g \cdot l^{-1}$ at standard ambient temperature and pressure (Hemmes *et al.*, 1986), it is possible to calculate the unit conversions for H_2 production yield given in Equation 5.13.

$$1\ mmolH_2 \cdot l^{-1} = 2\ mgH_2 \cdot l^{-1} = 22.5\ mlH_2 \cdot l^{-1} \qquad \textit{Equation 5.13}$$

H_2 production rates follow the same unit conversions as H_2 production yields. To calculate the H_2 production yield per unit of Chl ($mlH_2 \cdot mg^{-1}Chl$), it is necessary to simply divide the H_2 production yield ($mlH_2 \cdot l^{-1}$) by the Chl content ($mgChl \cdot l^{-1}$). Photochemical efficiency can be calculated using Equation 5.14 (Akkerman *et al.,* 2002).

$$Photochemical\ efficiency\,[\%] = \frac{H_2\ production\ rate\,[l \cdot s^{-1}] \cdot H_2\ energy\ content\,[J \cdot l^{-1}]}{Absorbed\ energy\,[J \cdot s^{-1}]} \cdot 100$$

Equation 5.14

The H_2 production rate is measured experimentally. The higher heating value for H_2 of 142 $J \cdot l^{-1}$ is used as the H_2 energy content (Hemmes *et al*., 1986). The absorbed energy depends on the irradiation incident on the PBR and on the active reactor surface area (Tamburic *et al*., 2011b).

Table 5.05: Important unit conversions

Variable	Alternative unit	Unit used in thesis
Light intensity	1 $\mu E \cdot m^{-2} \cdot s^{-1}$	0.2 $W \cdot m^{-2}$
SO_4^{2-} concentration	1 mM	0.096 $mg \cdot l^{-1}$
CH_3COO^- concentration	1 mM	0.059 $mg \cdot l^{-1}$
NH_4^+ concentration	1 mM	0.018 $mg \cdot l^{-1}$
PO_4^{3-} concentration	1 mM	0.095 $mg \cdot l^{-1}$
pO_2 concentration	1 $mg \cdot l^{-1}$	12%
OD_{663}	1 AU	17.9 $mg \cdot l^{-1}$Chl
OD_{875}	1 AU	28.0 $mg \cdot l^{-1}$Chl
H_2 yield	1 mmol$H_2 \cdot l^{-1}$	22.5 ml$H_2 \cdot l^{-1}$

5.3. Photobioreactors

5.3.1. Stirred-tank PBRs

The Solar Biofuels Consortium and the Solar Simulator stirred-tank PBRs were used in this thesis. The Solar Biofuels Consortium PBRs are a set of ten modified 250 ml conical flasks (Burgess *et al*., 2011). They are placed together on top of a shaker, which provides mechanical culture mixing in all the PBRs. Illumination is delivered by a pair of cool-white fluorescent arrays, one on each side of the shaker. The light intensity incident on the PBR surface is circa 25.0 $W \cdot m^{-2}$, but this depends on the specific PBR and on the particular surface that have been selected for measurement. The conical flasks have been modified to incorporate a sealed water displacement system. The water displacement system is essentially an inverted graduated pipette placed at the top of the reactor and filled with water. The volume of gaseous products, including H_2, is measured by observing the amount of water that has been displaced from the inverted pipette (Tamburic *et al*., 2011a). A septum is located at the top of the water displacement system. During H_2 production experiments, gaseous samples were extracted through this septum using a gas-tight syringe and analysed by injection mass spectrometry. A sketch of the PBR is shown in Figure 5.02a. In this thesis, the Solar Biofuels Consortium PBRs have been used to analyse *C. reinhardtii* growth under different light regimes. Since the PBRs are sealed, *C. reinhardtii* cells grew under heterotrophic conditions, with acetate in the growth medium acting as the predominant carbon source.

The Solar Simulator PBR is a modified transparent acrylic storage jar (Argos), with a diameter of 35 cm and a height of 25 cm, giving a working volume of approximately 2 litres. Mechanical culture mixing is provided by a magnetic stirrer-bar at the bottom of the reactor. Temperature is measured with a K-type thermocouple from Omega. Dissolved oxygen and pH are measured using electrodes supplied by Consort. Illumination is provided by a steady-state Solar Simulator (LOT). The Solar Simulator has a nominal field size of 10 cm^2 and a working distance of 0-1.5 m. It provides radiation that mimics the solar spectrum, with a maximum light intensity close to the Solar Constant of 1,360 $W \cdot m^{-2}$ (US DoE, 2005). The Solar Simulator PBR was used to investigate the photosaturation and photoinhibition effects on algal growth at high light intensities. A sketch of the reactor is shown in Figure 5.02b.

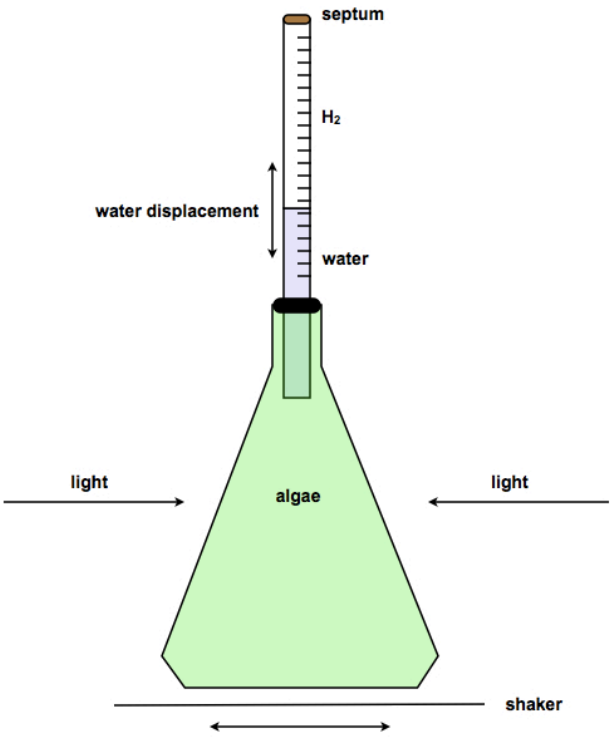


Figure 5.02a: Solar Biofuels Consortium PBR

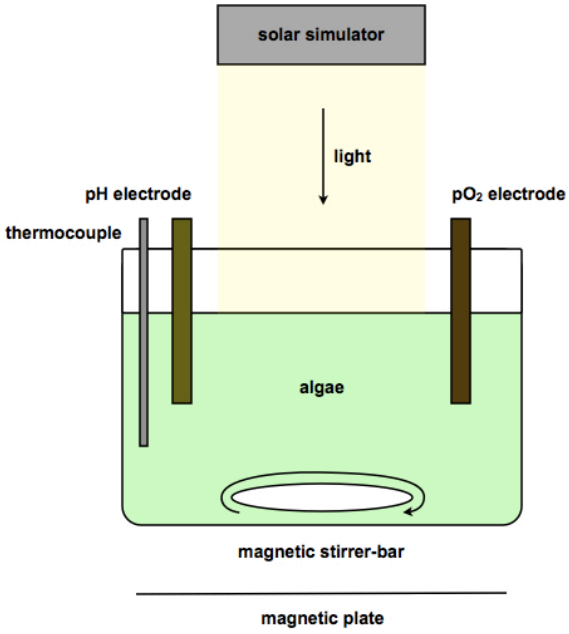


Figure 5.02b: Solar Simulator PBR

5.3.2. Vertical-column PBRs

Commercial Plankton Light Reactors (Aqua Medic) were used to grow *C. reinhardtii* stock cultures for use in subsequent experiments and to conduct preliminary algal growth experiments. The reactors have a working volume of approximately 1.5 litres. They are illuminated by a cool-white fluorescent tube, which spans the length of the reactor and supplies a fixed light intensity of 42.5 $W \cdot m^{-2}$. The incoming light is concentrated by a reflector, a process that also heats up the culture to the required 20-28ºC. The PBR is connected to an air compressor pump, which delivers gas-lift mixing to the system. This ensures that the *C. reinhardtii* cells do not sink to the bottom of the reactor and that the algal illumination and mineral nutrient requirements are satisfied throughout the growth process. The algal biomass can multiply four-fold within 24 hours and the culture is typically sufficiently grown in 3-7 days, depending on the initial cell density and the algal strain. Algae in vertical-column PBRs were grown mixotrophically, using both CO_2 and acetate as carbon sources. The vertical-column PBRs had two major experimental limitations, namely that only a fixed light intensity was available and that all concentration and OD measurements had to be carried out by sampling. A sketch of the vertical-column reactor is shown in Figure 5.03.

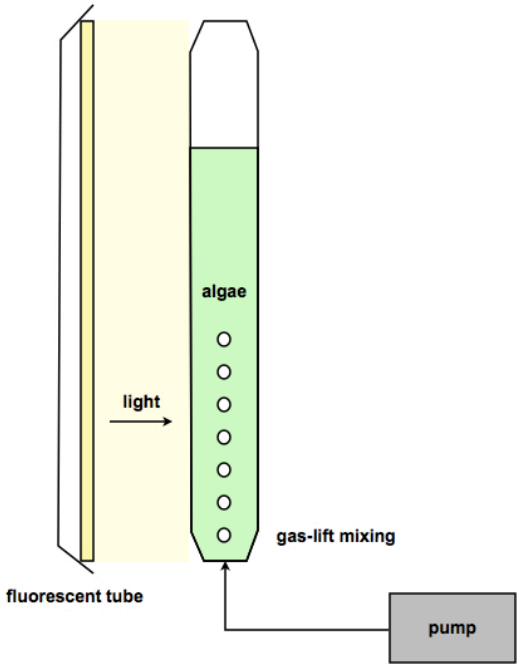


Figure 5.03: AquaMedic Plankton Light Reactor

5.3.3. Tubular PBR

The Sartorius Biostat PBR 2S is a tubular flow reactor with layer pipe illumination that is suitable for microalgal phototrophic applications. The Sartorius PBR is composed of a 1 litre central vessel, surrounded by a 2 litre helix and has a maximum working volume of 2.7 litres. All the sampling equipment, measuring probes and temperature control systems are located in the recirculation and conditioning vessel at the centre of the reactor. This central vessel houses a thermocouple as well as pH, pO_2 and OD probes that are used for *in situ* measurements. Variables such as the light intensity, temperature and pH are controlled using the touch-screen Micro DCU-System display on the control tower, which also logs measurement data using specialised software. The Sartorius PBR data acquisition system is shown in Figure 5.04a.

The 2 litre photosynthetic module has been designed using a helix geometry to provide optimum illumination efficiency per surface area. Algae within the helix are exposed to a circular array of cool white fluorescent lights, which is located between the central vessel and the helix (Figure 5.04b). The culture is efficiently circulated up and around the helix, through the central vessel, and back into the helix by means of a peristaltic pump (Figure 5.04c). The main limitation of the Sartorius PBR is that the complexity of its design with large numbers of joints on the fluid flow line, together with the nature of its peristaltic pump, makes it very difficult to minimise diffusive H_2 losses from the reactor. As a result, the Sartorius PBR was used primarily to measure *C. reinhardtii* growth kinetics under different light intensities. The Sartorius PBR was run as an open system to encourage mixotrophic algal growth.

The Sartorius PBR has the capacity to control the light intensity of the accompanying fluorescent light array, but the light intensity values are given as a percentage of the maximum light output. A light meter was used to determine a linear relationship between the Sartorius percentage units and PAR units, as shown in Figure 5.04d and Equation 5.15.

$$PAR\ (\mu E \cdot m^{-2} \cdot s^{-1}) = 3.8 \cdot Sartorius\ units\ (\%) - 55 \qquad \textit{Equation 5.15}$$

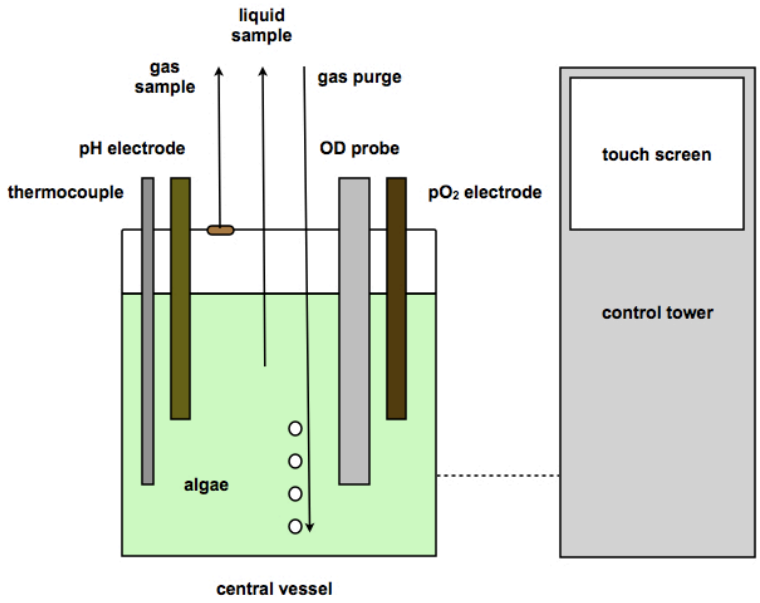


Figure 5.04a: Sartorius PBR; measurement, sampling and control

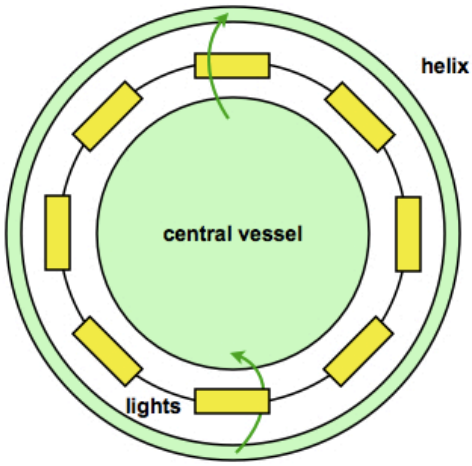


Figure 5.04b: Sartorius PBR; central vessel, helix and light

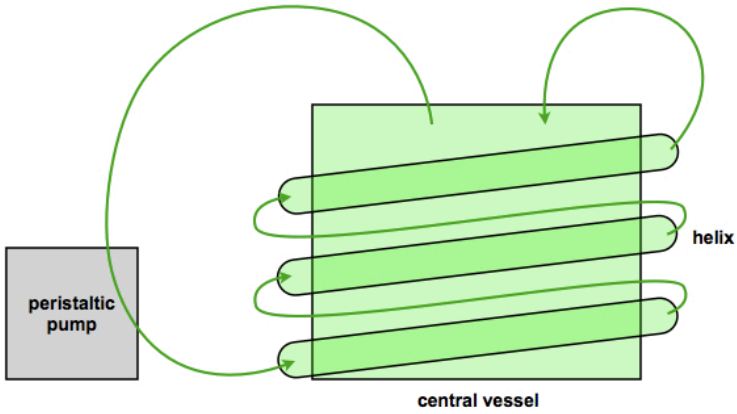


Figure 5.04c: Sartorius PBR; circulation and mixing

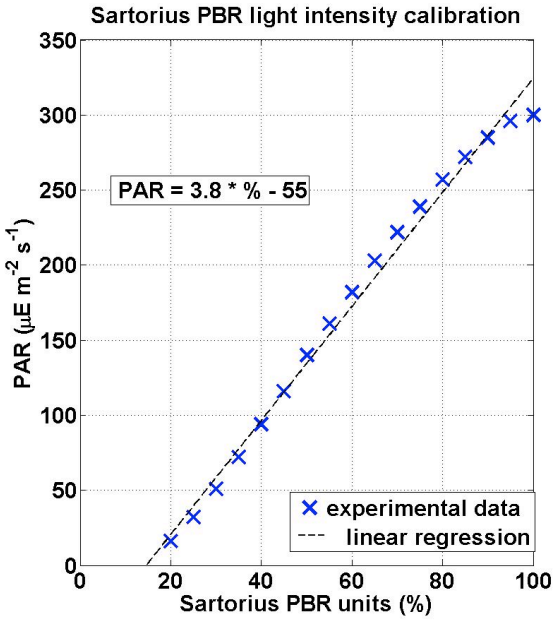


Figure 5.04d: Sartorius PBR; light intensity calibration

5.3.4. Flat-plate PBRs

The ICL Chemical Engineering flat-plate PBRs were specifically designed to facilitate *C. reinhardtii* H_2 production. The design, development, characterisation and commissioning of these PBRs represents a key development in this research and is described in detail in Chapter I (Tamburic *et al*., 2011b). The ICL Chemical Engineering PBRs were manufactured by Paul Crudge in the Chemical Engineering Workshop at Imperial College. The ICL Chemical Engineering PBR is illuminated with a cool-white LED array. The algal culture is mixed by means of a recirculating gas-lift flow powered by a diaphragm pump. The PBR has the capacity to control temperature, light intensity and wavelength, and to measure the pH, pO_2, temperature and OD of the culture. Measurement, datalogging and control were carried out using the National Instruments Compact RIO controller. A special mass spectrometry technique was developed to measure H_2 production *in situ*. A syringe-based dosing pump was used to perform sulphate re-addition experiments. Photographs of all the PBRs are shown in Figure 5.05.



Figure 5.05: Photobioreactor photographs

5.3.5. Cleaning and Maintenance

All PBRs require careful cleaning and maintenance to avoid damage and contamination. The stirred-tank, vertical-column and flat-plate PBRs were initially cleaned with common kitchen bleach. Occasionally, the bleach was not strong enough to remove all contaminants and it was eventually upgraded to Trigene. Trigene is a particularly powerful bleach that is used to sterilise medical equipment and to clean blood stains, faeces and other high-level contaminants. Trigene proved to be a very effective chemical sterilisation agent. The fungicide Carbendazim (Mahan *et al.,* 2005) was dissolved in small concentrations in the algal growth medium during periods of extremely bad fungal contamination.

The Sartorius PBR proved particularly difficult to clean because there is no direct access to the interior of the tubular helix. It is impractical to use Trigene since it is difficult to rinse out of the helix and it would therefore be likely to affect subsequent experiments. Instead, cleaning was carried out with dilute hydrogen peroxide (H_2O_2), a strong oxidising agent that is frequently used as a disinfectant and an antiseptic. H_2O_2 was used to rinse out and decontaminate the inside of the PBR. It offers the added benefit of dissociating into water and O_2 upon the addition of hot water, hence leaving no harmful chemicals in the PBR at the end of the cleaning procedure. After H_2O_2 was applied, the reactor was rinsed 2-3 times with warm water to remove all traces of H_2O_2 and any remaining algal cell clusters. The sensitive measuring probes (pH and pO_2) were not directly exposed to H_2O_2 but cleaned separately and later re-inserted into the reactor.

The cleaning procedures produce a large volume of algal biowaste that must be disposed of. In a large-scale industrial process, the algae would need to be dried and processed so that the biomass can be used for electricity generation, biodiesel production or fermentation (Morweiser *et al*., 2010; Stephens *et al*, 2010a). It is neither beneficial nor practical to do this with small algal volumes. Wild type *C. reinhardtii* cells were therefore left for 24 hours in a biowaste container containing Virkon tablets, at which point all cells were dead and could be disposed of safely down the sink. GM *C. reinhardtii* strains, such as pdc3-KD and s21, were disposed of separately according to the procedure for biohazardous waste (BBSRC, 2010).

5.4. Instrumentation

5.4.1. Measuring Instruments and Probes

A Pt100 Type 25-3 thermocouple was used to measure the temperature in the Sartorius tubular PBR and feed these data back to the Sartorius control tower. Temperature was maintained at 25°C by means of a water bath in the double-layered central vessel. The Hamilton Easyferm Plus K8 160 pH electrode was used to measure the activity of hydrogen ions surrounding this probe. The Oxyferm FDA 160 oxygen tension probe (Hamilton) was used to measure the pO_2 by means of a Clark electrode suspended in oxylyte electrolyte. The Sartorius Fundalux II OD probe, containing an LED that operates in the 870-910 nm wavelength range, was used to measure the optical density of the algal culture. This OD was correlated with the Chl content using Equation 5.12.

The temperature in the ICL Chemical Engineering PBRs was measured using a K-type thermocouple from Omega. Two probes were used: the SP10T pH electrode and the SZ10T galvanic pO_2 electrode (Consort). OD was measured using a photodiode operating with an absorption bandwidth of 650-700 nm. All the measurements were recorded using a National Instruments datalogging and control system based around the National Instrument Compact RIO processor and running LabView software (Tamburic *et al*., 2011b).

The Solar Simulator PBR also made use of the K-type thermocouple and the Consort pH and pO_2 electrodes. The data was collected using a Consort datalogging unit. OD in the Solar Simulator PBR, Solar Biofuels Consortium PBRs and AquaMedic Plankton Light Reactors was measured by sampling followed by spectrophotometer analysis at 663 nm.

5.4.2. Calibration

The pH probes were calibrated using three buffer solutions with known pH values (pH 4.01, pH 7.00 and pH 9.12). The pO_2 probes were calibrated to 0% oxygen in nitrogen-saturated water, 21% in air-saturated water and 100% in O_2-saturated water. These dissolved oxygen concentrations were established by purging a *C. reinhardtii* culture with N_2, air and O_2, respectively. The OD probe

reading was auto-zeroed in distilled water. The photodiode was calibrated using spectrophotometric measurements. Specific pH, pO_2 and OD calibrations will be discussed in Chapter I.

5.5. Medium Preparation

5.5.1. TAP

C. reinhardtii cultures are known to grow well in tris-acetate phosphate (TAP) growth medium. The TAP medium was prepared according to the classic recipe devised by Gorman & Levine (Gorman & Levine, 1966). Stock solutions of TAP salts, phosphate solution (P-solution) and Hutner's trace elements were prepared first. TAP salts were prepared by dissolving ammonium chloride (NH_4Cl), magnesium sulphate ($MgSO_4$) and calcium chloride ($CaCl_2$) in deionised water (Table 5.06a). P-solution is a buffer solution prepared from potassium phosphate monobasic (KH_2PO_4), potassium phosphate dibasic (K_2HPO_4) salts dissolved in deionised water (Table 5.06b). Hutner's trace elements include traces of iron, manganese, copper, zinc, boron, cobalt and molybdenum; this solution was supplied by colleagues from the Department of Biology at Imperial College London. The TAP recipe, shown in Table 5.06c, includes TAP salts, P-solution, Hutner's trace elements, acetic acid and tris-(hydroxymethyl)-aminomethane (Tris). Acetic acid provides the acetate ion, the carbon source for photoheterotrophic or photomixotrophic *C. reinhardtii* growth (Antal *et al*., 2003). Tris is the primary buffer of the TAP medium.

The TAP medium provides all the necessary nutrients for algal growth (carbon, nitrogen, sulphur, phosphorus and trace metals) but it also contains expensive ingredients such as acetate, ammonium and phosphate (Tsygankov *et al*., 2006). Optimising the use of acetate is important for limiting biohydrogen production costs, particularly in large-scale systems (Degrenne *et al*., 2010). Since S-deprivation induces the onset of anaerobic H_2 production, controlling sulphate levels is an intuitive way of controlling H_2 production. The TAP medium is overloaded with all key nutrients except for acetate, which normally runs out in the first three days of algal growth (Laurinavichene *et al*., 2004; Faraloni *et al.,* 2011).

The TAP growth medium was brought to the pH appropriate for algal growth (typically pH 7.0) by titration with hydrochloric acid and sodium hydroxide, using a standard pH sensor as the indicator. A magnetic stirrer bar was inserted into the glass flask containing the TAP medium to enable agitation of the system during this titration. Once the TAP medium was ready, the flask was

sterilised in an autoclave at 120°C to kill any contaminating microorganisms. Stock solutions of TAP salts, P-solution and Hutner's trace elements were prepared in 100-1,000 ml batches and stored in a refrigerator at 5°C. The TAP medium, on the other hand, was prepared and autoclaved shortly before an experiment to minimise the risk of bacterial or fungal contamination (Gorman & Levine, 1966).

C.reinhardtii cells were scraped off an agar plate and re-suspended in an autoclaved 25 ml flask filled with sterile TAP medium. This procedure was performed inside a laminar flow hood, a device that filters ambient air to minimise particulate concentrations. The working surface of the sterile hood and the nitrile lab gloves were washed with 70% ethanol. It is extremely important to maintain a sterile environment during the early stages of algal growth, because this is the period when the culture is most vulnerable to contamination. The 25 ml flask was kept under the optimal algal growth conditions recommended in the literature: at room temperature, with starting pH 7.0 and under cool white fluorescent light (Tsygankov *et al*., 2006). A mechanical shaker provided mixing and aeration. After approximately 5 days of growth, the culture was scaled up to a volume of 250 ml. Once again, a sterile hood was used to transfer the contents of the 25 ml flask into a 250 ml flask, which was then topped up with fresh TAP medium. As the cell density of *C.reinhardtii* increased, the culture became greener and less transparent. The entire growth process lasted less than 2 weeks. At that point, the culture was scaled up to 2-3 litres, a volume that is sufficient for use in PBRs (Amos, 2004). If the majority of algal cells die, either through contamination or as a result of S-deprivation, the culture begins to turn yellow and give out a strong smell. Eventually, black clusters of dead algal cells form and precipitate.

Table 5.06a: TAP salts recipe

Salt	Mass
NH_4Cl	15.0 g
$MgSO_4$	4.0 g
$CaCl_2$	2.0 g

dissolve in 1 litre of deionised water

Table 5.06b: P-solution recipe

Salt	Mass
KH_2PO_4	14.4 g
K_2HPO_4	28.8 g

dissolve in 100 ml of deionised water

Table 5.06c: TAP medium recipe

Component	Quantity
TAP salts	25 ml
P-solution	0.375 ml
Hutner’s trace elements	1 ml
Acetic acid	1 ml
Tris	2.42 g

dilute to 1 litre with deionised water, titrate to pH 7.0

5.5.2. TAP-S

Under standard conditions, *C. reinhardtii* will photosynthesise, using water and energy from sunlight to fix CO_2 and produce sugar and oxygen. The cells also undergo respiration using up O_2 and stored carbon to provide the energy needed for growth and reproduction. Sulphur deprivation (S-deprivation) results in metabolic changes within *C. reinhardtii*, with an initial accumulation of starch and breakdown of endogenous protein and fat. It also reduces photosynthetic rates as sulphur is required to repair PSII damage. The result is that O_2 evolution gradually decreases while respiration levels are maintained, causing the culture to become anaerobic. Once all O_2 in the system has been used up by respiration, the algal cells have the ability to switch to anaerobic fermentative metabolism, which involves both the use of solar energy to break down water, generating ATP and H_2, and the breakdown of starch into formic acid, ethanol, acetic acid, malic acid, carbon dioxide and H_2 (Melis, 2002).

The most practical way of inducing H_2 production is by replacing the sulphur-replete TAP medium with TAP-S (without sulphur; -S), its sulphur-deplete counterpart (Melis *et al*., 2000). This was typically achieved by replacing the sulphate salts in the TAP medium with their chloride derivatives to make TAP-S and exchanging the algal growth medium by centrifugation. In practical terms, it was first necessary to prepare a stock culture of TAP-S salts, achieved by replacing $MgSO_4$ with magnesium chloride ($MgCl_2$), as shown in Table 5.07a. Sulphur-deplete Hutner's trace elements were also prepared. Table 5.07b shows the recipe for preparing TAP-S; the procedure is very similar to the preparation of TAP.

5.5.3. HSM

High-salt medium (HSM) is a version of TAP without acetate that is used for photoautotrophic *C. reinhardtii* growth (Doebbe *et al.,* 2007). The acetic acid was removed, which also abolished the necessity for the Tris buffer. P-solution became the primary buffer and its concentration was increased to 5 ml per litre of HSM. The concentration of TAP salts and Hutner's trace elements was identical to the TAP medium. Table 5.08 gives the HSM recipe. HSM was titrated to a starting pH of 6.8 using hydrochloric acid and sodium hydroxide.

Table 5.07a: TAP-S salts recipe

Salt	Mass
NH_4Cl	15.0 g
$MgCl_2$	4.0 g
$CaCl_2$	2.0 g

dissolve in 1 litre of deionised water

Table 5.07b: TAP-S medium recipe

Component	Quantity
TAP-S salts	25 ml
P-solution	0.375 ml
Hutner's trace elements -S	1 ml
Acetic acid	1 ml
Tris	2.42 g

dilute to 1 litre with deionised water, titrate to pH 7.0

Table 5.08: HSM medium recipe

Component	Volume
TAP salts	25 ml
P-solution	5 ml
Hutner's trace elements	1 ml

dilute to 1 litre with deionised water, titrate to pH 6.8

5.5.4. Customised Media

It is possible to make other small variations to the TAP medium without reducing algal growth rates. For example, it is possible to reduce the concentrations of sulphate and ammonium salts in the TAP medium, as long as these changes do not result in the deprivation of one of these key nutrients. It is also possible to change the concentration of acetate if it is matched by an equivalent change in the concentration of the buffer solutions (Tris and P-solutions) and as long as the medium is titrated back to pH 7.0 using sodium hydroxide. The 5xTAP* medium (Table 5.09a) was overloaded with acetate (five times the standard TAP concentration) to investigate acetate uptake kinetics during the entire algal growth stage. The increase in the acetate concentration was balanced by an increase in the concentration of the phosphate buffer. The TAP_{12} medium (Table 5.09b) was prepared to facilitate nutrient-controlled H_2 production in the ICL Chemical Engineering PBR at a light intensity of 12 Wm^{-2}; the acetate and sulphate concentrations were optimised for these conditions, as will be demonstrated in Chapter III. The concentrations of the key biosynthesis ions in TAP, TAP-S, HSM, 5xTAP* and TAP_{12} media are shown in Table 5.10.

The duration of *C. reinhardtii* H_2 production may be increased by sulphur re-addition. Sulphur re-addition techniques and outcomes will be described in Chapter IV. One technique is to continuously feed a micromolar concentration of sulphate ions to an anaerobic, H_2-producing *C. reinhardtii* culture in order to facilitate PSII recovery. The components of this sulphur-feed medium are given in Table 5.11. The sulphur-feed medium contains 1,000 ppm of SO_4^{2-} and 10,000 ppm of CH_3COO^-. The sulphate concentration is based on the maximum sulphate uptake rate during *C. reinhardtii* growth, which is approximately 20 $ppm \cdot day^{-1}$ (Chapter III). A medium feed rate of less than 20 $ml \cdot day^{-1}$ is therefore required to satisfy PSII repair requirements, hopefully without overloading the medium with sulphate and terminating H_2 production. The intention was to keep sulphate concentrations of the algal medium below 2 ppm, the minimum tolerance level for H_2 production (Kim *et al.,* 2010). At the same time, it was necessary to provide a small acetate feed so that the culture would not fail due to a lack of carbon; the 1:10 SO_4^{2-}:CH_3COO^- ratio was established by trial and error. Since the nutrient feed was highly acid, a strong buffer was required. 4-(2-hydroxyethyl)-1-piperazineethanesulfonic acid (HEPES) buffer was used in accordance with the sulphur re-insertion technique developed by Kim and co-workers (Kim *et al*., 2010).

Table 5.09a: 5xTAP* medium recipe

Component	Quantity
TAP salts	25 ml
P-solution	1.875 ml
Hutner's trace elements	1 ml
Acetic acid	5 ml
Tris	12.10 g

dilute to 1 litre with deionised water, titrate to pH 7.0

Table 5.09b: TAP_{12} medium recipe

Component	Quantity
TAP salts	18 ml
P-solution	0.938 ml
Hutner's trace elements -S	1 ml
Acetic acid	2.5 ml
Tris	6.05 g

dilute to 1 litre with deionised water, titrate to pH 7.0

Table 5.10: Concentration of dissolved ion species in various growth media

		Algal growth medium				
	Species	**TAP**	**TAP-S**	**HSM**	**5xTAP***	**TAP_{12}**
Concentration ($mg \cdot l^{-1}$)	**CH_3COO^-**	1,020	1,020	0	5,100	2,550
	NH_4^+	126	126	126	126	91
	SO_4^{2-}	48[a]	0	48[a]	48[a]	29[b]
	PO_4^{3-}	0.4	0.4	5.3	2.0	1.0

a: 41 $mg \cdot l^{-1}$ from 25 ml TAP salts, 7 $mg \cdot l^{-1}$ from 1 ml Hutner's trace elements

b: 29 $mg \cdot l^{-1}$ from 18 ml TAP salts, sulphur-deplete Hutner's trace elements

Table 5.11: Sulphur-feed medium recipe

Component	Quantity
$MgSO_4$	0.8 g
Acetic acid	10 ml
HEPES	11.2 g

dilute to 1 litre with deionised water

5.6. Sulphur-deprivation Techniques

Centrifugation and dilution are accepted methods for causing S-deprivation in *C. reinhardtii* (Melis *et al*., 2000; Laurinavichene *et al.,* 2002). Nutrient control is a novel sulphur-deprivation technique that will be developed in this thesis. The details of each procedure are given below.

5.6.1. Centrifugation

The S-deprivation process has traditionally been initiated by centrifugation (Ghirardi *et al*., 2000). The algae were first grown in TAP medium until the required Chl content was obtained; approximately 20 $mg \cdot l^{-1}$ of culture is sufficient for H_2 production, but higher chlorophyll concentrations are desirable (Tsygankov *et al.,* 2006). Once ready, the culture was centrifuged at 14,000 rpm for 15 minutes and a dark green pellet of algal cells formed at the bottom of the centrifugation vessel. The TAP medium was discarded and the algae were washed with, and re-suspended in, TAP-S medium in the ICL Chemical Engineering PBR, where they proceeded to consume all available O_2 before commencing anaerobic H_2 production. At least 20% of algal cells were lost during centrifugation, with additional cells damaged by the compressive stress endured during the process (Kosourov *et al.,* 2002). The centrifugation process is very time, energy and labour intensive, and it is therefore impractical for any large scale application, thus motivating the need for a nutrient controlled method of H_2 production.

5.6.2. Dilution

The dilution method is an alternative way of inducing S-deprivation. A small inoculum of algal cells (growing in TAP) was diluted in a large volume of TAP-S. The algae continued to grow until all sulphur was used up, at which point the O_2 consumption stage and subsequent H_2 production began. A dilution of 10% cells/TAP-S has been shown to work experimentally (Laurinavichene *et al.,* 2002) and was therefore used in this thesis. The main disadvantage of the dilution method is that the algae never achieve the high cell densities common to the centrifugation method due to the significantly lower number of PSII reaction centres. The H_2 yield following dilution is approximately a factor of five lower than that of centrifugation (Laurinavichene *et al.,* 2006). On

the other hand, dilution is a lot more energy efficient, does not require any specialised equipment and does not impose shear stress on the algal cells.

5.6.3. Nutrient Control

The nutrient control method of H_2 production was developed in this thesis to optimise algal growth and maximise H_2 production without the need to exchange media by centrifugation at any stage of the process. This was achieved by accurately measuring algal growth rates and acetate and sulphate uptake rates under different growth conditions. The intention was that, given a set of initial conditions, it would be possible to predict exactly how quickly the algae would grow and precisely how much acetate and sulphate they would require to get there. On this basis, a growth medium (TAP_{12}, Table 5.09b) was designed to ensure that all sulphur would run out just as the algae attained their maximum OD, leading to spontaneous and effective H_2 production.

5.7. Analytical Techniques

5.7.1. Spectrophotometry

Spectrophotometry was used to determine the OD of an algal culture by light scattering. OD, measured in absorbance units (AU), has a linear correlation with the Chl content and the algal cell count of that culture (Figure 5.01). A Lambda 40 UV/Vis Spectrometer (Perkin-Elmer Instruments) running the UV WinLab software was used to measure OD at the algal PSII absorption peak of 663 nm. The OD reading at this photosynthetic wavelength maximum is the most responsive measurement to changes in the optical thickness of the culture (Tamburic *et al*., 2011b). At 663 nm, 1 AU is equal to 17.9 $mg \cdot l^{-1}$ of Chl, or approximately 26 million algal cells. Algal samples were analysed in a 1.5 ml cuvette and the instrument was auto-zeroed with the light scattering measurement from a cuvette filled with deionised water. Spectrophotometric OD measurements were also used to calibrate the flat-plate reactor photodiode for experiments at specific light intensities.

5.7.2. Ion Chromatography

Ion chromatography (IC) was carried out using the 882 Compact IC Plus instrument with an 863 Compact Autosampler (Metrohm) running the MagIC Net software. The technique used a Metrosep A Supp 10 separation column, which is capable of analysing compounds whose concentrations differ widely. The concentrations of compounds coming off the column were measured by means of a conductivity detector in units of microSiemens per centimetre ($\mu S \cdot cm^{-1}$). The sodium-based anion solution (liquid phase) consisted of 3.2 mM sodium carbonate, 1.0 mM sodium bicarbonate and 5.0 µM sodium perchlorate. Deionised water was used as the rinse and 0.1 M sulphuric acid as the regenerator. The liquid phase was pumped through the instrument using a peristaltic pump at a flow rate of 1.0 $ml \cdot min^{-1}$. Algal samples were spun down in a mini-centrifuge at 13,000 rpm for 10 min: the purified medium was used for IC and high-performance liquid chromatography and the algal pellet was discarded. Samples of 25 µl were injected into the IC instrument. The anion concentrations corresponded to the area occupied by their respective peaks. These areas were calibrated against concentration using CertiPUR Anion Multi-Element Standards (Merck) at

concentrations of 1 ppm, 10 ppm, 50 ppm, 100 ppm and 200 ppm (1 ppm = 1 $mg \cdot l^{-1}$). The anions coming off the column included PO_4^{3-} and SO_4^{2-} with a retention time of 12.2 min and 22.0 min respectively. It was subsequently determined that the phosphate concentrations present in the algal growth medium were not sufficiently high to be tracked by this technique. IC was therefore primarily used to measure the sulphate uptake during algal growth. The IC signal also contained peaks at 2.1 min and 3.9 min, which were believed to correspond to chloride (Cl^-) and CH_3COO^- respectively. It was not possible to calculate the concentrations of these ions from the conductivity signals generated using the A Supp 10 column. A representative IC result, showing the Cl^-, CH_3COO^-, PO_4^{3-} and SO_4^{2-} conduction peaks, is presented in Figure 5.06.

5.7.3. High-Performance Liquid Chromatography

High-performance liquid chromatography (HPLC) was performed using the Hewlett Packard Series 1050 instrument running HPCORE ChemStation software. The technique was based on a well-established procedure designed to investigate the concentration of fermentative products such as organic acids and alcohols (Ding *et al*., 1995). The Aminex HPX-87H Ion Exchange Column from BioRad (HPLC Organic Acid Analysis Column) was used at a temperature of 58.0ºC together with a BioRad guard column. Compounds were detected by means of an ultra-violet (UV) detector operating at 210 nm and measuring light absorption units of milliwatts per centimetre squared ($mW \cdot cm^{-2}$). The liquid phase consisted of 4 mM sulphuric acid, which was peristaltically pumped through the column at a flow rate of 0.6 $ml \cdot min^{-1}$. Having been spun down at 13,000 rpm for 10 min, 50 µl medium samples were injected into the instrument by means of an autosampler. HPLC was principally used to measure the acetate (CH_3COO^-) uptake during algal growth. A strong acetate peak was observed with a residence time of 15.1 min and the peak area was calibrated against acetate concentration using 20,000 ppm, 5,000 ppm 1,000 ppm and 200 ppm standards prepared from 99.99% pure acetic acid. This HPLC technique was also used to measure the fermentation products during anaerobic H_2 production, but those experiments fall outside the scope of this thesis. A representative HPLC result is depicted in Figure 5.07; the CH_3COO^- UV peak dominates all other signals.

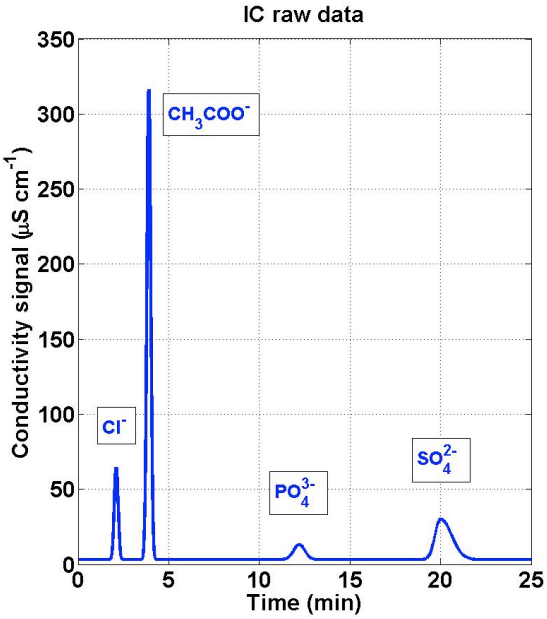


Figure 5.06: Representative ion chromatography (IC) results

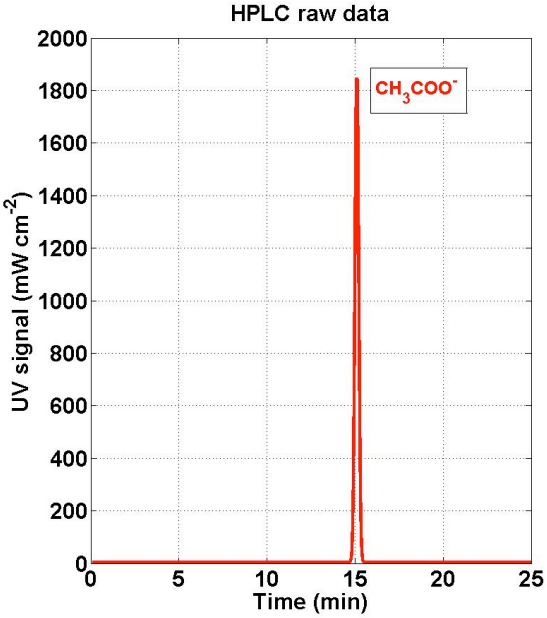


Figure 5.07: Representative high performance liquid chromatography (HPLC) results

5.7.4. Mass Spectrometry

The mass spectrometer (MS) is an instrument that identifies the chemical composition of a compound or sample by measuring the ionic mass-to-charge ratio of its constituent elements. The MS contains an ioniser to chemically fragment the compound into its charged particles, a detector to capture those particles and a suction pump that creates a vacuum system between the ioniser and the detector. Ions are separated on a mass basis; they impact the detector, inducing a current or a charge (Beckmann K. *et al*., 2009). A compact quadrupole Pfeiffer Vacuum Prisma MS running Windows Quadstar 422 software was used in this thesis.

Injection MS was used to identify the components of the gaseous product emitted by a sulphur-deprived *C. reinhardtii* culture. An argon (Ar) carrier gas flow of 25 $ml \cdot min^{-1}$ was fed into the MS, which was set to continuously scan across all mass-to-charge ratios and take measurements of the relevant atomic masses (H_2, water, N_2, O_2, Ar and CO_2; atomic mass = 2, 18, 28, 32, 40 and 44, respectively). Figure 5.08 shows a representative result of this scan; it represents the injection MS background measurement. A gas-tight syringe was used to inject 0.5 ml of gas phase from the sulphur-deprived culture into the Ar carrier gas stream via a septum. This produced a number of peaks in the MS readings corresponding to the presence of particular atomic masses in the injection. Injections were repeated three times to verify the consistency of the measurements. The syringe was dipped into acetone to sterilise it before injections were taken. It was important to use a heated (110°C) MS capillary to prevent any moisture in the injection from blocking the carrier gas path to the MS ioniser. Injection MS results will be described in Chapter III. Membrane-inlet mass spectrometry (MIMS) is an analytical technique used to measure *in situ* concentrations of dissolved gasses or volatile organic compound in aqueous solutions (Scott *et al*., 1983). The development of a MIMS system for the ICL Chemical Engineering PBR will be described in Chapter I.

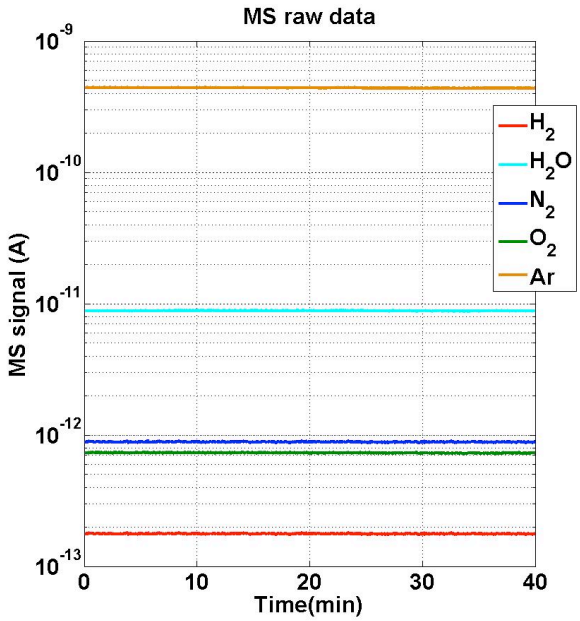


Figure 5.08: Representative result of an ion monitoring graph obtained using the mass spectrometer

5.8. Mathematical Models

5.8.1. Logistic Growth Model

A logistic (sigmoid) function has been frequently and effectively used to fit kinetic parameters to algal growth and nutrient uptake data (Kooijman *et al*., 1983; Lemesle & Mailleret, 2008). When modelling growth kinetics, OD may be described as a function of time using Equation 5.16. In this formulation, the parameter *K* represents the maximum OD obtained in a particular experiment. The parameter t_0 is the inflexion point of the function, which may be normalised to compare growth rates of algal cultures with diverse starting ODs and different start-up rates. The most important parameter is *r*, the specific growth rate of the culture. It is important to note that any use of 'specific growth rate' in this thesis will refer to *r*, the growth parameter defined by the logistic growth model. Equation 5.17 may be used to convert *r* to the doubling time (T_d), the most common unit for describing algal growth. By differentiating Equation 5.16 with respect to time, it is possible to determine the gradient at t_0 (Equation 5.18), which is the maximum growth rate (r_{max}) of the culture.

$$OD(t) = \frac{K}{(1 + e^{-r(t-t_0)})} \qquad \textit{Equation 5.16}$$

$$T_d = \frac{\ln(2)}{r} \qquad \textit{Equation 5.17}$$

$$r_{\max} = \frac{K \cdot r}{4} \qquad \textit{Equation 5.18}$$

In the case of nutrient uptake, an inverted form of the logistic function, shown in Equation 5.19, was fitted to experimental data in order to reflect the observed decrease in nutrient concentration. In this scenario, *K* becomes the total quantity of a nutrient that has been consumed and *r* becomes the corresponding consumption/uptake rate. *C(t)* is the time-dependent nutrient concentration function while C_f is the final nutrient concentration following the experiment. The final nutrient concentration can be calculated using the pre-determined initial nutrient concentration, C_i and the total quantity of nutrient consumed, *K* (Equation 5.20).

$$C(t) = \frac{K}{(1 + e^{r(t-t_0)})} + C_f \qquad \textit{Equation 5.19}$$

$$C_f = C_i - K \qquad \textit{Equation 5.20}$$

Fitting a logistic curve to discrete experimental data requires the simultaneous optimisation of three independent parameters, a task that has been studied extensively in the field of ecology (Cavallini, 1993). The accepted procedure is to assign a random initial value to K, then minimise the total least squared error in r and t_0. This assigns the correct shape to the logistic curve and K is subsequently recovered by linear optimisation. Mathematical solutions to the logistic growth model will be described in more detail (with examples) in Chapter II.

5.8.2. Aiba Growth Model

The algal-specific growth rate initially increases with light intensity, but it eventually saturates to a maximum value, μ_{max}. Previous work on algal growth kinetics has revealed that the growth rate not only saturates at μ_{max}, but may also experience subsequent photoinhibition (Molina Grima *et al*., 1999). This behaviour is described by the Aiba model (Equation 5.21).

$$\mu = \frac{\mu_{\max} \cdot I}{k_s + I + \frac{I^2}{k_i}} \qquad \textit{Equation 5.21}$$

where			
	μ	specific growth rate (also called r)	[h^{-1}]
	μ_{max}	maximum specific growth rate	[h^{-1}]
	I	light intensity	[$W \cdot m^{-2}$]
	k_s	light saturation term	[$W \cdot m^{-2}$]
	$\frac{I^2}{k_i}$	photoinhibition term	[$W \cdot m^{-2}$]

The parameters of the Aiba model were recovered in a similar way to their logistic model counterparts: k_s and k_i values were optimised using the method of least squares before μ_{max} was recovered by linear optimisation. Applications and examples of the Aiba growth model will be shown in Chapter II.

6. Results and Discussion

I. Flat-plate PBR Design and Characterisation

I.1. Introduction to PBR Design

A novel flat-plate PBR was designed, constructed, characterised, commissioned and operated within the Chemical Engineering Department at Imperial College London. It was manufactured by Paul Crudge in the departmental workshop. Consequently, it has been named the ICL Chemical Engineering PBR. Two of these ICL Chemical Engineering PBRs were used to carry out a number of the *C. reinhardtii* growth experiments and all of the H_2 production experiments described in this thesis.

The motivation for designing the ICL Chemical Engineering flat-late PBR was to create a simple system that would enable quick measurement of the key parameters in the biohydrogen production process under carefully controlled conditions. Since the availability of light is normally the limiting factor for algal growth and H_2 production, the reactor geometry that offers the highest surface-to-volume ratio was selected: the vertical flat-plate reactor. When selecting reactor materials, it was important to consider their strength, durability, spectral properties, toxicity to algal cells, and the permeability to H_2 (Skjånes *et al*., 2008). A dual-compartment reactor design was used to enable effortless control of the temperature and of the wavelength incident on the *C. reinhardtii* culture. The reactor was designed to be fully autoclavable to minimise the possibility of contamination, and completely modular to allow easy cleaning and maintenance between experiments (Nedbal *et al*., 2008). The choice of a minimalistic reactor design and the selection of materials and ancillary systems equipment were made with the intention of keeping the cost of this flat-plate PBR as low as possible, competitive with targets laid out in the literature (Ghirardi *et al*., 2000; Amos, 2004).

The flat-plate PBR ancillary systems were concerned with illumination, mixing, measurement, datalogging and the user control interface. Illumination was provided by an LED array and the main challenge was to select the correct geometric configuration for optimal light exposure (Janssen *et*

al., 2003). Diaphragm pumps were used to fulfil the mixing requirements by operating in the turbulent flow regime with appropriate mixing patterns and low levels of shear stress on the culture (Carvalho *et al*., 2006). As part of the design specification, the parameters that should be controlled and measured were selected. The critical control parameters were light intensity, wavelength, temperature and culture mixing (Carvalho *et al*., 2006). Commercial probes were used for *in situ* pH and pO_2 measurements. Membrane Inlet Mass Spectrometry (MIMS) was developed to accurately measure H_2 production rates and yields (Beckmann K. *et al*., 2009). The algal growth rate was monitored by continuously measuring the optical thickness of the culture using a photodiode. Datalogging and the user control interface were implemented by means of a National Instruments system.

This chapter will describe the ICL Chemical Engineering PBR design, including the rationale for, and the execution of, the compartmental design concept. The structure of the mixing and circulation ancillary system will be described. The application of MIMS to biohydrogen production measurement will be justified and the MIMS system design will be described and explained. The electronics and the software behind the datalogging and control system will be revealed. The second part of this chapter will deal with the flat-plate PBR characterisation. The light intensity distribution, wavelength modulation and heat transfer by the PBR will be explored. The calibration of the pH and pO_2 probes, the photodiode and the MIMS system will then be described. Finally, the flat-plate PBR and MIMS system will be operated to compare the dark H_2 production of *C. reinhardtii* cc124 WT strain with that of the pdc3-KD fermentation mutant.

I.2. Design and Construction

I.2.1. Compartmental Design

The novel dual-compartment flat-plate PBR design is shown in Figure I.01. The reactor body was made of Perspex (polymethyl methacrylate), a transparent polymer alternative to glass that is relatively inexpensive, autoclavable and easy to handle and process. The Perspex body consists of a 5 mm thick separator sheet sandwiched between a 25 mm thick front sheet and a 15 mm thick back sheet (Figure I.01a). Two rectangular compartments, the primary compartment and the secondary compartment, were machined into the front and back sheets, respectively. The SolidWorks design was programmed into the computer-aided machining software FeatureCam, which was used to run the Hardinge VMC800II computer numerical control machine. This machine cut the required reactor features into the Perspex sheets. Acrylic polish was applied to the machined surfaces to improve their optical transparency. A crucial element of the reactor design was that it should be impermeable to H_2. This means that special care had to be taken to ensure a good seal at all joints and points where devices and features were inserted through the reactor walls: at any location where the algal culture could potentially be exposed to the surroundings. The Perspex sheets were sealed with an inlaid grooved system of Viton fluoropolymer elastometer o-rings and compressed using a set of 12 stainless steel bolts. This layout also satisfied the requirements of a fully modular reactor design. The purpose of the primary compartment is to accommodate approximately one litre of growing or H_2-producing algal culture. The secondary compartment is filled with water, or alternatively with a light-absorbing aqueous solution, and provides both the temperature and wavelength control for the system. The flat-plate PBR compartment and reactor body dimensions are given in Figure I.01b.

A re-circulating gas-lift system was used to provide mixing to the *C. reinhardtii* culture in the primary compartment. The gas bubbling was introduced by means of a stainless steel sparger near the bottom of the compartment (Figure I.01c). A bi-directional flow of gas into the sparger provides an even pressure distribution within it, resulting in a well-balanced gas-lift profile. The gas leaves the compartment at the top of the reactor and is re-circulated. There is also liquid circulation in the secondary compartment; the liquid flows upwards from the bottom of the reactor. The holes in the

reactor body required for the mixing system were sealed with stainless steel Swagelok fittings incorporating Viton o-rings. Viton fluoropolymer elastometer o-rings are known to seal very effectively against H_2 diffusion leaks, with a low deuterium permeability of $1.25 \cdot 10^{-7}$ $cm^3 \cdot s^{-1} \cdot cm^{-1}$ of material at standard temperature and pressure (Derrick & McIntyre, 1974). Swagelok fittings are leak-tight and made from stainless steel SS316, a material that is relatively common and non-corrosive. The measuring instruments, including the thermocouple and the pO_2 and pH probes, were inserted via the appropriate slots at the top of the primary compartment. The MIMS system for H_2 measurement slots into the front of the reactor. These devices were all sealed by custom-made leak-tight o-ring connections. None of the materials in contact with the algal culture are known to be toxic to *C. reinhardtii* (Skjånes *et al.,* 2008).

The entire structure is screw-connected onto a firm, black (matt, to minimise surface reflection) polyoxymethylene base, which also holds the LED array with the aid of a support bracket (Figure I. 01d). The LED array selection is flexible – the main requirement is that it needs to be of the appropriate dimensions and intensity range/distribution. There is also a constraint on the LED spread and brightness to ensure uniformity of illumination across the reactor. The final dual-compartment reactor body dimensions were 250·240·65 mm (height·width·thickness), and the entire construction, including the base and LED array, could fit into a box with dimensions 270·340·220 mm.

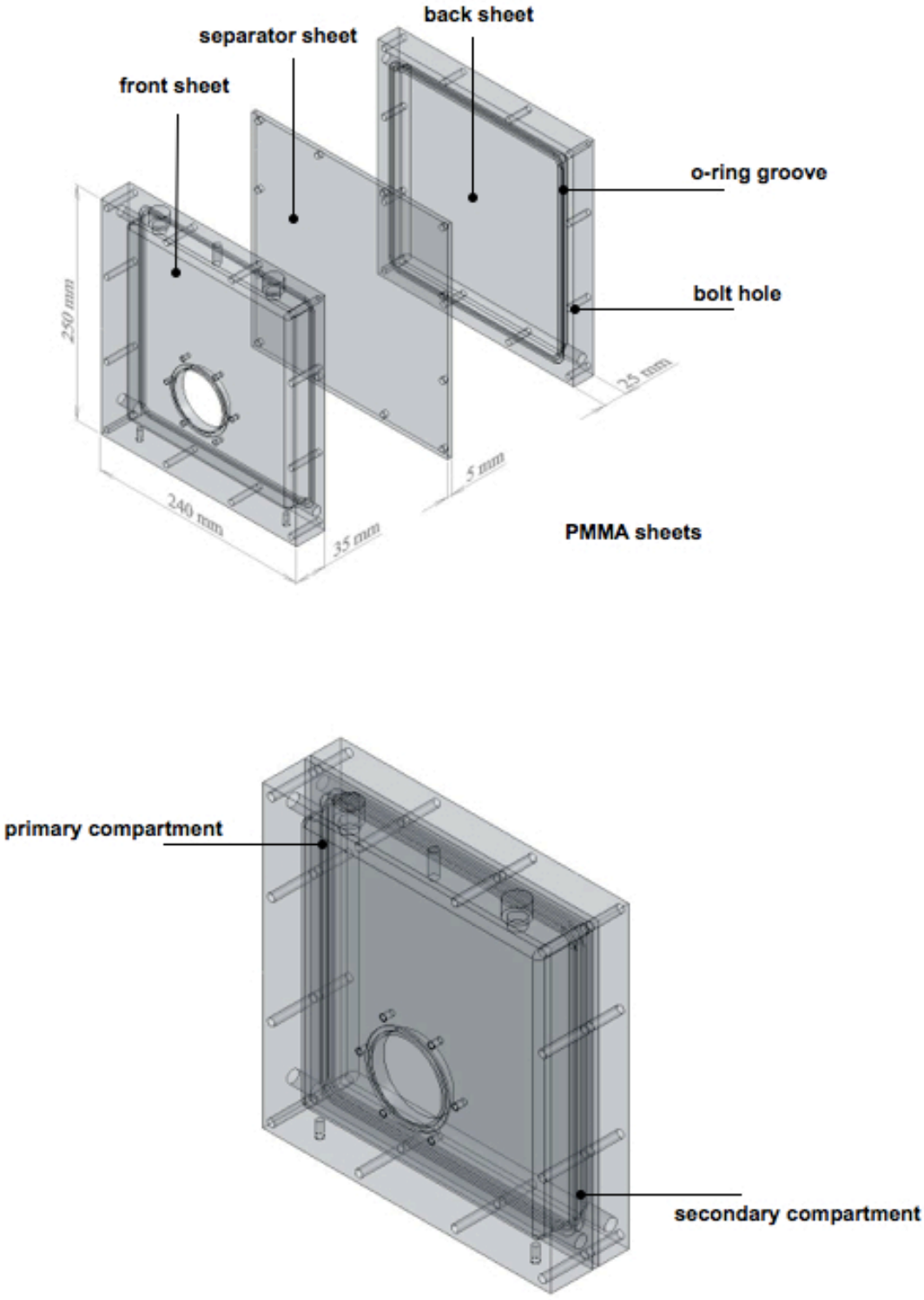


Figure I.01a: Flat-plate PBR; Assembly of the primary and secondary compartments

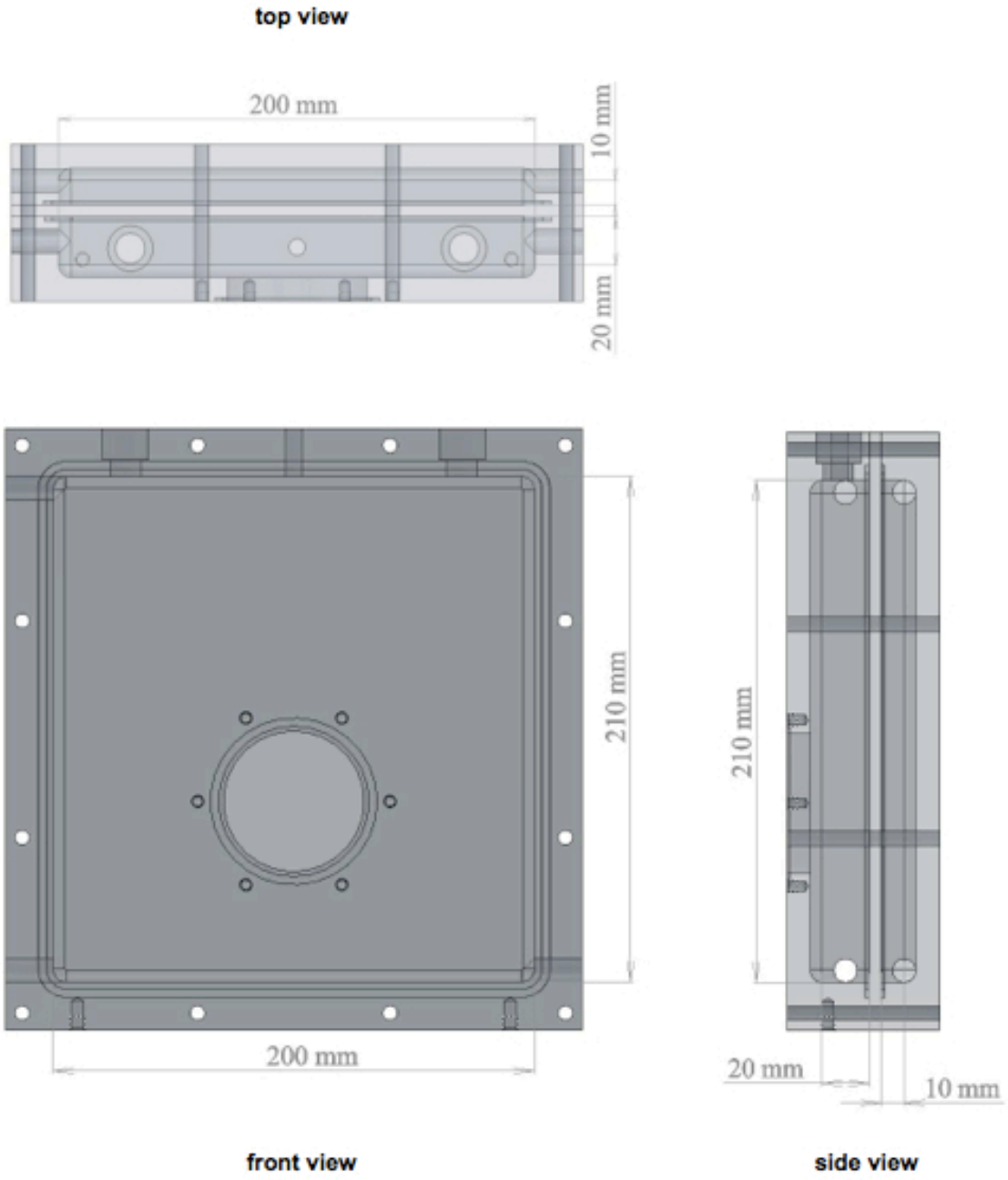


Figure I.01b: Flat-plate PBR dimensions

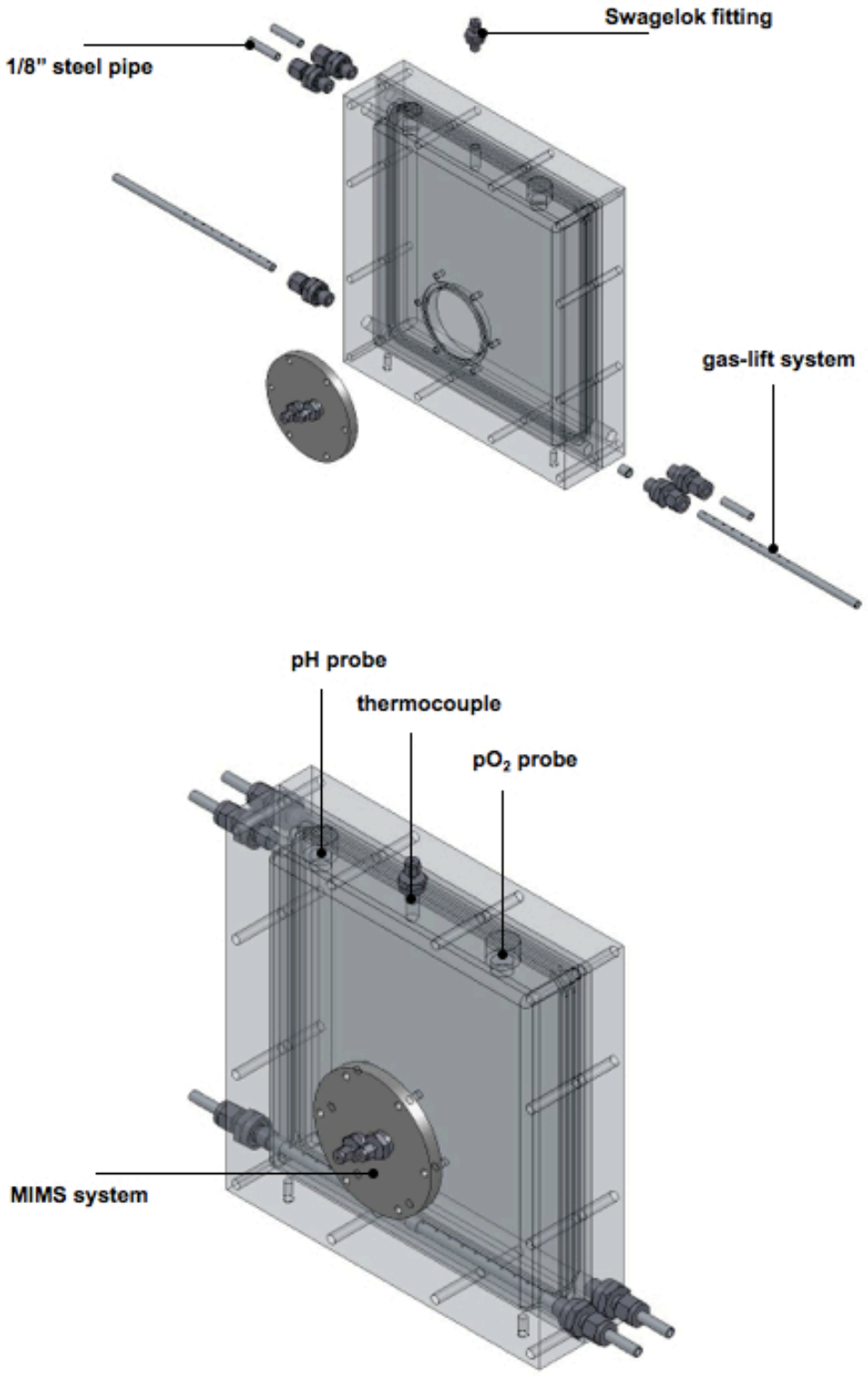


Figure I.01c: Flat-plate PBR; Mixing system features and measuring instruments

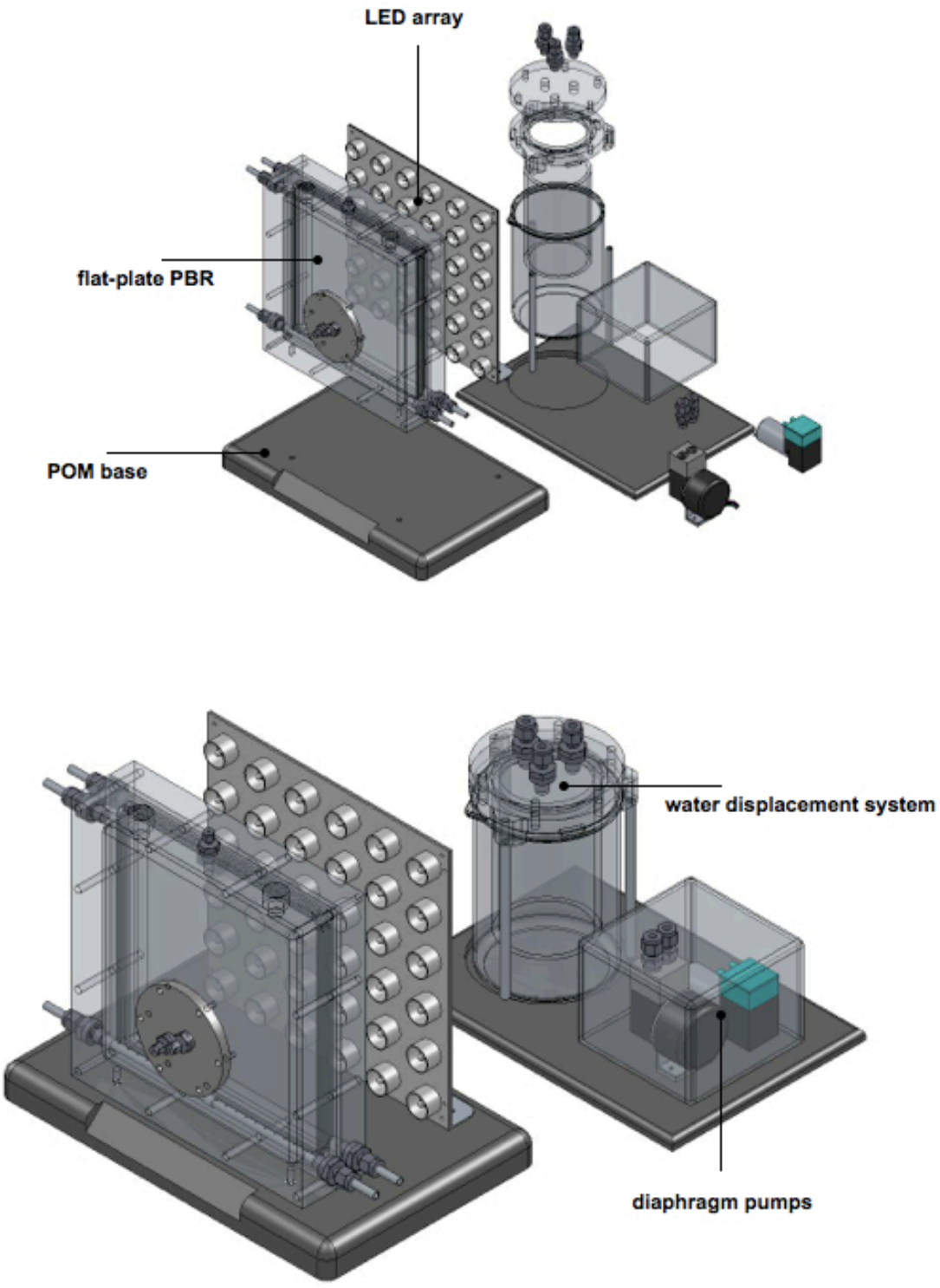


Figure I.01d: Complete PBR structure with reactor, base, LED array and ancillary equipment

I.2.2. Mixing and Circulation

A standard liquid diaphragm pump (KNF Neuberger) was used to circulate water, or a coloured aqueous solution, around the secondary compartment (Figure I.02, right-hand side of the diagram). The liquid diaphragm pump has a nominal flow rate of 0.3 $l \cdot min^{-1}$, but this rate is partially controllable by pulse width modulation (PWM) of the diaphragm frequency. A water-bath type heater was used to control the inlet temperature of the secondary compartment. The secondary compartment mixing system uses semi-transparent, flexible silicone tubing between the pump, heater and reactor body. The silicone tubing was slotted onto the pump, heater and reactor inlet and outlet ports, and secured with zip cable ties to prevent it from slipping during operation.

Primary compartment mixing was provided by a turbulent gas-lift system emanating from a dual-entry stainless steel sparger at the bottom of the compartment (Figure I.02, left-hand side of the diagram). The gas flow system was enclosed in quarter-inch perfluoroalkoxy (PFA) plastic piping and circulated around the reactor so that no gaseous hydrogen is lost to the environment. PFA is a flexible polymer with an excellent seal against H_2 diffusion; its permeability to H_2 has been measured to be $(2.3 \pm 0.6) \cdot 10^{-6}$ $cm^3 \cdot s^{-1} \cdot cm^{-1}$ (Extrand & Monson, 2006). Gas was circulated by means of a customised gas diaphragm pump (KNF Neuberger). This pump features a stainless steel pumping head with Swagelok inlet and outlet connections to minimise H_2 diffusion leaks in this critical region, as well as full PWM control of the pumping speed. The single gas diaphragm pump feeds both sparger inlets via a T-connector; in order to maintain a balanced bubble-emission distribution across the sparger, the two PFA pipes between the T-connector and each sparger inlet were machined to an identical length. The sparger itself was constructed from a 240 mm long, quarter-inch pipe made of stainless steel, and it was perforated with 20 evenly-spaced circular holes, each with a diameter of 1 mm. Due to the nature of this layout, bubbles are more likely to emerge from the holes closer to the edge of the primary compartment rather than the holes closer to the middle of the sparger. This produces a turbulent circular gas flow pattern that pushes *C. reinhardtii* cells towards the centre of the primary compartment and provides good mixing to the algal culture.

The primary compartment mixing system may also be connected directly to a gas cylinder via a mass flow controller rather than re-circulating resident gas using the gas diaphragm pump (Figure I.

02, left-hand side of the diagram). This provides additional operational flexibility to the flat-plate PBR. During the *C. reinhardtii* growth phase, it is possible to bubble the primary compartment with a mixture of CO_2 and air, thus providing an additional carbon source for photomixotrophic algal growth. Alternatively, an inert gas such as Argon may be used to purge O_2 out of the system and initiate anaerobic H_2 production.

While being circulated through the PFA piping system between the gas diaphragm pump and the flat-plate PBR primary compartment, the resident gas also passes through a Perspex water displacement and pressure release system (Figure I.01d; Figure I.02, left-hand side of the diagram). This system consists of an inverted, graduated Perspex cylinder suspended over a glass beaker and partially filled with water. When the algae generate gas-phase products, either O_2 during photosynthetic growth or H_2 under anaerobic conditions, this additional volume is detectable as a downward displacement of water in the inverted cylinder. This arrangement also prevents the build-up of pressure in the PBR. H_2 was also collected and analysed by a specially designed MIMS system, which is located on the front end of the primary compartment (Figure I.01c). The water displacement system, the liquid diaphragm pump and the gas diaphragm pump were mounted on a separate polyoxymethylene base, behind the LED array (Figure I.01d). Stick-on rubber feet were applied to the base of the diaphragm pumps to act as vibration dampers.

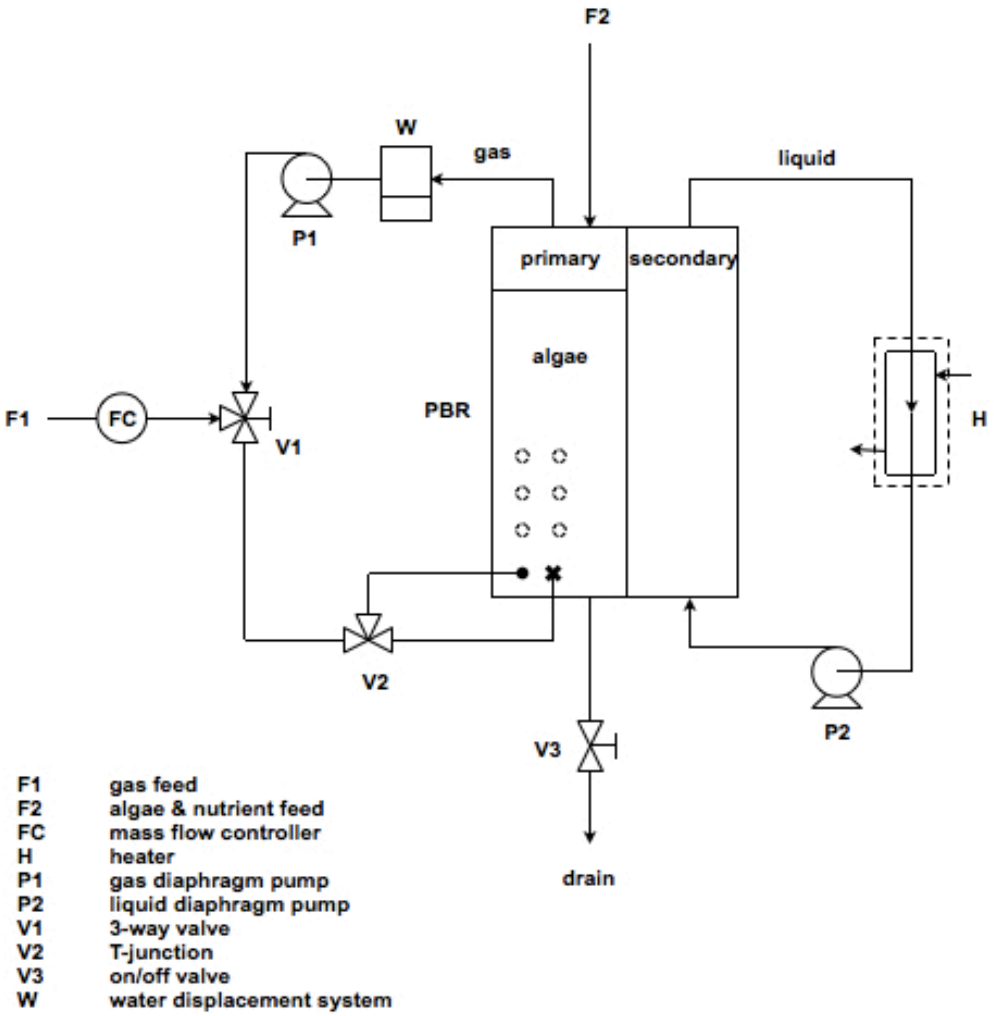


Figure I.02: Mixing and circulation in the flat-plate PBR

I.2.3. Membrane Inlet Mass Spectrometry (MIMS)

Various methods have been used to monitor the gaseous species (O_2, CO_2 and H_2) involved during photobiological H_2 production. The conventional method has been to use *in situ* Clark-type electrode measurements and/or analysis of gas samples by gas chromatography (Teplyakov *et al*., 2002). MIMS is another analytical technique used to measure *in situ* concentrations of dissolved gases or volatile organic compounds in aqueous solutions (Scott *et al*., 1983). The membrane system is the only interface between a liquid sample at atmospheric pressure and the vacuum chamber of a mass spectrometer. The membrane is made from different polymeric materials that allow gases to diffuse simultaneously or selectively depending on the investigation (Cournac *et al*., 2002). For selective H_2 diffusion, a semi-permeable polymer electrolyte membrane material such as Nafion is required. The technique allows direct comparison of the evolved gases and provides continuous monitoring of process conditions, i.e. light intensity, temperature, pH and system disturbances. Changes in these variables would be reflected in the MIMS gas concentration measurements. A MIMS system has been used in the literature to analyse relevant gases and determine the electron source during H_2 production by *C. reinhardtii* (Hemschemeier *et al*., 2009). In that experiment, MIMS was used to accurately measure the concentration of H_2 produced by *C. reinhardtii* under standard anaerobic conditions as well as in the presence of the PSII inhibitor DCMU. Consequently, the authors were able to conclude that the majority of electrons required for H_2 production originate from the photosynthetic mechanism of *C. reinhardtii*.

The ICL Chemical Engineering flat-plate PBR utilises the Aston Analytical Ultra-Trace MIMS System. The mass spectrometer is a compact quadrupole Pfeiffer Vacuum Prisma, running Windows Quadstar 422 software. Gases dissolved in the liquid phase within the primary compartment of the flat-plate PBR diffuse through a thin polydimethylsiloxane (PDMS) membrane, permeable to all the gases involved. The PDMS membrane was affixed on a disc holder inscribed with a perforated mesh (Figure I.03). It has a surface area of $1.36 \cdot 10^{-3}$ m^2 and a thickness of $3.20 \cdot 10^{-4}$ m. PDMS has a H_2 permeability of $6x10^{-15}$ $m^2 \cdot s^{-1} \cdot Pa^{-1}$ (Pinnau & He, 2004). The disk holder was sealed onto the stainless steel MIMS body by means of a Viton fluoropolymer elastometer o-ring. Inert gas introduced to the disc holder cavity carries diffused gaseous products, via a heatable capillary, into the mass spectrometer. Apart from the direct measurement of the kinetics of gaseous products, the

MIMS system offers the additional benefits of potential H_2 separation and collection, as well as the reduction of possible H_2 induced inhibition of the biophotolytic H_2 production process (Hemschemeier *et al*., 2009; Teplyakov *et al*., 2002).

MIMS extracts H_2 from the algal culture by a three-stage process called pervaporation. In the first step, H_2 molecules produced in the reactor are absorbed onto the membrane surface; this is followed by the permeation of these H_2 molecules through the membrane material, and finally by their desorption into the argon carrier gas stream on the other side (Lloyd *et al*., 2002). A modified form of Fick's First Law (Beckmann K. *et al*., 2009), shown in Equation I.01, was used to calculate the H_2 pervaporation rate through the membrane. This H_2 pervaporation rate of 9.3 $ml \cdot h^{-1}$ was significantly higher than the 2.0 $ml \cdot h^{-1}$ (per litre of culture) WT *C. reinhardtii* H_2 production rate typically quoted in the literature (Melis, 2002; Akkerman *et al*., 2002; Hankamer *et al*., 2007). Consequently, any H_2 produced by the algae would be rapidly stripped out of the system by MIMS; the rate of H_2 extraction through the PDMS membrane is equivalent to the H_2 production rate inside the flat-plate PBR. MIMS was therefore calibrated entirely in the gas-phase by substituting the H_2 pervaporating through the membrane/reactor interface with a known flow rate of hydrogen gas from a cylinder.

$$k_{trans} = \frac{P \cdot A \cdot \Delta p}{l} \qquad \textit{Equation I.01}$$

where,

P (H_2 permeability) = $6 \cdot 10^{-15}$ $m^2 \cdot s^{-1} \cdot Pa^{-1}$

A (membrane surface area) = $1.36 \cdot 10^{-3}$ m^2

l (membrane thickness) = $3.20 \cdot 10^{-4}$ m

Δp (partial pressure of H_2) = 1 atm = $1.01 \cdot 10^5$ Pa

k_{trans} (H_2 pervaporation rate) = $2.6 \cdot 10^{-9}$ $m^3 \cdot s^{-1}$ = 9.3 $ml \cdot h^{-1}$

Figure I.04 shows the technical design of the MIMS system, including the carrier gas flow, H_2 pervaporation, MIMS calibration and mass spectrometer (MS) connection components. Argon (Ar) carrier gas is drawn from a gas cylinder at a controlled flow rate of 15 $ml \cdot min^{-1}$. The carrier gas reaches a four-way valve, shown in the centre of Figure I.04, which may be operated in 'by-pass' or 'reactor' modes. In 'by-pass' operational mode, the carrier gas goes directly to the MS, although it is possible to inject a small gaseous sample into the carrier gas stream through a septum beforehand.

A 0.5 ml gas-tight syringe was used to carry out this injection mass spectrometry. Injection mass spectrometry was primarily used to qualitatively test for the presence of H_2 and other gaseous products during experiments in the Solar Biofuels Consortium and Sartorius PBRs. In 'reactor' operational mode, the carrier gas is diverted towards the MIMS system, where it picks up any H_2 pervaporating out of the membrane and carries it to the MS. The MIMS system operates based on partial pressure gradients, with H_2 pervaporating out of the PBR and Ar pervaporating in the opposite direction, so that mass is conserved within the PBR (Beckmann K. *et al*., 2009). The 'reactor' operational mode is also used during MIMS calibration. During calibration, the MIMS system was replaced by a known and variable flow of H_2, established by mixing pure H_2 from a gas cylinder with Ar using two mass flow controllers (Figure I.04). During both injection mass spectrometry and MIMS operational modes, the MS capillary was heated and the majority of MS inlet gas was vented out of the system. These precautions were implemented to protect the MS from water and pressure damage respectively (Lloyd *et al*., 2002).

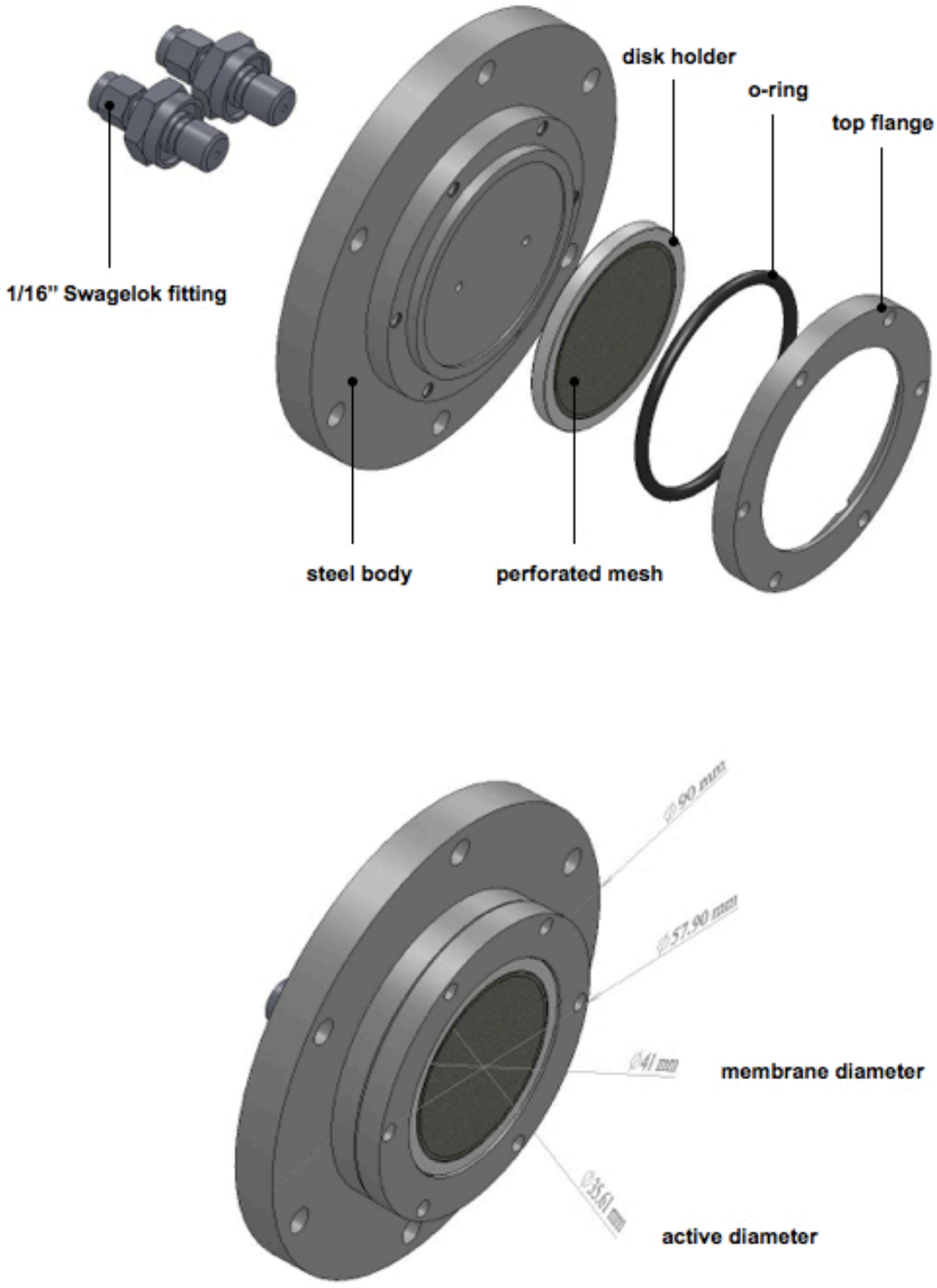


Figure I.03: Design of the Membrane Inlet Mass Spectrometry (MIMS) system

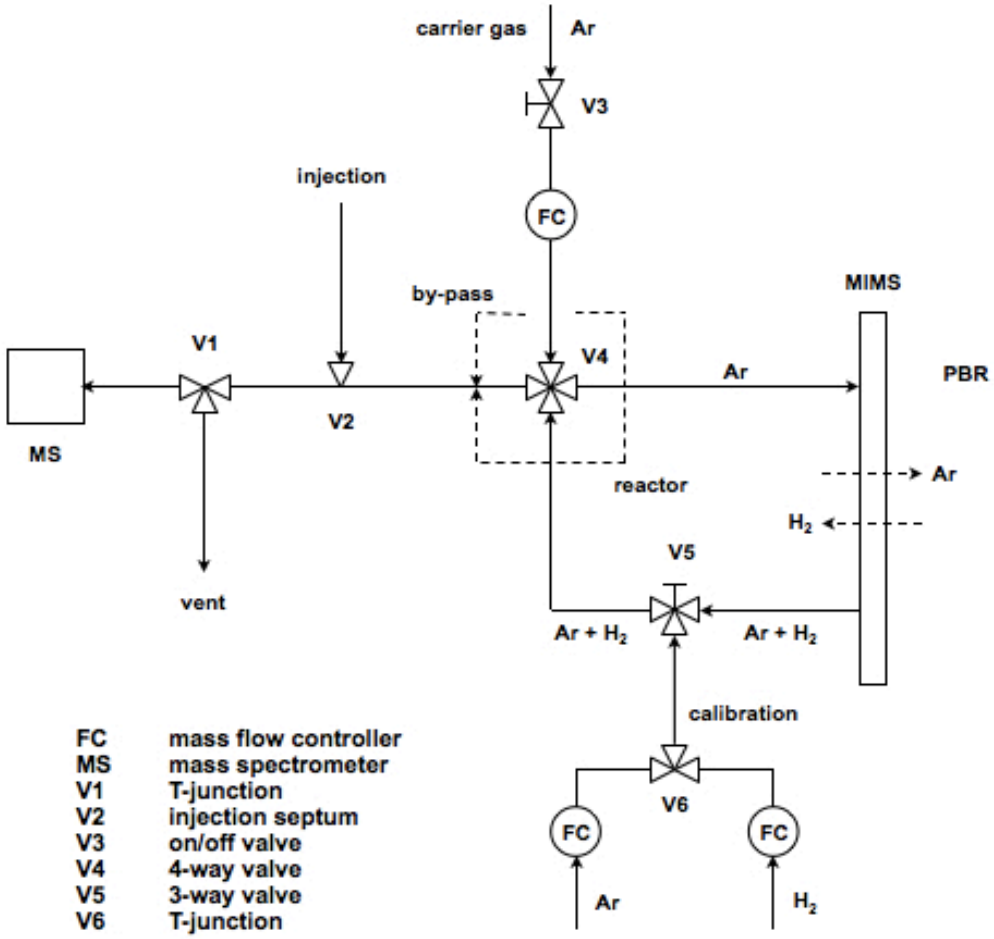


Figure I.04: Technical design of the MIMS system

I.2.4. Datalogging and Control

The key parameters that affect the H_2 production by *C. reinhardtii* include the pH, pO_2, temperature and OD of the culture. pH and pO_2 were measured using commercial probes from Consort – the SZ10T galvanic pO_2 electrode and the SP10T pH electrode. The temperature in the algal compartment was measured with a K-type thermocouple from Omega. The optical thickness was monitored using a photodiode with an absorption bandwidth of 650-700 nm. The photodiode detects the LED light-scattering by the algae in the photosynthetically-active region of the light spectrum. The measurements from all of these devices were recorded using the National Instruments datalogging system; this system was also set up to control the ancillary PBR equipment such as the LED array, the liquid diaphragm pump and the gas diaphragm pump. The datalogging and control system was centred on the National Instruments Compact RIO (Figure I.05). This device contains a real-time controller unit as well as its own independent hard drive, which was programmed via an Ethernet connection to a computer running Lab View software. The Compact RIO controller is powered by a 24 V direct current (DC) power supply, and it is connected to an eight-slot chassis, which carries various system-specific input/output modules.

The pH and pO_2 electrodes, as well as the photodiode signal, were datalogged with the NI-9205 analogue input module. It was necessary to use the PHTX pre-amplifier from Omega to increase the impedance of the electrode signals to 20 kΩ and make them compatible with the analogue input module specifications. All three of these raw voltage signals required calibration. The thermocouple was datalogged with the NI-9211 thermocouple analogue module. In this case, the module intrinsically carried out the calibration according to NIST-certified standards and a temperature output was obtained. The PBR system used a 24 V DC Brightest Day Light White LED array (LED Wholesalers) and a 12 V DC NF30 KPDC liquid diaphragm pump (KNF Neuberger). Both of these devices were controlled by PWM at a frequency of 1 kHz using an NI-9474 high-speed sourcing digital output module. However, due to the mismatch in input voltages, two separate NI-9474 modules were required. The PM24766 – NMP830 gas diaphragm pump from KNF Neuberger has been specifically designed for PWM control with a 0.9-5.0 V signal, which was provided by the NI-9401 TTL digital input/output module. In summary, the National Instruments Compact RIO was used to run the datalogging and control system in real-time with the aid of five input/output

modules: NI-9205, NI-9211, NI-9474 (24 V), NI-9474 (12 V) and NI-9401 (Figure 05). Overall, the National Instruments system allowed the careful control of the light intensity emitted by the LED array and of the flow rates through both diaphragm pumps. It enabled the datalogging of measurements from the pH and pO_2 probe, the thermocouple and the photodiode.

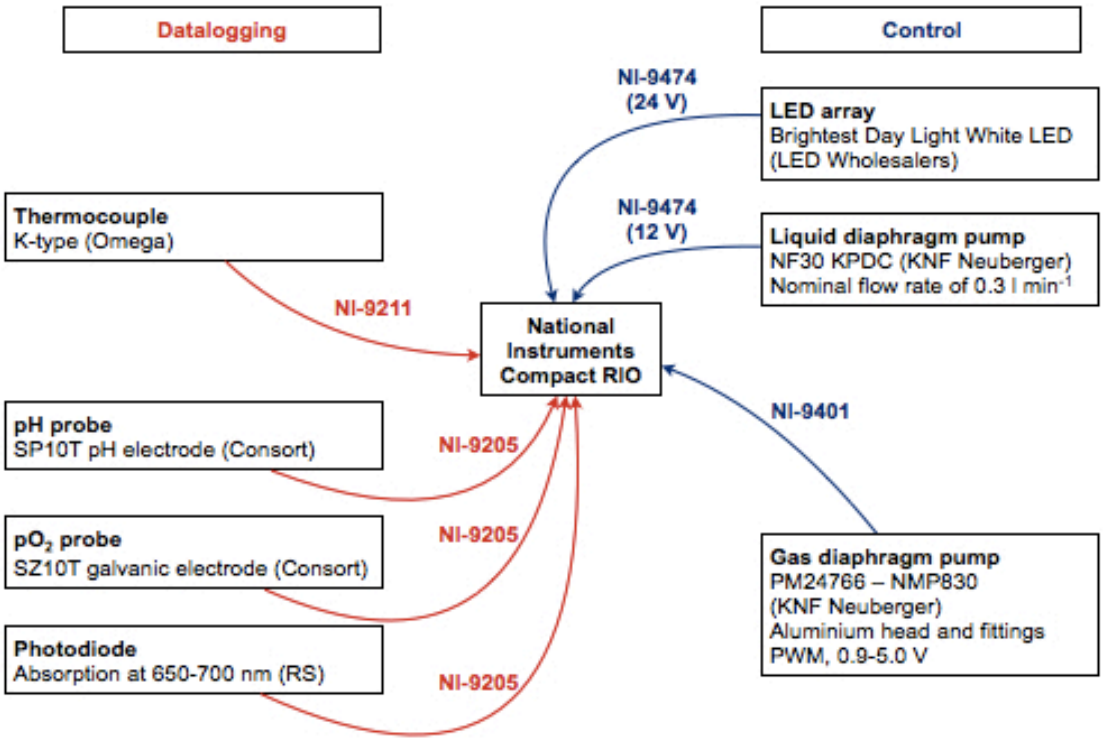


Figure I.05: Datalogging & control system architecture

I.3. Characterisation

I.3.1. Light Intensity Distribution

Overall, *C. reinhardtii* cells have modest light intensity requirements; the growth, S-deprivation and H_2 production processes need no more than 200 $\mu E \cdot s^{-1} \cdot m^{-2}$ of photosynthetically active radiation (PAR), approximately 40 $W \cdot m^{-2}$ (Table 5.05). Algal cells that remain in the dark for extended periods (dark zone) or that become overexposed to illumination (photic zone) will not grow or produce H_2 efficiently. The photic zone corresponds to an illumination exceeding 100 $W \cdot m^{-2}$, although this value is algal strain dependent (Melis, 2002). The objective was therefore to supply all *C. reinhardtii* cells with uniform illumination of the appropriate intensity (Akkerman *et al.,* 2002). An LED array provides illumination that is uniform, coherent, efficient and non-heating, all desirable properties for the flat-plate PBR. An LED array panel, approximately 200·200 mm in size, was purchased from LED Wholesalers. Its light intensity was varied using the National Instruments datalogging and control system. A light meter, operating on integrating sphere principles, was used to measure the spatial light intensity distribution of the LED array operating at maximum power (Figure I.06).

The spatial light intensity distribution, measured across a plane parallel to, and located at a distance of 30 cm directly away from, the cool-white LED array, appeared relatively constant across the surface area of measurement, with a light intensity of 58±3 $W \cdot m^{-2}$ (Figure I.06, top surface). When the Perspex flat-plate PBR was placed between the LED array and the light meter, the light intensity fell to 43±8 $W \cdot m^{-2}$ (Figure I.06, bottom surface). This result is primarily due to limitations in the transparency of machined Perspex, but there is also evidence of additional shading effects radially away from the reactor centre. It is therefore important to provide sufficient mixing to cycle the algal culture through all parts of the reactor in order to prevent the build-up of localised light gradients, and to ensure that the majority of algal cells receive the illumination they require. It is also possible to use a light meter or photodiode in a similar setup as described above to measure the optical density (OD) of the culture, which is directly proportional to the algal growth rate (Posten, 2009). The optical density, or absorbance, of a liquid is a quantity used to describe the transmission of light through that liquid. The Beer-Lambert law describes the optical density as a logarithmic ratio

between the light intensity incident on the liquid (I_{in}) and the light intensity transmitted through the liquid (I_{out}) (Equation I.02).

$$OD = -\log_{10}\left(\frac{I_{out}}{I_{in}}\right) \qquad \textit{Beer-Lambert Law} \qquad \text{Equation I.02}$$

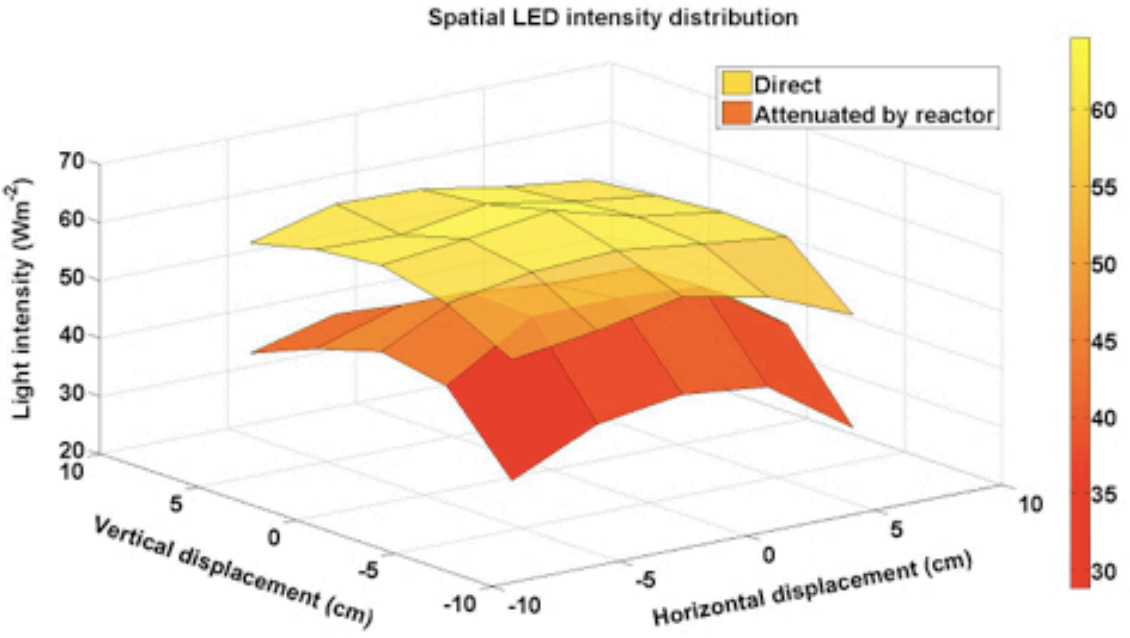


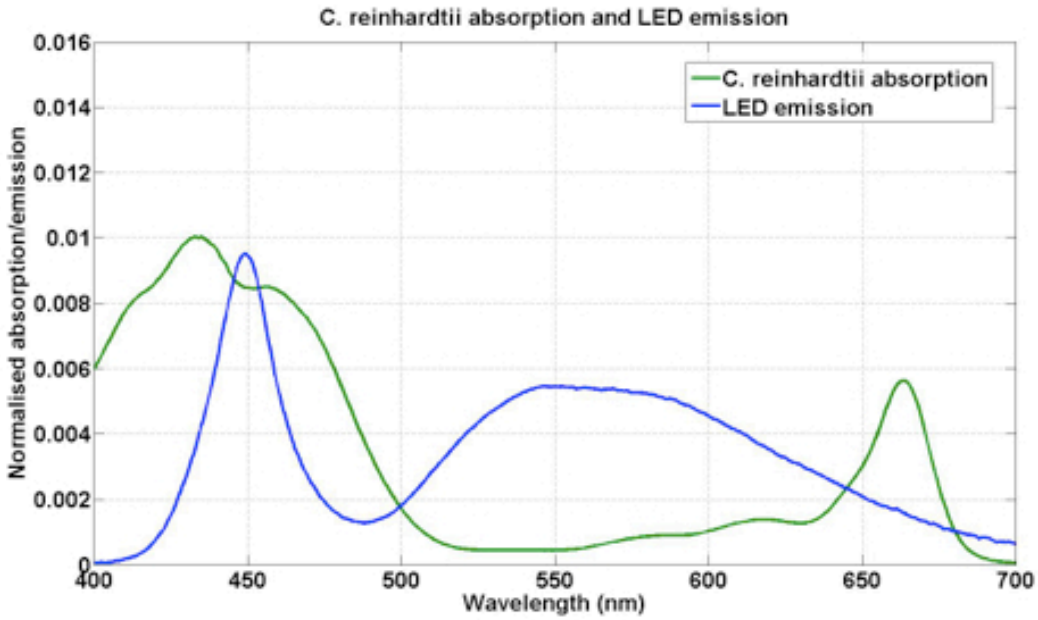
Figure I.06: Variations in the spatial light intensity distribution in the flat-plate PBR

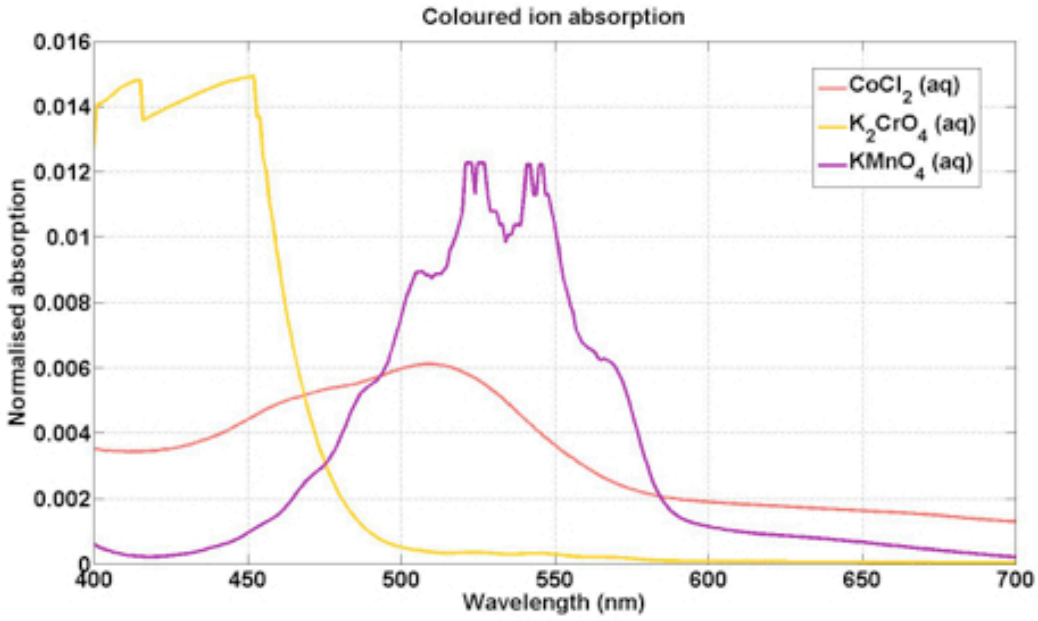
I.3.2. Wavelength Modulation

A spectrophotometer was used to analyse *C. reinhardtii* absorption in the visible region of the electromagnetic spectrum and a light meter was used to measure the corresponding cool-white LED emission spectrum. The spectral match between the *C.reinhardtii* absorption and LED emission is shown in Figure I.07a; the absorption and emission spectra have been normalised by setting the area under both curves equal to unity. There are two major light absorption mechanisms in *C. reinhardtii* – the carotenoid absorption in the 400-500 nm spectral range and the PSII absorption in the red region of the spectrum centred on the 663 nm peak; the algae also reflect green light. PSII absorption is a threshold mechanism, that is to say the algae could use photons of any wavelength less than or equal to 680 nm for photosynthesis, but preferentially use 663 nm, as evidenced by the strong absorption peak at this wavelength (Akkerman *et al*., 2002). The cool-white LED array provides powerful, well-balanced illumination over the entire visible spectrum, but a closer look at the normalised LED emission spectrum reveals a significant spectral mismatch with *C. reinhardtii* absorption in the green and red regions of the spectrum. This could potentially cause unnecessary oversaturation at certain wavelengths, resulting in photoinhibition of the algal growth and H_2 production processes (Janssen *et al*., 2003).

It was therefore important to incorporate the capacity to modulate wavelength into the flat-plate PBR design. This could have been accomplished by changing between different LED arrays, but a more practical solution was to apply a light filter between the cool-white LED array and the main reactor body. The dual-compartment flat-plate PBR design offers the possibility to modulate wavelength without any external filters, while at the same time providing temperature control for the reactor system. Aqueous solutions (*aq*) of various coloured ions were circulated around the secondary compartment to modulate the wavelength of LED illumination incident on the algal culture in the primary compartment (Figure I.07b). For example, the purple potassium permanganate (*aq*) may be used to reduce the photoinhibition of PSII by filtering out the suboptimal green light. Orange potassium chromate (*aq*) could be used to switch-off parts of the carotenoid absorption spectrum, potentially diverting additional photons to PSII, while red cobalt chloride (*aq*) could be used to combine the above effects.

(a)





(b)

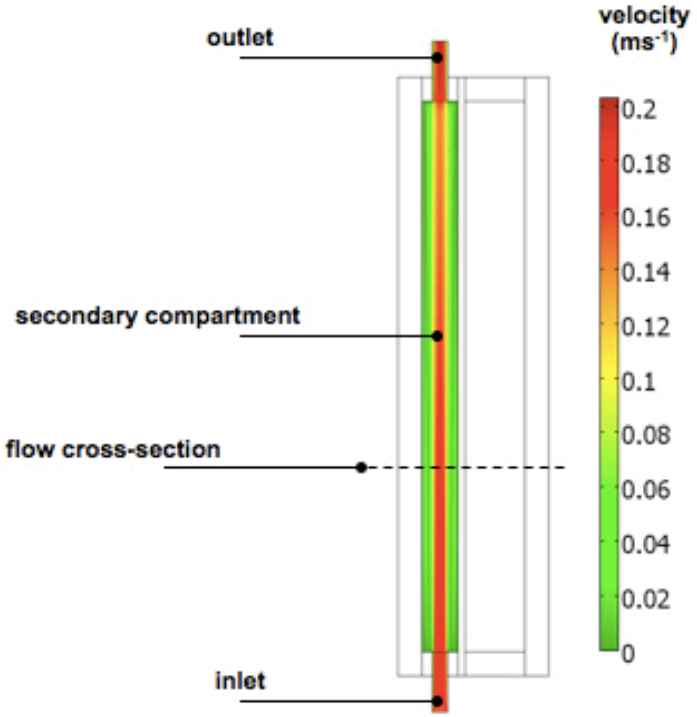
Figure I.07: Use of the secondary flat-plate PBR compartment for wavelength modulation

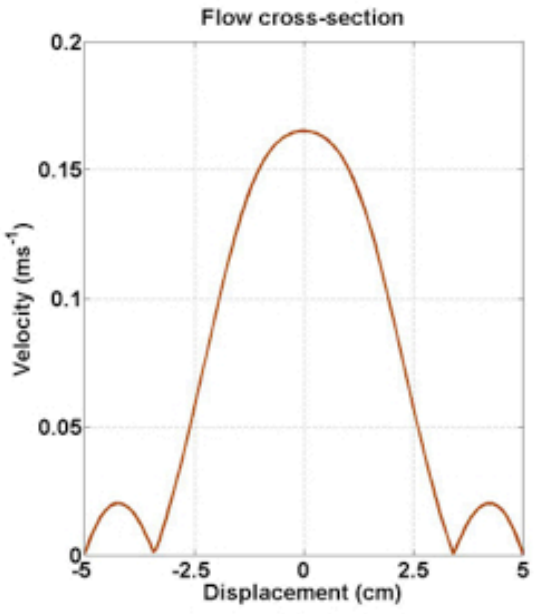
I.3.3. Heat Transfer

The secondary compartment of the flat-plate PBR was also used to control the temperature of the algal culture. A simple model was developed in Comsol multiphysics modelling and simulation software to examine the heat transfer properties of the PBR, focusing on estimating the Perspex wall thickness, inlet temperature and flow rate that could be used to maintain the appropriate primary compartment temperature for *C. reinhardtii* cultivation (Figure I.08; Figure I.09). This model featured a number of simplifications – it is based on a two-dimensional vertical cross-section through the reactor body, and mixing is assumed to take place in the secondary compartment only, with the inlet and outlet located in this same two-dimensional plane. Within this model, the secondary compartment is represented by the rectangular cavity on the left of Figure I.08a and the primary compartment by the larger rectangular cavity on the right of Figure I.08a; they are separated and insulated from each other and from the environment by a layer of Perspex. Mass transfer in the secondary compartment follows the incompressible Navier-Stokes equation, with no pressure and no viscous stress present at any point in the compartment, and gravity acting downwards on the water jet rising from the inlet at the bottom (Figure I.08a). The model predicts laminar flow profile throughout the secondary compartment, and the water jet slows down and spreads out on the way up. Figure I.08b shows a horizontal cross-section of the flow profile in Figure I.08a, indicating the distinguishable laminar flow pattern.

The physics of mass transfer were coupled to convective and conductive heat transfer in the secondary compartment by means of the inlet velocity, so that the water jet transferred heat upwards through the compartment. The heat transfer properties are strongly influenced by the physical properties of water and Perspex listed in Table I.01. All water and Perspex physical data were available in the Comsol internal database.

(a)

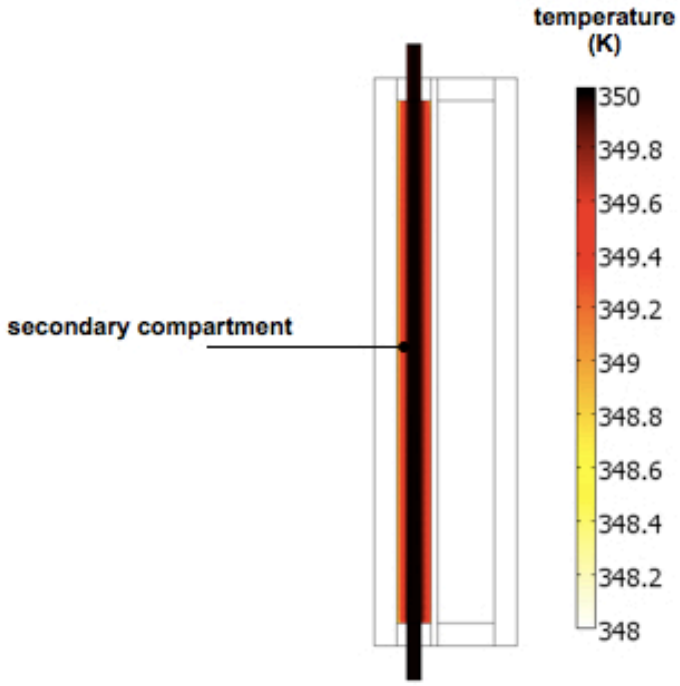




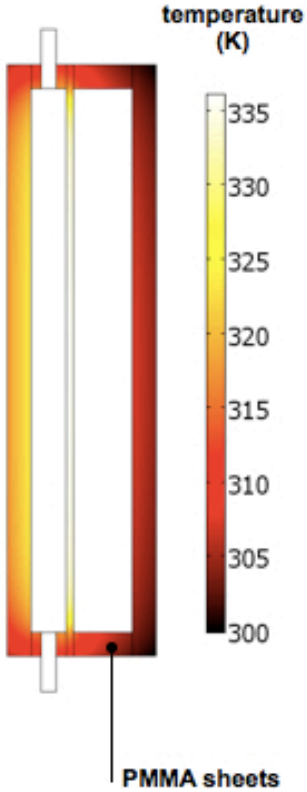
(b)

Figure I.08: Mass transfer in the secondary flat-plate PBR compartment

(a)



(b)



(c)

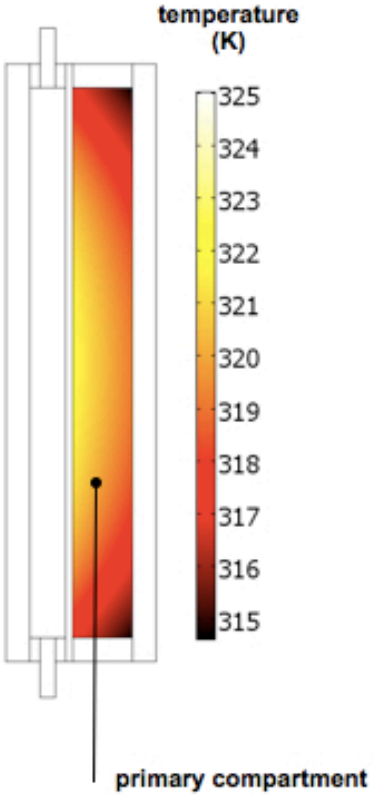


Figure I.09: Heat transfer through the flat-plate PBR compartments

Table I.01: Physical properties of water and Perspex

Property	Water	Perspex
Density, ρ	1000 $kg \cdot m^{-3}$	1190 $kg \cdot m^{-3}$
Viscosity, η	$8.9 \cdot 10^{-4}$ Pa·s	-
Conductivity, k	0.58 $W \cdot m^{-1} \cdot K^{-1}$	0.20 $W \cdot m^{-1} \cdot K^{-1}$
Heat capacity, C_p	2108 $J \cdot kg^{-1} \cdot K^{-1}$	1450·$J \cdot kg^{-1} \cdot k^{-1}$

Table I.02: Comparison between primary compartment temperature predictions by the Comsol model and experimental data

Pump flow rate ($l\ min^{-1}$) controlled	$T_{secondary}$ (°C) controlled	$T_{primary}$ (°C) predicted	$T_{primary}$ (°C) measured	$\Delta T_{primary}$ (°C) calculated
0.30	10	15.6	15.4	-0.2
0.30	20	21.2	20.9	-0.3
0.30	30	27.3	27.9	+0.6
0.30	40	33.4	34.7	+1.3
0.15	10	15.3	15.0	-0.3
0.15	20	21.1	20.4	-0.7
0.15	30	27.5	28.7	+0.8
0.15	40	33.8	35.0	+1.2

The conductive heat transfer coefficient of Perspex, *h*, is also of primary importance and it varies linearly with Perspex thickness: it takes a value of 5.8 $W \cdot m^{-2} \cdot K^{-1}$ in the case of a 3 mm thick sheet and a value of 3.4 $W \cdot m^{-2} \cdot K^{-1}$ for a 10 mm thick sheet (Comsol database). The heat transfer is principally governed by the heat flux boundary condition between surfaces at different temperatures. For example, in the Perspex boundary layer between the secondary compartment and the surroundings, heat flows into the Perspex layer based on the temperature of the water in the secondary compartment and it flows out of the layer based on the temperature of the surroundings, thus determining the temperature distribution within the Perspex layer itself. This information may be summarised by the heat flux Equations I.03-I.05, where *q* is the heat flux.

$q = h \cdot \Delta T$	*heat flux*	*Equation I.03*
$q = h \cdot (T_{water} - T_{perspex})$	*inner boundary of Perspex layer*	*Equation I.04*
$q = h \cdot (T_{surroundings} - T_{perspex})$	*outer boundary of Perspex layer*	*Equation I.05*

Figure I.09 shows the results of this Comsol heat transfer model for a specific set of input parameters. With a vertical inflow velocity of 0.155 $m \cdot s^{-1}$ (calculated from the nominal pump flow rate of 0.3 $l \cdot min^{-1}$) and an inlet temperature of 350 K (77°C), the secondary compartment appears well-insulated, cooling only by a fraction close to the Perspex boundaries and creating a temperature differential of approximately 2 K in the compartment (Figure I.09a). Conductive heat transfer takes place in the Perspex layer between the two compartments and the surroundings. Assuming an ambient temperature of 293 K (20°C), good heat transfer within the 5 mm Perspex separator between the two compartments was observed. The temperature differential in the Perspex layer was approximately 35 K, and the greatest heat loss to the surroundings occurred through the back of the reactor, i.e. away from the primary compartment (Figure I.09b). Assuming conductive and convective heat transfer, as well as ideal mixing in the primary compartment, the mean temperature of the algae may be calculated to be 320 K (47°C) (Figure I.09c). The model allows variables such as inflow velocity, inlet temperature and Perspex layer thickness to be modified and computes the corresponding change in the temperature of the algal culture. An experiment was conducted to provide a comparison between the primary compartment temperature predicted by the model and the corresponding temperature measured experimentally (Table I.02).

The ambient temperature during this experiment was 23 °C. The pump flow rate was controlled by the NI system and the secondary compartment temperature was controlled and measured using a Grant LTC1 heating/cooling water bath unit. The temperature in the water bath therefore takes a constant pre-set value and all heat transfer takes place subsequently as the water is pumped around via the secondary compartment. The primary compartment temperature was measured using a K-type thermocouple.

The results show that primary compartment temperatures of 15-35 °C are easily attained and controlled – this is the accepted temperature range for *C. reinhardtii* growth (Akkerman *et al.,* 2002). The model is correct to ±1.3°C in all instances, usually significantly better. These experimental data also reveal that a longer residence time distribution in the secondary compartment (resulting from a lower flow rate) gives slightly better temperature control, an effect that is also seen by the model. The model is therefore useful in providing a holistic overview of the heat transfer properties in the flat-plate PBR. In reality, the flat-plate PBR is actually better at controlling primary compartment temperature than the model predicts. The model would need to be extended to a more complex three-dimensional geometry with gas-lift mixing introduced in the primary compartment before the numerical values resulting from the model may be considered completely reliable.

I.4. Operation

I.4.1. Calibrations of Probes

As part of the flat-plate PBR commissioning, it was necessary to calibrate the pH and pO_2 probes, the photodiode and the MIMS system. Figure I.10 shows an example calibration for each of these four instruments. In practise, these calibrations were repeated once every month to ensure consistency of results and protect against systematic errors. The pO_2 probe proved to be particularly unstable and prone to blockage by algal cells; as a precaution, the pO_2 electrolyte was replaced and the pO_2 probe was recalibrated prior to the start of every major experiment.

The pH probe signal was measured in three buffer solutions of known pH values: pH 4.00, pH 7.00 and pH 9.12 (Figure I.10a). The probe-buffer contact was maintained over a brief period of time to ensure that the pH signal, measured in mV, was stable. The pH probe signal was assigned the corresponding buffer pH value and the remainder of the pH scale was then interpolated linearly. Equation I.06 gives the correlation between pH probe signal and pH.

$$pH = -0.019 \cdot signal + 6.0 \qquad \textit{Equation I.06}$$

The pO_2 signal was set to 0% in N_2-saturated water, 21% in air-saturated water and 100% in O_2-saturated water (Figure I.10b). The pO_2 measurement consequently takes a percentage value based on the oxygen saturation of the liquid, given in Equation I.07.

$$pO_2\,(\%\,saturation) = 0.35 \cdot signal + 9.1 \qquad \textit{Equation I.07}$$

The photodiode measurement depends on the light intensity of the LED array; a different calibration is required for each different LED setting. Figure I.10c shows the photodiode OD calibration at a light intensity of 12 $W \cdot m^{-2}$, which was the commonly used light intensity throughout this thesis. To carry out the photodiode OD calibration, it was necessary to start with a very dense *C. reinhardtii* culture. The photodiode measurement was recorded and an algal sample was extracted in order to measure its chlorophyll content using a spectrophotometer (Arnon, 1949;

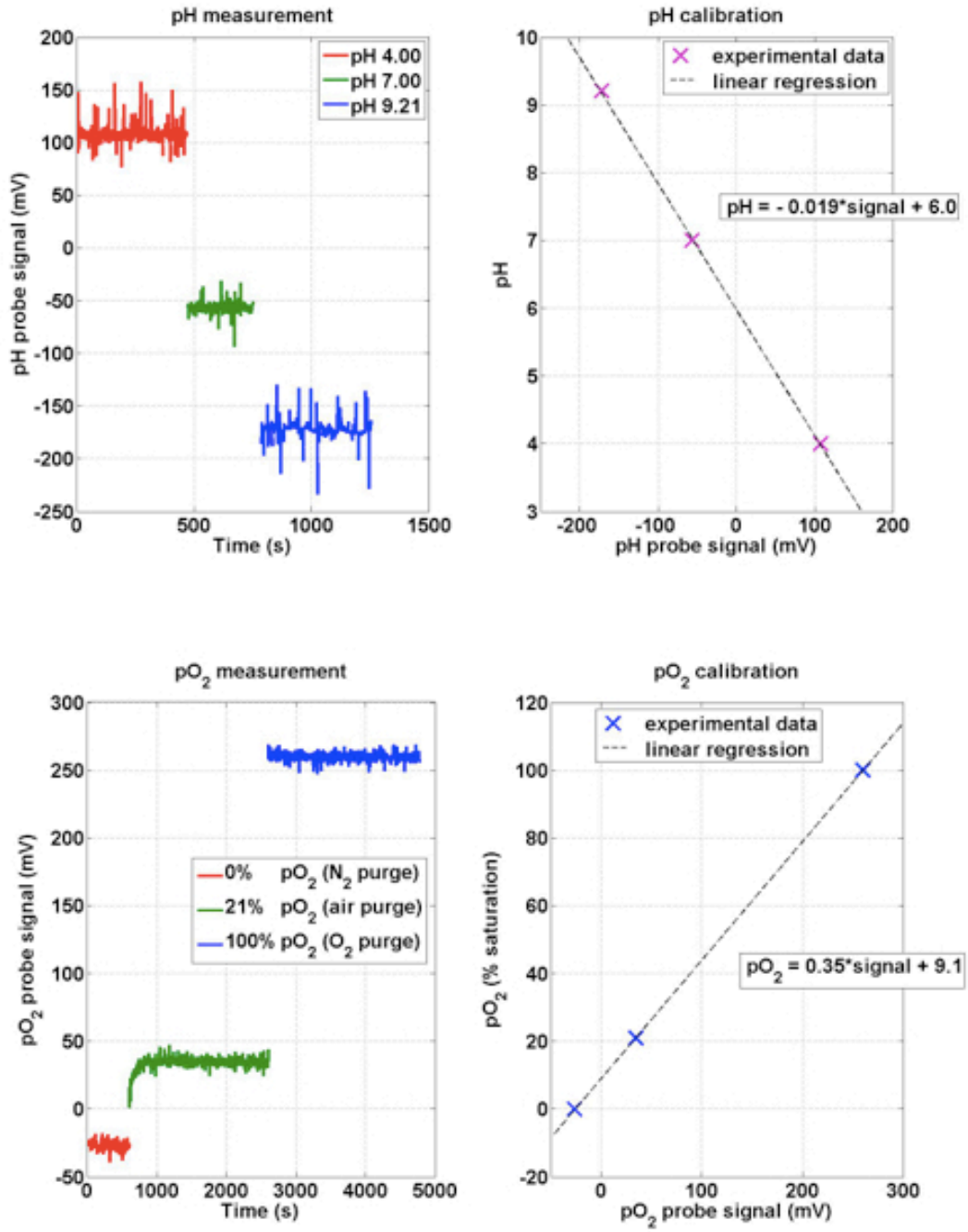
Equations 5.06-5.08). In this case, a photodiode measurement of 430 mV, corresponding to a chlorophyll content of 32.3 $mg \cdot l^{-1}$ was obtained. The algal culture was then progressively diluted with distilled water, with photodiode and chlorophyll content measurements repeated at each stage of the dilution. Eventually, the relationship given in Equation I.08 was obtained.

$$OD_{663}\ (mg\ l^{-1}\ Chl) = -0.46 \cdot signal + 230 \qquad \textit{Equation I.08}$$

MIMS calibration was carried out entirely in the gas phase by replacing the H_2 pervaporating through the PDMS membrane with a known and variable flow of H_2 from a gas cylinder according to the setup shown in Figure I.04. Although the intention was to inject H_2 flows similar to the *C. reinhardtii* H_2 production rate (2 $ml \cdot h^{-1}$) into the carrier gas stream, limitations imposed by the available mass flow controllers ensured that the lowest controllable H_2 flow was in fact 33 $ml \cdot h^{-1}$. The H_2 flow was therefore varied between 33 and 86 $ml \cdot h^{-1}$, with the corresponding MS signal measured (Figure I.10d). This linear correlation may be extrapolated for low H_2 production/flow rates and the relationship between H_2 flow and MS signal is given in Equation I.09.

$$H_2\ (ml\ h^{-1}) = 3.8 \cdot 10^{10} \cdot signal \qquad \textit{Equation I.09}$$

(a)



(b)

Figure I.10a: pH probe calibration

Figure I.10b: pO_2 probe calibration

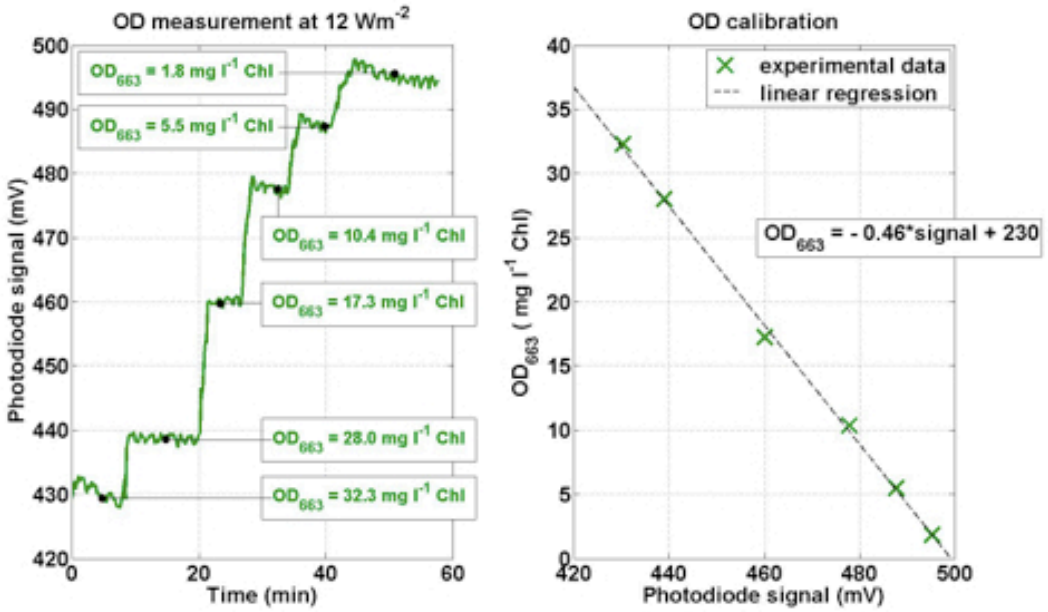


Figure I.10c: Photodiode OD calibration

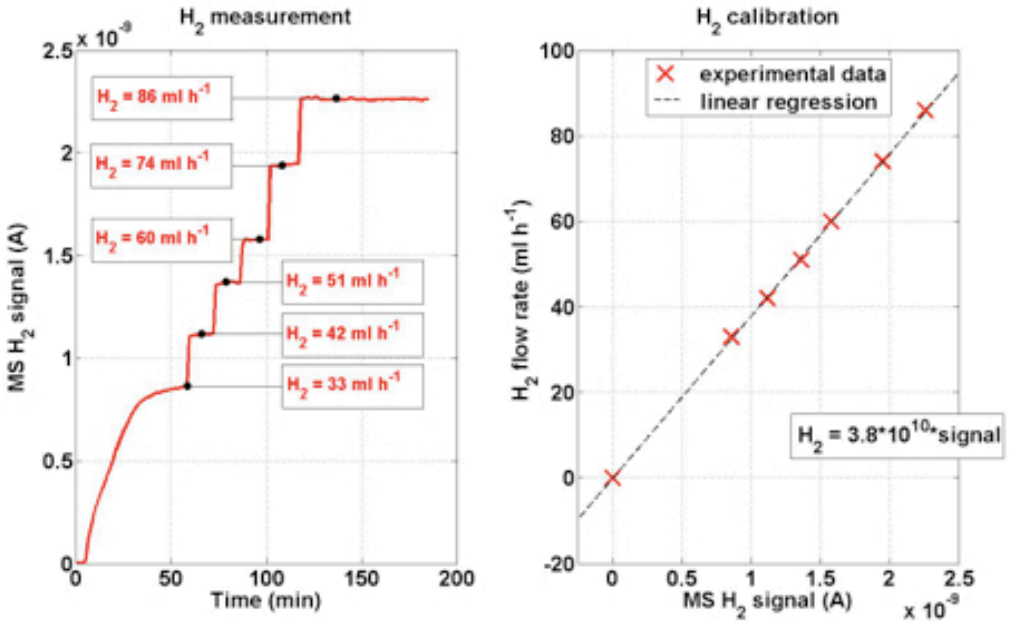


Figure I.10d: MIMS calibration

1.4.2. Dark H_2 Production Experiments

The hydrogenase enzyme has the capacity to utilise photosynthetic, catabolic and fermentative electrons (Ghirardi *et al*., 2009). One possibility of genetically engineering *C. reinhardtii* cells for improved H_2 production is to knock-down fermentative pathways that compete with the PFR H_2 production pathway (Burgess *et al*., 2011). These include the pdc3 pathway, which involves the enzymes PDC and ADH, and results in ethanol production, and the pfl1 pathway, which involves the enzymes PFL and AcDH, and results in ethanol and formic acid production (Figure 3.07). Dr Steven Burgess, working under the supervision of Professor Peter Nixon in the Department of Biology at ICL, was able to create a knock-down mutant of the pdc3 pathway, appropriately named the pdc3-KD mutant (Burgess *et al*., 2012). Additionally, the pfl1 pathway can be blocked using the inhibitor hypophosphite (Hemschemeier & Happe, 2005). It was therefore possible to design an experiment to measure the effect on H_2 production of knocking-down the pdc3 pathway only (pdc3-KD), inhibiting the pfl1 pathway only (cc124+IN) or knocking-down pdc3 and inhibiting pfl1 (pdc3-KD+IN), as shown in Figure I.11.

Since the proportion of fermentative electrons is much smaller than that of photosynthetic electrons, it is difficult to observe any difference in H_2 production rates using the standard S-deprivation procedure. H_2 production was therefore initiated by dark incubation and the experiments were carried out in the dark. However, this raised another concern, namely that the H_2 production rates in the dark are more than a factor of 10 lower than the already low H_2 production rates under illumination. On the other hand, it provided an excellent opportunity to test the ICL flat-plate PBR and its MIMS system. The dark H_2 production experiments consisted of four components: H_2 production by cc124, cc124+IN, pdc3-KD and pdc3-KD+IN. Each one of these components was run in triplicate. A fully-grown *C. reinhardtii* WT or mutant strain was prepared and placed in the flat-plate PBR and hypophosphite was added where appropriate. The PBR was covered by a dark cloth and all O_2 was purged out of the system with Argon. The PBR was then sealed shut and the MIMS system was activated. MIMS was used to measure the H_2 production rates over the next 4 hours. The results are shown in Figure I.12a.

The H_2 production rate using cc124+IN was lower than that of simply using cc124. This result highlights one of the pitfalls of deactivating metabolic pathways: it does not necessarily achieve the desired result. In this case, removing the pfl1 pathway actually reduced the electron flow to the hydrogenase enzyme, perhaps by encouraging additional ethanol production via the pdc3 pathway. The H_2 production rate using pdc3-KD was similar to that of using cc124. The main difference is that the pdc3-KD results were more variable. This is to be expected with a knock-down mutant strain, because not all cells will have had their pdc3 pathway knocked-down to the same degree, increasing the random error in the H_2 production measurement. Finally, pdc3-KD+IN showed a considerable increase in the H_2 production rate compared to the WT. In terms of the H_2 yield after 4 hours, pdc3-KD+IN produced 9.4±0.5 $\mu l \cdot mgChl^{-1}$ compared with 6.0±0.3 $\mu l \cdot mgChl^{-1}$ for cc124, a 57% increase (Figure I.11b). The dark H_2 production experiments have shown that it is possible to improve the H_2 production rate by knocking-down fermentative pathways in *C. reinhardtii*, provided that enough of the right pathways have been successfully knocked-down. On the other hand, it is now apparent that the best genetic improvements are those that target the photosynthetic electron transport pathway, such as the chlorophyll antenna mutants (Kosourov *et al*., 2011). In engineering terms, the dark H_2 production experiments have validated the use of MIMS to measure green algal biohydrogen production rates and yields, including for very low H_2 pervaporation rates.

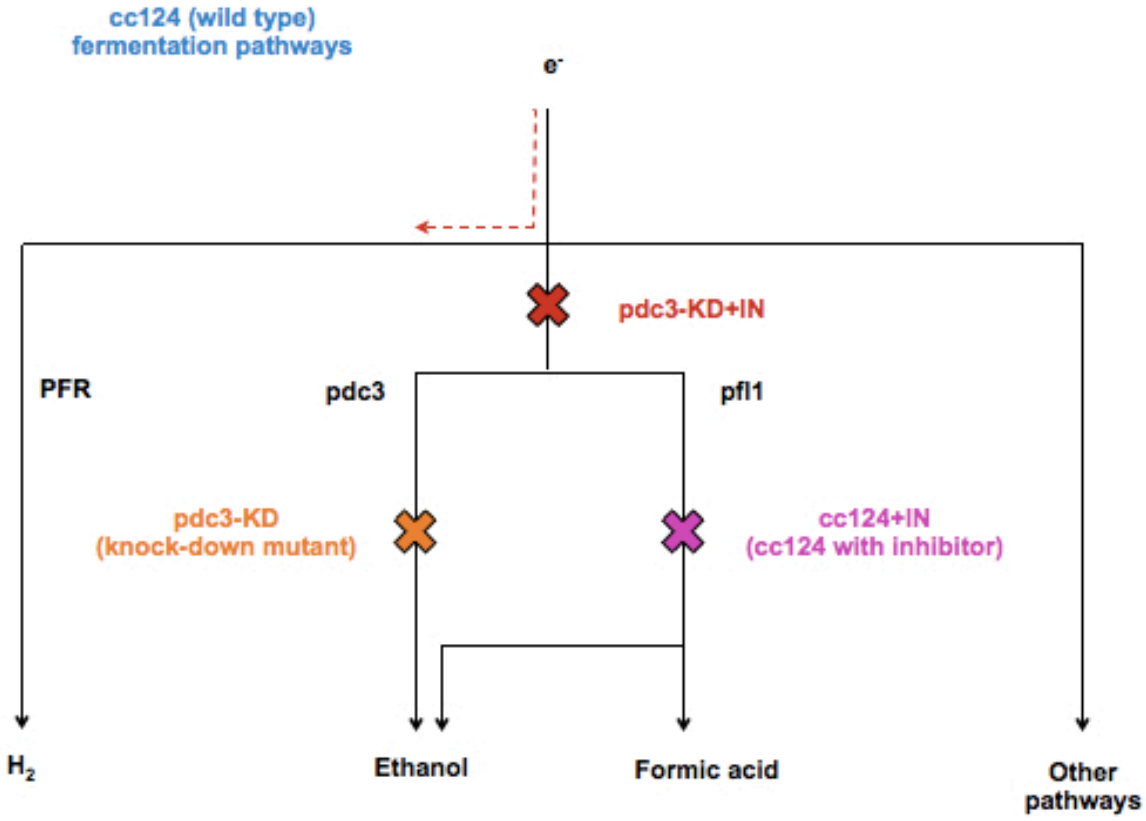
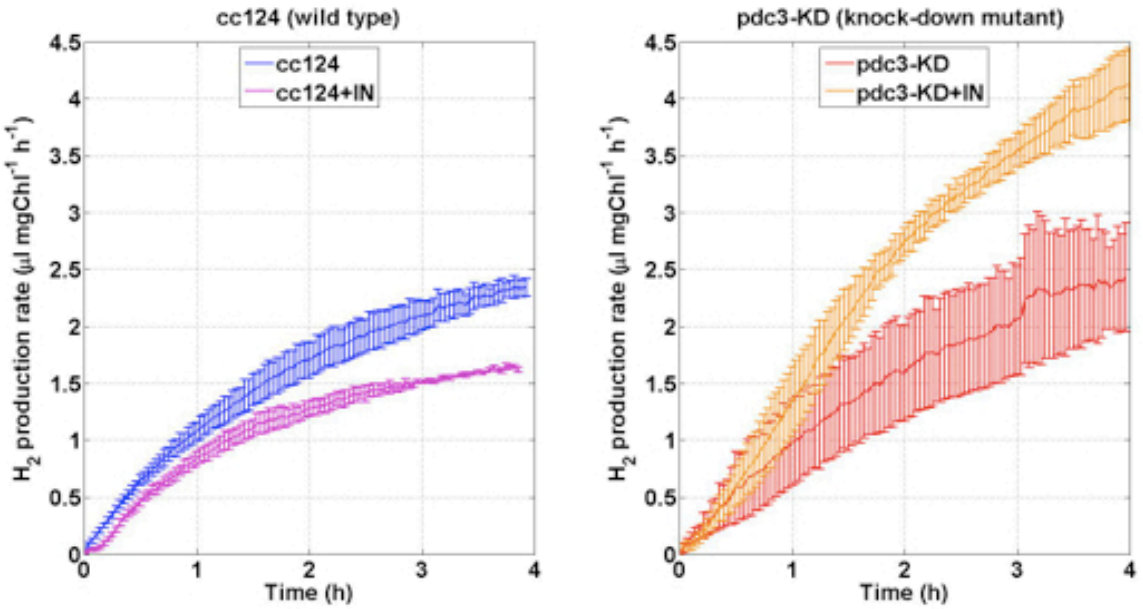
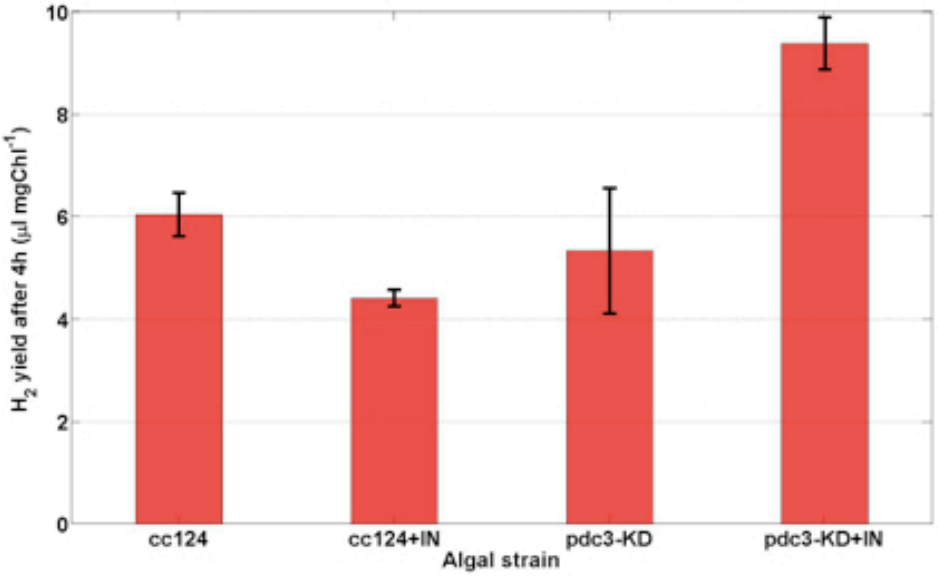


Figure I.11: Mutation pathways in *C. reinhardtii*

(a)





(b)

Figure I.12: Dark H_2 production by different *C. reinhardtii* strains

I.5. Summary

A flat-plate vertical one-litre photobioreactor that facilitates the biophotolytic H_2 production process has been designed and constructed (Tamburic *et al*., 2011b). The flat-plate reactor geometry was chosen due to its superior surface-to-volume ratio, which results in the highest observed photochemical efficiencies for H_2 production. The reactor was shown to enable rapid and accurate measurements of the key parameters in the biohydrogen production process under carefully controlled conditions. A novel dual-compartment flat-plate reactor was constructed from Perspex, using hydrogen-impermeable o-rings and stainless steel fittings. The primary compartment holds the algal culture and contains the key measuring instruments, including the MIMS system developed for *in situ* H_2 detection and extraction. The secondary compartment is used to control the system temperature and incident wavelength. Turbulent culture mixing is achieved by a circulating gas-lift system while a cool-white LED array provides uniform, coherent, non-heating illumination to the system. A comprehensive real-time datalogging and control system was developed. The ICL flat-plate PBR was successfully commissioned and calibrated. The validity of using MIMS to measure green algal H_2 production was confirmed by dark H_2 production experiments involving the fermentation mutant pdc3-KD. From July to November 2010, the reactor was operated and demonstrated in the Antenna Exhibition of contemporary science at the London Science Museum. Photos of PBR operation in the laboratory as well as in the Science Museum are shown in Figure I. 13.

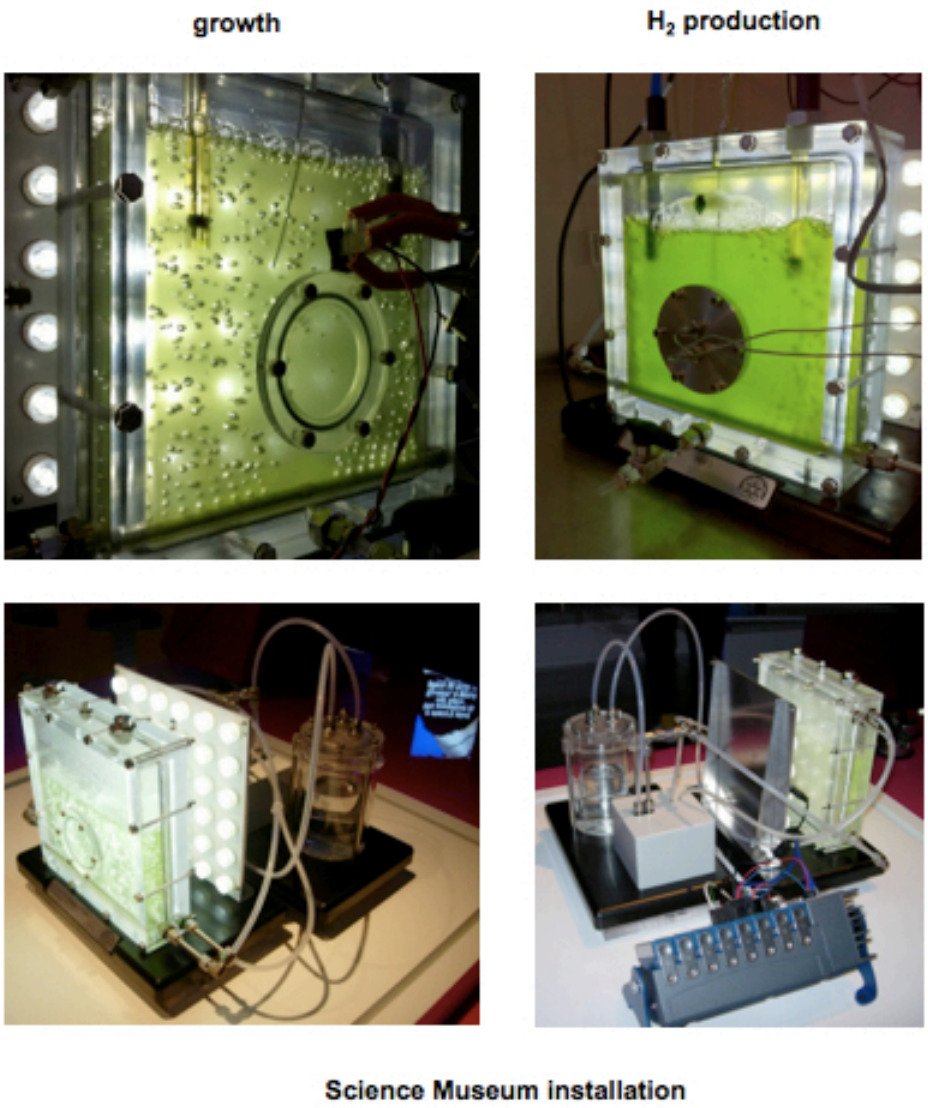


Figure I.13: Photographs of the complete and operational dual-compartment flat-plate PBR

II. Growth of *Chlamydomonas reinhardtii*

II.1. Introduction

Growing dense and healthy *C. reinhardtii* cultures is a prerequisite for effective biohydrogen production. The quantity of functioning algal cells directly determines the number of light-harvesting complexes, oxygen-evolving centres, hydrogenase enzymes and other reaction centres that are critical to the H_2 production process. In addition to enabling H_2 production, the agglomeration of *C. reinhardtii* biomass also facilitates the buildup of lipids, fatty acids, vitamins, carotenoids and other cellular components. These may be extracted and used to produce biodiesel, food additives and precursor chemicals, either as individual products, or as side-products that add value to the H_2 production process.

Due to its importance in various industries, algal biomass growth has been extensively studied and is consequently well understood. The *C. reinhardtii* growth medium recipes were finalised in the 1960s (Gorman & Levine, 1966). However, the growth medium recipes are generic, and there is still plenty of opportunity to optimise them for specific growth conditions. The effects of critical growth parameters, such as the specific algal strain (Sheehan *et al*., 1998), temperature (Kunjapur & Eldridge, 2010), light regime (Molina Grima *et al*., 1999), carbon source (Kosourov *et al*., 2007), light intensity (Janssen *et al*., 2003) and photobioreactor geometry (Posten, 2009) have all been investigated. What is missing is a well-developed growth model that can reach across all these different growth conditions and photobioreactor geometries.

This chapter will feature the development of a simple logistic *C. reinhardtii* growth model, which may be fitted to experimental results to extract important growth kinetic parameters. The aim is to determine which parameters are important for optimising algal growth. The chapter will describe the evolution of this model, from its initial application to well-understood phenomena, such as the effect of algal strain and temperature on *C. reinhardtii* growth, to its implementation in more complex scenarios, such as the growth under different light regimes and using different carbon sources. Eventually, a detailed study of *C. reinhardtii* growth under different light intensities will be conducted. The focus in all these experiments has been to grow *C. reinhardtii* cultures to high

densities as quickly and as economically as possible. As well as covering a number of environmental parameters that affect algal growth, this chapter will also examine algal growth using all the available PBRs and PBR geometries: vertical-column, stirred-tank, tubular and flat-plate.

II.2. Effect of *C. reinhardtii* Strain

One of the first decisions made during the course of this thesis involved the selection of a *C. reinhardtii* strain to be used in the majority of algal growth and biohydrogen production experiments. At the time, few genetically modified strains were available locally at Imperial College London and the laboratory had not yet passed the health and safety clearance for using GM organisms. The choice was therefore limited to three naturally-occurring *C. reinhardtii* strains: the laboratory WT cc124, the starch-accumulating mutant dum24 and the cell-wall-deficient mutant cc406. Growth experiments were carried out in triplicate in the vertical-column Plankton Light Reactors (AquaMedic) at 42.5 $W \cdot m^{-2}$ using the 5xTAP* growth medium. The acetate-replete 5xTAP* medium was used to ensure that there is sufficient organic substrate available to facilitate dum24 growth. The OD was measured at regular time intervals by extracting a 10 ml algal sample from the vertical-column reactor and analysing its light-scattering properties at 663 nm using a spectrophotometer. This OD measurement, initially in absorbance units, was converted to units of chlorophyll concentration (Equation 5.09). The raw growth results are shown in Figure II.01, with the vertical error bars representing the standard error of the triplicate OD measurements.

The results in Figure II.01 matched the logical hypothesis. Laboratory WT cc124 grew to an OD of 36 $mg \cdot l^{-1}$Chl over a period of approximately 70 hours. The mutant dum24 required more time to synthesise additional starch; it grew more slowly but attained a higher final OD than cc124. The final OD of 44 $mg \cdot l^{-1}$Chl was 22% higher than that of cc124, but this density was only attained after 140 hours of biomass synthesis. The cell-wall-deficient cc406 grew slightly faster than dum24, but it grew slower than cc124 and resulted in a lower final OD. The lack of a cell wall makes cc406 easier to genetically modify, but it also reduces its ability to grow effectively. Based on these results, cc124 was chosen as the primary experimental strain. This experiment also presented an excellent early opportunity to put the logistic growth model to the test.

The logistic curve takes on the sigmoid shape observed, for example, in Figure II.03 as a result of a number of competing environmental effects. At the start of the experiment, the *C. reinhardtii* culture is very dilute and all *C. reinhardtii* cells have access to sufficient illumination and nutrients. Consequently, the algae grow and reproduce by mitosis, generating 4 to 8 daughter cells for each

mother cell. This is the stage of exponential growth. As the culture becomes denser, the cells closer to the illumination source begin to shade the cells behind them, reducing their ability to photosynthesise and grow. The growth rate decreases and eventually becomes linear: this is the midpoint of the sigmoid curve. As the cell density increases further, the transport, or logistics, of light and key nutrients becomes a limiting factor (Posten, 2009). The growth rate decreases to zero and the culture has reached a final stable concentration based on that particular set of environmental conditions.

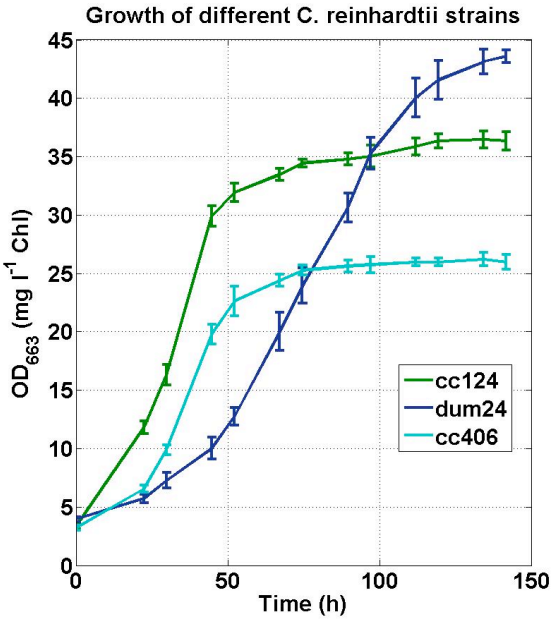
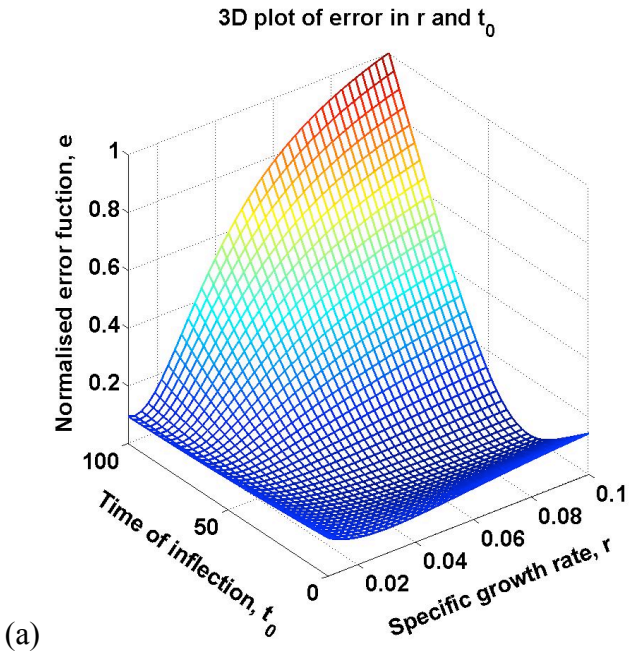
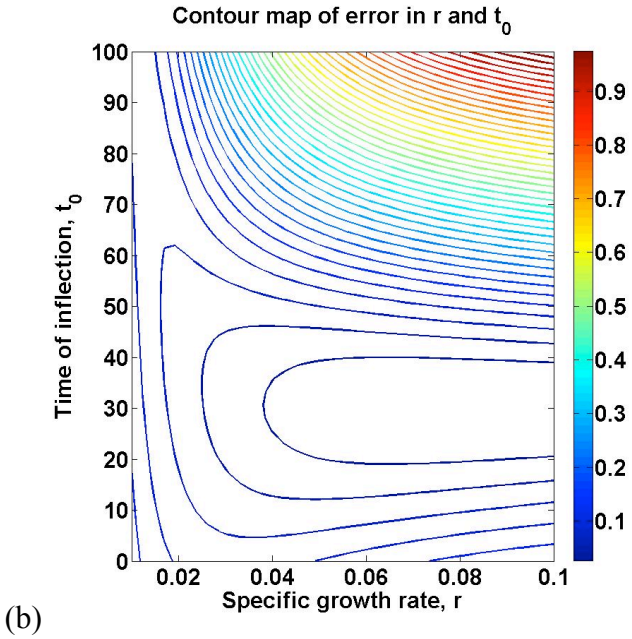


Figure II.01: Growth curves for the cc124, dum24 and cc406 strains of *C. reinhardtii* in the vertical-column PBR, raw data



(a)



(b)

Figure II.02: Fitting the logistic model parameters r and t_0 using the method of least squares

(a) 3D plot of the normalised error function, e

(b) Contour map of the normalised error function, e

The logistic model aims to fit a sigmoid function (Equation 5.16) to experimental *C. reinhardtii* growth data. The sigmoid function has three kinetic parameters: the maximum OD obtained during growth K, the specific growth rate r, and the time of inflection t_0. The model is solved by setting K to unity and calculating r and t_0 using the method of least squares, before recovering K by linear optimisation. Figure II.02 shows a graphical representation of the method of least squares. A normalised error function, e, was defined to indicate the magnitude of the error that would be made for each possible combination of r and t_0 values. The colour red indicates regions of high error within this matrix, while dark blue indicates regions of low error. From the contour plot in Figure 02b, it is clear that $r > 0.04$ and that $20 < t_0 < 40$. The MatLab program that produced the graphs in Figure II.02 was written to find the exact minimum of e in order to extract all three kinetic parameters from any given growth experiment, and to reconstruct and plot the corresponding optimised logistic functions (Figure II.03).

As shown in Figure II.03, the logistic model provides a very accurate description for the growth of all three *C. reinhardtii* strains. The maximum standard error in the triplicate growth experiments was 3 $mg \cdot l^{-1}$Chl, observed during dum24 growth. All logistic curves stay comfortably within that error range and in most cases approach very close to the mean experimental measurements. The biggest error occurs in the case of the initial 0 hour measurement, where the logistic model consistently underestimates the experimental measurement. This error is probably caused by sluggish *C. reinhardtii* growth within the first few hours of the experiment as the cells become acclimatised to their new environment. Kinetic parameters extracted by the logistic model (Figure II.03) make it possible to collect some additional observations about the growth of different *C. reinhardtii* strains that were not immediately obvious from the raw data. For example, it is interesting to note that cc124 ($r = 0.093\ h^{-1}$) and cc406 ($r = 0.094\ h^{-1}$) have an almost identical specific growth rate. Another observation is that the dum24 experiment was concluded before the algae had completely finished growing and that they would have actually attained a final OD of 46.9 $mg \cdot l^{-1}$Chl had the experiment been continued. Finally, the logistic model enables a much more accurate comparison between the different growth curves. It is now possible to conclude that cc124 ($r = 0.093\ h^{-1}$) was chosen over dum24 ($r = 0.042\ h^{-1}$) because the cells grew 2.2 times faster, ensuring that twice as many growth and H_2 production experiments could be conducted using cc124.

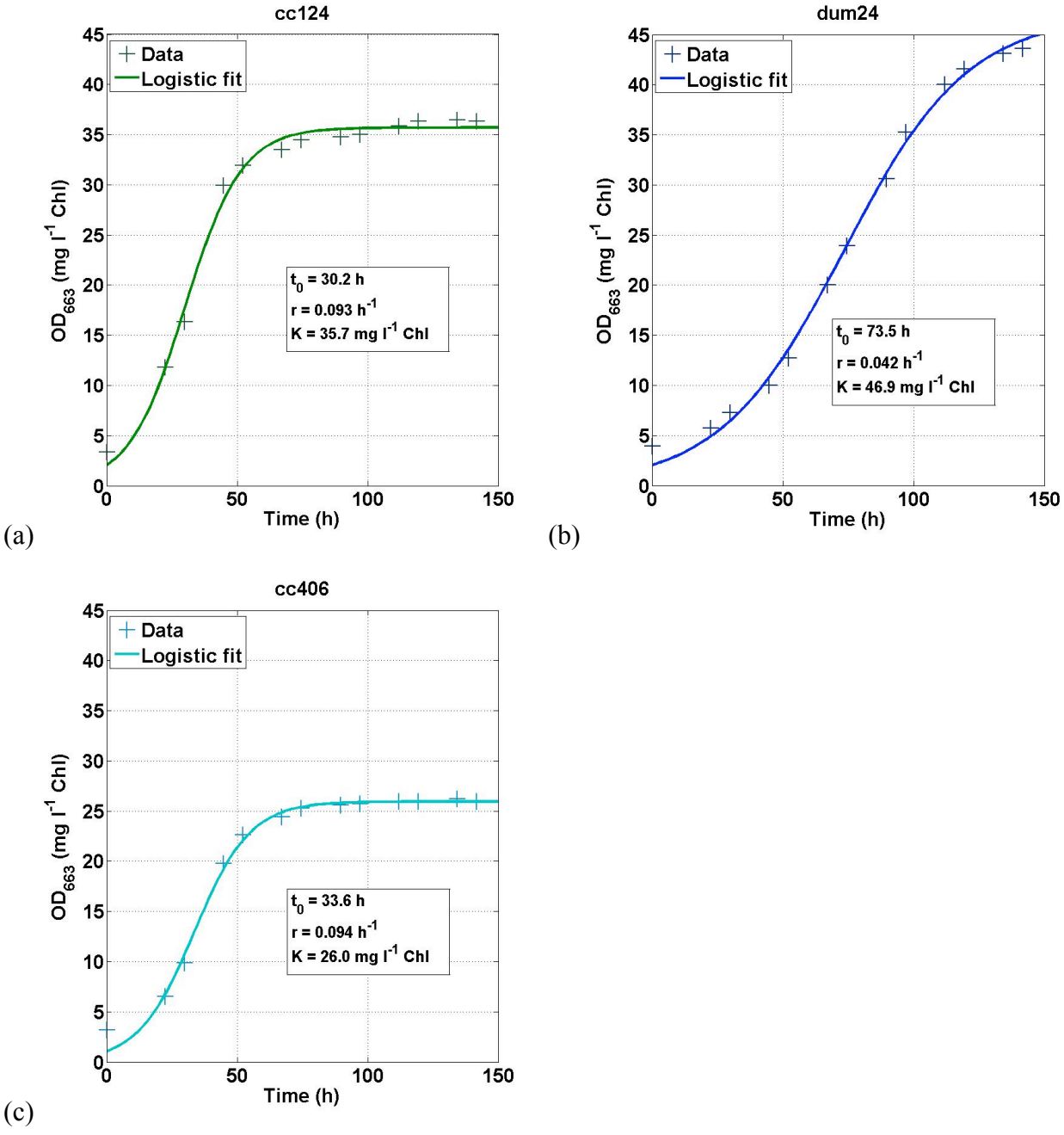


Figure II.03: Logistic model fit to experimental growth data for different *C. reinhardtii* strains

(a) cc124

(b) dum24

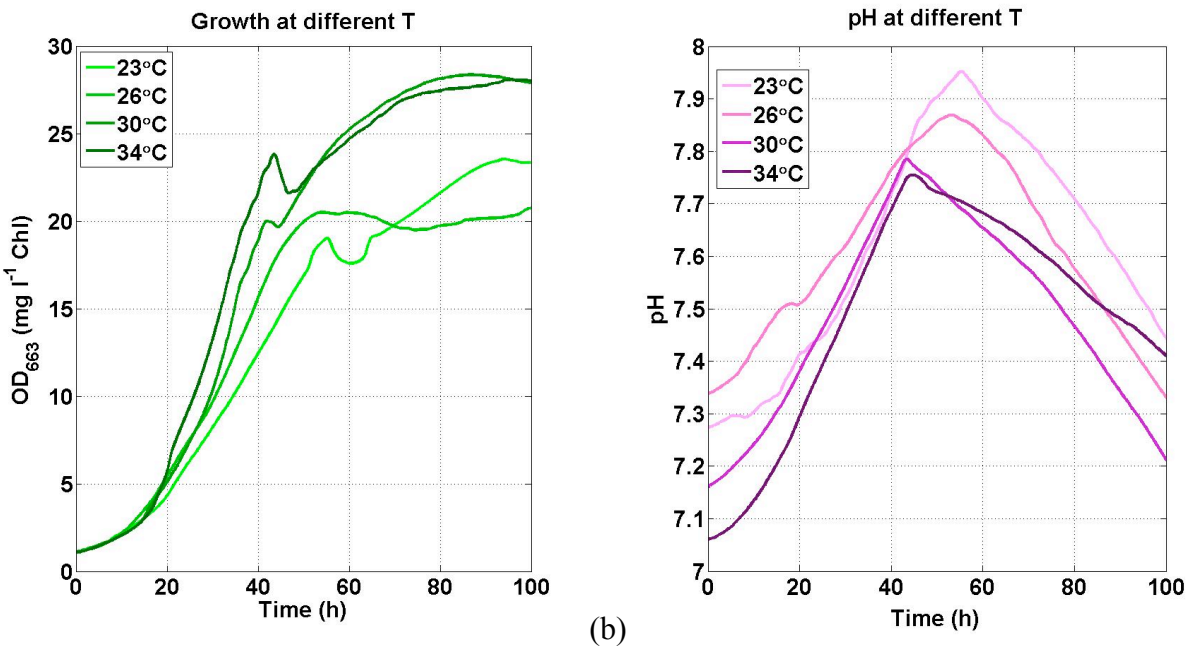
(c) cc406

II.3. Effect of Temperature

Experiments to measure the effect of temperature on *C. reinhardtii* cc124 growth were carried out in the Sartorius tubular PBR using the TAP algal growth medium at a light intensity of 30 $W \cdot m^{-2}$. Temperature was controlled by means of a heated water jacket that encompasses the central vessel of the PBR. A Pt100 thermocouple was used to measure the temperature of the algal culture; this measurement was immediately fed into the Sartorius control tower, which operated a feedback loop that controlled the temperature of the water jacket accordingly. Experiments were carried out at temperatures of 23°C, 26°C, 30°C and 34°C (Figure II.04). OD was measured using the Fundalux OD probe and pH was measured with the Easyferm pH electrode. OD measurements at 875 nm were converted to units of chlorophyll content (Equation 5.10).

The raw temperature data (Figure II.04a) suggests that cc124 cultures grow better at higher temperatures. However, it is difficult to be certain of this result, because an anomaly is observed during the 40-60 hour period in the case of all cc124 growth curves. Figure II.04b shows that the pH of the algal cultures initially increases until it reaches a sharp maximum during this 40-60 hour period, and then it subsequently decreases. The initial increase in pH is caused by acetic acid consumption (Chen & Johns, 1994). The pH maximum likely occurs once the entire acetate supply of the TAP medium has been used up (this hypothesis will be corroborated by later results). The subsequent decrease in pH may be partially attributed to the tendency of *C. reinhardtii* cells to self-buffer (Faraloni *et al*., 2011). Under alkaline conditions, the cells were found to secrete traces of malic, succinic and formic acid in an attempt to return the growth medium to a more neutral pH (analysis carried out by HPLC, results not shown). Although self-buffering processes may contribute towards forming the growth anomalies observed in Figure II.04a, a more likely culprit is the need to switch from a largely photoheterotrophic to an entirely photoautotrophic growth mechanism in the absence of acetate. The Sartorius PBR was operated as an open system so that there was a continuous supply of CO_2 available in the headspace of the PBR. On the other hand, this CO_2 was poorly mixed with the algal culture since the peristaltic mixing system was designed for liquid circulation and tubular reactors have substandard gas transfer properties (Chisti & Jauregui-Haza, 2002). Some CO_2 did eventually become absorbed by the algal culture, as evidenced by continued growth following acetate depletion, and by the simultaneous decrease in pH, which

was partially caused by the absorption of acidic CO_2 molecules. The growth curve anomalies in Figure II.04a result from a delay in switching between different phototrophic growth mechanisms and the limited availability of dissolved CO_2.



(a) (b)

Figure II.04: Growth of *C. reinhardtii* cc124 at different temperatures in the Sartorius tubular reactor, raw data

(a) OD curves at different temperatures

(b) pH curves at different temperatures

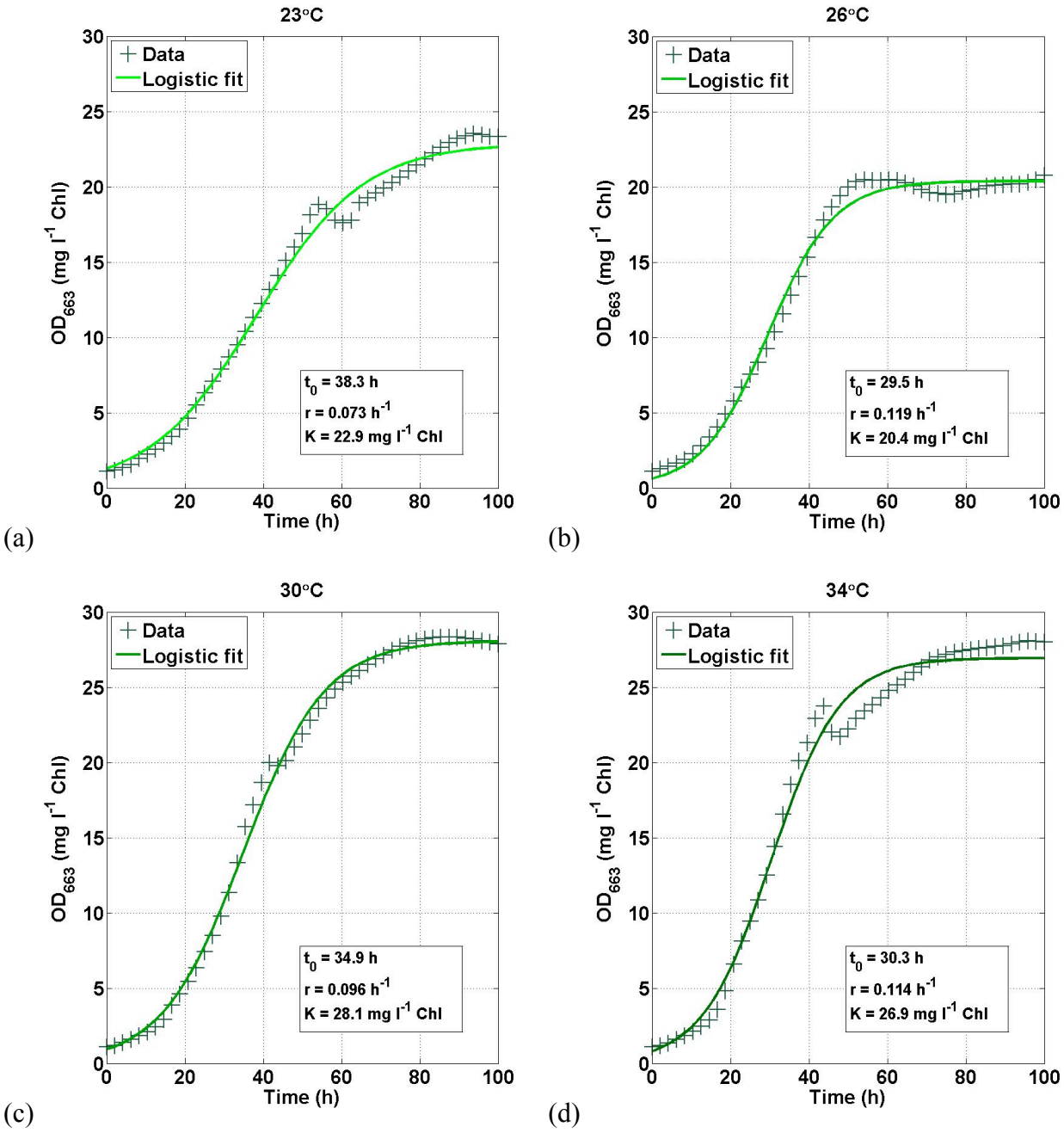


Figure II.05: Logistic model fit to experimental data for *C. reinhardtii* cc124 grown at different temperatures

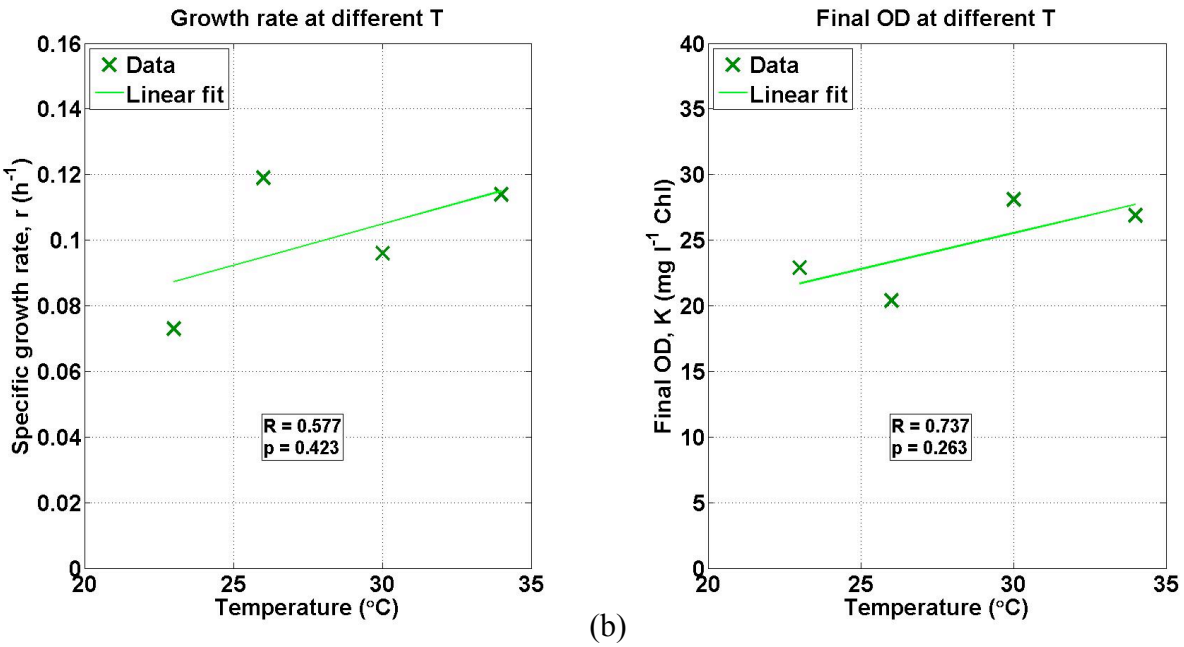
(a) 23°C

(b) 26°C

(c) 30°C

(d) 34°C

The logistic model was applied to the cc124 growth curves at different temperatures (Figure II.05). The logistic model fit was imperfect because of the growth anomalies described previously. Nevertheless, the logistic model provides a good estimate of the specific growth rates and final ODs of the algal cultures. The specific growth rate, r, and the final OD, K, were plotted as functions of temperature in Figures II.06a and II.06b, respectively. The statistical significance of the resulting correlations was assessed using the correlation coefficient, R, and the p-value, p. The Pearson's product-moment correlation coefficient R is a measure of the linear dependence between two variables. An R value of ±1 indicates perfect correlation, while a value of zero indicates no correlation. The correlation coefficients of r (R = 0.577) and K (R = 0.737) both indicate some positive correlation between that kinetic parameter and the temperature, confirming the initial observation that cc124 cells grow better at higher temperatures. The p-value is a test of the statistical significance of the observed correlation. A p-value less than 0.010 is typically taken to indicate that the correlation is significant. Neither the p-value of r (p = 0.423) nor that of K (p = 0.263) confirms statistical significance. The limited effect of temperature on cc124 growth is also supported by the literature (Bosma *et al*., 2007; Kunjapur & Eldridge, 2010). The temperature was controlled at 25°C in all subsequent experiments in the Sartorius tubular PBR and in the ICL flat-plate PBR.



(a) (b)

Figure II.06: Growth parameter correlations with temperature

(a) Growth rate, *r*, at different temperatures, linear fit

(b) Final OD, *K*, at different temperatures, linear fit

II.4. Growth under different Light Regimes

II.4.1. Growth in TAP

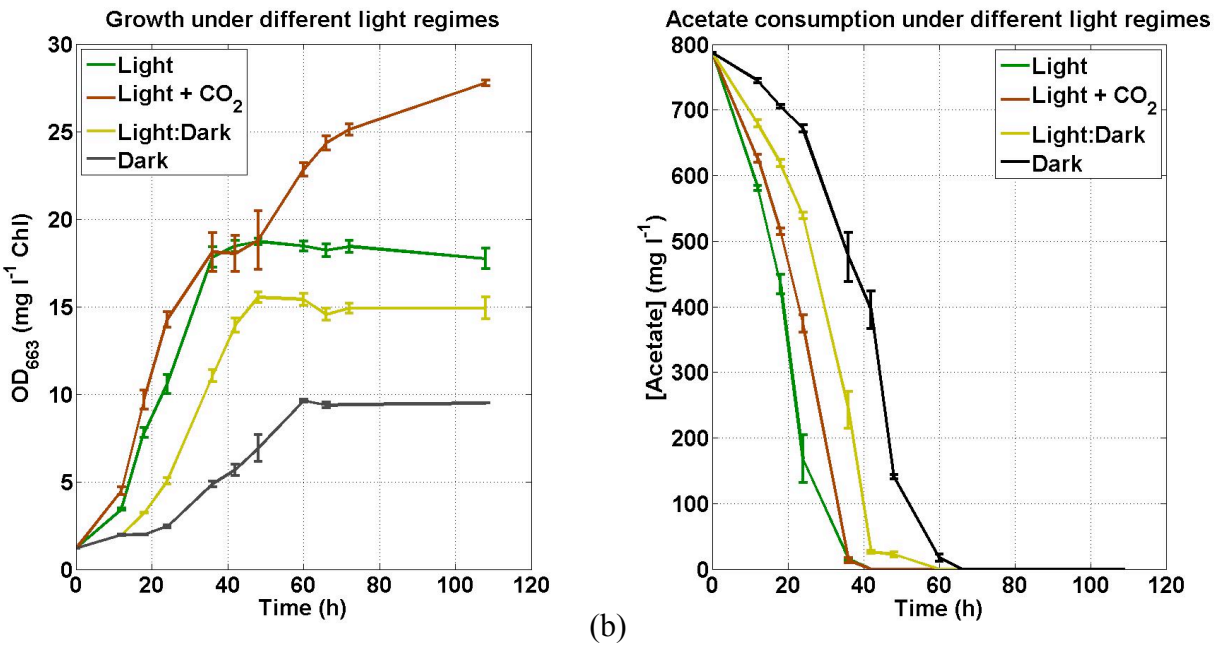
Experiments to investigate cc124 growth under different light regimes were carried out in the Solar Biofuels Consortium stirred-tank PBRs using the TAP growth medium. OD was measured by sampling followed by spectrophotometry at 663 nm. In addition, the acetate concentration of these samples was also measured by HPLC (Chapter 5.7.3.). Four different light regimes were investigated: continuous illumination (light), continuous illumination with CO_2 bubbling (light + CO_2), 12h:12h light:dark cycles, and no illumination (dark) (Figure II.07). The CO_2 was bubbled from a 2% CO_2 (in air) gas cylinder at a flow rate of 100 ml·min^{-1}. The light intensity in the stirred-tank PBRs was approximately 25.0 W·m^{-2}. In the 12h:12h light:dark cycle experiment, 25.0 W·m^{-2} was the light intensity during the light period (the mean light intensity was 12.5 W·m^{-2}). The reactors used for all other light regimes were sealed throughout the course of the experiments and had very limited gaseous headspace. All the experiments were conducted in triplicate; the error bars indicate the standard error in the measurements.

One observation from the raw growth data (Figure II.07a) is that cc124 cultures grow to a higher OD under continuous illumination with, as opposed to without, CO_2 bubbling. This indicates that photomixotrophic growth results in better algal yields than photoheterotrophic growth (Kosourov *et al*., 2007). In addition, growth under light-dark cycles is worse than growth under continuous illumination. This result has repercussions once algal growth and biohydrogen production are scaled up from laboratory systems with artificial illumination (Tamburic *et al*., 2011b) to larger outdoor facilities (Scoma *et al*., 2011). At the same time, growth at a mean light intensity of 12.5 W·m^{-2} is more efficient under light:dark cycles than it would be under a continuous light source. The reason for this is that light:dark cycles are a better representation of the natural environment of *C. reinhardtii*. The growth of cc124 cultures in the dark was used as a control to indicate the capacity of the cells to grow purely on substrate as opposed to the photosynthetically-assisted growth witnessed in the other experiments.

Figure II.07b proves that acetate was depleted 40-60 hours from the start of a growth experiment in the TAP medium. Algal cultures growing under continuous illumination without CO_2 (light), under light:dark cycles, and those growing in the dark experienced heterotrophic growth; the higher their growth rate, the quicker they used up the available acetate. On the other hand, cultures growing under continuous illumination with CO_2 bubbling consumed their acetate more slowly than those growing under continuous illumination without CO_2 bubbling despite a slightly higher growth rate, indicating that some CO_2 was also used for biomass synthesis. While growth in the three heterotrophic growth experiments is clearly acetate-limited, the CO_2-bubbled culture continues to grow following acetate depletion. As observed in previous experiments, a growth curve anomaly occurs while the culture adjusts from a mostly photoheterotrophic growth mechanism to an entirely photoautotrophic growth mechanism. Following this adjustment period, the culture continues to grow.

Logistic model curves were fitted to experimental data to extract kinetic growth parameters and enable more precise comparisons of growth under different light regimes (Figure II.08). The maximum error in the logistic fit is 3.5 $mg \cdot l^{-1}$Chl, which arises when fitting kinetic parameters to the staggered data of the experiment with continuous illumination and CO_2 (Figure II.08b); all the other logistic fits are visually excellent. The first point of interest is that cc124 cultures growing in the dark can achieve a final OD of 10.1 $mg \cdot l^{-1}$Chl, an important benchmark value. Cultures growing under 12h:12h light:dark cycles have a lower growth rate ($r = 0.142\ h^{-1}$) and a lower final OD ($K = 15.3\ mg \cdot l^{-1}$Chl; only 5.2 $mg \cdot l^{-1}$Chl above the benchmark value), compared with the growth rate ($r = 0.161\ h^{-1}$) and final OD ($K = 18.5\ mg \cdot l^{-1}$Chl, 8.4 $mg \cdot l^{-1}$Chl above the benchmark value) of cultures growing under continuous illumination. It is therefore not realistic to extrapolate laboratory growth results to real outdoor systems, even before temperature control requirements and the hazards of contamination, predation and evaporation are taken into account. The final OD under continuous illumination was enhanced by CO_2 bubbling ($K = 26.4\ mg \cdot l^{-1}$Chl, compared to 18.5 $mg \cdot l^{-1}$Chl without CO_2 bubbling, an increase of 43%), but it comes at the cost of a significantly slower growth rate ($r = 0.067\ h^{-1}$, compared to $0.161\ h^{-1}$ without CO_2 bubbling). This inferior growth rate under continuous illumination with CO_2 bubbling is probably caused by a major delay (approximately 10 hours) while switching between different growth mechanisms as well as by the subsequent low

photoautotrophic growth rate. It was possible to remove both of these effects by overloading the growth medium with acetate, as explored below.



(a) (b)

Figure II.07: Growth of *C. reinhardtii* cc124 in TAP medium under different light regimes in the stirred-tank PBRs, raw data

(a) OD curves under different light regimes

(b) Acetate consumption under different light regimes

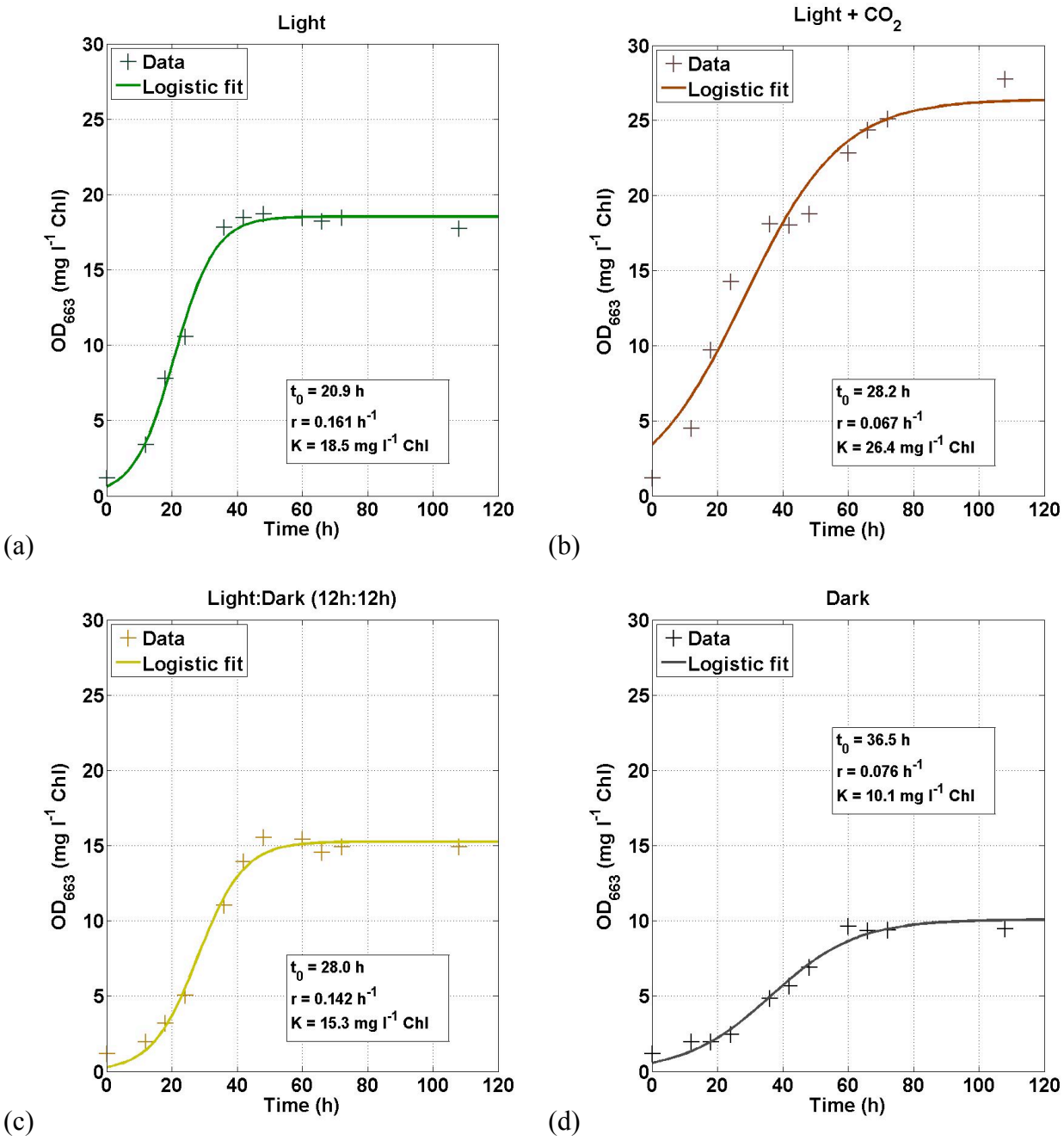


Figure II.08: Logistic model fit to experimental data for *C. reinhardtii* cc124 grown under different light regimes in TAP medium

(a) Constant illumination

(b) Constant illumination with CO_2 bubbling

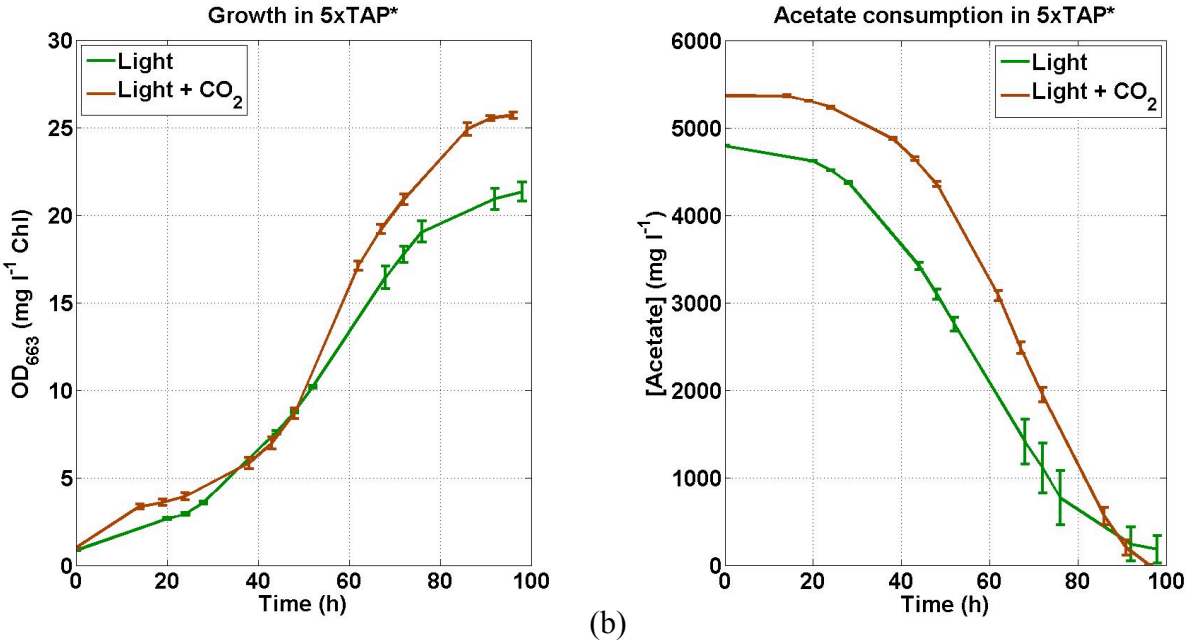
(c) 12h:12h light-dark cycles

(d) No illumination

II.4.2. Growth in 5xTAP*

The 5xTAP* growth medium was prepared by increasing the acetate concentration and the buffer concentration in the TAP medium by a factor of five, while leaving the other ingredients unchanged (Table 5.09a). The 5xTAP* medium was used to facilitate growth experiments that were not acetate-limited. These experiments were not subject to growth anomalies because a consistent carbon source regime (either photoheterotrophic or photomixotrophic) was maintained throughout the experiment. Experiments under continuous illumination, with and without CO_2 bubbling, were repeated in 5xTAP* to investigate the effect of CO_2 bubbling (as opposed to both CO_2 bubbling and acetate limitation) on cc124 culture growth (Figure II.09a). The experiments were carried out in triplicate. Acetate consumption was measured by HPLC (Figure II.09b). The acetate supply was not exhausted during the course of either experiment. Logistic model curves were fitted to the experimental data (Figure II.10).

The two experiments in 5xTAP* resulted in very similar growth rates ($r = 0.066\ h^{-1}$ and $0.063\ h^{-1}$) but the final OD with CO_2 bubbling ($K = 28.7\ mg \cdot l^{-1}Chl$) was 26% higher than the final OD without CO_2 bubbling ($K = 22.8\ mg \cdot l^{-1}Chl$). This proves with certainty that photomixotrophic growth is superior to photoheterotrophic growth and that CO_2 bubbling should be applied to growing *C. reinhardtii* cc124 cultures. On the other hand, the algal growth rate in 5xTAP* under continuous illumination without CO_2 bubbling ($r = 0.066\ h^{-1}$) was significantly lower than the growth rate of the corresponding experiment in TAP ($r = 0.161\ h^{-1}$), although the final OD was slightly higher ($K = 22.8\ mg \cdot l^{-1}Chl$, compared with $18.5\ mg \cdot l^{-1}Chl$). These results suggest that some acetate-inhibition is probably taking place in the 5xTAP* medium (Chen & Johns, 1994). The most favourable concentration of acetate in the growth medium and the optimal partial pressure of CO_2 bubbling will be investigated in the following section.

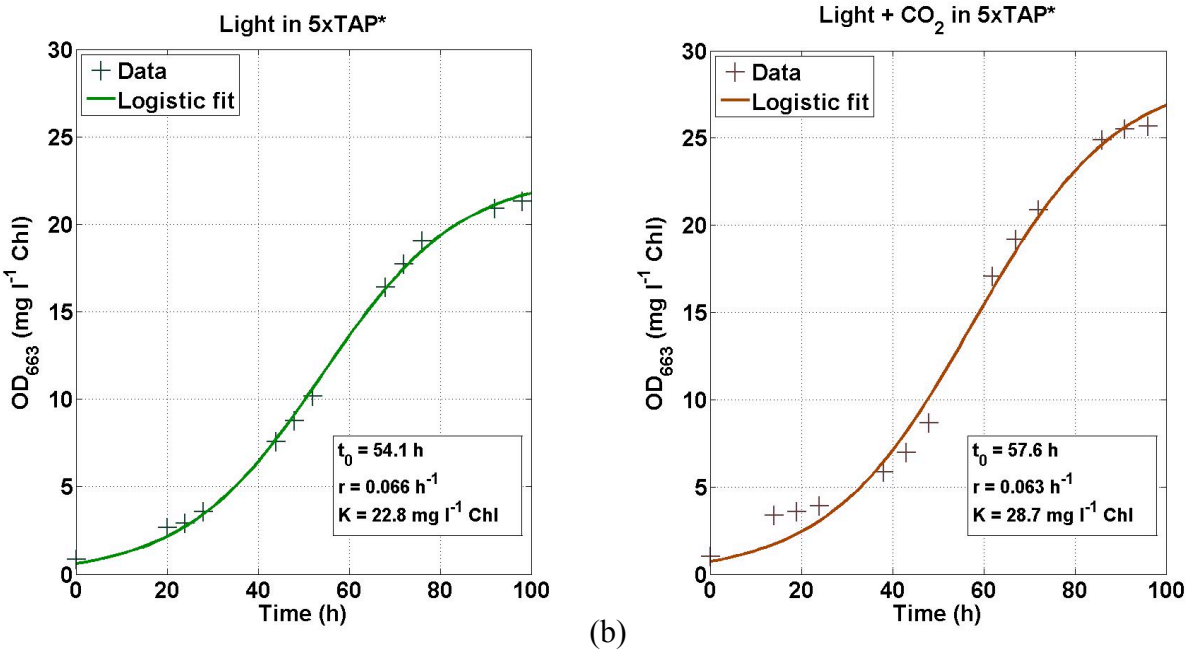


(a) (b)

Figure II.09: Growth of *C. reinhardtii* cc124 in 5xTAP* medium under different light regimes in the stirred-tank PBRs, raw data

(a) OD curves under different light regimes

(b) Acetate consumption under different light regimes



(a) (b)

Figure II.10: Logistic model fit to experimental data for *C. reinhardtii* cc124 grown under different light regimes in 5xTAP* medium

(a) Constant illumination

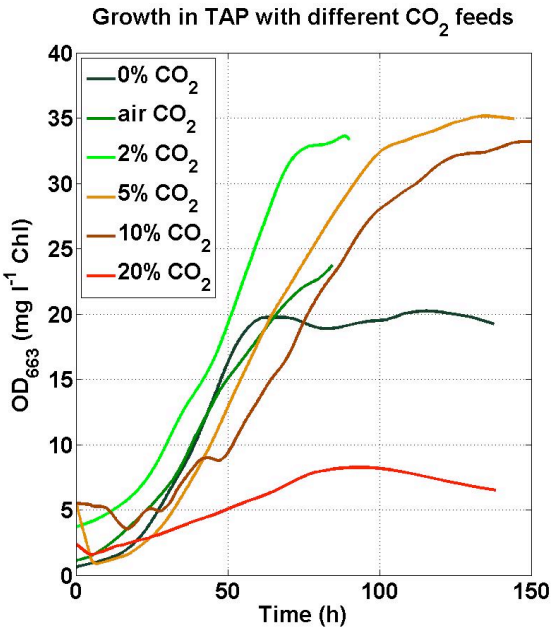
(b) Constant illumination with CO_2 bubbling

II.5. Growth using different Carbon Sources

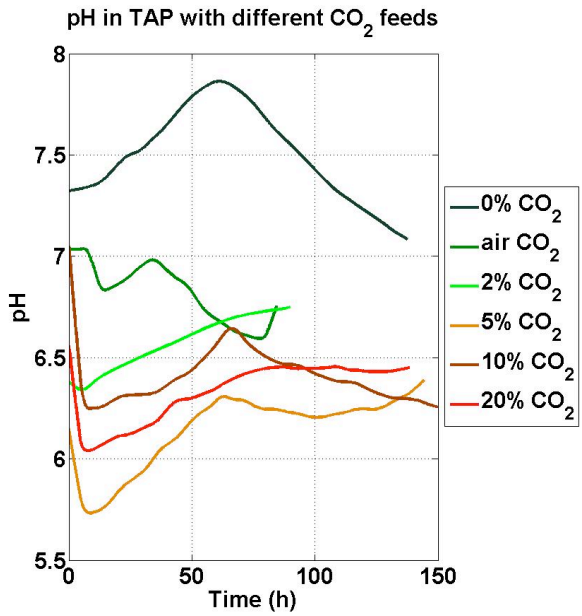
II.5.1. Growth in TAP with CO_2 bubbling

The aim of this section is to discover the optimum concentration of CO_2 that should be bubbled into a PBR to encourage *C. reinhardtii* cc124 growth. A series of experiments was carried out with cc124 in the Sartorius tubular reactor. The temperature was controlled at 25°C, the light intensity was controlled at 30 $W \cdot m^{-2}$ and the TAP growth medium was used. CO_2 was bubbled via a finely-perforated sparger at the bottom of the central vessel of the Sartorius PBR, at a flow rate of 100 $ml \cdot min^{-1}$. All experiments were operated in an open PBR system. The Sartorius PBR enabled on-line monitoring of the OD and pH of the culture. Small liquid samples (10 ml) were extracted at regular intervals to measure the acetate concentration by HPLC. Six different experiments were carried out: 0% CO_2 feed (the reactor was bubbled with N_2; this was the control experiment), 0.039% CO_2 (the reactor was bubbled with air), 2% CO_2 (2% CO_2 in air from a gas cylinder), 5% CO_2, 10% CO_2, and 20% CO_2 (Figure II.11).

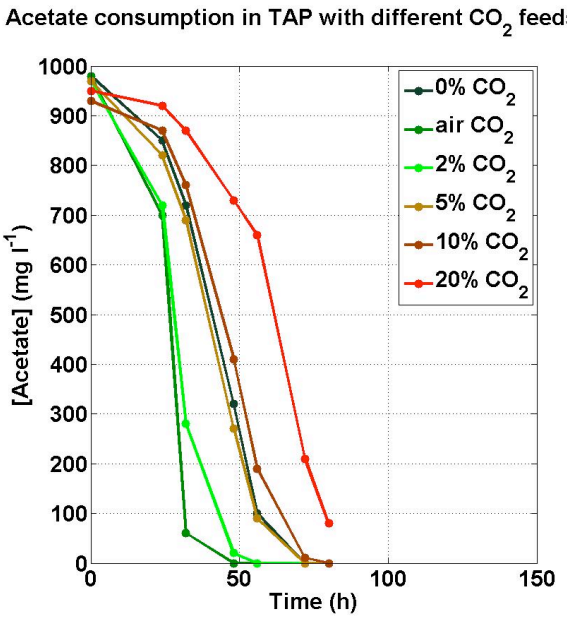
The raw growth data (Figure II.11a) indicate that CO_2 feeds of 2%, 5% and 10% result in the best algal growth, but it is difficult to differentiate between them without applying the logistic model. The pH drops quite low as the acidic CO_2 is bubbled through and absorbed by the algal culture (Figure II.11b). It even falls beneath pH 6 in the case of the 5% CO_2 feed, but the pH does not appear to have a significant, reproducible effect on the algal growth rate. The pH profile of the 0% CO_2 feed is markedly different from the other pH profiles (including air feed), but it lacks the sharp pH maximum of the pH profiles observed in Figure II.04b. This would suggest that continuous bubbling ensures that gases in the algal culture are well-mixed, including the gas phase CO_2 in the PBR headspace. As a result, there was no major delay in switching between different growth mechanisms and consequently no anomaly in the growth curves (Figure II.11a) once the acetate supply ran out (Figure II.11c). The general trend in the acetate data (Figure II.11c) is for slower acetate consumption at higher CO_2 concentrations because more CO_2 is used as a replacement for acetate during biomass synthesis.



(a)



(b)



(c)

Figure II.11: Growth of *C. reinhardtii* cc124 in TAP medium bubbled with different CO_2 partial pressures

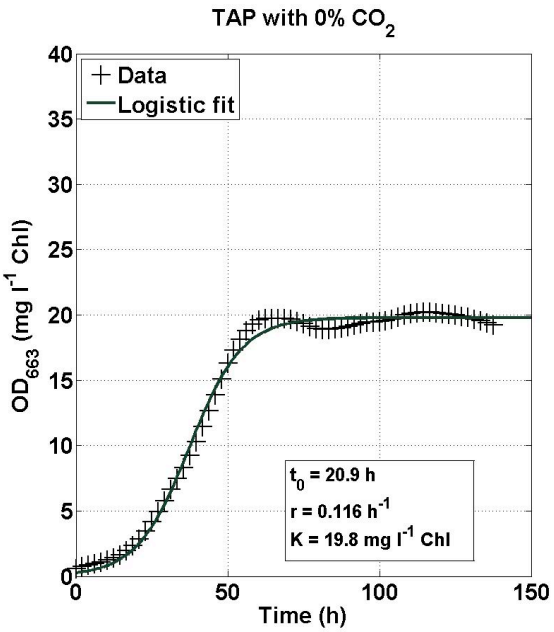
(a) OD curves in TAP with different CO_2 feeds

(b) pH curves in TAP with different CO_2 feeds

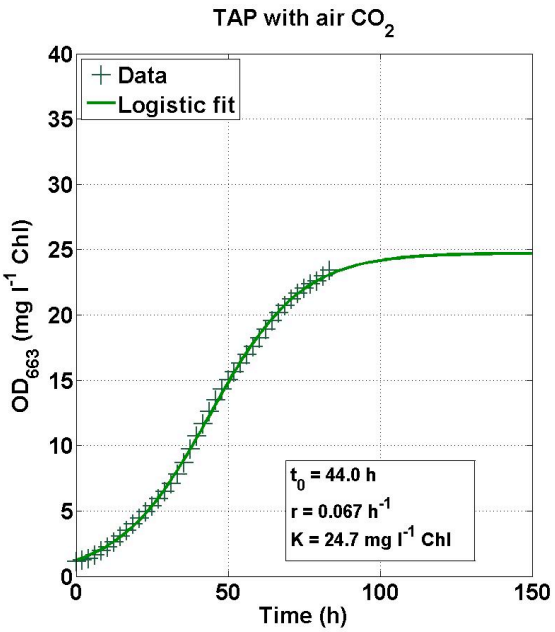
(c) Acetate consumption curves in TAP with different CO_2 feeds

Figure II.12 shows the application of the logistic fit parameters to experimental growth data. In general, the logistic curves provided a good fit to experimental data. However, there was a discrepancy between logistic model estimates and experimental measurements at high CO_2 concentrations during the first 5-15 hours of algal growth. It was observed that during the early stages of these experiments, gas bubbles became attached to the OD probe and affected the light scattering measurements. This highlighted the limitation of using an OD probe *in situ*; subsequent experiments used sampling and spectrophotometry to obtain backup OD data. The accumulation of gas bubbles on the OD probe is unlikely to be related to the CO_2 concentration of the gas feed. Correlations between the algal growth rate and the CO_2 feed concentration (Figure II.13a), and between the final OD and the CO_2 feed concentration (Figure II.13b) have been plotted. A second-order polynomial fit was used in anticipation of a kinetic parameter maximum at the optimal CO_2 feed.

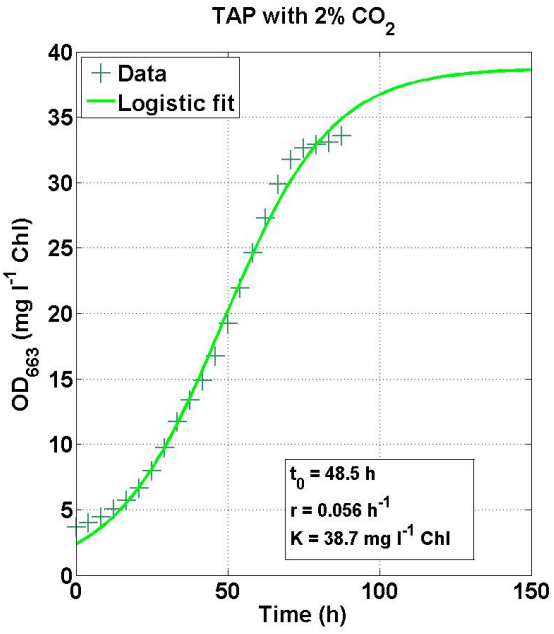
It turned out that the fastest cc124 culture growth rate ($r = 0.087\ h^{-1}$) was actually observed with the 0% CO_2 feed (Figure II.13a). This result shows that *C. reinhardtii* cc124 cells use acetate as a carbon source much more effectively than they use CO_2, and that providing any CO_2 to an acetate-replete medium such as TAP can only reduce the growth rate. On the other hand, the maximum final OD ($K = 37.9\ mg \cdot l^{-1}Chl$) was calculated to occur at a CO_2 feed of 7.9%. There is therefore a trade-off between the algal cell density and the growth rate. The best H_2 production rates would be attained by growing *C. reinhardtii* cc124 in TAP with a CO_2 feed of 8%, but this configuration would not necessarily result in the best H_2 production yield.


TAP with 0% CO2
Data
Logistic fit
t0 = 20.9 h
r = 0.116 h-1
K = 19.8 mg l-1 Chl
OD663 (mg l-1 Chl)
Time (h)

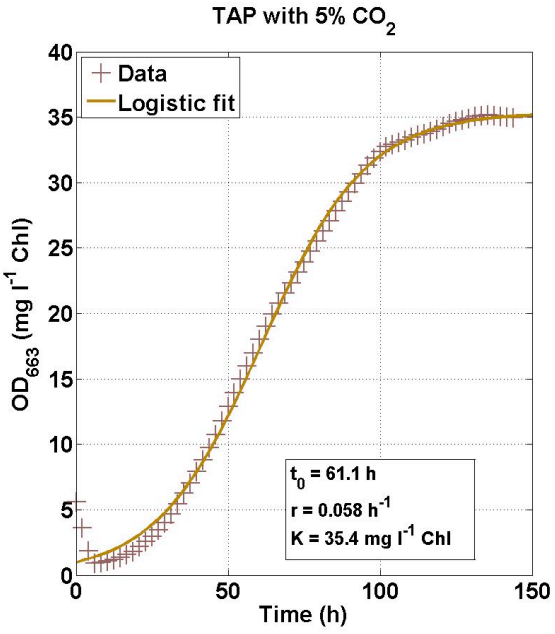
(a)


TAP with air CO2
Data
Logistic fit
t0 = 44.0 h
r = 0.067 h-1
K = 24.7 mg l-1 Chl
OD663 (mg l-1 Chl)
Time (h)

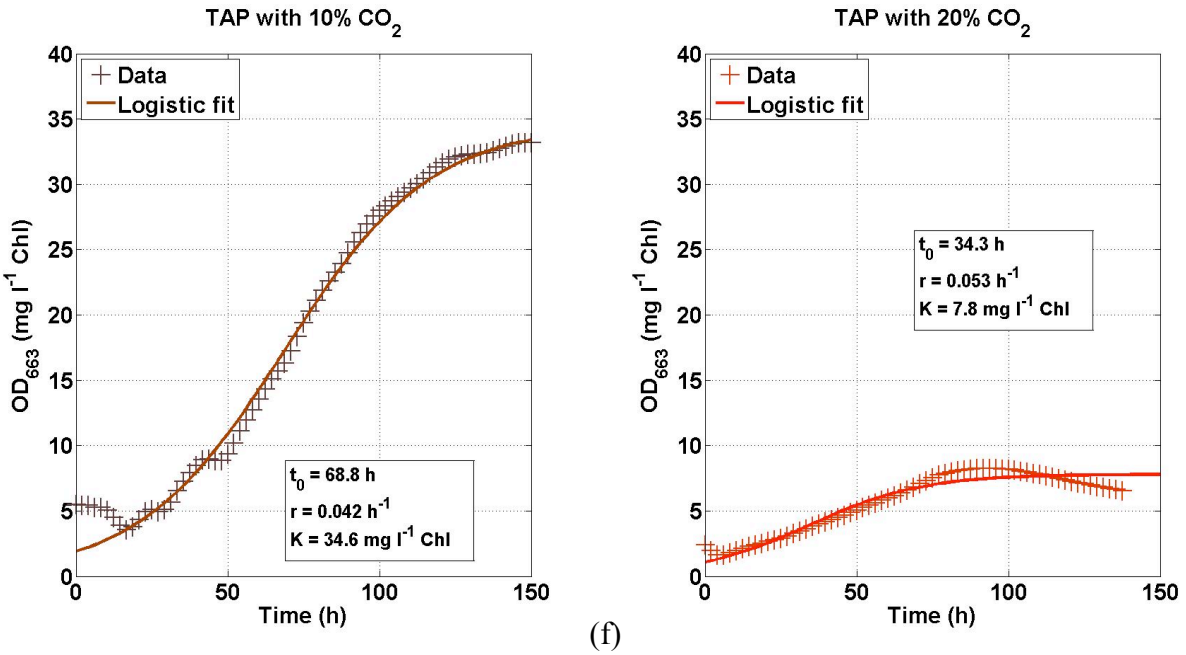
(b)


TAP with 2% CO2
Data
Logistic fit
t0 = 48.5 h
r = 0.056 h-1
K = 38.7 mg l-1 Chl
OD663 (mg l-1 Chl)
Time (h)

(c)


TAP with 5% CO2
Data
Logistic fit
t0 = 61.1 h
r = 0.058 h-1
K = 35.4 mg l-1 Chl
OD663 (mg l-1 Chl)
Time (h)

(d)



(e) (f)

Figure II.12: Logistic model fit to experimental data for *C. reinhardtii* cc124 grown in TAP medium bubbled with different CO_2 partial pressures

(a) 0% CO_2 (no bubbling)

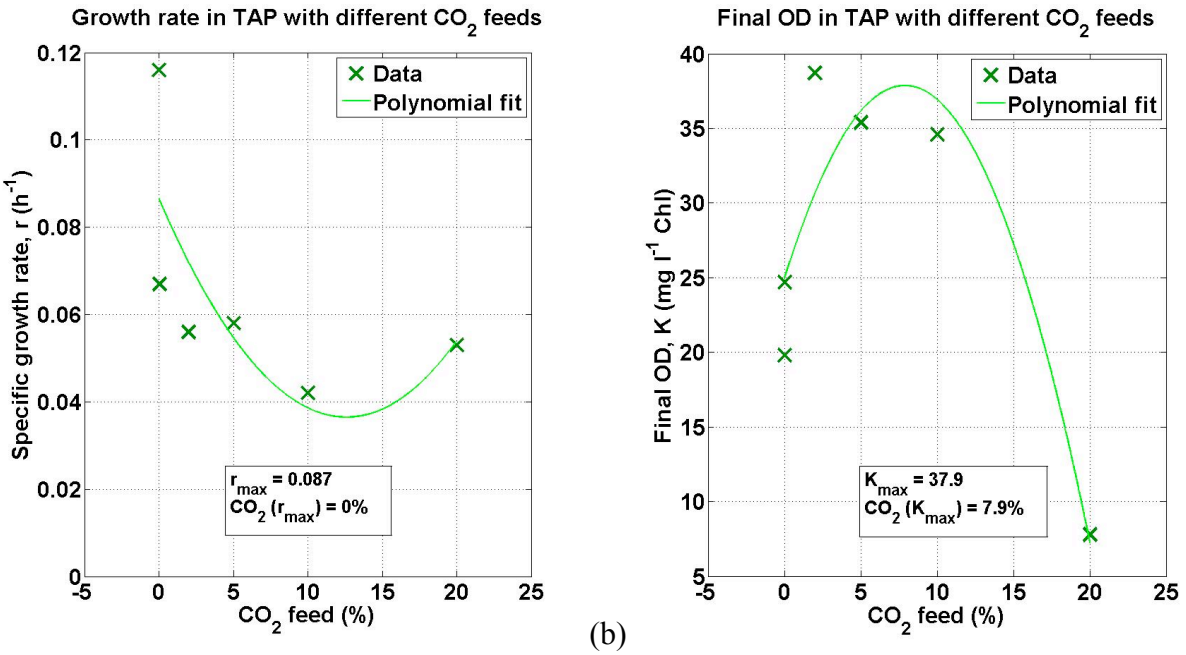
(b) 0.039% CO_2 (bubbled with air)

(c) 2% CO_2

(d) 5% CO_2

(e) 10% CO_2

(f) 20% CO_2



(a) (b)

Figure II.13: Growth parameter correlations with CO_2 feed in TAP

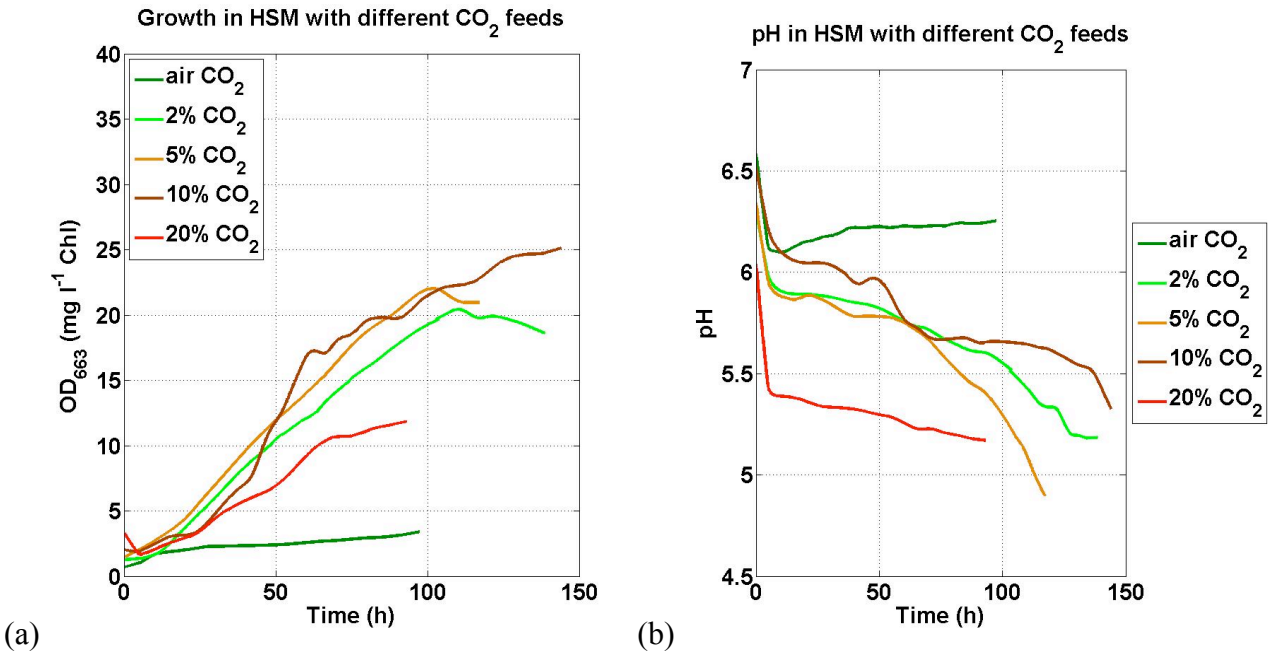
(a) Growth rate, *r*, at different CO_2 feeds, polynomial fit

(b) Final OD, *K*, at different CO_2 feeds, polynomial fit

II.5.2. Growth in HSM with CO_2 bubbling

The CO_2 bubbling experiments were repeated in HSM (Table 5.08) to determine the effect of CO_2 concentration under purely photoautotrophic growth conditions. HSM contains no acetate, so it is the medium that is the most applicable for economic scale-up of algal growth. Once again, the experiments were carried out in the Sartorius tubular reactor, at a temperature of 25°C and with a CO_2 feed of 100 ml·min^{-1}. *C. reinhardtii* cc124 could not grow in HSM without any access to CO_2, but the other five conditions were repeated: 0.039% CO_2, 2% CO_2, 5% CO_2, 10% CO_2, and 20% CO_2 (Figure II.14). The raw data suggest that cc124 growth was improved with increasing CO_2 concentrations up to a maximum at 5-10% CO_2, before decreasing again (Figure II.14a). The pH dropped below pH 5.5 in most experiments (Figure II.14b), although these acidic conditions only appeared to delay growth at 20% CO_2. At 20% CO_2, the pH rapidly fell to pH 5.4 within the first 3 hours of the experiment (Figure II.14b), which probably prevented the dilute algal culture from self-buffering and growing.

The HSM growth curves (Figure II.14a) are not as steady as the TAP medium growth curves (Figure II.11a). This is because growth in HSM relies entirely on the CO_2 distribution inside the PBR. Small variations in the CO_2 distribution, caused by the formation of gas pockets within the tubular helix of the Sartorius PBR, are probably responsible for the wavy deviations in the HSM growth curves. Nevertheless, the logistic model fits remain a very good representation of the experimental data (Figure II.15). HSM correlations of the algal growth rate and CO_2 feed (Figure II. 16a) and the final OD with CO_2 feed (Figure II.16b) were plotted and approximated using a second-order polynomial fit. The maximum growth rate ($r = 0.056$ h^{-1}) occurred at a CO_2 feed of 10.9% (Figure II.16a). Similarly, the maximum final OD ($K = 27.0$ mg·l^{-1}Chl) was observed at a CO_2 feed rate of 10.7% (Figure II.16b). Growth in HSM with a CO_2 feed rate of circa 11% is therefore the optimal solution for large-scale *C. reinhardtii* cc124 biomass production. However, even an optimised cc124 culture grown in HSM is not ideal for H_2 production because of its relatively low cell density ($K = 27.0$ mg·l^{-1}Chl in HSM, compared with 37.9 mg·l^{-1}Chl in TAP). Some acetate in the growth medium is required for effective H_2 production. The next results chapter will aim to optimise the acetate (and sulphate) concentrations of the *C. reinhardtii* cc124 growth medium.

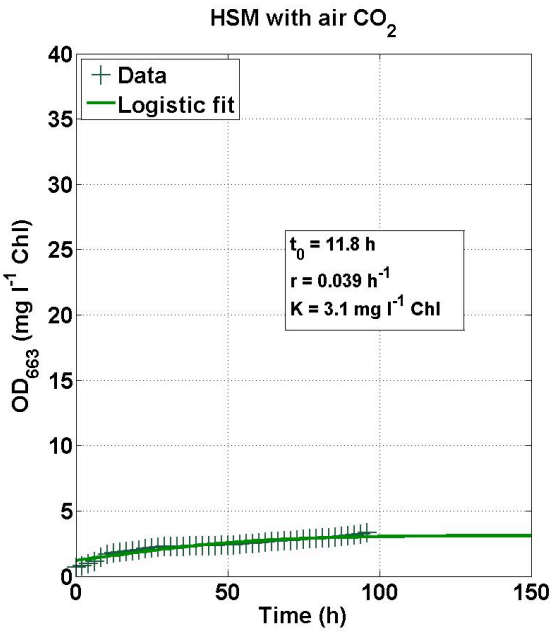


(a) (b)

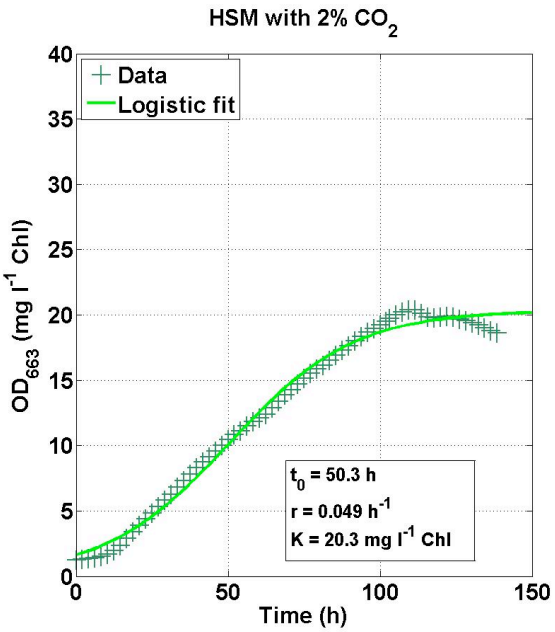
Figure II.14: Growth of *C. reinhardtii* cc124 in HSM bubbled with different CO_2 partial pressures

(a) OD curves in HSM with different CO_2 feeds

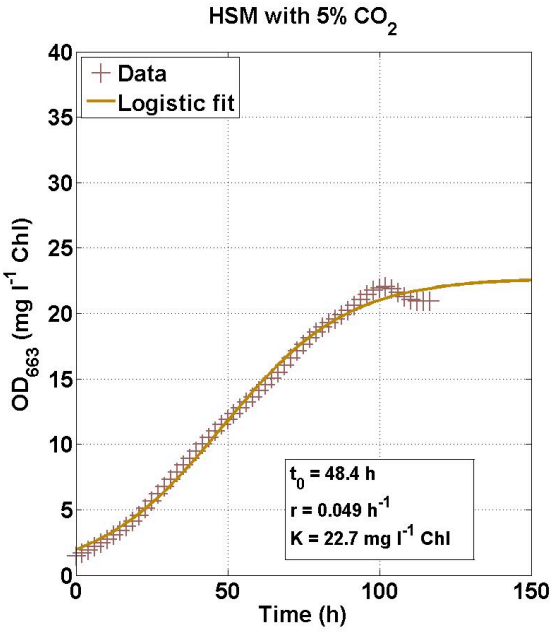
(b) pH curves in HSM with different CO_2 feeds


HSM with air CO2
Data
Logistic fit
t0 = 11.8 h
r = 0.039 h-1
K = 3.1 mg l-1 Chl
OD663 (mg l-1 Chl)
Time (h)

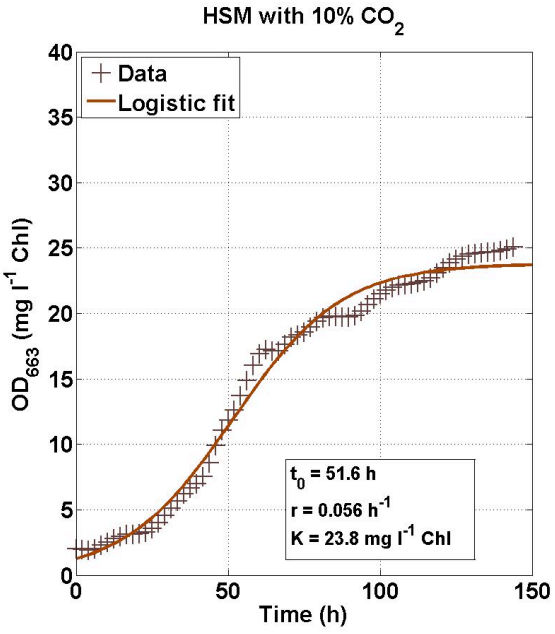
(a)


HSM with 2% CO2
Data
Logistic fit
t0 = 50.3 h
r = 0.049 h-1
K = 20.3 mg l-1 Chl
OD663 (mg l-1 Chl)
Time (h)

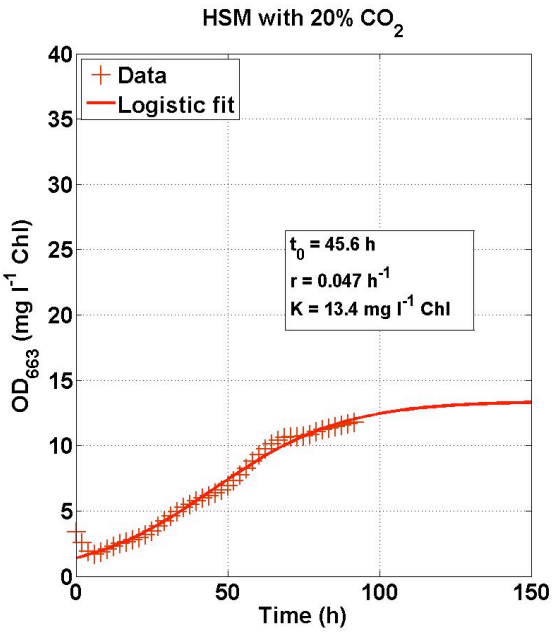
(b)


HSM with 5% CO2
Data
Logistic fit
t0 = 48.4 h
r = 0.049 h-1
K = 22.7 mg l-1 Chl
OD663 (mg l-1 Chl)
Time (h)

(c)


HSM with 10% CO2
Data
Logistic fit
t0 = 51.6 h
r = 0.056 h-1
K = 23.8 mg l-1 Chl
OD663 (mg l-1 Chl)
Time (h)

(d)



(e)

Figure II.15: Logistic model fit to experimental data for *C. reinhardtii* cc124 grown in HSM bubbled with different CO_2 partial pressures

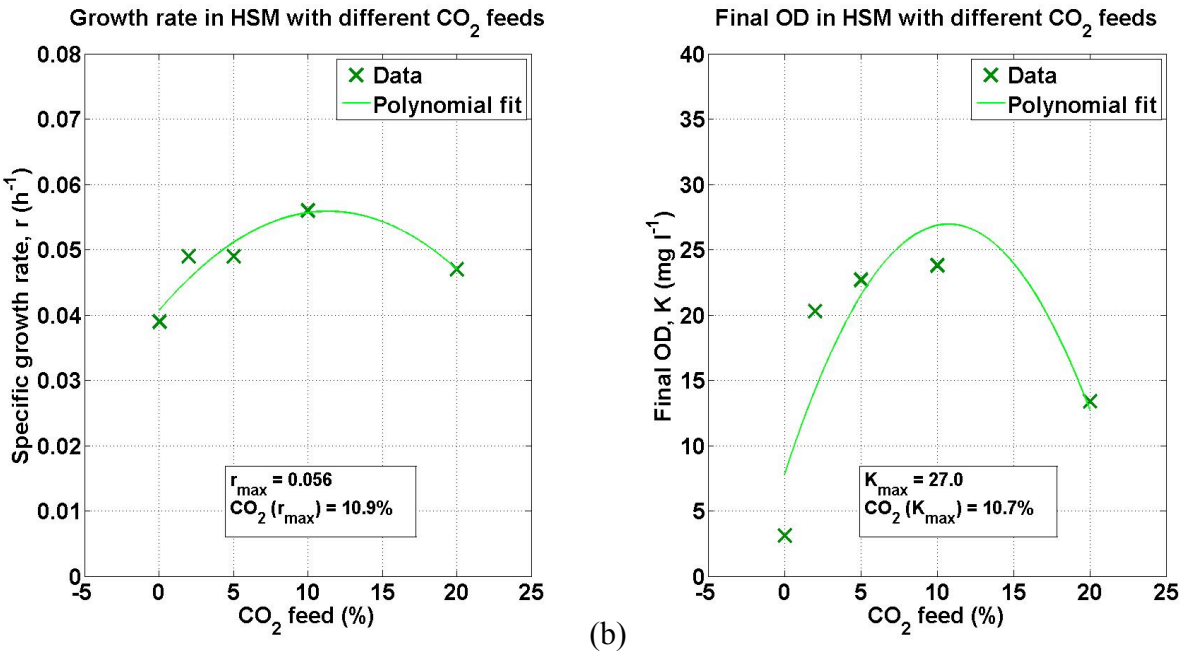
(a) 0.039% CO_2 (bubbled with air)

(b) 2% CO_2

(c) 5% CO_2

(d) 10% CO_2

(e) 20% CO_2



(a) (b)

Figure II.16: Growth parameter correlations with CO_2 feed in HSM

(a) Growth rate, *r*, at different CO_2 feeds, polynomial fit

(b) Final OD, *K*, at different CO_2 feeds, polynomial fit

II.6. Effect of Light Intensity

II.6.1. Growth in Sartorius PBR

Light intensity is the most important environmental parameter that affects *C. reinhardtii* growth. An increase in the light intensity normally facilitates better photosynthetic electron transport, improving both the growth rates and the H_2 production rates of the algal cells (Hallenbeck & Benemann, 2002). Light intensities in excess of the photosaturation limit cause photoinhibition and cell death (Nixon *et al*., 2010). The effect of light intensity was investigated in the Sartorius tubular PBR, the ICL flat-plate PBR and the Solar Simulator stirred-tank PBR.

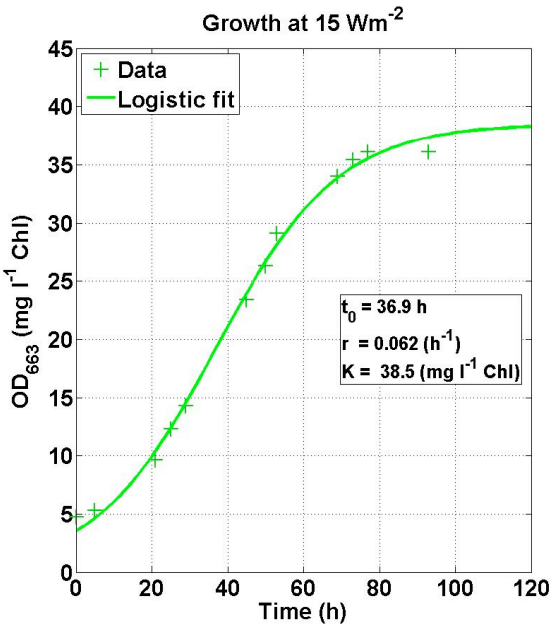
C. reinhardtii cc124 cells were grown in the Sartorius tubular reactor under six different light intensities: 15, 20, 25, 30, 45 and 60 $W \cdot m^{-2}$. It has been previously shown that *C. reinhardtii* grows well within this light intensity range: there is a sufficiently high photon flux density to drive photosynthesis without causing photoinhibition (Kosourov *et al.,* 2002; Janssen *et al*., 2000a). Algae were grown using the 5xTAP* medium. The temperature (25°C) and mixing rate (flow rate of 2,200 $ml \cdot min^{-1}$) were constant for all experiments. Algal OD was measured by a spectrophotometer at 663 nm and correlated to the chlorophyll content of the culture. In the abundance of light and nutrients, the algae initially grew exponentially, with a doubling time of 6.2 to 11.1 hours, depending on the light intensity. As the culture became thicker, algal cells increasingly inhibited their own access to illumination. This became a saturating factor that slowed down the growth rate and eventually terminated growth. This behaviour was accurately fitted by a logistic curve, as shown in Figure II.17. Residuals between the experimental data and the logistic fit have been minimised by the method of least squares and the largest remaining residual is only 1.7 $mg \cdot l^{-1}$Chl (4.8%). The application of the logistic model facilitates the extraction of two important kinetic parameters: the specific growth rate, *r*, and the maximum OD, *K*, which are both functions of light intensity.

The starting OD, age, circadian rhythm and reproductive phase of the starter culture used during an algal growth experiment are all difficult to control and may influence initial growth kinetics (Lemesle & Mailleret, 2008; Kosourov *et al*., 2007). This results in a large temporal spread of

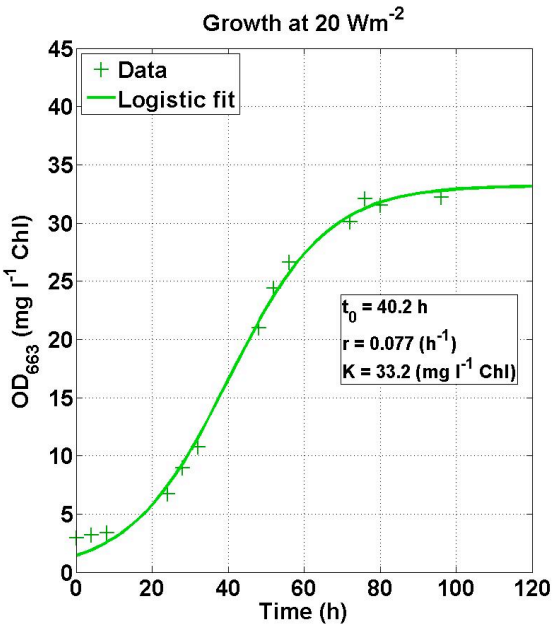
experimental algal growth curves, with a wide variety of t_0 values. Since t_0 is by definition the mid-point of any logistic curve, we have chosen to standardise it to 60 hours to enable a more effective comparison of algal growth curves at different light intensities, as shown in Figure II.18a.

Increasing the light intensity has two main effects on *C. reinhardtii* growth kinetics. Firstly, the higher light intensity leads to a higher photosynthesis rate (Rupprecht *et al*., 2006), increasing the overall algal growth rate. Secondly, the higher light intensity increases the overall irradiation incident on the culture, increasing the maximum OD. Plotting the specific algal growth rate against the light intensity (Figure II.18b) revealed a non-linear correlation between these two parameters. While the specific growth rate did increase with light intensity, it also saturated to a maximum value μ_{max}. Previous work on algal growth kinetics has revealed that the growth rate not only saturates at μ_{max}, but may also experience subsequent photoinhibition (Molina Grima *et al*., 1999). This behaviour has been summarised by the Aiba model (Equation 5.21). For the purpose of this correlation, the artificial point (0,0) was introduced into Figure II.18b. In reality, the *C. reinhardtii* cell actually requires a small maintenance energy to simply remain alive prior to using excess energy for biomass synthesis and reproduction (Posten & Schaub, 2009).

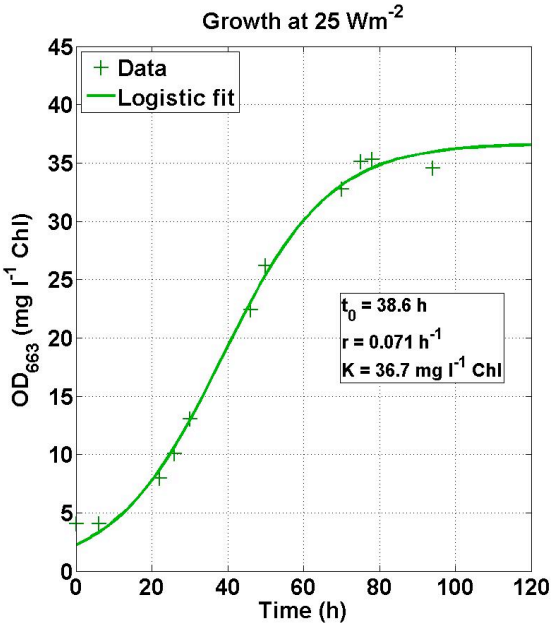
The parameters of the Aiba model were recovered in a similar way to their logistic model counterparts: k_s and k_i values were optimised using the method of least squares before μ_{max} was recovered by linear optimisation. The algal growth rate was determined to saturate to a μ_{max} of 0.154 h^{-1} (doubling time of 4.5 hours) and no photoinhibition was observed in the 15-60 $W \cdot m^{-2}$ light intensity range. The maximum OD did not show a statistically significant increase with light intensity; the linear correlation coefficient R was equal to 0.250 with a *p-value* of 0.633 (Figure II. 18c). This result supports the claim (Giannelli *et al*., 2009) that the PBR geometry and hydrodynamic conditions have a more significant influence on the maximum OD than light intensity does.


Growth at 15 Wm-2
Data
Logistic fit
t0 = 36.9 h
r = 0.062 (h-1)
K = 38.5 (mg l-1 Chl)
OD663 (mg l-1 Chl)
Time (h)

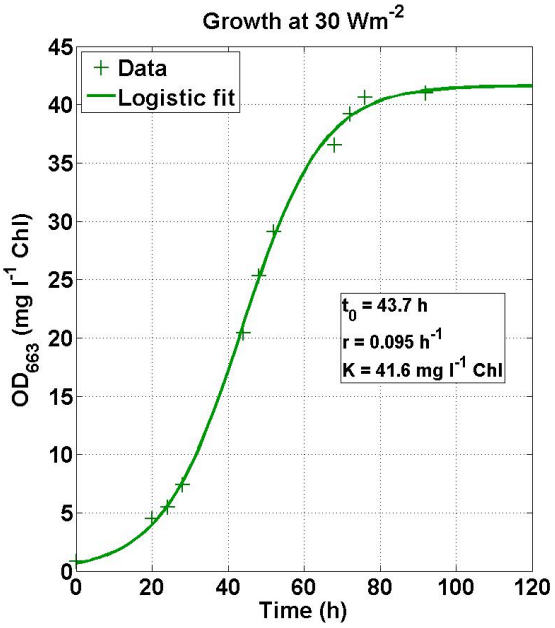
(a)


Growth at 20 Wm-2
Data
Logistic fit
t0 = 40.2 h
r = 0.077 (h-1)
K = 33.2 (mg l-1 Chl)
OD663 (mg l-1 Chl)
Time (h)

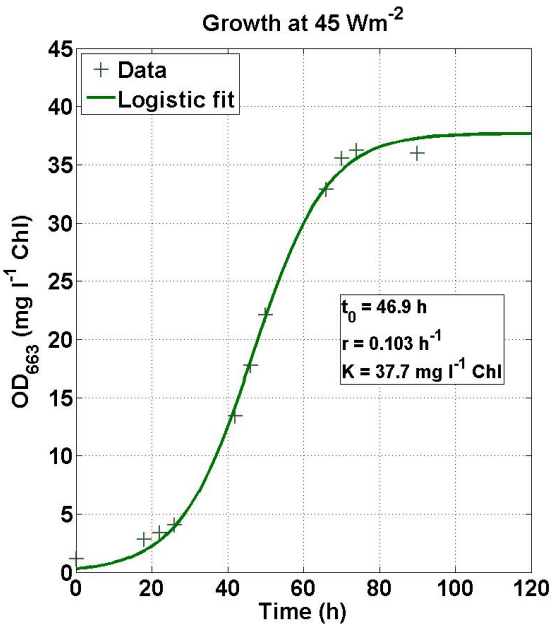
(b)


Growth at 25 Wm-2
Data
Logistic fit
t0 = 38.6 h
r = 0.071 h-1
K = 36.7 mg l-1 Chl
OD663 (mg l-1 Chl)
Time (h)

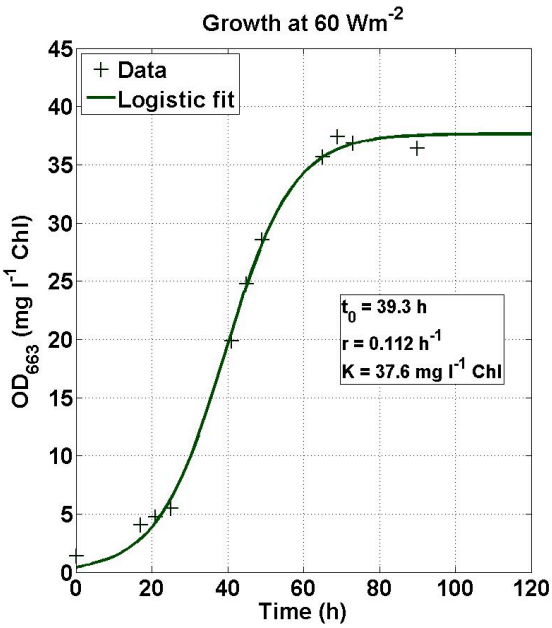
(c)


Growth at 30 Wm-2
Data
Logistic fit
t0 = 43.7 h
r = 0.095 h-1
K = 41.6 mg l-1 Chl
OD663 (mg l-1 Chl)
Time (h)

(d)



(e)



(f)

Figure II.17: Logistic model fit to experimental data for *C. reinhardtii* cc124 at different light intensities in the Sartorius tubular PBR

(a) 15 Wm^{-2}

(b) 20 Wm^{-2}

(c) 25 Wm^{-2}

(d) 30 Wm^{-2}

(e) 45 Wm^{-2}

(f) 60 Wm^{-2}

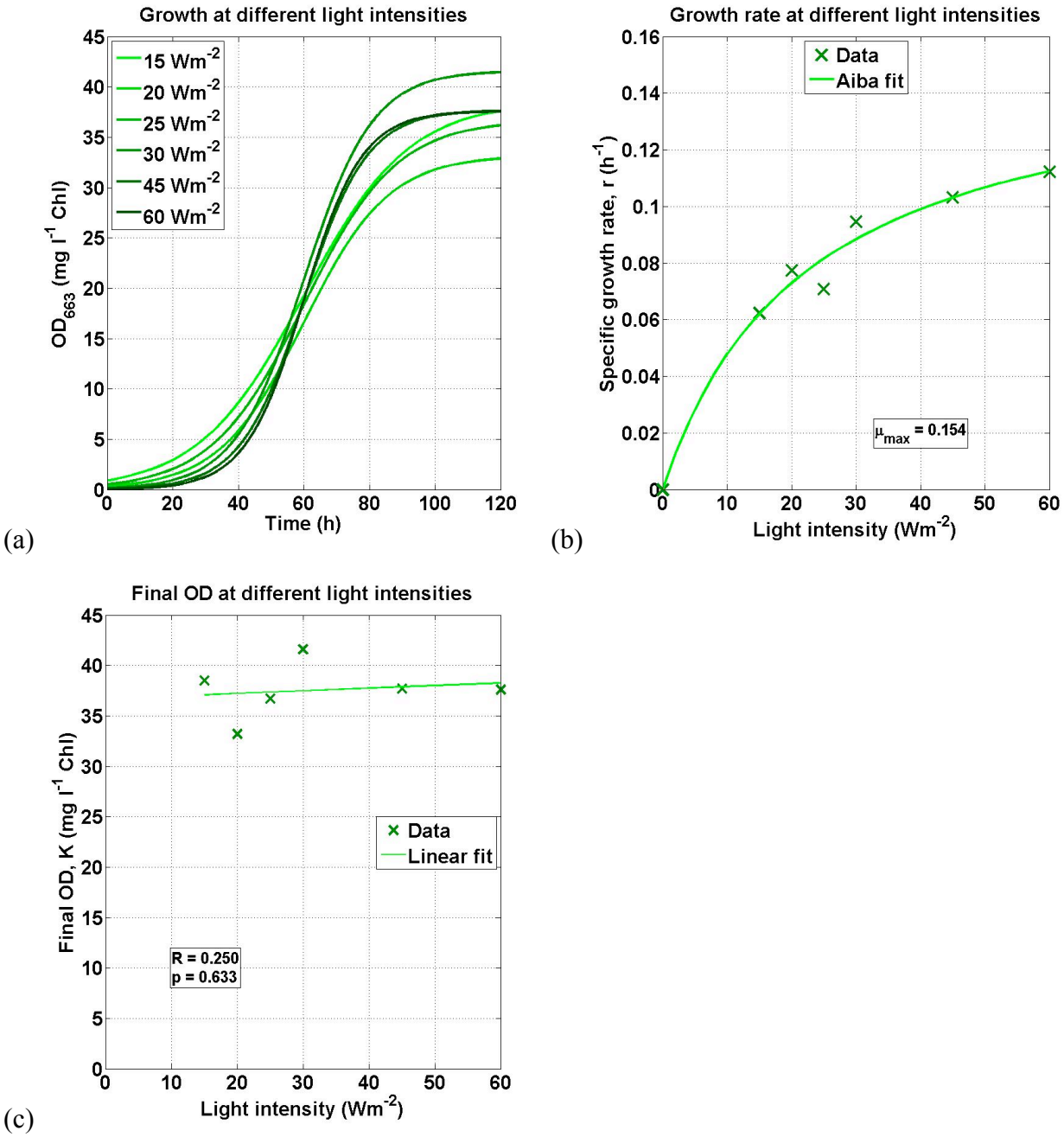


Figure II.18: Growth parameter correlations with light intensity in the Sartorius tubular PBR

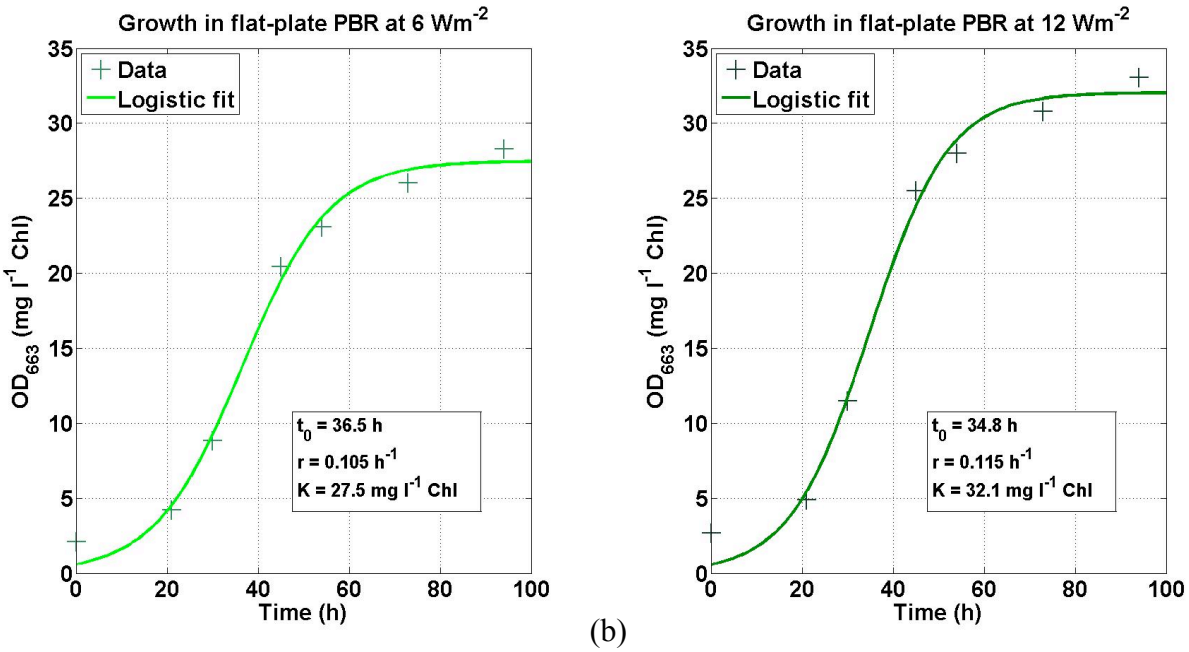
(a) Collection of growth curves at different light intensities, t_0 = 60h

(b) Growth rate, *r*, at different light intensities, Aiba fit

(c) Final OD, *K*, at different light intensities, linear fit

II.6.2. Growth in Flat-plate PBR

The commissioning of the ICL flat-plate PBR involved algal growth at two different light intensities: 6 $W \cdot m^{-2}$ and 12 $W \cdot m^{-2}$. Algae were grown in the 5xTAP* medium and the temperature was controlled at 25°C by using the secondary compartment as a heating water jacket. OD was measured using the calibrated photodiode. The experimental results and logistic fit are presented in Figure II.19. A higher specific growth rate (r = 0.115 h^{-1}, compared to 0.105 h^{-1} at 6 $W \cdot m^{-2}$) and a higher final OD (K = 32.1 $mg \cdot l^{-1}$Chl, compared with 27.5 $mg \cdot l^{-1}$Chl at 6 $W \cdot m^{-2}$) were observed at the higher light intensity of 12 $W \cdot m^{-2}$. It was difficult to compare growth rates at different light intensities across the various PBR geometries. One reason for this is that LED light provides a better spectral match to *C. reinhardtii* absorption than fluorescent light (Figure I.07a), so that 12 $W \cdot m^{-2}$ of LED light actually delivers more PAR than 12 $W \cdot m^{-2}$ of fluorescent light. There are also many reactor-dependent parameters such as the fluid dynamics, the residence time distribution and the gas transfer rates that also influence growth.



a) (b)

Figure II.19: Logistic model fit to experimental data for *C. reinhardtii* cc124 at different light intensities in the ICL flat-plate PBR

(a) 6 Wm^{-2}

(b) 12 Wm^{-2}

II.6.3. Growth under High Light Intensity

The Solar Simulator stirred-tank PBR may be a primitive system compared with the other PBRs used in this thesis, but it does facilitate algal growth under the high light intensities of the Solar Simulator. *C. reinhardtii* cc124 were grown in the TAP medium under light intensities of: 85, 150, 300 and 600 $W \cdot m^{-2}$ (Figure II.20). The combined growth data is shown in Figure II.21a. The highest OD of 30.9 $mg \cdot l^{-1}$Chl was measured at a light intensity of 300 $W \cdot m^{-2}$. The photosaturating light intensity is therefore in the region of 300 $W \cdot m^{-2}$. Unfortunately, the temperature of the Solar Simulator stirred-tank PBR was not controllable (Figure II.21b), which means that possible temperature inhibition at 300 $W \cdot m^{-2}$ and especially 600 $W \cdot m^{-2}$ cannot be ruled out. Future experiments under the Solar Simulator should use a water bath or other temperature-control strategies to reduce the likelihood of temperature inhibition. Kinetic growth parameters were extracted from the experimental data by means of the logistic model and used to plot the correlations in Figure II.22. There appeared to be no correlation between the cc124 culture growth rate and light intensity for growth under high light intensities (Figure II.22a). A second-order polynomial provided a good description of the correlation between the final OD and the light intensity (Figure II.22b). The maximum final OD (K = 30.9 $mg \cdot l^{-1}$Chl) corresponded to a light intensity of 273 $W \cdot m^{-2}$. This is the light intensity of photosaturation. Beyond this point, clear evidence of photoinhibition, in the form of a greatly reduced final OD, was observed at the light intensity of 600 $W \cdot m^{-2}$ (K = 10.5 $mg \cdot l^{-1}$Chl).

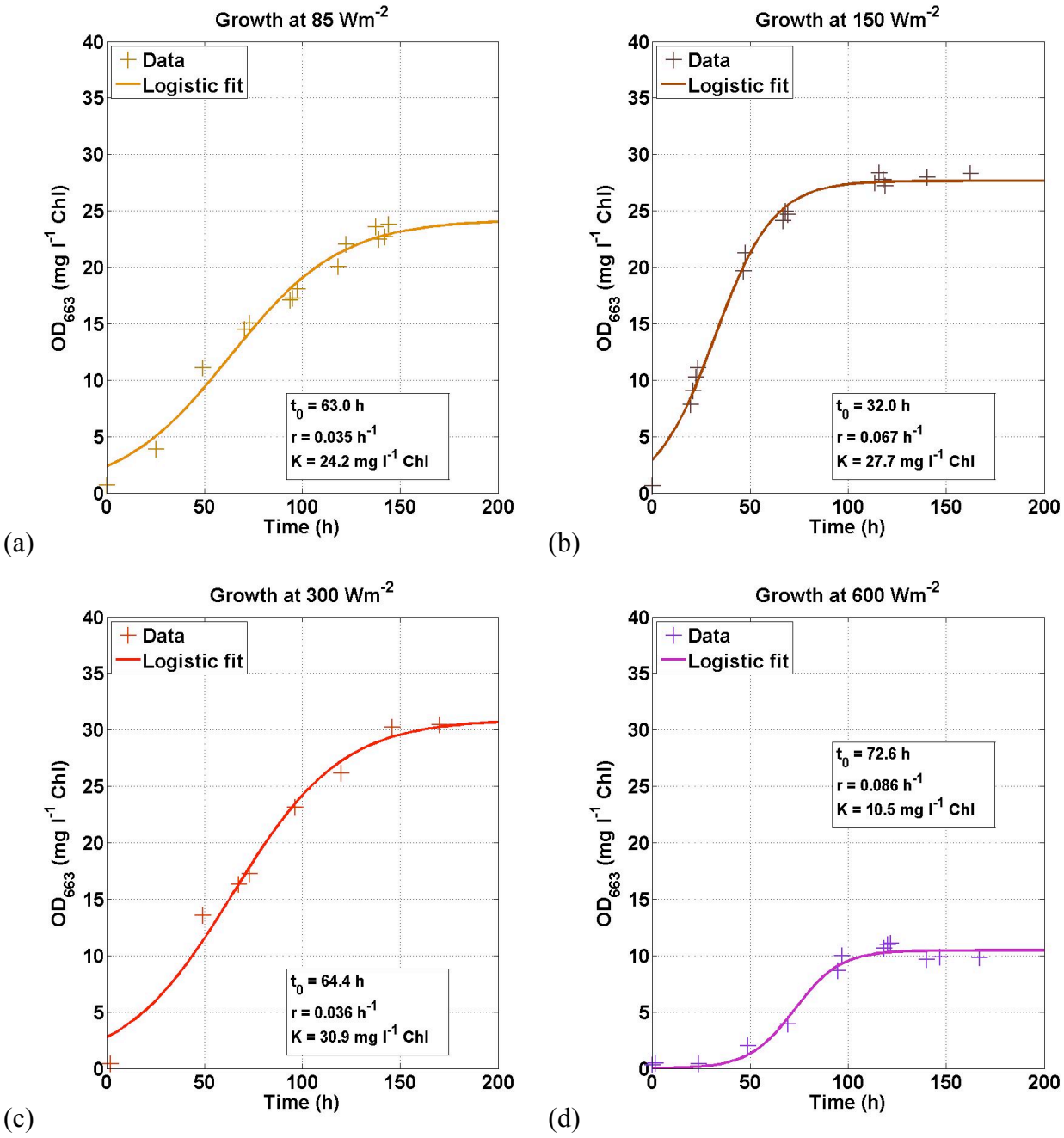


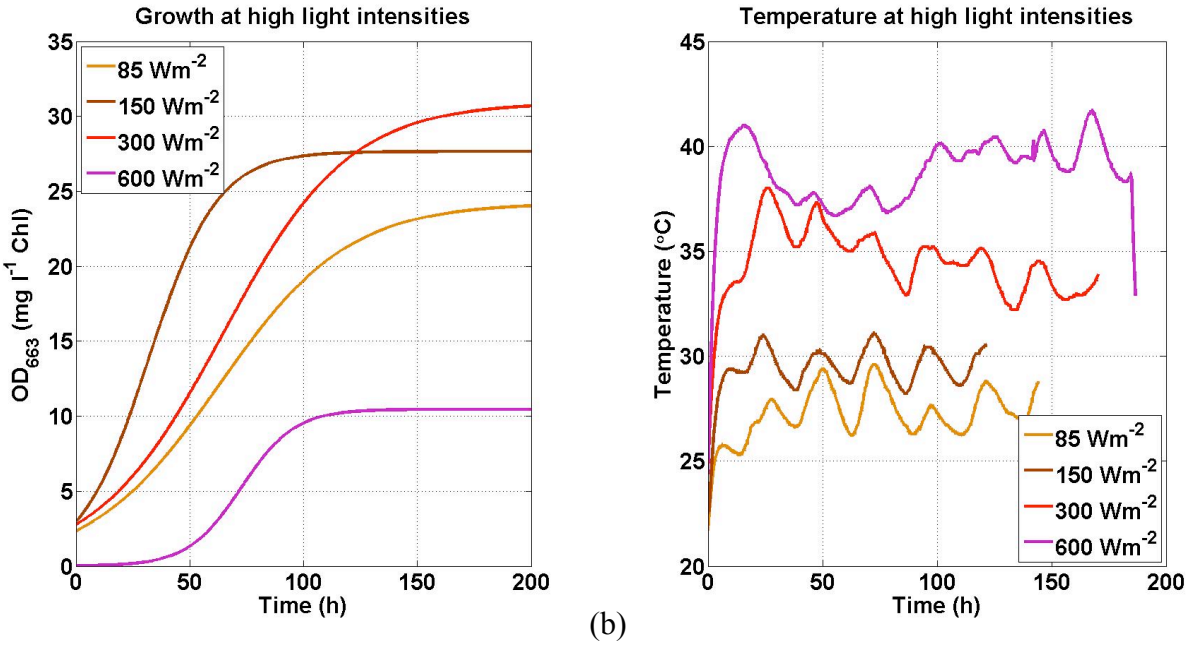
Figure II.20: Logistic model fit to experimental data for *C. reinhardtii* cc124 at high light intensities under the Solar Simulator

(a) 85 Wm^{-2}

(b) 150 Wm^{-2}

(c) 300 Wm^{-2}, photosaturation

(d) 600 Wm^{-2}, photoinhibition



(a) (b)

Figure II.21: Growth of *C. reinhardtii* cc124 at high light intensities under the Solar Simulator

(a) OD curves at different light intensities

(b) Temperature at different light intensities, raw data

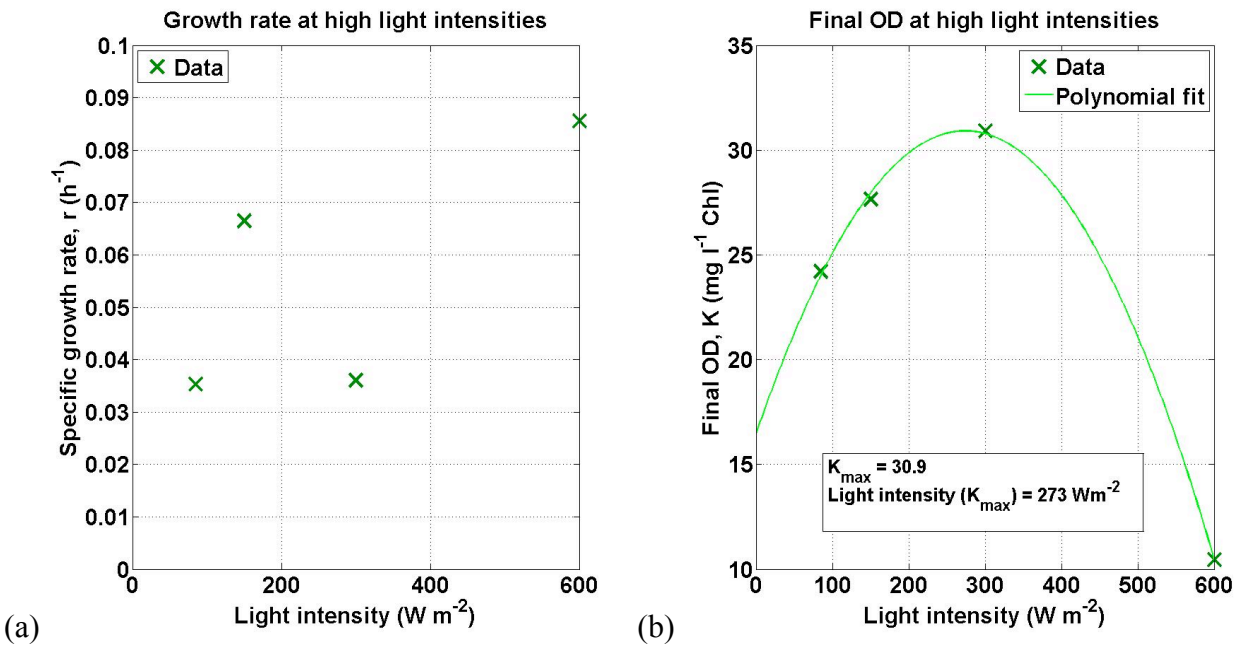


Figure II.22: Growth parameter correlations with light intensity at high light intensities

(a) Growth rate, *r*, at different light intensities, no correlation

(b) Final OD, *K*, at different light intensities, polynomial fit

II.7. Summary

A logistic growth model that accurately describes algal growth has been developed and used to determine the parameters that are important for optimising algal growth. The *C. reinhardtii* laboratory WT cc124 strain exhibited a faster growth rate than the dum24 and cc406 mutants. It was selected for use in future growth and H_2 production experiments. Experiments carried out in the following chapter will demonstrate that high growth rates and cell densities are crucial for effective H_2 production. Increasing the temperature was shown to improve cc124 culture growth slightly, but this effect was not deemed significant enough for in-depth study. A fixed temperature of 25°C was used whenever possible in subsequent experiments. Growth under light-dark cycles proved to be inferior to growth under continuous illumination, which has negative implications for outdoor PBR operation and scale-up. Bubbling a source of CO_2 improved the final OD of cc124 cultures grown under continuous illumination. A similar effect was observed when the cc124 cells were grown in the acetate-enriched 5xTAP* medium. This CO_2 effect was investigated further with a series of experiments at different CO_2 feed concentrations in TAP and HSM media. In the TAP medium, maximum final OD was obtained at 7.9% CO_2, but the fastest growth rate occurred in the absence of CO_2 bubbling. In HSM, optimum growth was obtained at circa 11% CO_2, but the maximum cell density was significantly lower than in the TAP medium. An optimised acetate-based medium therefore needs to be developed for H_2 production. Increasing light intensity up to 60 $W \cdot m^{-2}$ increased the cc124 culture specific growth rate according to the Aiba model, but had little effect on the final OD. Photosaturation of cc124 cultures occurred at 273 $W \cdot m^{-2}$. Clear evidence of photoinhibition was detectible at 600 $W \cdot m^{-2}$. In summary, the conditions which lead to optimal algal growth, providing a system that can be exploited for H_2 production, are a temperature of 25°C, continuous illumination at 5-100 $W \cdot m^{-2}$ and photomixotrophic growth conditions.

III. Hydrogen Production by Nutrient Control

III.1. Introduction

H_2 production by *C. reinhardtii* takes place under anaerobic conditions, which may be imposed metabolically by depriving the algae of sulphur. S-deprivation normally requires the spatial and temporal separation of the algal growth and H_2 production stages. This would typically require separate PBRs for each stage as well as a costly and energy-intensive medium exchange technique such as centrifugation, making the process difficult to scale up. H_2 production has previously been achieved by growing *C. reinhardtii* at low light intensities (Degrenne *et al*., 2011), or by initiating S-deprivation using centrifugation (Melis *et al*., 2000) or dilution (Laurinavichene *et al*., 2002) procedures.

The aim of this chapter is to develop a novel nutrient control procedure for S-deprived H_2 production in order to improve the scalability of the process (Tamburic *et al*., 2012). To achieve this, the sulphate and acetate uptake rates during algal growth will be investigated under different illumination conditions. The experiment will be repeated in various photobioreactor geometries in order to determine a reactor-independent relationship between the algal growth and nutrient consumption kinetics. Using this relationship, the initial sulphur and acetate concentrations of the algal medium will be optimised so that these nutrients run out at the exact moment when the maximum algal cell density is reached. This nutrient control method will allow a fully-grown algal culture to enter spontaneous hydrogen production mode, eliminating the need for a medium separation technique and for an additional PBR.

H_2 production rates and yields will be measured by MIMS in the ICL flat-plate PBR. The *C. reinhardtii* cc124 H_2 production properties following S-deprivation by centrifugation, dilution and nutrient control methods will be analysed and compared. In addition, the H_2 production of cc124 under low light intensities will be probed by injection mass spectrometry. The H_2 production of the *C. reinhardtii* fermentation mutant s21 will also be investigated.

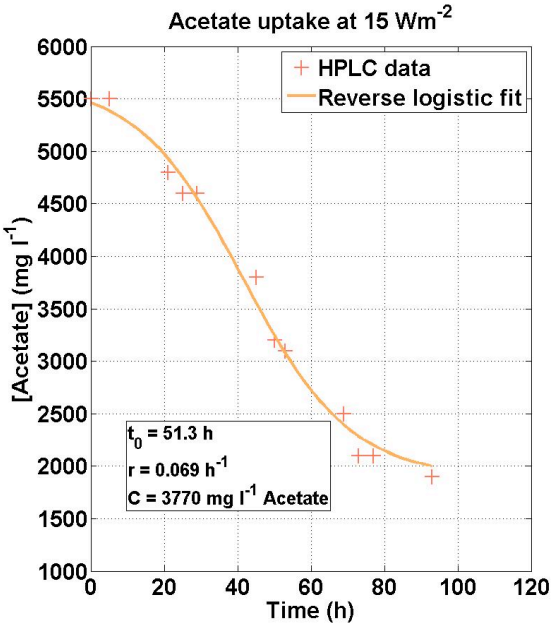
III.2. Nutrient Uptake Kinetics

III.2.1. Acetate Demand

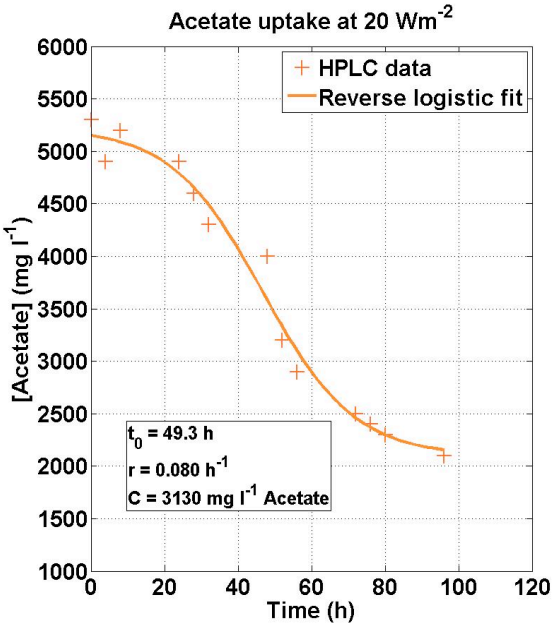
As described previously (Chapter II.6.1), the growth of *C. reinhardtii* cc124 in 5xTAP* medium was investigated at different light intensities in the Sartorius PBR. At the same time, acetate and sulphate uptake rates were also measured; the investigation of nutrient uptake kinetics will be described in this chapter. The 5xTAP* medium was used to ensure that the growth was not acetate-limited, making light availability the primary limiting factor of algal growth. The growth conditions are mixotrophic because the *C. reinhardtii* cells can obtain carbon from the acetate in the 5xTAP* medium or from the ambient CO_2. Algal samples were extracted at regular intervals in order to measure the nutrient uptake of the culture. Acetate uptake and sulphate uptake were measured by HPLC and IC respectively (Chapter 5.7.). The acetate uptake raw data at different light intensities is shown in Figure III.01. A reverse logistic model (Equations 5.19 & 5.20) was used to fit a sigmoid curve to the acetate uptake data. The reverse logistic fit does not stray further than 300 $mg \cdot l^{-1}$ acetate away from the raw data, indicating that the fit is better than 95% accurate. Three kinetic parameters were extracted from this logistic model: t_0, the time of inflection, r, the acetate uptake rate, and C, the total quantity of acetate consumed.

The acetate and sulphate uptake kinetics were analysed in a similar way to the algal growth kinetics. Figure III.02a shows a comparison of the acetate uptake reverse logistic curves at different light intensities, with t_0 standardised to 60 hours and the initial sulphate concentration, C_i, set to 5,100 mg l^{-1} to offset any small variations in the initial acetate concentration of the 5xTAP* medium. Acetate uptake rates were found to increase with light intensity and follow an Aiba model with a μ_{max} of 0.154 (Figure III.02b), producing a similar curve to the variation of specific algal growth rate with light intensity (Figure II.18b). However, the total acetate uptake appears to decrease linearly with light intensity (Figure III.02c: the correlation coefficient R is -0.893 with a p-value of 0.016). Acetate is the main source of carbon during *C. reinhardtii* growth (Degrenne *et al*., 2010). Higher light intensities increase the algal growth rate, resulting in an increased demand for carbon and consequently an increase in the acetate uptake rate. At the same time, the increase in the rate of photosynthesis leads to higher rates of inorganic carbon fixation via the Calvin cycle (Burgess *et*

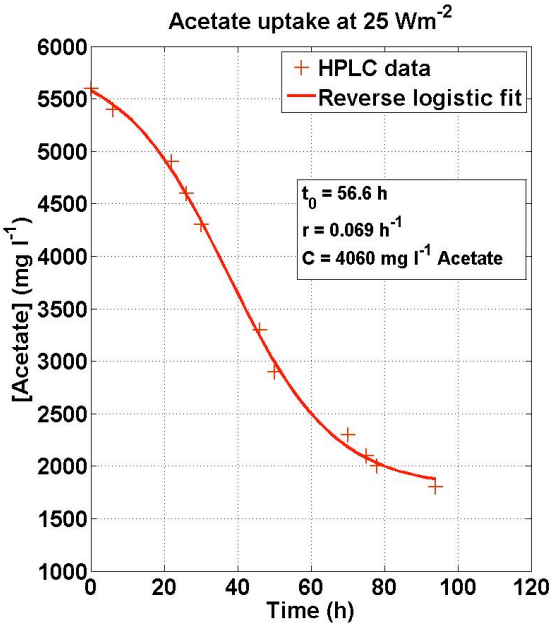
al., 2011). A higher proportion of the overall carbon required by the algal cells can therefore be obtained from the ambient carbon dioxide via the Calvin cycle, resulting in a decrease in the total acetate uptake. This observation only holds if the algae are grown under these photomixotrophic conditions, in the presence of both carbon dioxide and acetate.



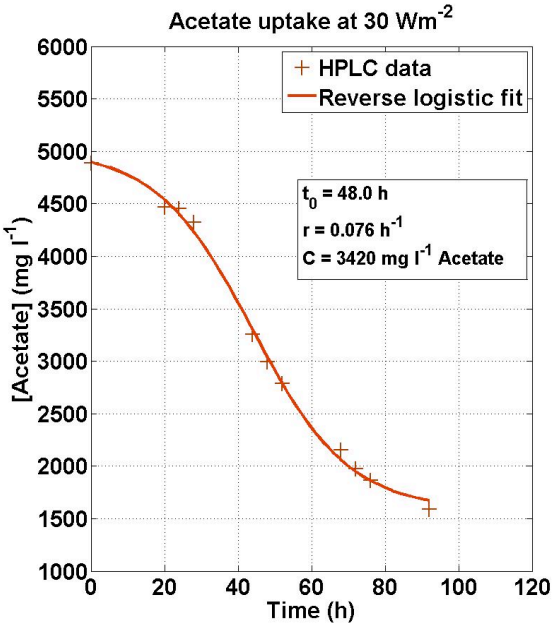
(a)



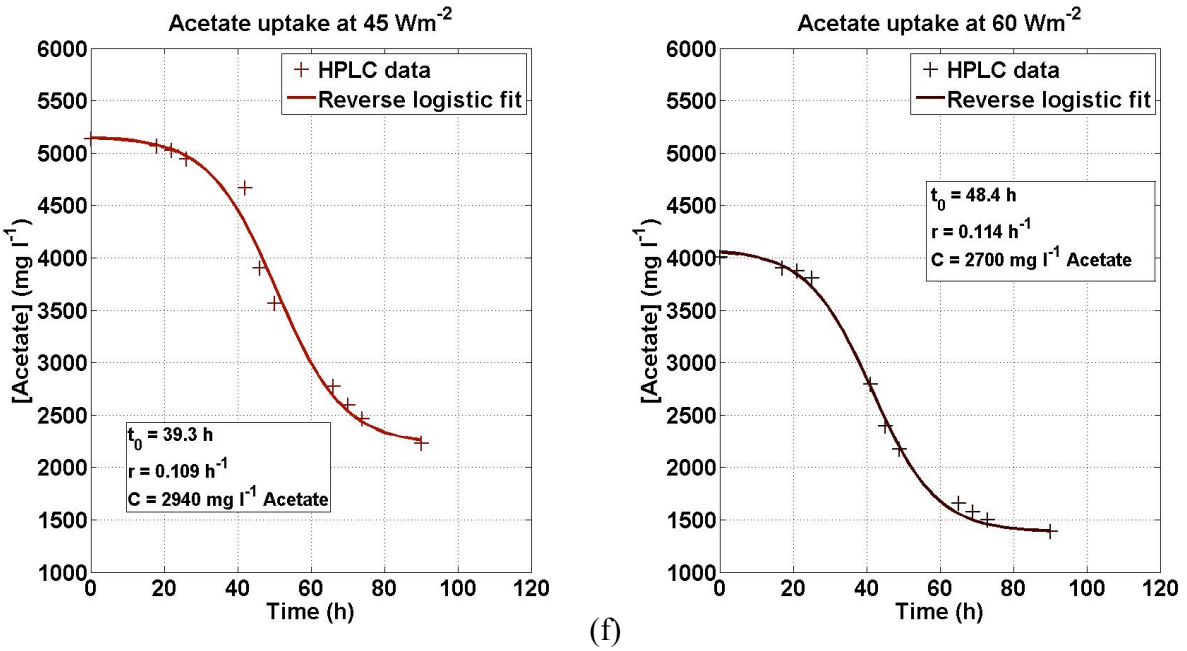
(b)



(c)



(d)



(e) (f)

Figure III.01: Reverse logistic model fit to experimental data for *C. reinhardtii* cc124 acetate uptake at different light intensities in the Sartorius tubular PBR

(a) 15 Wm^{-2}

(b) 20 Wm^{-2}

(c) 25 Wm^{-2}

(d) 30 Wm^{-2}

(e) 45 Wm^{-2}

(f) 60 Wm^{-2}

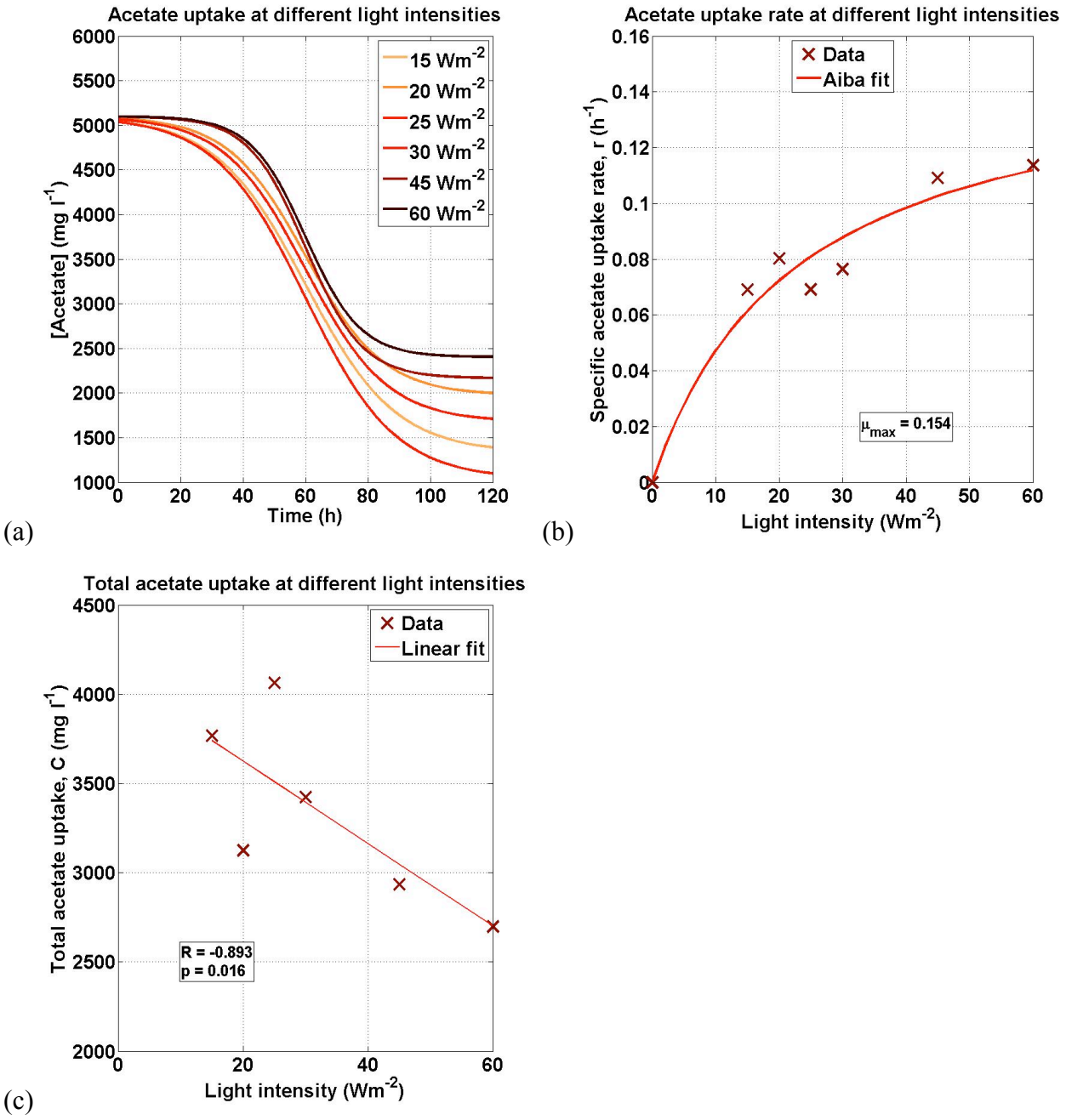


Figure III.02: Acetate uptake parameter correlations with light intensity in the Sartorius tubular PBR

(a) Collection of acetate uptake curves at different light intensities, t_0 = 60 hours

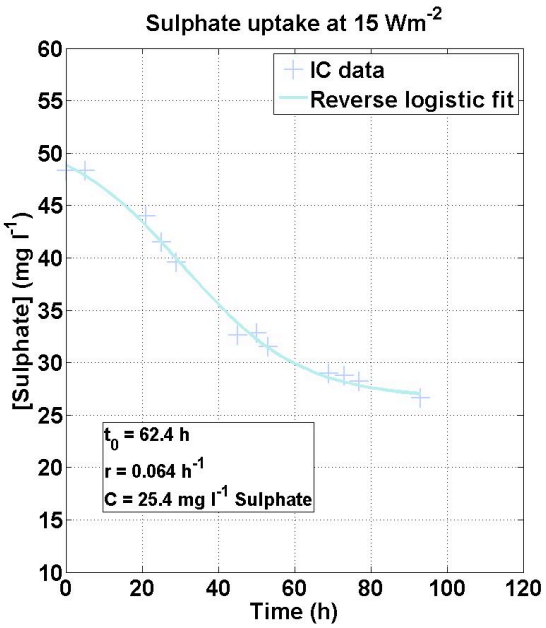
(b) Acetate uptake rate, r, at different light intensities, Aiba fit

(c) Total acetate uptake, C, at different light intensities, linear fit

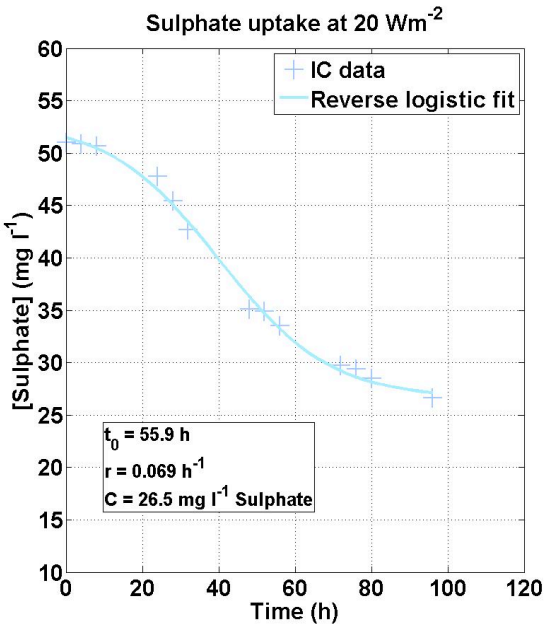
III.2.2. Sulphate Demand

The sulphate uptake raw data at different light intensities are shown in Figure III.03 together with reverse logistic model fits to this data. The logistic fit has a maximum error of 2 $mg \cdot l^{-1}$ of sulphate, which implies that the fit is at least 96% accurate. Figure III.04a shows a comparison of the sulphate uptake reverse logistic curves at different light intensities, with t_0 standardised to 60 hours and the initial sulphate concentration set to 48 $mg \cdot l^{-1}$. The sulphate uptake rate was also shown to follow the Aiba light saturation model, with a μ_{max} of 0.231 (Figure III.04b). The total sulphate uptake demonstrated a linear increase with light intensity over the range studied (Figure III.04c: the correlation coefficient R is 0.626 with a p-value of 0.184). Sulphur is a key component of the photosynthetic mechanism of *C. reinhardtii*; it is required to repair the D1 protein, a major component of the PSII reaction centre (Ghirardi *et al*., 2009). Higher light intensities result in higher photosynthesis rates, increasing the overall photo-damage to PSII proteins and therefore increasing both the sulphur uptake rate and the overall demand for sulphur.

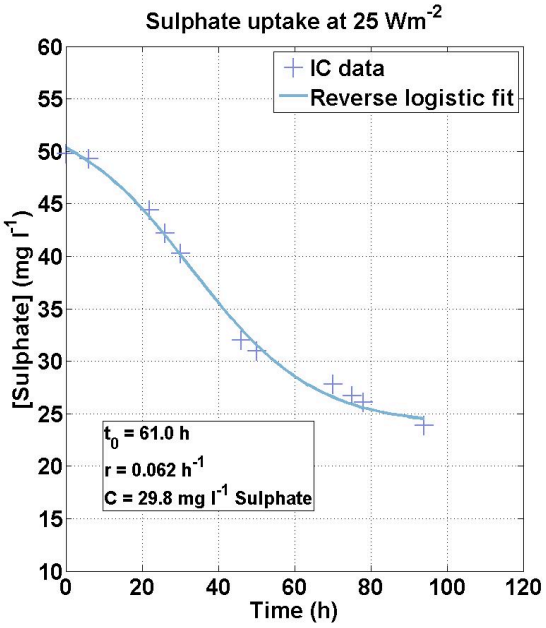
The correlations in Figure III.02c and Figure III.04c may be used to design an algal growth medium to facilitate batch H_2 production by nutrient control for any light intensity in the Sartorius reactor. For example, at a light intensity of 40 $W \cdot m^{-2}$, a medium with an initial acetate concentration of 3,160 $mg \cdot l^{-1}$ and an initial sulphate concentration of 29.4 $mg \cdot l^{-1}$ is required. Given these starting nutrient concentrations, the algae would use up all sulphate and acetate just as they obtain their maximum OD, leading to spontaneous H_2 production by S-deprivation. However, these relationships between light intensity and total nutrient uptake are specific to a particular PBR under a particular set of controlled conditions (temperature of 25°C, turbulent mixing), and their application is therefore very limited. More data are needed to increase the certainty in the acetate and sulphate uptake correlations at different light intensities. A reactor-independent correlation is required to develop a more flexible nutrient control technique.


Sulphate uptake at 15 Wm-2
IC data
Reverse logistic fit
[Sulphate] (mg l-1)
Time (h)
t0 = 62.4 h
r = 0.064 h-1
C = 25.4 mg l-1 Sulphate

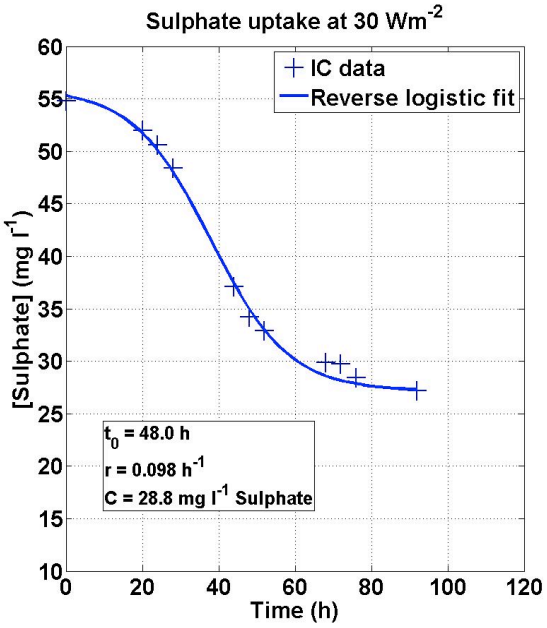
(a)


Sulphate uptake at 20 Wm-2
IC data
Reverse logistic fit
[Sulphate] (mg l-1)
Time (h)
t0 = 55.9 h
r = 0.069 h-1
C = 26.5 mg l-1 Sulphate

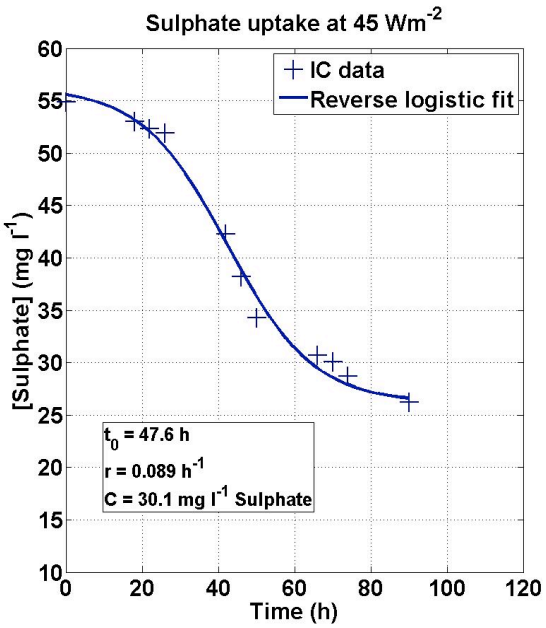
(b)


Sulphate uptake at 25 Wm-2
IC data
Reverse logistic fit
[Sulphate] (mg l-1)
Time (h)
t0 = 61.0 h
r = 0.062 h-1
C = 29.8 mg l-1 Sulphate

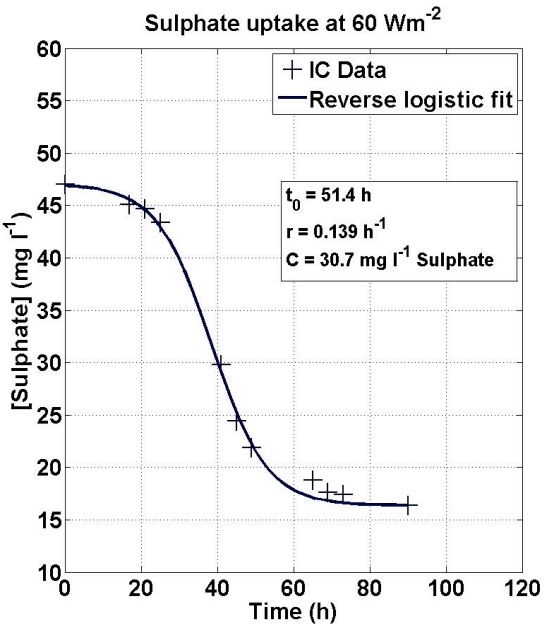
(c)


Sulphate uptake at 30 Wm-2
IC data
Reverse logistic fit
[Sulphate] (mg l-1)
Time (h)
t0 = 48.0 h
r = 0.098 h-1
C = 28.8 mg l-1 Sulphate

(d)



(e)



(f)

Figure III.03: Reverse logistic model fit to experimental data for *C. reinhardtii* cc124 sulphate uptake at different light intensities in the Sartorius tubular PBR

(a) 15 Wm^{-2}

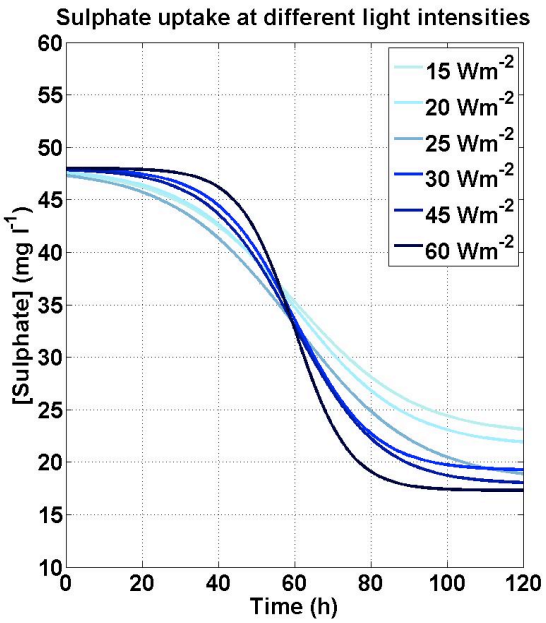
(b) 20 Wm^{-2}

(c) 25 Wm^{-2}

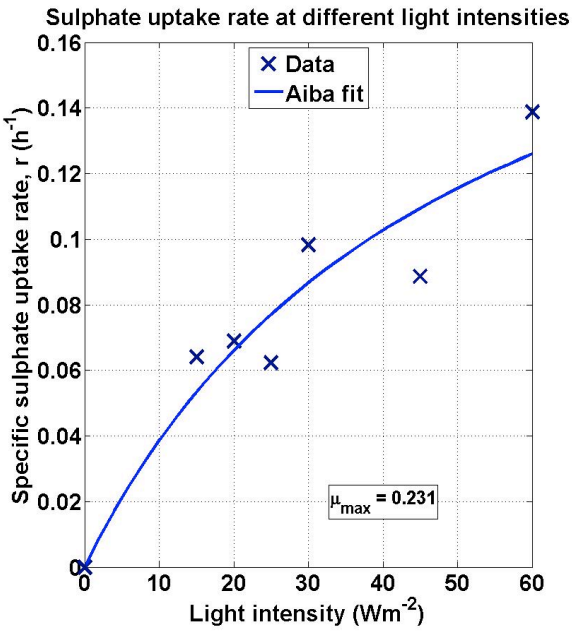
(d) 30 Wm^{-2}

(e) 45 Wm^{-2}

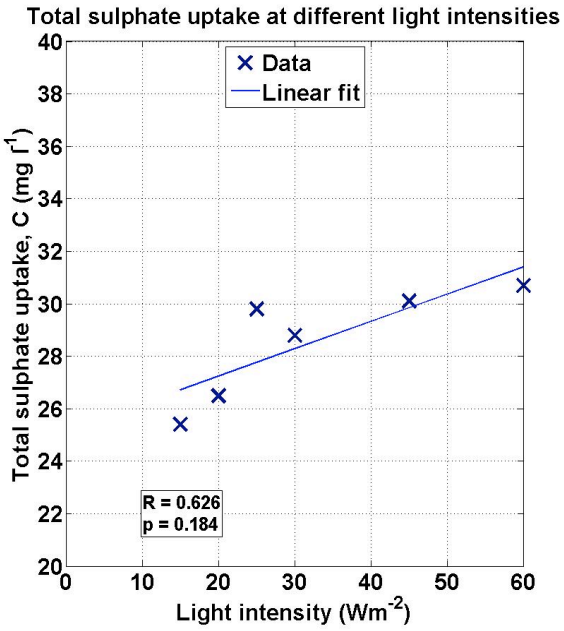
(f) 60 Wm^{-2}



(a)



(b)



(c)

Figure III.04: Sulphate uptake parameter correlations with light intensity in the Sartorius tubular PBR

(a) Collection of sulphate uptake curves at different light intensities, t_0 = 60 hours

(b) Sulphate uptake rate, r, at different light intensities, Aiba fit

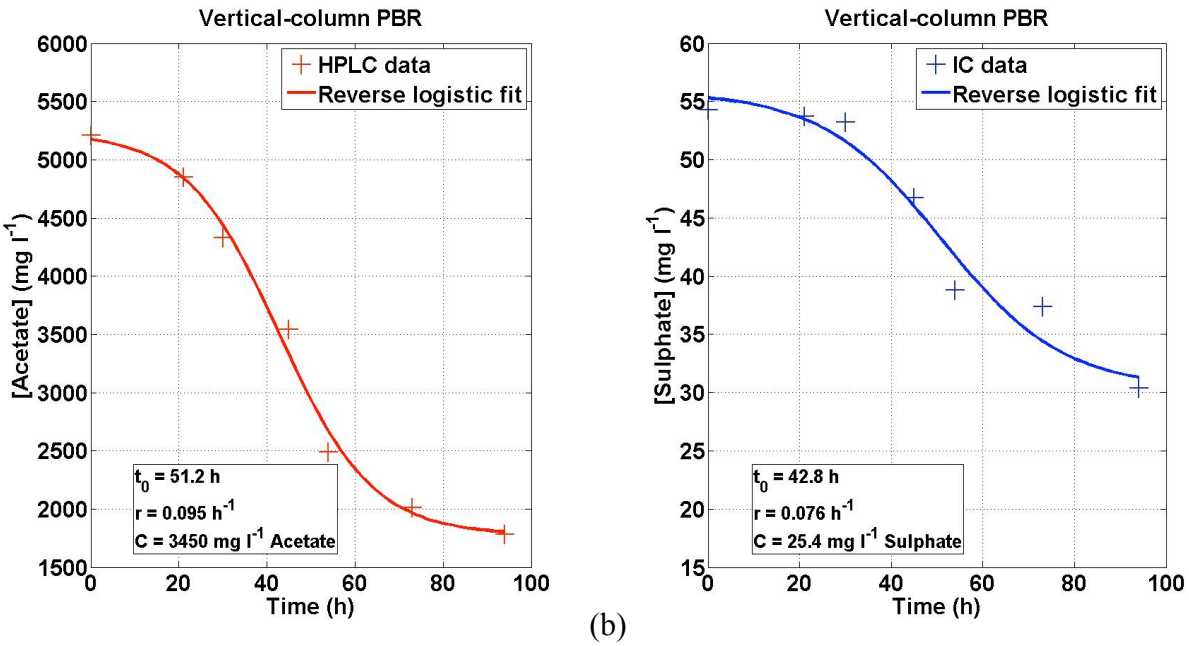
(c) Total sulphate uptake, C, at different light intensities, linear fit

III.3. Reactor-independent Nutrient Uptake

III.3.1. Additional Nutrient Uptake Results

In addition to the Sartorius tubular reactor, *C. reinhardtii* cc124 growth experiments using the 5xTAP* medium were also carried out in AquaMedic vertical-column, Solar Biofuels consortium stirred-tank and ICL flat-plate PBRs. The AquaMedic vertical-column PBR provides a fixed light intensity of 42.5 $W \cdot m^{-2}$. The nutrient uptake kinetics corresponding to cc124 growth in 5xTAP* (Figure II.03a) are shown in Figure III.05. Similarly, the Solar Biofuels consortium stirred-tank PBRs supply a fixed light intensity of 25.0 $W \cdot m^{-2}$, but cc124 growth experiments were carried out in both constant illumination (Figure II.10a) and constant illumination with CO_2 bubbling (Figure II.10b) modes. The corresponding acetate and sulphate uptake rates are given in Figure III.06. Unlike the other PBRs, the stirred-tank reactor was a closed system and the algal growth conditions were consequently photoheterotrophic (acetate only). As a result, the overall system was different from that of the experiments in other PBRs in that a higher proportion of acetate was consumed per unit of biomass produced. Since these results provided insufficient data to develop a separate photoheterotrophic correlation of acetate consumption and algal growth, they were excluded from further study.

Finally, the ICL flat-plate PBR was commissioned by measuring cc124 growth at light intensities of 6 $W \cdot m^{-2}$ (Figure II.19a) and 12 $W \cdot m^{-2}$ (Figure II.19b); the corresponding nutrient uptake is shown in Figure III.07. Some of the quickest growth rates were observed in the flat-plate reactor, even though it was operated at a lower light intensity than the other reactors. This is because irradiation is incident on a flat reactor surface, and this PBR features a large surface-to-volume ratio and a turbulent mixing system, which maximise photon use efficiency (Tamburic *et al*., 2011b). The reverse logistic fits in Figures III.05-III.07 have a similar accuracy to those of the nutrient uptake in the Sartorius PBR, which have already been analysed in more detail. An aggregation of all the algal growth and nutrient uptake kinetic data is shown in Table III.01.



(a) (b)

Figure III.05: Reverse logistic model fit to experimental data for *C. reinhardtii* cc124 acetate and sulphate uptake in the AquaMedic vertical-column PBR

(a) Acetate uptake

(b) Sulphate uptake

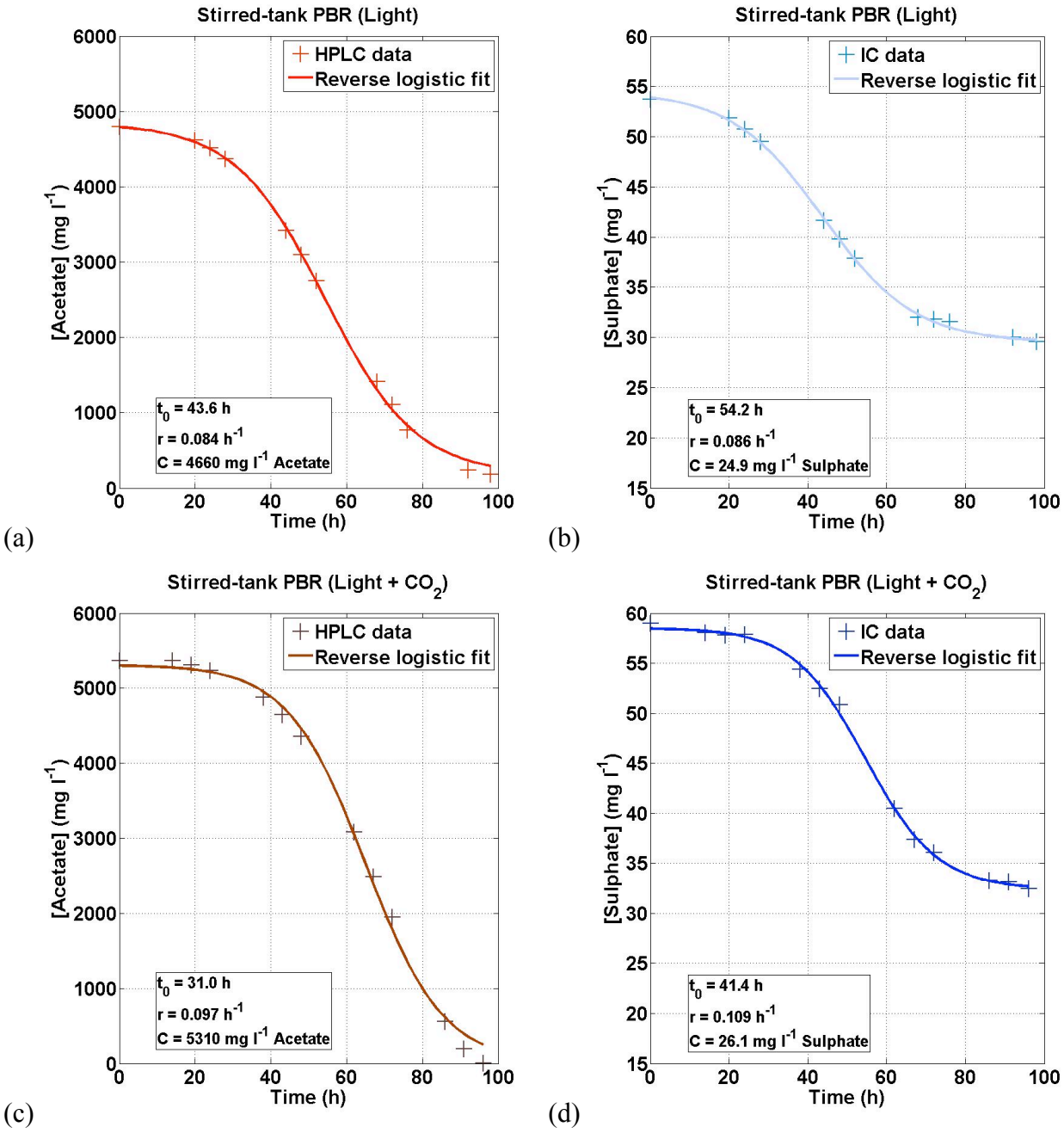


Figure III.06: Reverse logistic model fit to experimental data for *C. reinhardtii* cc124 acetate and sulphate uptake in the Solar Biofuels Consortium stirred-tank PBR

(a) Acetate uptake under continuous illumination

(b) Sulphate uptake under continuous illumination

(c) Acetate uptake under continuous illumination with CO_2 bubbling

(d) Sulphate uptake under continuous illumination with CO_2 bubbling

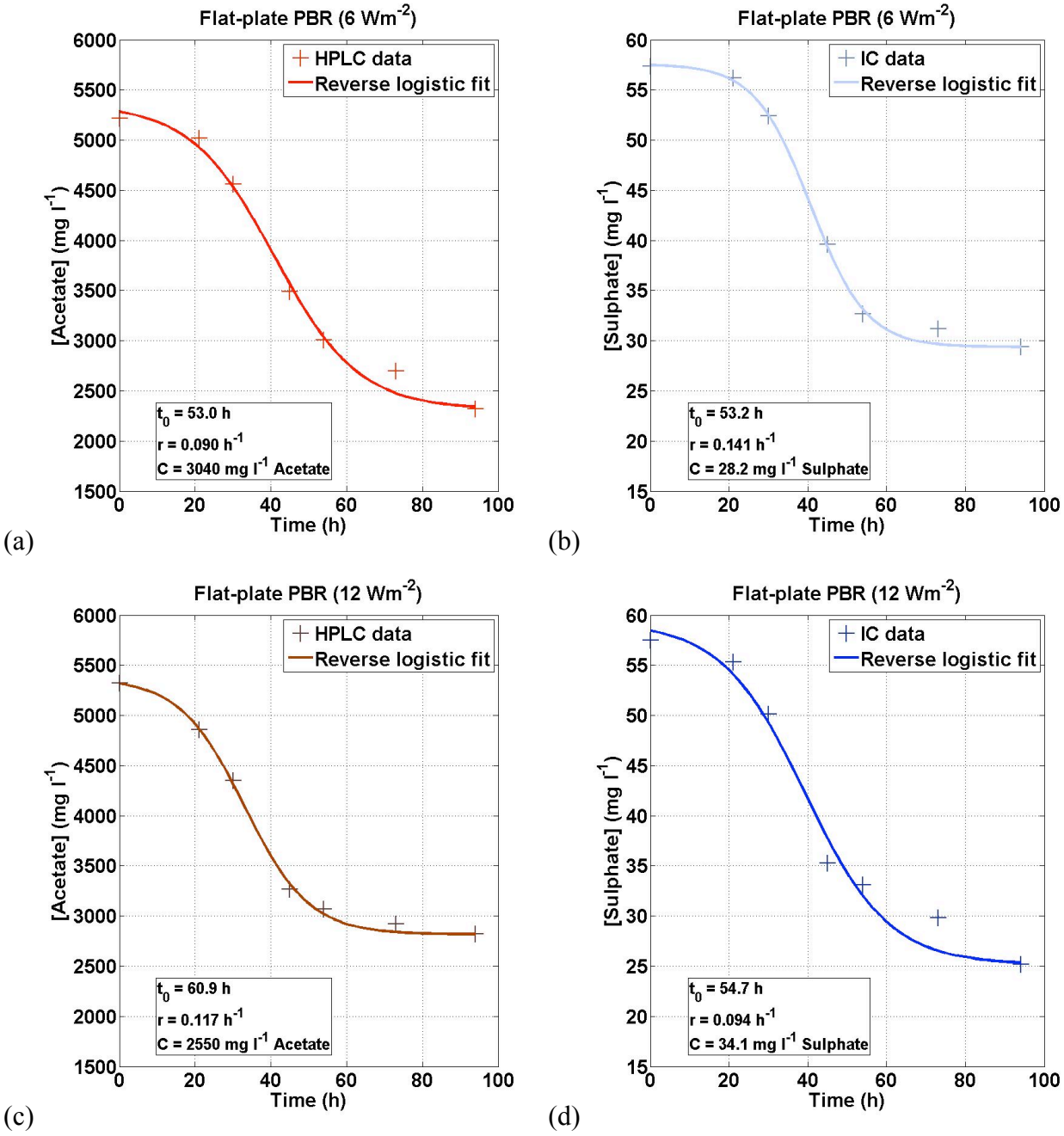


Figure III.07: Reverse logistic model fit to experimental data for *C. reinhardtii* cc124 acetate and sulphate uptake in the ICL flat-plate PBR

(a) Acetate uptake at 6 Wm^{-2}

(b) Sulphate uptake at 6 Wm^{-2}

(c) Acetate uptake at 12 Wm^{-2}

(d) Sulphate uptake at 12 Wm^{-2}

Table III.01: Collection of *C. reinhardtii* cc124 growth and nutrient uptake kinetic parameters in different reactors and under different illumination conditions

Reactor (light)	Algal growth		Acetate uptake		Sulphate uptake	
	Growth rate (h^{-1})	Final OD ($mg \cdot l^{-1}$Chl)	Uptake rate (h^{-1})	Consumption ($mg \cdot l^{-1}$)	Uptake rate (h^{-1})	Consumption ($mg \cdot l^{-1}$)
Tubular (15 $W \cdot m^{-2}$)	0.062	38.6	0.069	3,770	0.064	25.4
Tubular (20 $W \cdot m^{-2}$)	0.077	33.3	0.080	3,130	0.069	26.5
Tubular (25 $W \cdot m^{-2}$)	0.071	36.8	0.069	4,060	0.062	29.8
Tubular (30 $W \cdot m^{-2}$)	0.095	41.7	0.076	3,420	0.098	28.8
Tubular (45 $W \cdot m^{-2}$)	0.103	37.7	0.109	2,930	0.089	30.1
Tubular (60 $W \cdot m^{-2}$)	0.112	37.7	0.114	2,700	0.139	30.7
Vertical-column	0.093	35.7	0.095	3,450	0.076	25.4
Stirred-tank (light)	0.066	22.8	0.084	4,660	0.086	24.9
Stirred-tank (light+CO_2)	0.063	28.7	0.097	5,310	0.109	26.1
Flat-plate (6 $W \cdot m^{-2}$)	0.105	27.5	0.090	3,040	0.141	28.2
Flat-plate (12 $W \cdot m^{-2}$)	0.115	32.1	0.117	2,550	0.094	34.1

III.3.2. Reactor-independent Correlations

As discussed previously, the specific acetate and sulphate uptake rates are determined by the rate of photosynthesis and are therefore functions of the specific algal growth rate. It follows from the same argument that the total acetate and sulphate uptake quantities should also be functions of the specific algal growth rate. These correlations have been substantiated in Figures III.08a and III.08b for acetate, and Figures III.08c and III.08d for sulphate.

The acetate uptake rate increases linearly with algal growth rate (Figure III.08a: the correlation coefficient R is 0.97 with a p-value of 0.000). The total acetate uptake decreases linearly with the algal growth rate (Figure III.08b: the correlation coefficient R is -0.86 with a p-value of 0.003) because higher algal growth rates imply higher photosynthesis rates and a lower contribution of acetate towards the overall carbon requirements of the algal cells. Correlations with a p-value lower than 0.010 are considered to be statistically significant. The random spread of different PBR data points above and below the linear regression line indicates that the correlation is reactor-independent. Both the sulphate uptake rate (Figure III.08c: the correlation coefficient R is 0.81 with a p-value of 0.010) and the total sulphate uptake (Figure III.08d: the correlation coefficient R is 0.74 with a p-value of 0.009) have been found to increase linearly with the algal growth rate. All sulphate-related correlations are also statistically significant and reactor-independent.

It is now possible to prepare a medium for batch H_2 production by nutrient control for any photomixotrophic PBR under a wide variety of ambient conditions. All that is required is an initial measurement of the algal growth rate under those conditions. For example, if the growth rate is measured to be 0.1 h^{-1}, the nutrient control medium needs to contain 29.5 $mg \cdot l^{-1}$ of sulphate and 3,060 $mg \cdot l^{-1}$ of acetate. The proposition that S-deprived H_2 production can be initiated by nutrient control will be experimentally verified later in this chapter.

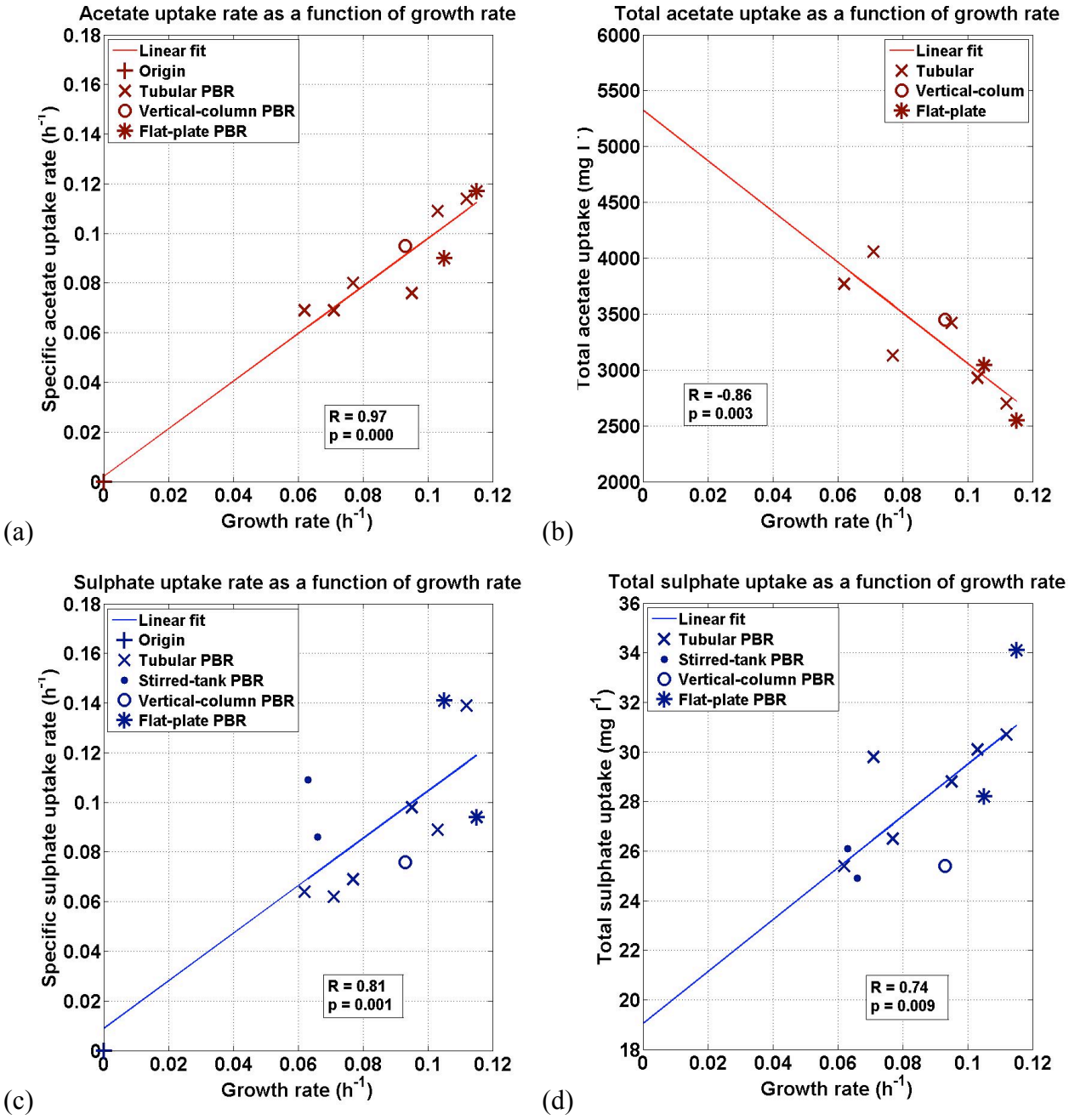


Figure III.08: Reactor-independent sulphate and acetate uptake kinetics during *C. reinhardtii* cc124 growth

(a) Acetate uptake rate as a function of algal growth rate

(b) Total acetate uptake as a function of algal growth rate

(c) Sulphate uptake rate as a function of algal growth rate

(d) Total sulphate uptake as a function of algal growth rate

III.4. H_2 Production at Low Light Intensities

The discovery of a reactor-independent relationship between *C. reinhardtii* growth rate and nutrient uptake rates has set the stage for carrying out nutrient-controlled H_2 production. However, it is now time to take a step back and evaluate a number of alternative H_2 production techniques, which were used prior to the development of the nutrient-control procedure. Comparing and contrasting the different H_2 production techniques will provide a useful insight into the H_2 production process, and it will make the benefits of using nutrient-controlled H_2 production apparent. During the course of this thesis, biophotolytic H_2 production was also induced by a number of alternative routes: using low light intensity, centrifugation, dilution and nutrient control.

H_2 production at low light intensities was initially identified almost by accident. It occurred during *C. reinhardtii* cc124 growth experiments in the Sartorius tubular PBR. The algae were grown in TAP medium, at a light intensity of 12 $W \cdot m^{-2}$ and a temperature of 25°C, and the PBR was operated as a closed system. The pO_2 signal was observed to decrease to 0% at the very beginning of the algal growth stage, after approximately 10 hours of experimental time (Figure III.09a). This raised the question of whether H_2 production was possibly taking place. A gas sample was extracted using a gas-tight syringe and analysed by injection mass spectrometry. Although there was no H_2 production after 16 hours, the results do show clear H_2 production peaks at 40, 64 and 88 hours (Figure III.09b). No H_2 was detected at 112 hours, but by this time, the pO_2 was beginning to increase again. A review of literature revealed that such H_2 production at low light intensities had already been observed and investigated (Skjånes *et al*., 2008; Degrenne *et al*., 2011). The reason for H_2 production is that the algae do not produce enough O_2 by photosynthesis to satisfy metabolic requirements, the environment becomes anaerobic and H_2 production commences. A number of additional experiments (Figure III.09c-III.09h) were carried out to prove this hypothesis using *in situ* O_2 measurements. In the absence of MIMS, H_2 production was measured by injection mass spectrometry, which enables a qualitative comparison of the H_2 production results. A quantitative analysis was not possible because the MS injection peaks could not be calibrated to actual H_2 production volumes.

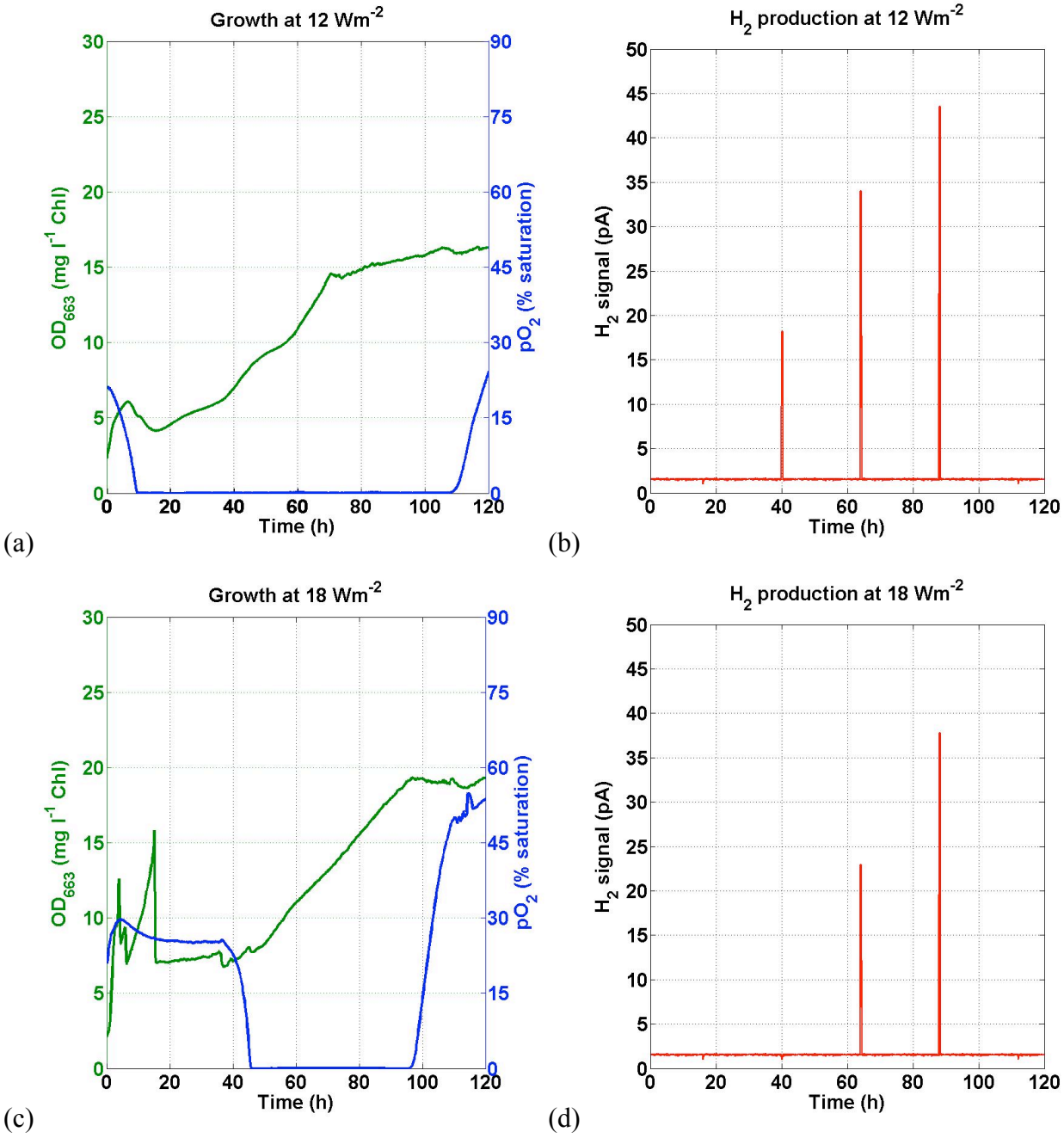


Figure III.09a-d: Growth and H_2 production (measured by injection mass spectrometry) by cc124 *C. reinhardtii* at low light intensities in the Sartorius tubular reactor

(a) OD and pO_2 at 12 Wm^{-2}

(b) H_2 production at 12 Wm^{-2}

(c) OD and pO_2 at 18 Wm^{-2}

(d) H_2 production at 18 Wm^{-2}

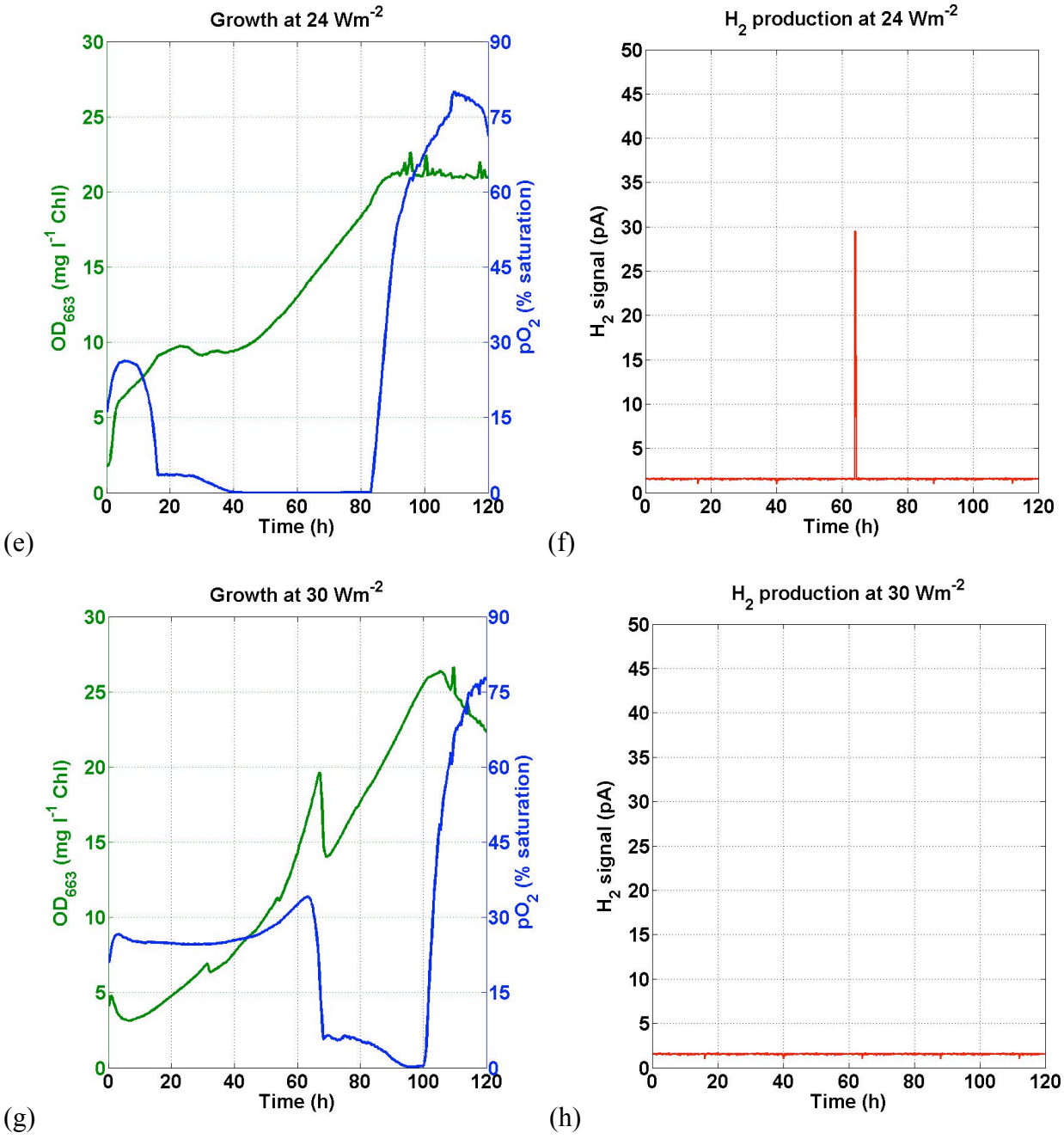


Figure III.09e-h: Growth and H_2 production (measured by injection mass spectrometry) by cc124 *C. reinhardtii* at low light intensities in the Sartorius tubular reactor

(e) OD and pO_2 at 24 Wm^{-2}

(f) H_2 production at 24 Wm^{-2}

(g) OD and pO_2 at 30 Wm^{-2}

(h) H_2 production at 30 Wm^{-2}

As the light intensity was increased from 12 to 18, 24, and eventually 30 $W \cdot m^{-2}$, the algae grew quicker and grew to a higher final OD, indicating improved rates of photosynthesis with each increase. At the same time, the duration of the anaerobic period decreased from approximately 100 hours at 12 $W \cdot m^{-2}$ (Figure III.09a), to 45 hours at 18 $W \cdot m^{-2}$ (Figure III.09c), 22 hours at 24 $W \cdot m^{-2}$ (Figure III.09e), and 6 hours at 30 $W \cdot m^{-2}$ (Figure III.09g). By counting the number of H_2 peaks it was possible to determine the duration of anaerobic H_2 production. At 12 $W \cdot m^{-2}$, three H_2 production peaks were observed with a maximum H_2 signal of 43 pA (Figure III.09b), at 18 $W \cdot m^{-2}$, there were only two H_2 peaks with a 38 pA maximum (Figure III.09d), at 24 $W \cdot m^{-2}$, there was one H_2 peak at 30 pA (Figure III.09f), and no H_2 production was detected at 30 $W \cdot m^{-2}$ (Figure III.09h). These results prove that duration of anaerobic conditions is longer at lower light intensities and that H_2 production does occur as a result of these anaerobic conditions. The results also show that inducing H_2 production by low illumination is ultimately a self-defeating process because it is most efficient at extremely low light intensities, which do not encourage algal growth to high cell densities, hence limiting the number of reaction centres available for H_2 production. The limitation of these results is that they do not allow quantitative analysis of H_2 production and therefore cannot be compared to the H_2 production rates and yields induced by S-deprivation and measured by MIMS. H_2 production at low light intensity will be measured by MIMS and quantified in a later nutrient control experiment.

III.5. H_2 Production by Centrifugation

Centrifugation was the original S-deprivation technique (Melis *et al*., 2000) and it continues to be used by algal researchers worldwide (Eroglu & Melis, 2011; Hemschemeier & Happe, 2011). The technique involves the extraction of fully-grown algal cells from the growth medium using a centrifuge and the re-suspension of those cells in the sulphur-deplete TAP-S medium. The algal culture proceeds to use up any O_2 in the system before entering the anaerobic H_2 production stage. Centrifugation experiments were carried out in the ICL flat-plate PBR at a light intensity of 12 $W \cdot m^{-2}$ and a temperature of 25°C. A light intensity of 12 $W \cdot m^{-2}$ was used because the recipe for a nutrient control medium (TAP_{12}) at that light intensity was previously developed. The OD and pO_2 of the algal culture were continuously measured. H_2 production was measured by MIMS. There were two primary objectives for carrying out the centrifugation experiments: to compare H_2 production by centrifugation to the H_2 production by alternative S-deprivation techniques and to compare the H_2 production of the WT cc124 *C. reinhardtii* strain with the H_2 production of the s21 fermentation mutant.

H_2 production under centrifugation by cc124 is shown in Figure III.10. The experiment was started following the centrifugation of a fully-grown *C. reinhardtii* cc124 culture and its subsequent re-suspension in TAP-S. The initial OD of the re-suspended algal culture was 24.5 $mg \cdot l^{-1}$Chl (Figure III.10a). A period of 24 hours was required before the rate of photosynthesis became sufficiently downgraded by S-deprivation to induce anaerobic conditions (Figure III.10b). H_2 production was initiated at this time and lasted for 147 hours, reaching a maximum H_2 production rate of 1.11 $ml H_2 \cdot l^{-1} \cdot h^{-1}$ at 66 hours (after 42 hours of anaerobic conditions). The OD decreased over the course of the experiment, reaching a final value of 13.4 $mg \cdot l^{-1}$Chl, indicating that almost half of the available photosynthetic biomass was used for the production of H_2 and other fermentative by-products such as organic acids and alcohols. The cumulative H_2 yield was 102.7 $ml H_2 \cdot l^{-1}$. The H_2 production rates and yields measured here using the centrifugation technique are consistent with those measured in the literature for WT *C. reinhardtii* (Melis *et al*., 2000; Kruse *et al*., 2005b).

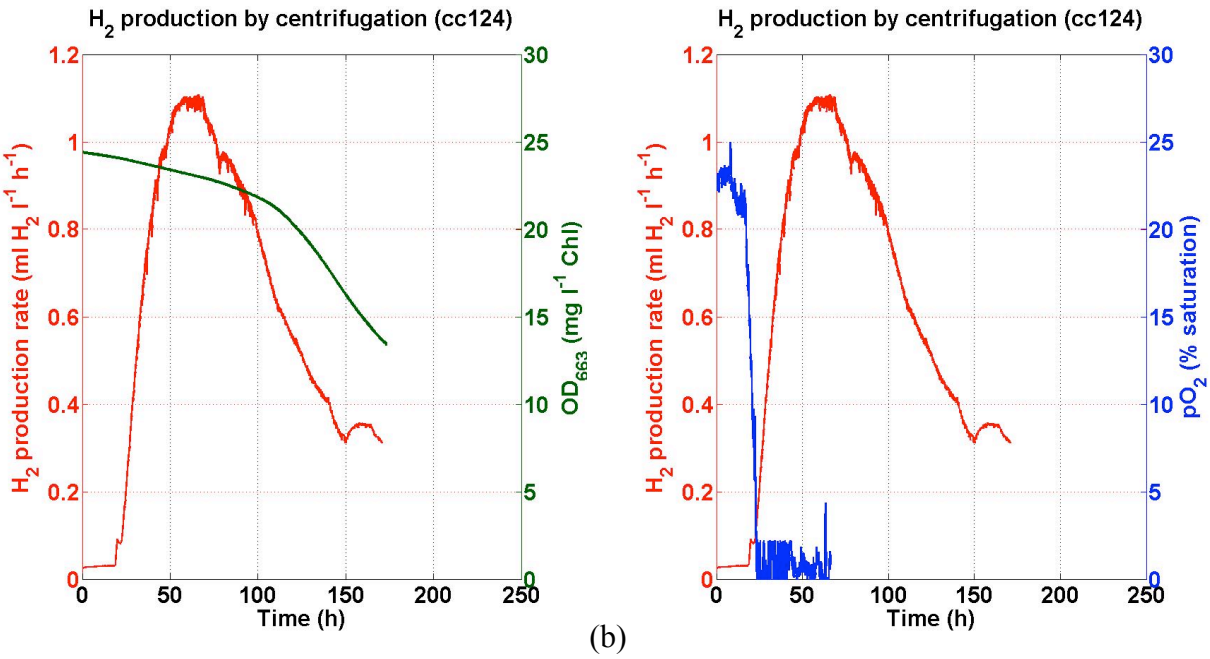


Figure III.10: *C. reinhardtii* cc124 WT H_2 production by centrifugation in the ICL flat-plate PBR

(a) OD_{663} and H_2 production against time

(b) pO_2 and H_2 production against time

The *C. reinhardtii* s21 mutant was prepared by Dr Steven Burgess under the supervision of Professor Peter Nixon in the Biology department of ICL. It was designed to be a knock-down mutant of the PFL metabolic pathway in *C. reinhardtii* and Western blots had shown that the mutation was successful; however, H_2 production by s21 was being tested for the first time in this experiment. H_2 production under centrifugation by s21 is shown in Figure III.11. Following centrifugation, the s21 cells were diluted to exactly 24.5 $mg \cdot l^{-1}$Chl (Figure III.11a), which was identical to the starting OD used for the corresponding cc124 experiment. The O_2 consumption period lasted for 30 hours, followed by a 220 hour period of anaerobic H_2 production (Figure III. 11b). The maximum H_2 production rate was 0.85 $mlH_2 \cdot l^{-1} \cdot h^{-1}$ and the total H_2 yield was 107.1 $mlH_2 \cdot l^{-1}$. The OD at the end of the experiment was 19.1 $mg \cdot l^{-1}$Chl.

The cc124 and s21 H_2 production results are compared in Figure III.12. The fermentation mutant s21 has a lower maximum H_2 production rate than cc124 (0.85 $mlH_2 \cdot l^{-1} \cdot h^{-1}$ compared to 1.11 $mlH_2 \cdot l^{-1} \cdot h^{-1}$, Figure III.12a) but H_2 production lasts for a longer time period, resulting in a slightly higher H_2 yield (107.1 $mlH_2 \cdot l^{-1}$ compared to 102.7 $mlH_2 \cdot l^{-1}$, Figure III.12b). In addition, fewer catabolic processes take place in s21, as indicated by a smaller decrease in the algal OD. The differences between the two experiments indicate that a successful metabolic mutation was achieved in s21. However, these results also support a conclusion made previously during experiments using the fermentation mutant pdc3-KD in the dark (Chapter I.4.2): knocking-down a single metabolic pathway is not a sufficient condition to significantly increase the H_2 production by *C. reinhardtii*.

It is also possible to observe oscillation in the H_2 production rate in Figure III.12a, as well as in subsequent figures depicting the H_2 production rate. These oscillations have a period of approximately 24 hours, indicating the sensitivity of H_2 production to diurnal cycles in the laboratory. Although continuous LED illumination is the dominant light source to *C. reinhardtii* cultures in the ICL flat-plate PBR, sunlight and artificial laboratory light also play a role in driving H_2 production. The diurnal oscillations were not investigated further because it was difficult to quantitatively determine the variation in light intensity that they related to. The oscillations do provide another indication of the sensitivity of the MIMS system to very small variations in H_2 production conditions.

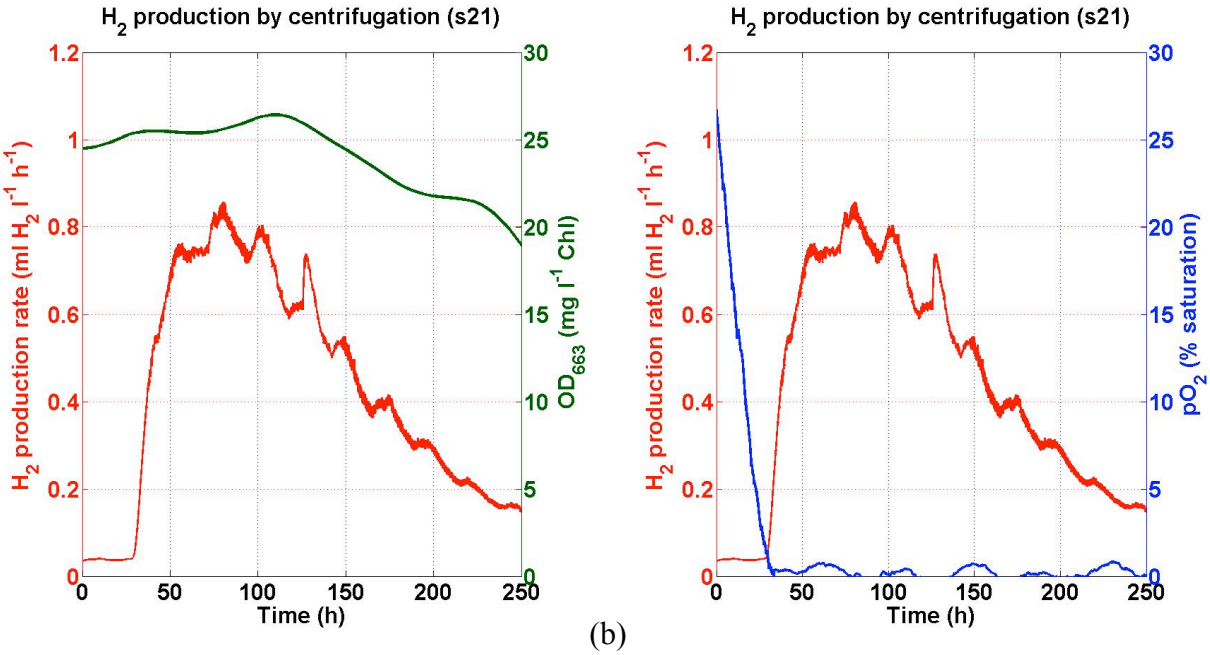


Figure III.11: *C. reinhardtii* s21 mutant H_2 production by centrifugation in the ICL flat-plate PBR

(a) OD_{663} and H_2 production against time

(b) pO_2 and H_2 production against time

(a) (b)

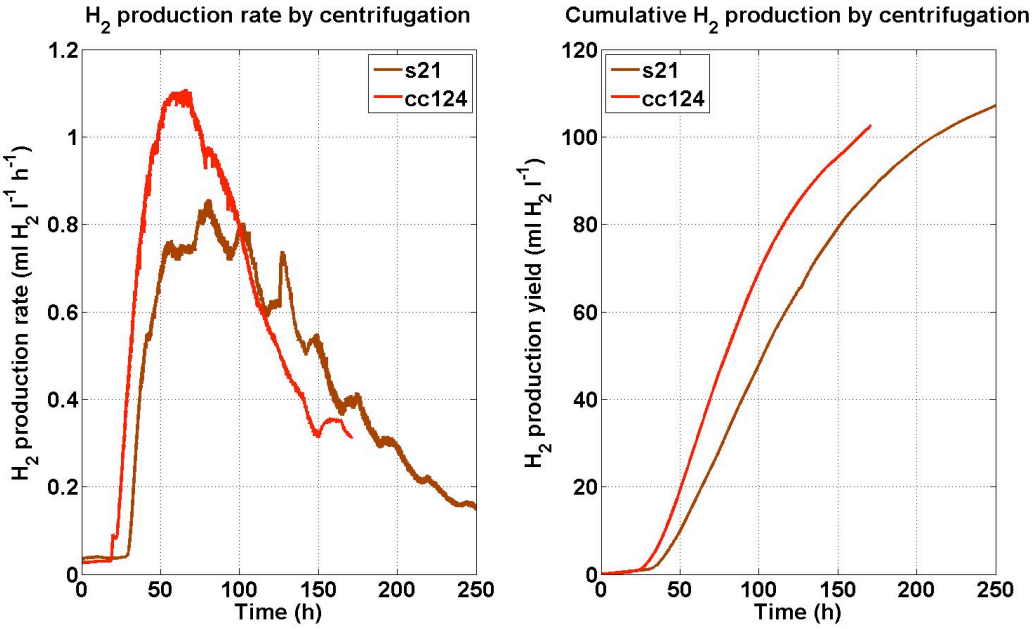


Figure III.12: Comparison of the H_2 production by cc124 and s21 strains of *C. reinhardtii* under centrifugation

(a) H_2 production rates

(b) H_2 production yields

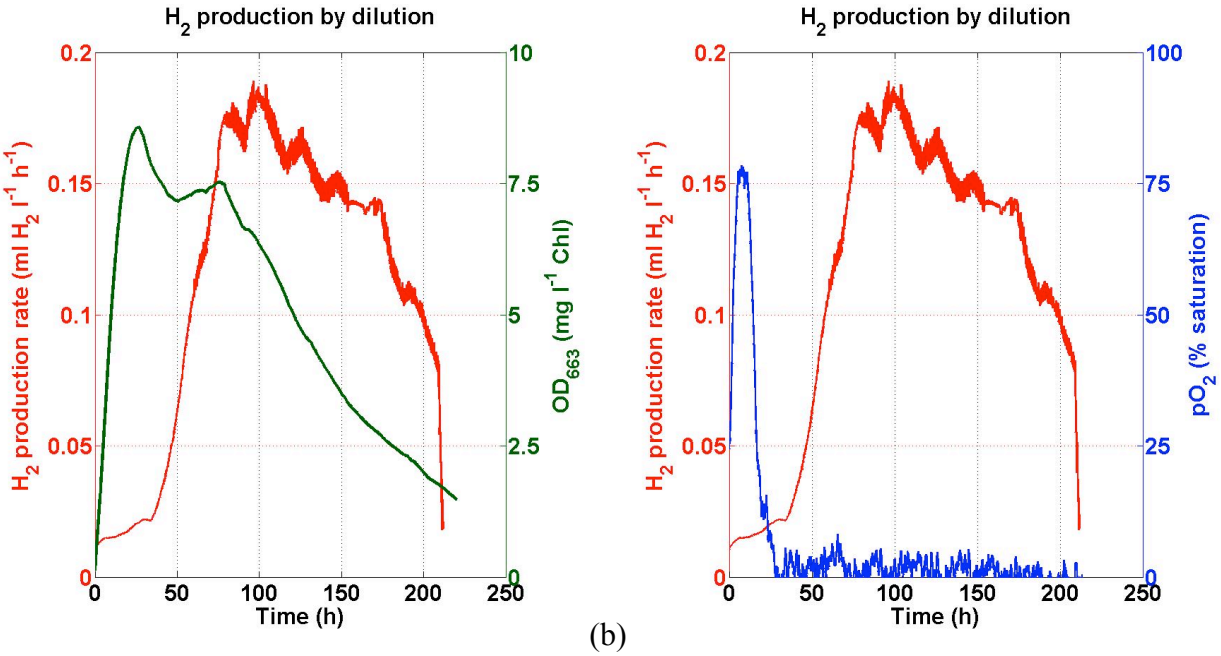
III.6. H_2 Production by Dilution

Dilution was initially developed as a more practical and scalable S-deprivation alternative to centrifugation (Laurinavichene *et al*., 2002). The dilution technique involves growth in a sulphur-limited medium until all sulphate has been used up, followed in turn by an O_2 consumption stage and a H_2 production stage. Sulphur-limited conditions are achieved by diluting a small inoculum of sulphur-replete growing algal culture in the sulphur-deplete TAP-S medium. The dilution experiment was carried out in the ICL flat-plate PBR at a light intensity of 12 $W \cdot m^{-2}$ and a temperature of 25°C. The *C. reinhardtii* WT cc124 was used. MIMS was used to measure H_2 production rates and yields as described previously (Tamburic *et al*., 2011b). A 10% v/v inoculum of growing algal cells was diluted in the TAP-S medium.

Sulphur-limited growth and H_2 production by cc124 under dilution is shown in Figure III.13. In the first 25 hours of the experiment, the algae grew aerobically to a maximum OD of 8.6 $mg \cdot l^{-1}$Chl (Figure III.13a). At this point, the algae had already run out of the little sulphur that was present in the inoculum and the culture promptly became anaerobic 30 hours into the experiment (Figure III. 13b). H_2 production commenced as soon as the anaerobic conditions were imposed and a maximum H_2 production rate of 0.18 $mlH_2 \cdot l^{-1} \cdot h^{-1}$ was reached at 96 hours (after 66 hours of anaerobic conditions). In addition to photolytic H_2 production, some H_2 was also produced by the catabolism of substrate, as evidenced by the decrease in OD from 8.6 $mg \cdot l^{-1}$Chl to 1.5 $mg \cdot l^{-1}$Chl over the course of the experiment. The H_2 production duration was 182 hours, resulting in a H_2 yield of 23.6 $mlH_2 \cdot l^{-1}$. This yield is consistent with that measured in other dilution experiments in the literature (Laurinavichene *et al*., 2002; Kosourov *et al*., 2007).

An inoculum of 10% v/v was used because Laurinavichene and colleagues had determined, by trial and error, that this was the best ratio for H_2 production (Laurinavichene *et al*., 2002). While this was the case under their operating conditions, it is evident that the dilution method is not optimised for H_2 production in the ICL flat-plate PBR at 12 $W \cdot m^{-2}$. The maximum OD reached during the dilution experiment was 8.6 $mg \cdot l^{-1}$Chl, almost three times lower than the initial OD during the corresponding centrifugation experiment, which was 24.5 $mg \cdot l^{-1}$Chl. This low OD did not provide enough PSII reaction centres for effective H_2 production, resulting in a considerably lower H_2

production rate (0.18 $mlH_2 \cdot l^{-1} \cdot h^{-1}$ compared to 1.11 $mlH_2 \cdot l^{-1} \cdot h^{-1}$) and total H_2 yield (23.6 $mlH_2 \cdot l^{-1}$ compared to 102.7 $mlH_2 \cdot l^{-1}$) compared with centrifugation. It would certainly be possible to improve the H_2 production by dilution using a trial and error approach. An obvious correction to make would be to increase the size of the inoculum with the aim of improving algal growth and increasing the starting OD available for H_2 production. However, any improvements would become void as soon as an operating condition was changed or the PBR was changed. Fortunately, the nutrient control procedure creates the opportunity to effectively operate a fully-optimised dilution procedure under any set of conditions.



(a) (b)

Figure III.13: *C. reinhardtii* cc124 WT H_2 production by dilution in the ICL flat-plate PBR

(a) OD_{663} and H_2 production against time

(b) pO_2 and H_2 production against time

III.7. H_2 Production by Nutrient Control

The nutrient control technique of S-deprivation combines the high starting OD of the centrifugation technique with the spontaneous H_2 production of the dilution technique. It was developed by determining a reactor-independent correlation between *C. reinhardtii* cc124 growth, and the corresponding acetate and sulphate consumption, as shown in Figure III.08b and in Figure III.08d, respectively. As with previous centrifugation and dilution experiments, nutrient-control experiments were carried out using *C. reinhardtii* WT cc124 in the ICL flat-plate PBR at 12 $W \cdot m^{-2}$ and 25°C. The optimised TAP_{12} medium was used (Table 5.09b). H_2 production was measured by MIMS, acetate consumption was measured by HPLC and sulphate consumption was measured by IC. OD and pO_2 were continuously monitored and recorded. Two similar nutrient-control experiments were carried out. In the first experiment, MIMS was operated throughout the experiment, both during the algal growth and the H_2 production stage. In the second experiment, MIMS was only operated during the H_2 production stage.

The results of the first nutrient control experiment are shown in Figure III.14. Since the TAP_{12} growth medium was carefully optimised to provide just enough acetate and sulphate for *C. reinhardtii* growth, the algae attain a substantial maximum OD of 32.3 $mg \cdot l^{-1} \cdot Chl$ (Figure III.14a) 91 hours from the start of the experiment. This OD was even higher than the starting OD of the centrifugation method because an excess of 20% of the algal cells are typically lost during the centrifugation and re-suspension procedure (Tsygankov *et al.*, 2006). The entire acetate concentration of 2,550 $mg \cdot l^{-1}$ was also used up during the algal growth stage at a specific uptake rate of 0.112 h^{-1} (Figure III.14c). The entire sulphate concentration of 28.0 $mg \cdot l^{-1}$ was also consumed during the 90 hours of algal growth at a specific uptake rate of 0.127 h^{-1} (Figure III.14d). The nutrient control experiment underwent two anaerobic stages: a brief anaerobic stage between 15 and 69 hours and a longer anaerobic stage from 90 hours until the end of the experiment (Figure III.14b). The first anaerobic stage was likely caused by a large increase in the O_2 demand of the rapidly growing algal culture, which could not entirely be satisfied by photosynthesis. Since the flat-plate reactor was operated as a closed system, this resulted in anaerobic conditions during the mid-point of the algal growth stage. This phenomenon was already observed at low light intensities in the Sartorius tubular PBR (Figure III.09), and it has also been investigated in the literature

(Degrenne *et al*., 2011). The use of MIMS enabled the quantification of this H_2 production at low light intensity. A peak H_2 production rate of 0.25 $mlH_2 \cdot l^{-1} \cdot h^{-1}$ was observed during this first anaerobic stage. Although this H_2 production period was not insignificant, the maximum H_2 production rate was more than five times lower than the subsequent S-deprived H_2 production rate. The second anaerobic stage was the result of the regular S-deprivation procedure. It lasted for 210 hours and reached a maximum H_2 production rate of 1.30 $mlH_2 \cdot l^{-1} \cdot h^{-1}$ at 130 hours (40 hours into the second anaerobic stage). The OD reduced to 21.3 $mg \cdot l^{-1}$ Chl by the end of the experiment and the H_2 yield was 112.7 $mlH_2 \cdot l^{-1}$. The H_2 yield achieved by nutrient control was 9.7% higher than the H_2 yield achieved by centrifugation. This is because the nutrient control method takes advantage of every grown algal cell, while the centrifugation procedure loses a proportion of available cells during the medium separation and exchange stages.

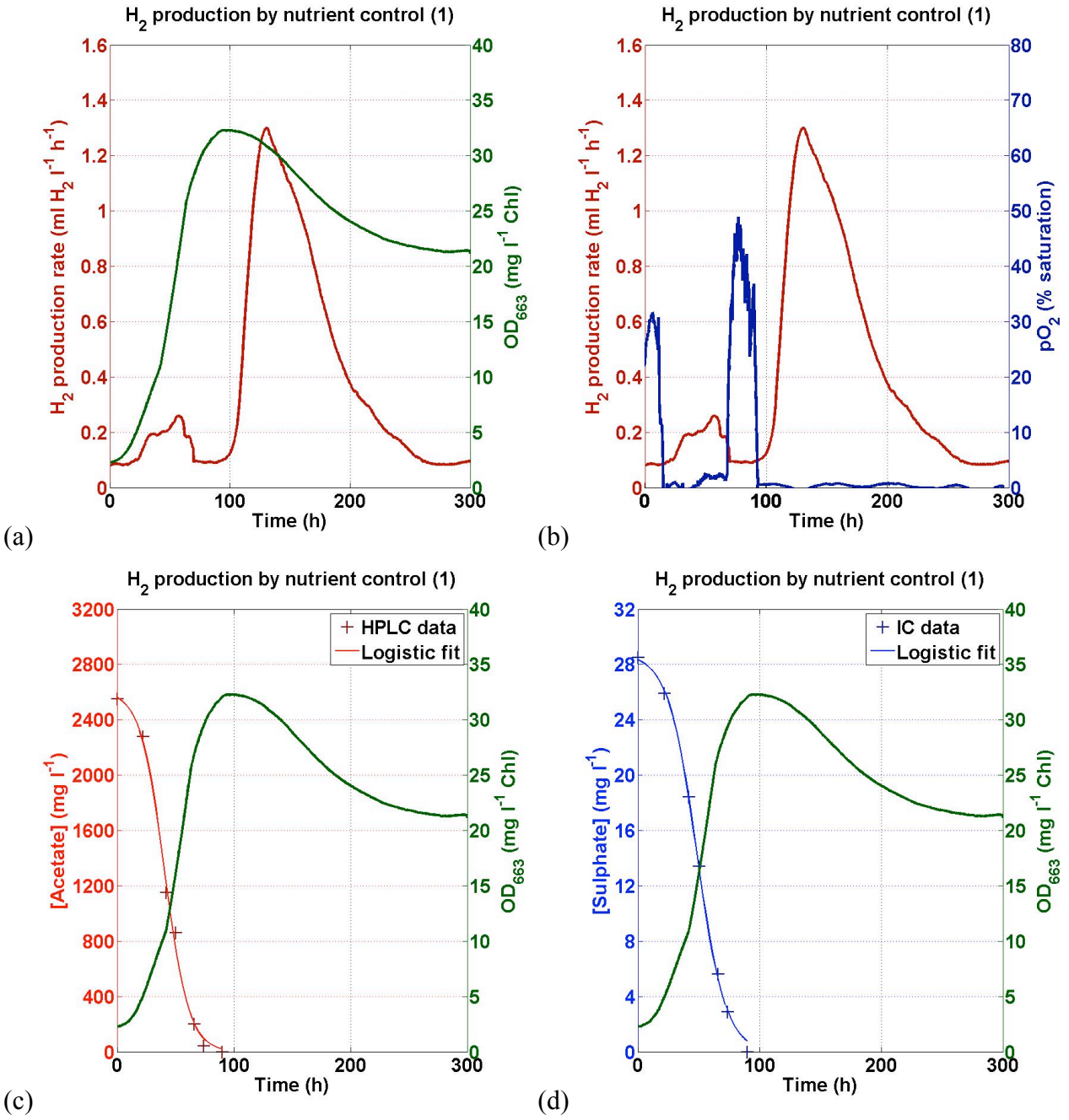


Figure III.14: *C. reinhardtii* cc124 H_2 production by nutrient control in the ICL flat-plate PBR; 1st experiment

(a) OD_{663} and H_2 production against time

(b) pO_2 and H_2 production against time

(c) Acetate uptake during algal growth

(d) Sulphate uptake during algal growth

The results of the second nutrient control experiment are shown in Figure III.15. MIMS was operated only during the H_2 production stage of the experiment. The intention was not to record H_2 production due to low light intensity during algal growth in order to achieve a fairer comparison between the S-deprived H_2 production by centrifugation, dilution and nutrient control. There was also a concern that the operation of MIMS during algal growth might be extracting O_2 out of the system and therefore contributing towards the onset of anaerobic conditions. During the second nutrient control experiment, the algal culture required 104 hours to grow to an even higher maximum OD of 35.9 $mg \cdot l^{-1}$Chl, which eventually reduced to 23.4 $mg \cdot l^{-1}$Chl as a result of catabolic processes (Figure III.15a). All acetate was used up at a specific uptake rate of 0.103 h^{-1} (Figure III. 15c) and all sulphate was used up at a specific uptake rate of 0.110 h^{-1} (Figure III.15d). The anaerobic period associated with S-deprivation lasted from approximately 130 hours until the end of the experiment at 260 hours (Figure III.15b). A maximum H_2 production rate of 1.52 $mlH_2 \cdot l^{-1} \cdot h^{-1}$ was measured at 167 hours.

A comparison of the H_2 production rates and yields of *C. reinhardtii* cc124 under the centrifugation, dilution and nutrient control methods of S-deprivation is shown in Figure III.16. The second nutrient control experiment was used in this comparison. The nutrient control method of S-deprivation resulted in a higher H_2 production rate (Figure III.16a) and a larger H_2 yield (Figure III. 16b) than either the centrifugation or dilution methods. A H_2 yield of 119.8 $mlH_2 \cdot l^{-1}$ at a maximum H_2 production rate of 1.52 $mlH_2 \cdot l^{-1} \cdot h^{-1}$ was measured during the second nutrient control experiment. The nutrient control method does not require the energy intensive medium exchange procedure central to the centrifugation method. Unlike the dilution method, the initial concentrations of sulphate and acetate have been optimised to facilitate effective algal growth, and subsequent H_2 production, for a specific set of ambient conditions in the ICL flat-plate PBR. The H_2 production by nutrient control does take a longer time to get started, but this time delay has been used effectively to grow algal biomass with optimum acetate and sulphate input. Nutrient control is also the only technique that can easily be scaled up for use in large continuous systems because it is based on a universal model that is independent of reactor geometry and size.

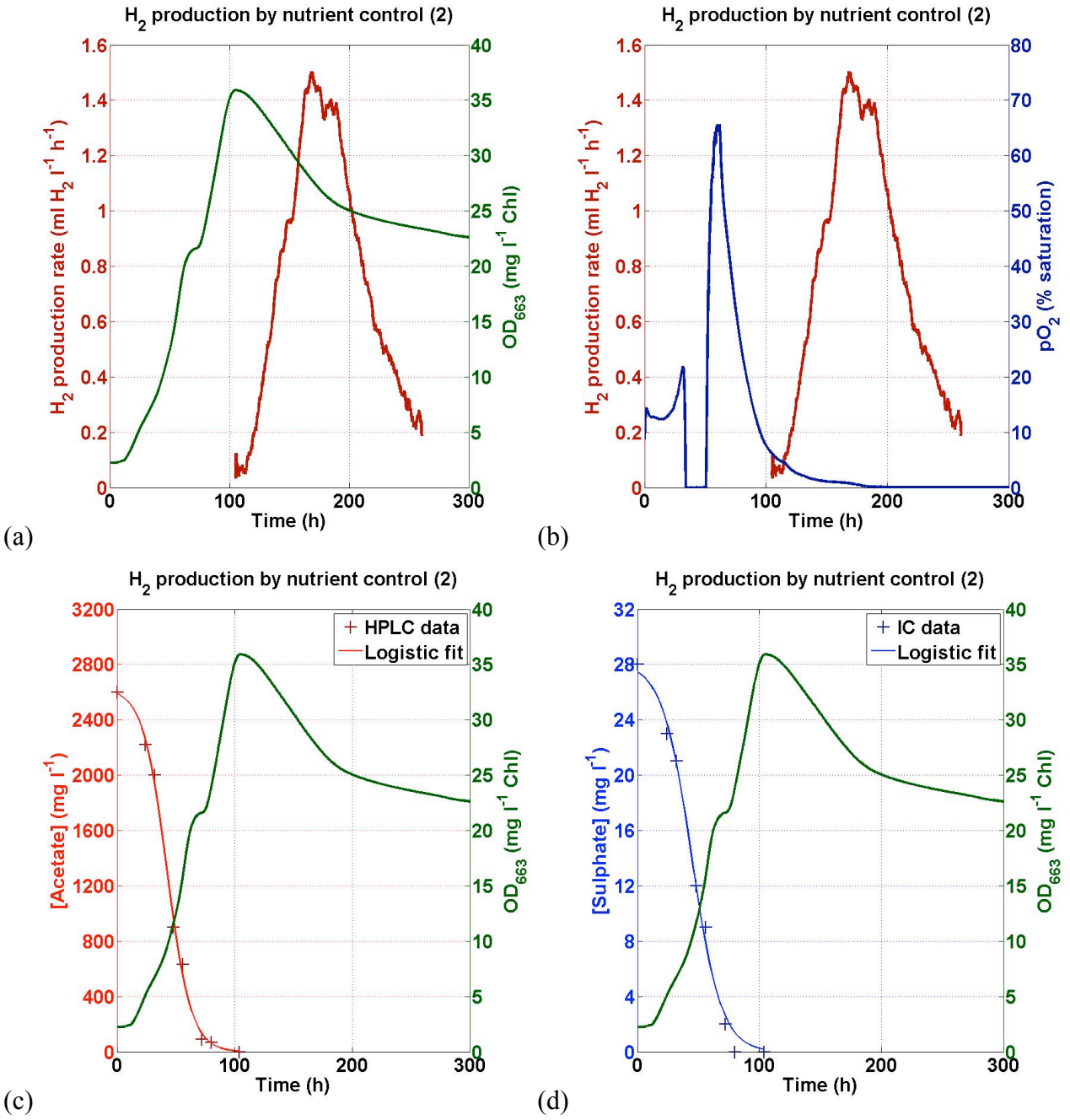


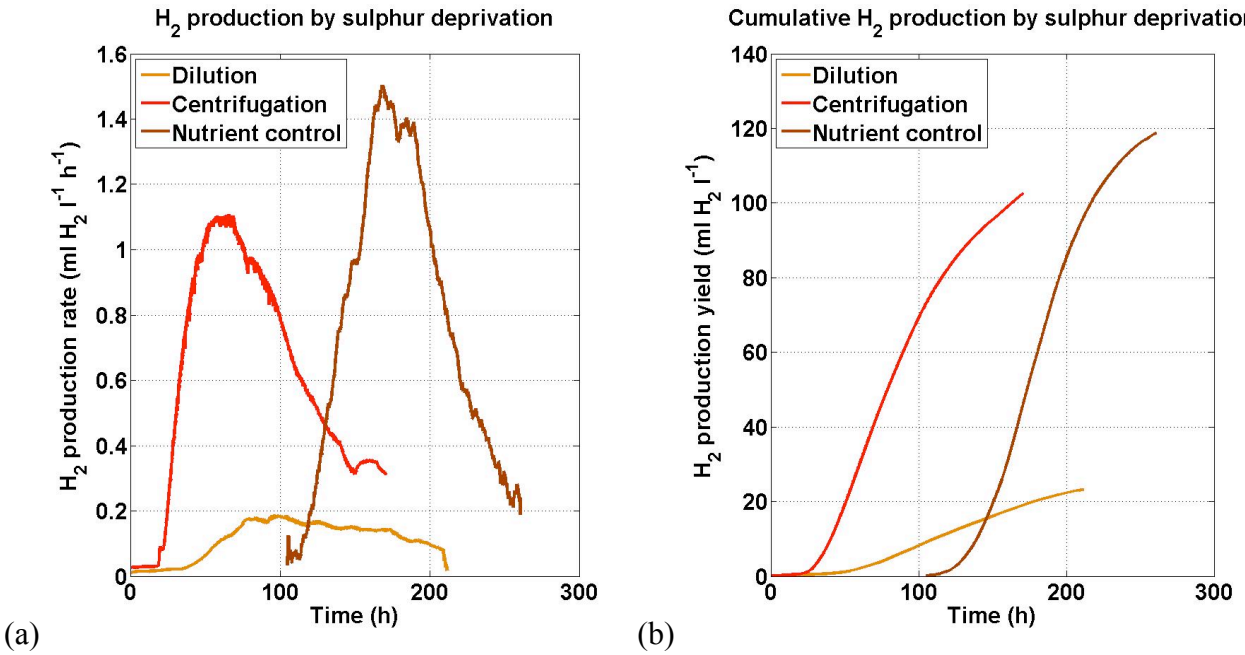
Figure III.15: *C. reinhardtii* cc124 H_2 production by nutrient control in the ICL flat-plate PBR; 2nd experiment

(a) OD_{663} and H_2 production against time

(b) pO_2 and H_2 production against time

(c) Acetate uptake during algal growth

(d) Sulphate uptake during algal growth



(a) (b)

Figure III.16: Comparison of the H_2 production by the dilution, centrifugation and nutrient control methods of S-deprivation

(a) H_2 production rates

(b) H_2 production yields

III.8. Summary

A reverse logistic model has been used to fit sulphate and acetate uptake kinetics and to obtain the specific nutrient uptake rates and the total quantities of nutrient consumed during algal growth. These two parameters are functions of the light intensity as well as of the specific algal growth rate. Higher light intensities (or higher specific growth rates) imply higher photosynthesis rates, increasing the turnover of the PSII repair mechanism and therefore increasing the demand for sulphur, both in terms of the specific sulphate uptake rate and of the total quantity of sulphur required. Similarly, higher light intensities (higher specific growth rates) lead to an increase in the specific acetate uptake rate. On the other hand, they also result in increased CO_2 fixation by the Calvin cycle and a corresponding decrease in the total quantity of acetate consumed. Evaluating the nutrient uptake rates and the total nutrient consumption as functions of the algal growth rate has revealed a set of statistically significant correlations, with a random distribution of data points indicating reactor independence. It is now possible to prepare an algal growth medium to facilitate batch or continuous H_2 production by nutrient control in any photomixotrophic PBR geometry under ambient conditions as soon as the algal growth rate at those conditions has initially been measured.

H_2 production was measured during algal growth at low light intensities by both injection mass spectrometry and MIMS. The maximum H_2 production rate during algal growth at 12 $W \cdot m^{-2}$ in the ICL flat-plate PBR was 0.25 $mlH_2 \cdot l^{-1} \cdot h^{-1}$, more than five times lower than the maximum H_2 production rate during subsequent S-deprivation (1.30 $mlH_2 \cdot l^{-1} \cdot h^{-1}$). The centrifugation procedure was used to compare H_2 production by WT cc124 and s21 fermentation mutant strains of *C. reinhardtii*. It was concluded that the PFL metabolic pathway mutation was successful, but that it was not sufficient to significantly increase H_2 production. A H_2 yield of 107.1 $mlH_2 \cdot l^{-1}$ was measured during the s21 experiment, compared with a H_2 yield of 102.7 $mlH_2 \cdot l^{-1}$ during the cc124 experiment.

Three different methods of S-deprivation were compared under identical ambient conditions in the Imperial College flat-plate PBR. The dilution method of S-deprivation resulted in a maximum H_2 production rate of 0.18 $mlH_2 \cdot l^{-1} \cdot h^{-1}$; the H_2 production duration was 182 hours, giving a H_2 yield of

23.6 $mlH_2 \cdot l^{-1}$. The centrifugation method was more energy intensive overall, but the higher initial OD led to an improved H_2 production rate of 1.11 $mlH_2 \cdot l^{-1} \cdot h^{-1}$. The H_2 production lasted for a period of 147 hours with a H_2 yield of 102.7 $mlH_2 \cdot l^{-1}$. The nutrient control method of H_2 production developed in this chapter combined the high initial OD of the centrifugation method with the spontaneous H_2 production of the dilution method. A starting sulphate concentration of 28.0 $mg \cdot l^{-1}$ and a starting acetate concentration of 2,550 $mg \cdot l^{-1}$ were used to achieve algal growth up to an OD of as much as 35.9 $mg \cdot l^{-1}$Chl (after 104 hours) under nutrient-optimised conditions. The subsequent H_2 production stage lasted for approximately 170 hours, with a maximum H_2 production rate of 1.52 $mlH_2 \cdot l^{-1} \cdot h^{-1}$ and a H_2 yield of 119.8 $mlH_2 \cdot l^{-1}$.

The nutrient control method of S-deprivation was easy to implement and it proved superior to its counterparts based on all the relevant H_2 production criteria, indicating that it should be the method of choice for H_2 production experiments as well as for scaled-up applications of biophotolytic H_2 production. It creates the opportunity for automated and spontaneous H_2 production using a single PBR. Unfortunately, it does not address the main shortcoming of green algal H_2 production, namely the short duration of the H_2 production period. Biophotolytic H_2 production remains a batch process with a lifetime of approximately one week. The next chapter will aim to apply the lessons learned during the development of the nutrient control technique to the procedure of re-inserting sulphur into a depleted *C. reinhardtii* culture, with the objective of increasing process lifetime.

IV. Extended Hydrogen Production by Sulphur Re-Addition

IV.1. Introduction

One of the main limitations of green algal biophotolysis is the short duration of anaerobic H_2 production. Under anaerobic conditions, *C. reinhardtii* cells cycle their photosynthetic electrons, creating a proton gradient that is responsible for both ATP synthesis and H_2 production via the $h_2$ase enzyme (Hallenbeck & Benemann, 2002; Hemschemeier *et al*., 2008). *C. reinhardtii* cells use ATP as their primary energy source, but it does not provide sufficient energy to satisfy their long-term metabolic requirements. Anaerobic conditions therefore result in gradual cell death and the *C. reinhardtii* culture can only survive for 5-7 days (Kosourov *et al*., 2002). This H_2 production duration needs to be significantly extended in order for large-scale biophotolysis applications to become viable. Anaerobic H_2 production is typically induced by sulphur-deprivation. In the previous chapter, it was shown that careful control of sulphate concentration in the algal growth medium is the key to achieving spontaneous and effective H_2 production. A similar approach also has the potential to increase the H_2 production duration. Since the availability of sulphur governs the rate of photosynthesis, and consequently the pO_2 levels of the *C. reinhardtii* culture, sulphur re-addition following the onset of anaerobic conditions should encourage algal cell recovery, and enable additional H_2 production over a longer time frame.

The aim of this chapter is to extend the duration of biohydrogen production of *C. reinhardtii* by sulphur re-addition. Two different sulphur re-addition techniques will be used: sulphur dilution and sulphur feed. The objective of the sulphur dilution method is to initiate cycles of algal growth and H_2 production. In a sulphur dilution experiment, the *C. reinhardtii* cc124 culture will be allowed to complete one full cycle of growth and H_2 production. The culture will then be diluted with a sulphur-optimised medium in an attempt to induce a secondary cycle of growth and H_2 production. Different percentage dilutions will be used and compared. The objective of the sulphur feed technique will be to achieve long-term continuous H_2 production. A micromolar sulphur feed will be applied to *C. reinhardtii* cultures while they are producing H_2. This sulphur feed will need to contain a nutrient concentration that is sufficient to nourish the *C. reinhardtii* cells without raising photosynthesis rates too high and stopping the anaerobic H_2 production.

IV.2. Sulphur Dilution

IV.2.1. Sulphur Dilution Experiments

Sulphur re-addition by dilution experiments were carried out using the *C. reinhardtii* WT cc124 in the ICL flat-plate PBR. A temperature of 25°C and a light intensity of 12 $W \cdot m^{-2}$ were used. This made the results comparable to those recorded in the previous chapter. In addition, it meant that the TAP_{12} medium could once again be utilised as an optimised source of sulphate and acetate. As in previous experiments, H_2 production was measured by MIMS, pO_2 was measured using an electrode and sulphate and acetate concentrations were measured by IC and HPLC respectively. Sulphur re-addition by dilution has already been demonstrated in the literature (Laurinavichene *et al*., 2006; Kim *et al*., 2010), but those experiments lacked the rigorous measurement techniques used in this study.

The aim of the sulphur re-addition by dilution experiments was to follow up a complete H_2 production cycle with subsequent *C. reinhardtii* cell recovery and secondary H_2 production cycles. In the interest of time, the initial H_2 production period was initiated by centrifugation, although this could also have been achieved by nutrient control, as described in the previous chapter. Upon the completion of a full H_2 production cycle, sulphur (and acetate) were re-inserted by means of a dilution with TAP_{12} medium. Dilutions of 20% and 50% (both shown in Figure IV.01), and 95% (Figure IV.02) volume/volume (v/v) were attempted. A dilution of 20% implies that 80% v/v of the depleted *C. reinhardtii* culture was diluted with 20% v/v of fresh TAP_{12} medium. The remaining 20% v/v of the depleted algal culture (200 ml, since the ICL flat-plate PBR has a 1 litre working volume) was drained from the PBR, deactivated with Trigene and discarded. Since the TAP_{12} medium was developed to provide optimum batch sulphate and acetate feed for an algal culture growing at 12 $W \cdot m^{-2}$ in the ICL flat-plate PBR, it follows that a 20% v/v dilution with TAP_{12} should provide the optimal nutrient feed to encourage the recovery of 20% of the *C. reinhardtii* culture growing under the same ambient conditions.

Figure IV.01 shows the results of the first sulphur re-addition by dilution experiment, where a centrifugation-induced H_2 production period was followed up by a 20% dilution with TAP_{12}, and

later also a 50% dilution. In the primary H_2 production cycle, the pO_2 fell to zero within 24 hours and a maximum H_2 production rate of 1.12 $mlH_2 \cdot l^{-1} \cdot h^{-1}$ was achieved (Figure IV.01a). This result is consistent with the previous centrifugation experiment with cc124, where a maximum H_2 production rate of 1.11 $mlH_2 \cdot l^{-1} \cdot h^{-1}$ was observed (Figure III.10). During the primary H_2 production stage, the algal OD reduced from 30.0 to 23.3 $mg \cdot l^{-1}$Chl as a result of catabolic processes (Figure IV.01b) and the entire starting acetate concentration provided by the TAP-S medium of 950 $mg \cdot l^{-1}$ was used up (Figure IV.01d). 155 hours from the start of the experiment, the *C. reinhardtii* culture was depleted, the sulphate and acetate had run out, the H_2 production had become negligible and clusters of dead algal cells were observed accumulating at the bottom of the reactor, indicating that it was the right time to attempt sulphur re-addition by dilution. A 20% v/v dilution was initiated at 155 hours, supplying the depleted algal culture with 7.2 $mg \cdot l^{-1}$ of sulphate (Figure IV.01c) and 540 $mg \cdot l^{-1}$ of acetate (Figure IV.01d). Although the OD initially decreased from 23.3 $mg \cdot l^{-1}$Chl to 17.5 $mg \cdot l^{-1}$Chl as a result of the actual dilution, the algal culture proceeded to recover to an OD of 25.0 $mg \cdot l^{-1}$Chl within 24 hours (Figure IV.01b). While this OD was an improvement on the OD of the depleted algal culture prior to dilution, it was nevertheless significantly lower than the starting OD of 30 $mg \cdot l^{-1}$Chl. Following this 24 hour recovery period, all the sulphate and acetate in the replenished growth medium were used up (Figure IV.01c-d). During the recovery period, the rate of photosynthesis did not increase sufficiently to raise the pO_2 of the culture above zero (Figure IV. 01d). As a result, the culture entered a secondary H_2 production stage at 179 hours, immediately after the re-inserted sulphur was used up, without needing to undergo an O_2 consumption stage. The secondary H_2 production stage lasted for 30 hours and a maximum H_2 production rate of 0.20 $mlH_2 \cdot l^{-1} \cdot h^{-1}$ was measured. During this secondary H_2 production stage, the algal OD reduced from 25.0 $mg \cdot l^{-1}$Chl to 20.8 $mg \cdot l^{-1}$Chl (Figure IV.01b). Given that the maximum H_2 production rate following 20% v/v dilution with TAP_{12} was almost 6 times lower than the original maximum H_2 production rate, it was concluded that the 20% dilution did not provide sufficient nutrients or time to allow an adequate recovery of the depleted *C. reinhardtii* culture. The most likely explanation of this result is that only a small fraction of the *C. reinhardtii* culture was successfully re-activated by the 20% dilution. Only the re-activated algal cells were able to recover and subsequently engage in H_2 production. The remainder of the culture remained sulphur-deplete and inactive. A larger dilution was required to encourage a more substantial secondary H_2 production cycle.

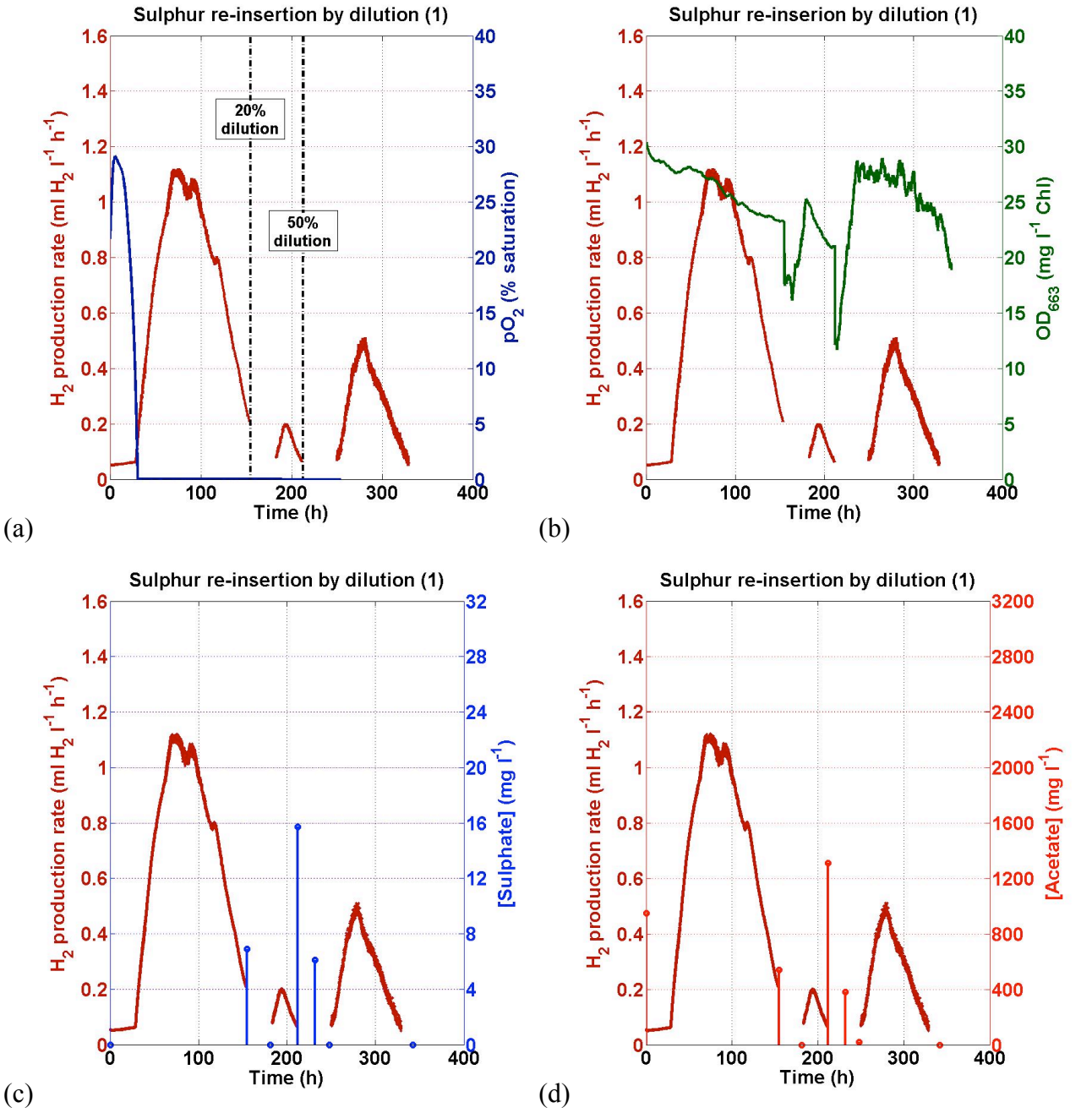


Figure IV.01: H_2 production by *C. reinhardtii* cc124 in the ICL flat-plate PBR following sulphur re-insertion by dilution, 20% and 50% dilutions

(a) H_2 production and pO_2 against time

(b) H_2 production and OD_{663} against time

(c) H_2 production and sulphate consumption against time

(d) H_2 production and acetate consumption against time

Following 209 hours of experiment, a second dilution of 50% v/v was attempted (Figure IV.01). The 50% dilution initially reduced the OD from 20.8 $mg \cdot l^{-1}$Chl to 11.8 $mg \cdot l^{-1}$Chl, while supplying an additional 16.0 $mg \cdot l^{-1}$ of sulphate and 1,320 $mg \cdot l^{-1}$ of acetate. The recovery period lasted for 40 hours. In this time, the algal OD increased from 11.8 $mg \cdot l^{-1}$Chl to 29.1 $mg \cdot l^{-1}$Chl, the entire nutrient supply was used up, and the pO_2 surprisingly remained at zero. The *C. reinhardtii* culture immediately entered a third H_2 production period, which lasted for 83 hours. Although the culture cell density had recovered to a value close to that of the initial OD, the maximum H_2 production rate following 50% dilution was a disappointing 0.53 $mlH_2 \cdot l^{-1} \cdot h^{-1}$, higher than the 0.20 $mlH_2 \cdot l^{-1} \cdot h^{-1}$ production rate following 20% dilution, but about half the initial 1.12 $mlH_2 \cdot l^{-1} \cdot h^{-1}$ production rate. Once again, the conclusion was that the 50% dilution did not provide sufficient time for full metabolic recovery of the *C. reinhardtii* cells. This result is consistent with the hypothesis that only a fraction of algal cells have been successfully re-activated by dilution. The 50% dilution appears to have re-activated approximately half of the algal culture, resulting in a halved H_2 production rate compared to the primary H_2 production stage. At this time, 332 hours from the start of the sulphur dilution experiment, the accumulation of dead algal cells had formed a thick layer of material near the bottom of the PBR that was beginning to obstruct the reactor mixing system. Although it provided an excellent environment for biohydrogen production and detection, the ICL flat-plate PBR proved to be limited in its ability to facilitate long-term H_2 production using multiple sulphur dilution procedures. Better drainage and dead cell separation capability will be required for future scaled-up PBR design.

A second experiment was started with the intention of investigating the effects of a 95% v/v dilution with TAP_{12} (Figure IV.02). The initial H_2 production phase was once again initiated by centrifugation. The pO_2 dropped to zero after 18 hours, resulting in anaerobic H_2 production with a maximum H_2 production rate of 1.03 $mlH_2 \cdot l^{-1} \cdot h^{-1}$ (Figure IV.02a). This H_2 production stage lasted over a period of 132 hours; the OD reduced from 28.1 $mg \cdot l^{-1}$Chl to 21.5 $mg \cdot l^{-1}$Chl during this time (Figure IV.02b). Following 150 hours of experiment, the depleted *C. reinhardtii* culture was diluted with 95% TAP_{12}. This dilution reduced the OD from 21.5 $mg \cdot l^{-1}$Chl to 6.1 $mg \cdot l^{-1}$Chl, but it supplied the cells with 29.0 $mg \cdot l^{-1}$ of sulphate (Figure IV.02c) and 3,130 $mg \cdot l^{-1}$ of acetate (Figure IV.02d). The OD did not reduce to 5% of the initial value as expected by this dilution due to imperfections in the flat-plate PBR drainage system. Some living *C. reinhardtii* cells remained clustered on the walls

and corners of the PBR during the dilution and were subsequently re-suspended in the fresh medium. The true value of the dilution was therefore lower than 95% and difficult to quantify accurately. This observation does not affect the conclusions drawn in this chapter. During the cell recovery stage, which lasted for 80 hours, the entire nutrient supply was consumed and the algal OD eventually increased to 31.2 $mg \cdot l^{-1}$Chl, higher than the original OD following centrifugation (Figure IV.02b). The pO_2 remained at zero throughout the recovery period (Figure IV.02a). Following the consumption of sulphur, the algae immediately entered a secondary H_2 production period with a maximum H_2 production rate of 1.13 $ml H_2 \cdot l^{-1} \cdot h^{-1}$ and a duration of 145 hours. The OD decreased from 31.2 $mg \cdot l^{-1}$Chl to 23.1 $mg \cdot l^{-1}$Chl in this time. The 95% dilution proved to be an effective way of inducing a secondary H_2 production period. This was not a surprising result because a 95% dilution is not dissimilar to starting a fresh experiment. The main difference is that a 95% dilution allows prolonged cyclic H_2 production within a single PBR without the need to completely empty and clean it. The lack of a pO_2 recovery also decreases the amount of time required to initiate the secondary H_2 production stage because it eliminates a time-consuming O_2 consumption stage. The secondary H_2 production stage of the experiment in Figure IV.02 was superior to the primary H_2 production stage because there was a higher initial algal cell density. This occurred because the secondary H_2 production stage was initiated by nutrient control rather than centrifugation, so that no algal cells were lost during centrifugation.

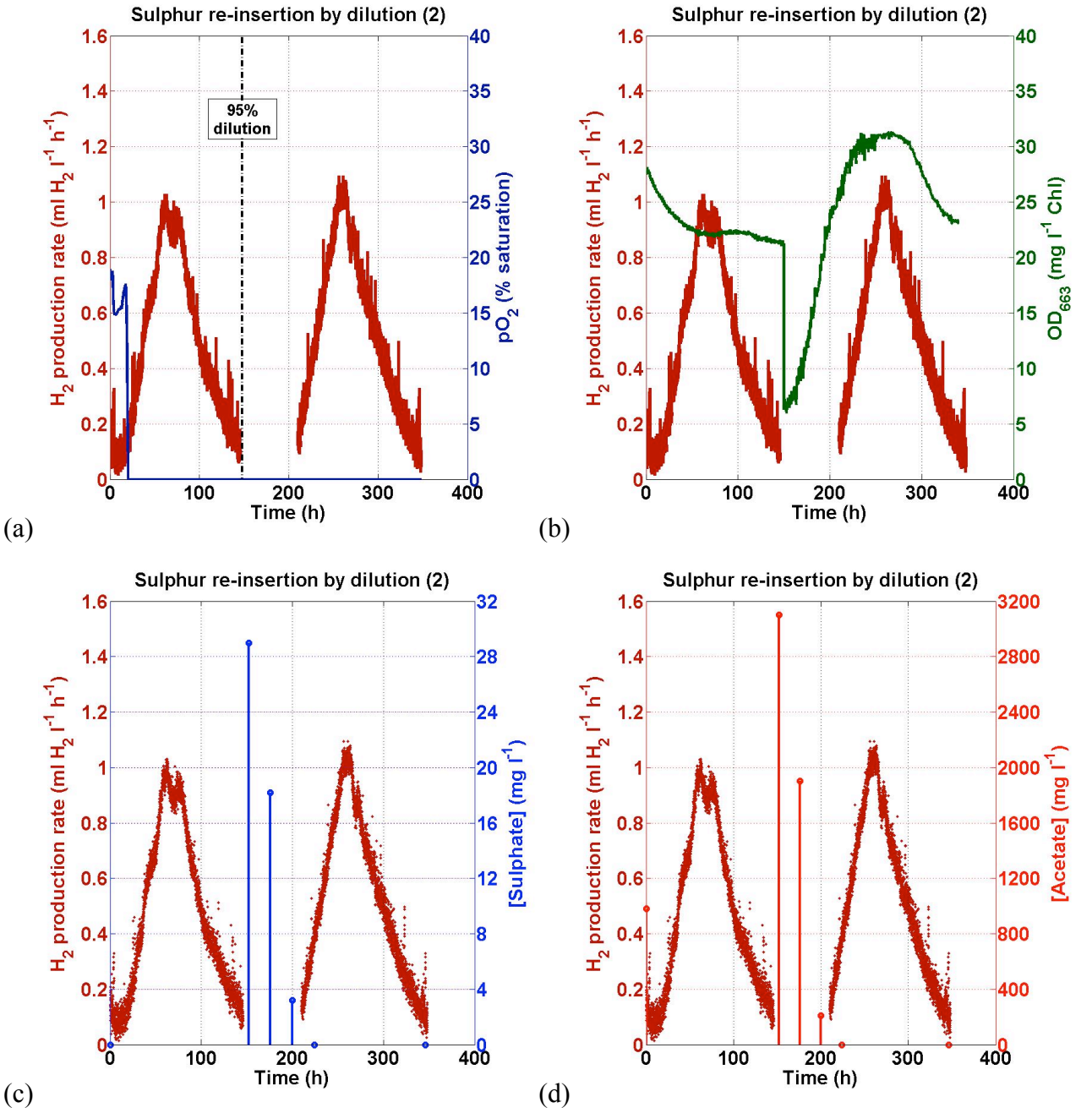


Figure IV.02: H_2 production by *C. reinhardtii* cc124 in the ICL flat-plate PBR following sulphur re-insertion by dilution, 95% dilution

(a) H_2 production and pO_2 against time

(b) H_2 production and OD_{663} against time

(c) H_2 production and sulphate concentration against time

(d) H_2 production and acetate concentration against time

IV.2.2. Process Scale-up by Sulphur Dilution

A paper exercise was conducted to determine the scale-up consequences of the data obtained in the laboratory-scale flat-plate PBR. It is clear from the experimental results that a 95% v/v dilution in TAP_{12} is the most effective way of encouraging an additional H_2 production stage. However, it is not immediately obvious just how much better a 95% dilution is than, for example, a 50% dilution. Also, the maximum H_2 production rate is not in itself sufficient to define the performance of this system. Sulphur re-addition by dilution creates a complex and interdependent system of cyclic H_2 production, algal biomass synthesis and consumption, and sulphate and acetate consumption. In order to investigate all of these parameters and their implications for the scale-up of H_2 production by sulphur dilution, four variables were defined: the cumulative H_2 yield, the dry biomass synthesis, the cumulative sulphate consumption and the cumulative acetate consumption (Figure IV.03). The cumulative H_2 yield is a calculation of the combined H_2 yield from all the individual H_2 production stages. Similarly, the cumulative sulphate and acetate consumptions define the total combined sulphate and acetate consumption respectively, following multiple dilutions with TAP_{12}. The dry biomass yield defines the amount of biomass that may be harvested from the fraction of algal culture that is drained out of the PBR during the dilution procedure. Additional biomass is first synthesised during the algal recovery stage before some of it is consumed by catabolic processes during the H_2 production stage. Since a cumulative chlorophyll concentration does not make practical sense, biomass synthesis is defined in units of dry biomass instead. The unit conversion from chlorophyll concentration to dry biomass is based on the recent experiments carried out by Torri and colleagues on *C. reinhardtii* WT cc124 and it is given in Equation IV.01 (Torri *et al*., 2011).

$$1\ g \cdot l^{-1}\ of\ dry\ biomass = 17\ mg \cdot l^{-1} Chl \qquad \textit{Equation IV.01}$$

These four variables were calculated over a time period of 1,000 hours (circa 6 weeks) by extrapolating the experimental sulphur dilution results over this time frame. In reality, the progressive accumulation of dead algal cells, contaminants and other debris would ensure that the actual continuous H_2 yield and dry biomass synthesis would be lower than those described in Figure

IV.03. Figure IV.03 is therefore a description of the maximum potential to produce H_2 and biomass while consuming nutrients over a period of 6 weeks by the sulphur dilution procedure.

Figure IV.03a shows the extrapolated cumulative H_2 production under the three different sulphur dilutions investigated experimentally: 20%, 50% and 95%. The cyclic peaks and troughs identify the H_2 production and recovery stages respectively. The 20% dilution has the potential to produce 67 $mlH_2 \cdot l^{-1}$ over 1,000 hours, the 50% dilution has the potential to produce 160 $mlH_2 \cdot l^{-1}$, and the 95% dilution could produce as much as 400 $mlH_2 \cdot l^{-1}$ (Figure IV.03a). As well as producing by far the largest volume of H_2, the 95% dilution only requires 5 cycles over a period of six weeks, which makes it easier to control and automate in a scaled-up application. The 95% dilution also synthesises the most dry biomass, namely 6.0 $g \cdot l^{-1}$ dry biomass, compared with approximately 3.8 $g \cdot l^{-1}$ dry biomass synthesised by both the 20% and 50% dilutions (Figure IV.03b). Unlike H_2 production, which is determined by the amount of time the *C. reinhardtii* cells are given to recover following a complete H_2 production stage, the biomass synthesis is a direct function of the corresponding nutrient consumption (Figure IV.03c-d). Regardless of the sulphur dilution percentage, one gram of dry biomass is synthesised for approximately every 30 mg of sulphate and every 3,000 mg of acetate supplied in the growth medium. While the sulphate consumption is defined by the nutrient control procedure and is therefore inflexible, there is the potential to improve biomass synthesis by supplementing (Figure II.11) or replacing (Figure II.12) acetate with a source of concentrated CO_2. The main lesson learned for biohydrogen production scale-up is that a 95% v/v dilution is an effective way of achieving cyclic H_2 production by sulphur dilution, resulting in an average H_2 production rate of 0.4 $mlH_2 \cdot l^{-1} \cdot h^{-1}$. This average H_2 production rate was obtained by dividing the overall H_2 yield (400 $mlH_2 \cdot l^{-1}$) by the 1,000 hour time period required to obtain it. The instantaneous H_2 production rate is in fact as high as 1.13 $mlH_2 \cdot l^{-1} \cdot h^{-1}$ during the H_2 production maximum, and 0 $mlH_2 \cdot l^{-1} \cdot h^{-1}$ during the *C. reinhardtii* growth and recovery stages. However, this H_2 production is cyclic rather than continuous, suggesting that a semi-continuous system consisting of a group of PBRs operating in a cyclic manner may be a good solution for large-scale H_2 production.

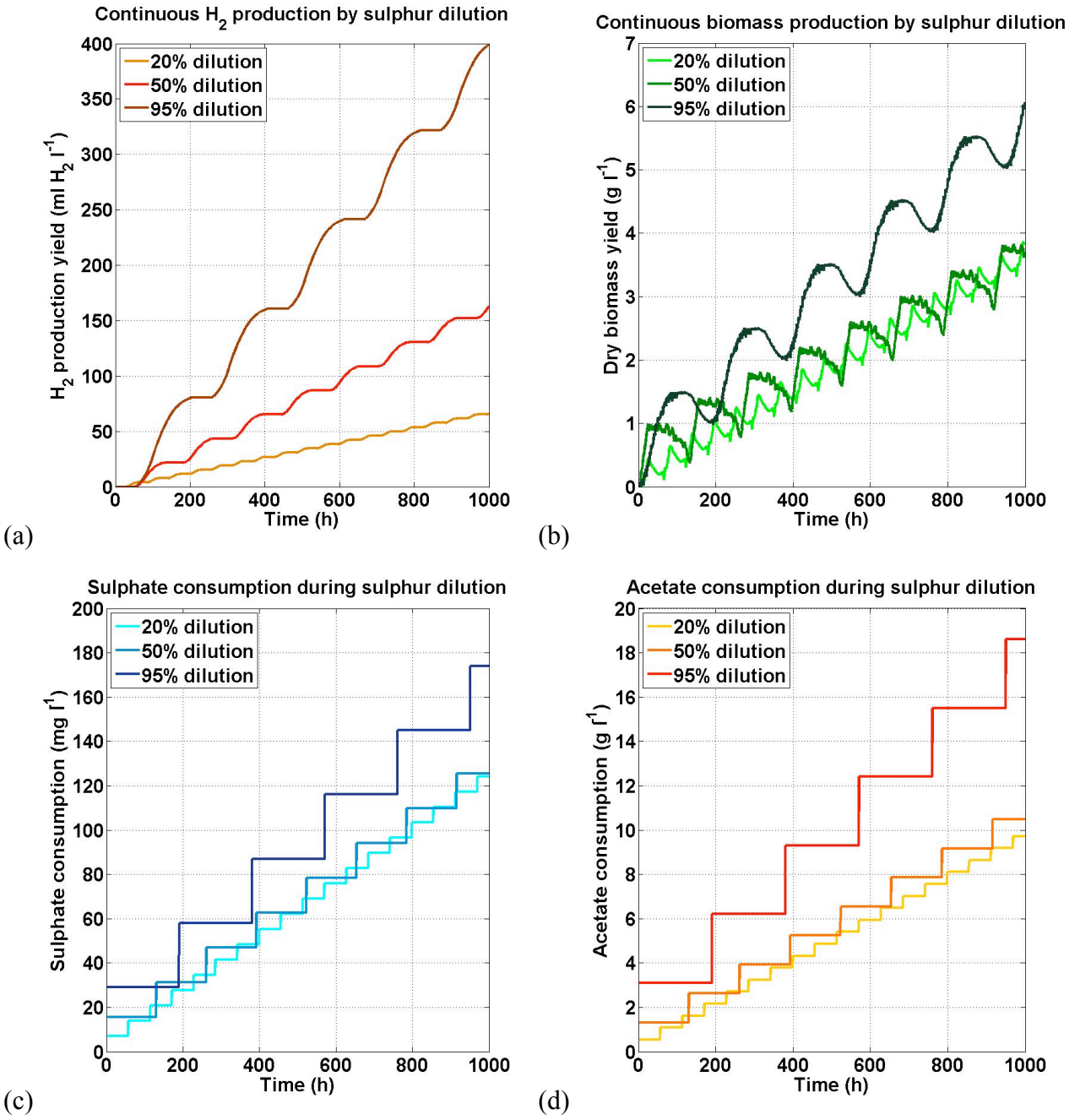


Figure IV.03: Sulphur-re insertion by dilution (20%, 50% and 95%) results extrapolated over a period of 1,000 hours (circa 6 weeks)

(a) Continuous H_2 production

(b) Continuous biomass production

(c) Sulphate consumption

(d) Acetate consumption

One possible design of a scaled-up continuous batch biohydrogen production application is shown in Figure IV.04. This conceptual design is the current best suggestion of what a near-continuous large scale process might look like based on the findings of the small scale research conducted in this thesis. The application consists of several PBRs, each facilitating cyclic H_2 production and algal recovery by sulphur dilution; there is also a time lag between the PBRs, so that the algal culture in each reactor is at a different stage of the cyclic sulphur dilution process. Figure IV.04 illustrates this concept using three PBRs. In the first reactor (R1), fresh nutrients have been delivered to a depleted *C. reinhardtii* culture via valve V1 and the algal recovery process is about to begin. In R2, the algal culture has grown to its final OD, the nutrients have been consumed and H_2 production is about to commence. Finally, in R3, H_2 production has been completed and algal biomass is about to be harvested via valve V6. Given a sufficiently large number of reactors, it is possible to achieve continuous biomass and H_2 production using this system. A gravity-assisted flow system is used for biomass harvesting (green arrows) and nutrient delivery (blue arrows). Algal biomass flows down into a cross-flow micro-filter (Rossignol *et al*., 1999), which separates the usable solid mass from the recyclable liquid growth medium. A nutrient concentration detector measures the nutrient composition of the recycled growth medium, which is enhanced using fresh nutrients delivered by a dosing pump. The nutrient feed is raised above the PBR level by means of an energy-efficient Archimedes screw (Sheehan *et al*., 1998); the nutrient feed then flows down into the appropriate PBRs. The gas flow system has been labeled with red arrows. Pre-processed flue gas, the waste gas output of a fossil fuel power station, delivers concentrated CO_2 and mixing to all the PBRs, while also picking up any H_2 that has been produced. The H_2 product is separated using a H_2-permeable membrane and the majority of the CO_2 is sequestered by the growing algal culture. The system described in Figure IV.04 therefore provides H_2 production and extraction, solid biomass production and extraction, nutrient control and recycling, and temporary CO_2 sequestration.

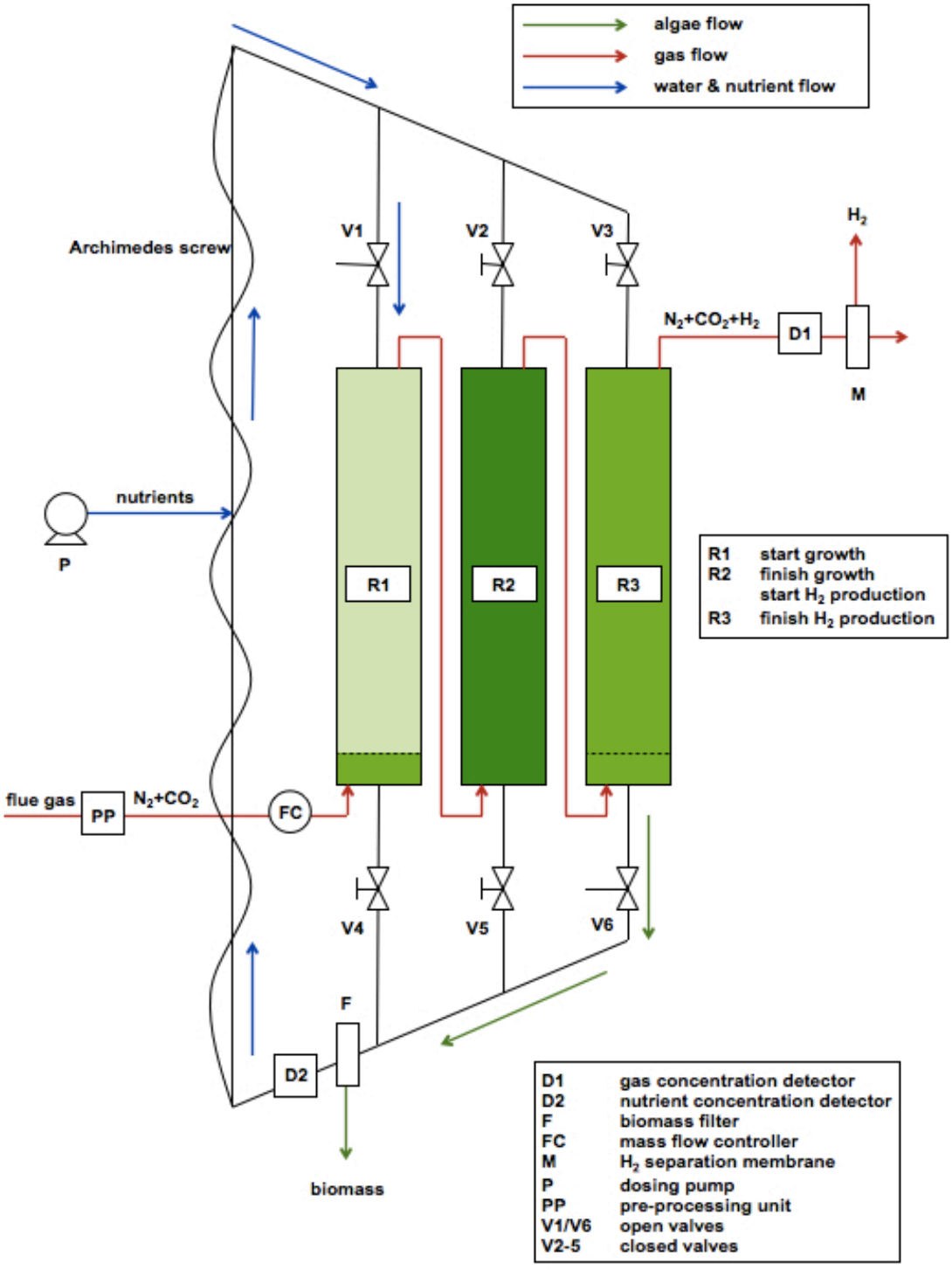


Figure IV.04: Proposed PBR design for green algal H_2 production scale-up

IV.3. Sulphur Feed

IV.3.1. Sulphur Feed Experiments

The aim of the sulphur feed experiments was to achieve continuous H_2 production by *C. reinhardtii*, as opposed to the cyclic H_2 production already achieved by sulphur dilution. The sulphur feed experiments were carried out using *C. reinhardtii* WT cc124 in the ICL flat-plate PBR at a constant temperature of 25°C and a light intensity of 12 $W \cdot m^{-2}$. Different concentrations of the sulphur-feed medium (Table 5.11) were used to attempt micromolar sulphur re-addition during the algal H_2 production stage. The sulphur-feed medium supplied sulphate and acetate at a 1:10 ratio and contained HEPES buffer, which minimised pH variations created by the acidic nature of the sulphur feed (Mussgnug *et al*., 2007). On-line *in situ* H_2 production was measured continuously by MIMS. This ensured that any variations in the H_2 production rate resulting from the sulphur feed were immediately and accurately measured. Sulphate and acetate concentrations were subsequently measured by IC and HPLC respectively. Algal culture OD was measured using the ICL flat-plate PBR photodiode and expressed in units of chlorophyll concentration. Since the OD during the H_2 production stage proved difficult to control experimentally, H_2 production rates were expressed per unit of OD according to the technique introduced by Zhang & Melis (Zhang & Melis, 2002). This technique normalises the H_2 production rate with respect to the quantity of PSII reaction centres available in a given volume and therefore facilitates a systematic comparison between the results of different sulphur feed experiments. Extended H_2 production using a micromolar sulphur feed has been attempted previously by Oncel & Vardar Sukan with limited success (Oncel & Vardar Sukan, 2009).

The sulphur-feed medium contains 1,000 $mg \cdot l^{-1}$ (1 $mg \cdot ml^{-1}$) of sulphate. This sulphur supply was dripped into the 1 litre working volume of the ICL flat-plate PBR with the aid of a dosing pump at four different delivery rates: 5 $ml \cdot day^{-1}$, 10 $ml \cdot day^{-1}$, 15 $ml \cdot day^{-1}$ and 20 $ml \cdot day^{-1}$. The 5 $ml \cdot day^{-1}$ delivery rate is equivalent to a delivery rate of 0.21 $ml \cdot h^{-1}$, or 0.21 $mg \cdot l^{-1} \cdot h^{-1}$ in terms of the concentration of sulphate delivered. The four delivery rates therefore supplied the depleted *C. reinhardtii* culture with 0.21 $mg \cdot l^{-1} \cdot h^{-1}$, 0.42 $mg \cdot l^{-1} \cdot h^{-1}$, 0.63 $mg \cdot l^{-1} \cdot h^{-1}$ and 0.84 $mg \cdot l^{-1} \cdot h^{-1}$ of sulphate respectively. The effect of this sulphur feed on the H_2 production by *C. reinhardtii* is

shown in Figure IV.05. The vertical dotted line identifies the time when the sulphur feed was initiated. The sulphur feed was applied towards the beginning of the H_2 production stage, at a point when the H_2 production rate was still increasing. This timing was chosen in order to maximise the observability of any negative effect of the sulphur feed on the algal H_2 production rate. Chronologically, the first experiment was carried out using the 0.84 $mg \cdot l^{-1} \cdot h^{-1}$ sulphate feed (Figure IV.05g-h). Within the first 8 hours following the introduction of the sulphur feed, the H_2 production rate stabilised at a value of circa 17.9 $(\mu lH_2 \cdot l^{-1} \cdot h^{-1})/(mg \cdot l^{-1}Chl)$ before rapidly decreasing to an inconsequential 3.3 $(\mu lH_2 \cdot l^{-1} \cdot h^{-1})/(mg \cdot l^{-1}Chl)$. Following this collapse of the H_2 production rate, a significant accumulation of both sulphate and acetate was detected in the algal growth medium. The sulphate concentration had increased to 3.9 $mg \cdot l^{-1}$; with a sulphate concentration of 2.0 $mg \cdot l^{-1}$ being considered as the upper limit of sulphur tolerance during anaerobic H_2 production by *C. reinhardtii* (Kim *et al*., 2010). It is believed that a sulphate concentration exceeding this limit significantly increases photosynthetic O_2 production and deactivates the $h_2$ase enzyme. At the same time, the acetate concentration increased to 140 $mg \cdot l^{-1}$, which is more than sufficient for algal cell recovery. The conclusion from this initial experiment was that a sulphur feed of 0.84 $mg \cdot l^{-1} \cdot h^{-1}$ was too high to permit prolonged H_2 production, and the sulphur feed rate was decreased in subsequent experiments.

Although the sulphur feed rate was eventually reduced all the way to 0.21 $mg \cdot l^{-1} \cdot h^{-1}$, the overarching result of all four sulphur feed experiments remained the same. In all four cases, the H_2 production stabilised for a brief period of time before rapidly decreasing to negligible levels. At the same time as the H_2 production decreased, the concentration of sulphate in the growth medium increased. At a sulphur feed of 0.63 $mg \cdot l^{-1} \cdot h^{-1}$, the final sulphate concentration was 2.2 $mg \cdot l^{-1}$ (Figure IV.05e), at 0.42 $mg \cdot l^{-1} \cdot h^{-1}$ it was 1.8 $mg \cdot l^{-1}$ (Figure IV.05c), and at 0.21 $mg \cdot l^{-1} \cdot h^{-1}$ it was 0.8 $mg \cdot l^{-1}$ (Figure IV.05a). These relatively low final sulphate concentrations would appear to imply that the *C. reinhardtii* H_2 production metabolism responds to the presence of sulphur itself as opposed to any increase in the PSII activity. If this hypothesis is correct, it would signify bad news for the prospect of continuous H_2 production using any type of sulphur feed.

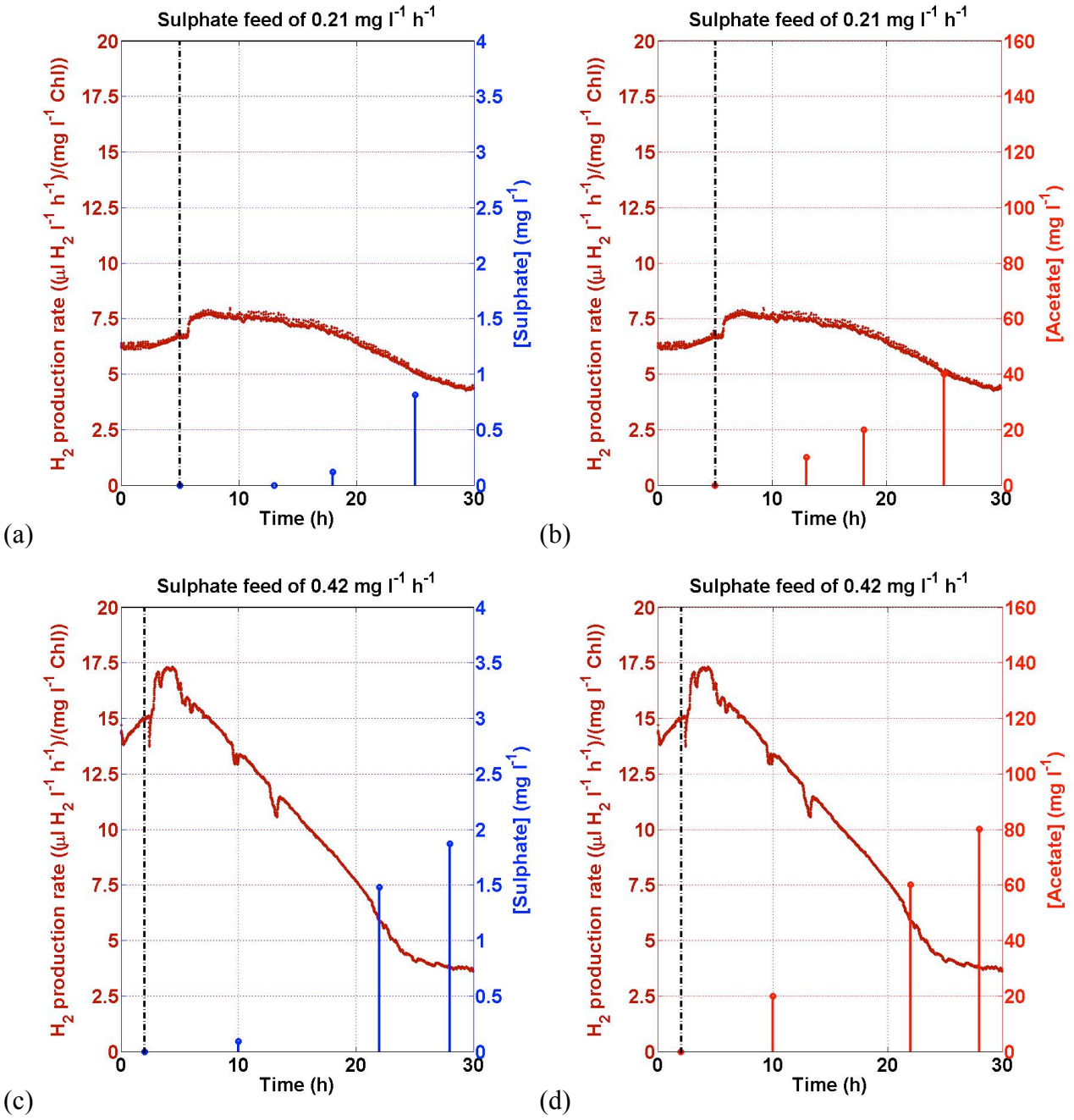


Figure IV.05a-d: Effect of sulphate feed on H_2 production by *C. reinhardtii* cc124 in the ICL flat-plate PBR

(a) H_2 production and sulphate consumption at a feed of 0.21 mg l^{-1} h^{-1}

(b) H_2 production and acetate consumption at a feed of 0.21 mg l^{-1} h^{-1}

(c) H_2 production and sulphate consumption at a feed of 0.42 mg l^{-1} h^{-1}

(d) H_2 production and acetate consumption at a feed of 0.42 mg l^{-1} h^{-1}

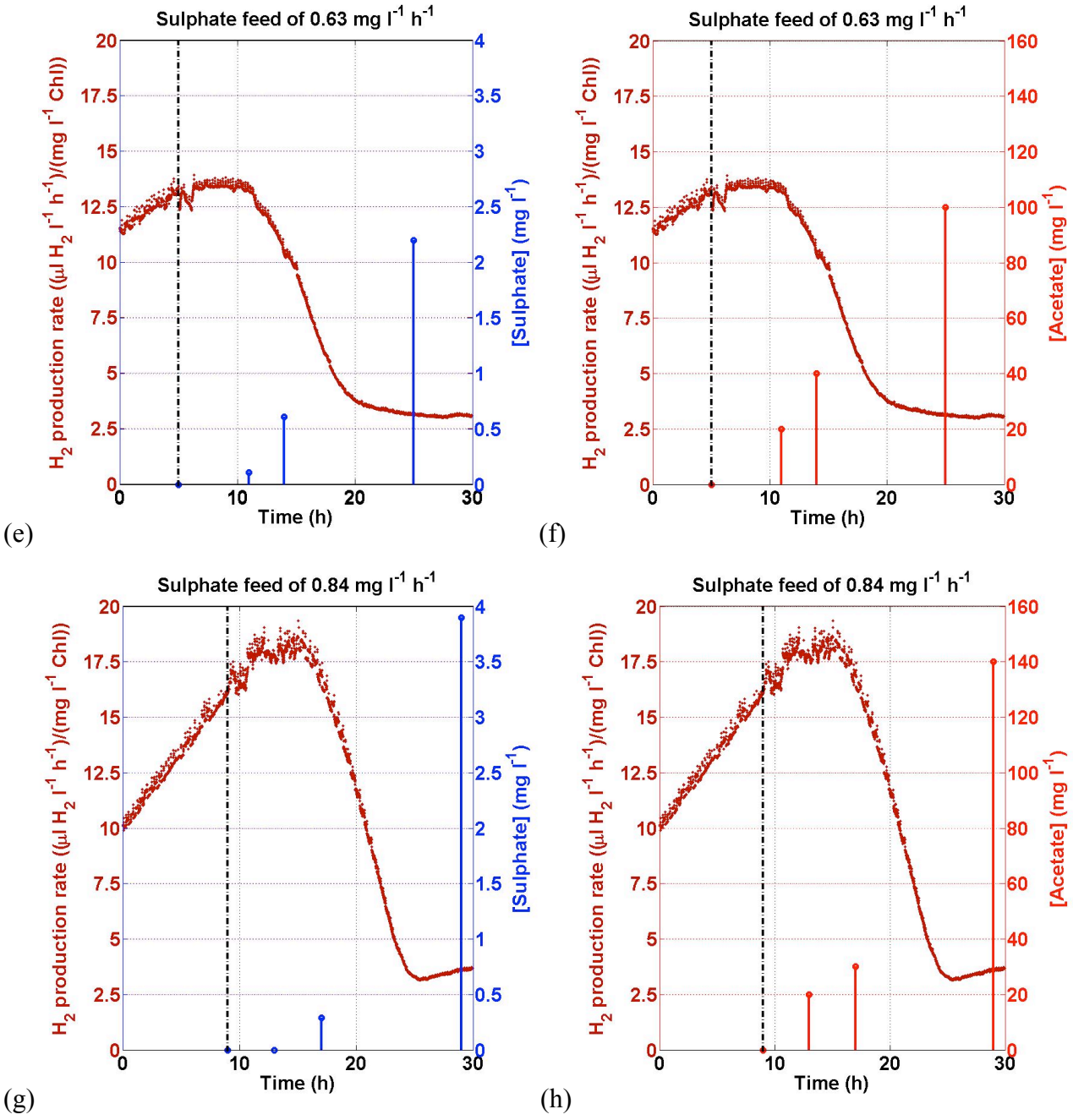


Figure IV.05e-h: Effect of sulphate feed on H_2 production by *C. reinhardtii* cc124 in the ICL flat-plate PBR

(e) H_2 production and sulphate consumption at a feed of 0.63 mg l^{-1} h^{-1}

(f) H_2 production and acetate consumption at a feed of 0.63 mg l^{-1} h^{-1}

(g) H_2 production and sulphate consumption at a feed of 0.84 mg l^{-1} h^{-1}

(h) H_2 production and acetate consumption at a feed of 0.84 mg l^{-1} h^{-1}

IV.3.2. Prospects for Continuous H_2 Production by Sulphur Feed

Upon closer examination of the sulphur feed data (Figure IV.05), one piece of good news does emerge: the decrease in the H_2 production rate as a result of the sulphur feed is well-defined and linear in all the experiments. As a result, it was possible to define the variable ΔH to represent this linear change in the H_2 production rate (since the H_2 production rate decreases, ΔH is negative). Figure IV.06 shows the application of a linear fit to the decrease in H_2 production rate for all four sulphur feed experiments. Not surprisingly, the absolute value of ΔH decreases with a decrease in the sulphur feed rate, from 1.84 $(\mu lH_2 \cdot l^{-1} \cdot h^{-2})/(mg \cdot l^{-1}Chl)$ at a sulphur feed rate of 0.84 $mg \cdot l^{-1} \cdot h^{-1}$, to 0.24 $(\mu lH_2 \cdot l^{-1} \cdot h^{-2})/(mg \cdot l^{-1}Chl)$ at 0.21 $mg \cdot l^{-1} \cdot h^{-1}$. The next step was to express ΔH as a function of the sulphur feed rate (Figure IV.07). In order for continuous H_2 production by sulphur feed to be successful, the curve describing ΔH as a function of sulphur feed would need to cross the ΔH=0 axis. At this point,, the sulphur feed would be sufficiently low to allow *C. reinhardtii* cell recovery without adversely affecting the H_2 production rate. In reality, the relationship between ΔH and sulphur feed rate is best described by a curved interpolant function, which passes through the origin (Figure IV.07). The fact that the interpolant passes though the origin implies that the only way not to decrease anaerobic H_2 production by *C. reinhardtii* is to provide no sulphur feed whatsoever. This outcome may be disappointing, but it is the most realistic interpretation of the sulphur feed experimental data. It is also consistent with the sulphur dilution results, in the sense that it confirms that *C. reinhardtii* cultures require a long time frame to become re-activated by sulphur re-insertion following a period of sulphur depletion.

It is important to note that these results do not completely rule out the possibility of achieving continuous biohydrogen production using a sulphur feed. A number of relevant parameters were not sufficiently investigated during these sulphur feed experiments. For example, it is possible that the decrease in H_2 production is a function of the sulphate:acetate ratio or of the HEPES concentration in the sulphur-feed medium. A more favourable result could possibly have been achieved by applying the sulphur feed towards the end of the H_2 production phase, once the algal culture was fully depleted and the H_2 production rate was already decreasing naturally. The rationale for this is that the *C. reinhardtii* culture would have remained sulphur deplete for a longer period of time, and would therefore be more sulphur-hungry, increasing the possibility that it would tolerate a low

sulphur feed. One promising observation, which indicates the potential viability of the sulphur feed technique, is that the H_2 production rate initially plateaus once the sulphur feed is applied, before decreasing linearly. This plateau was maintained for a period of approximately 10 hours in the case of the 0.21 $mg \cdot l^{-1} \cdot h^{-1}$ sulphur feed rate. It is possible that even lower sulphur feed rates could result in an even longer plateau and therefore significantly increase the H_2 production duration. Additional sulphur feed experiments would supplement and enhance the results obtained in this thesis, and provide a more complete understanding of the prospects for continuous H_2 production by sulphur feed.

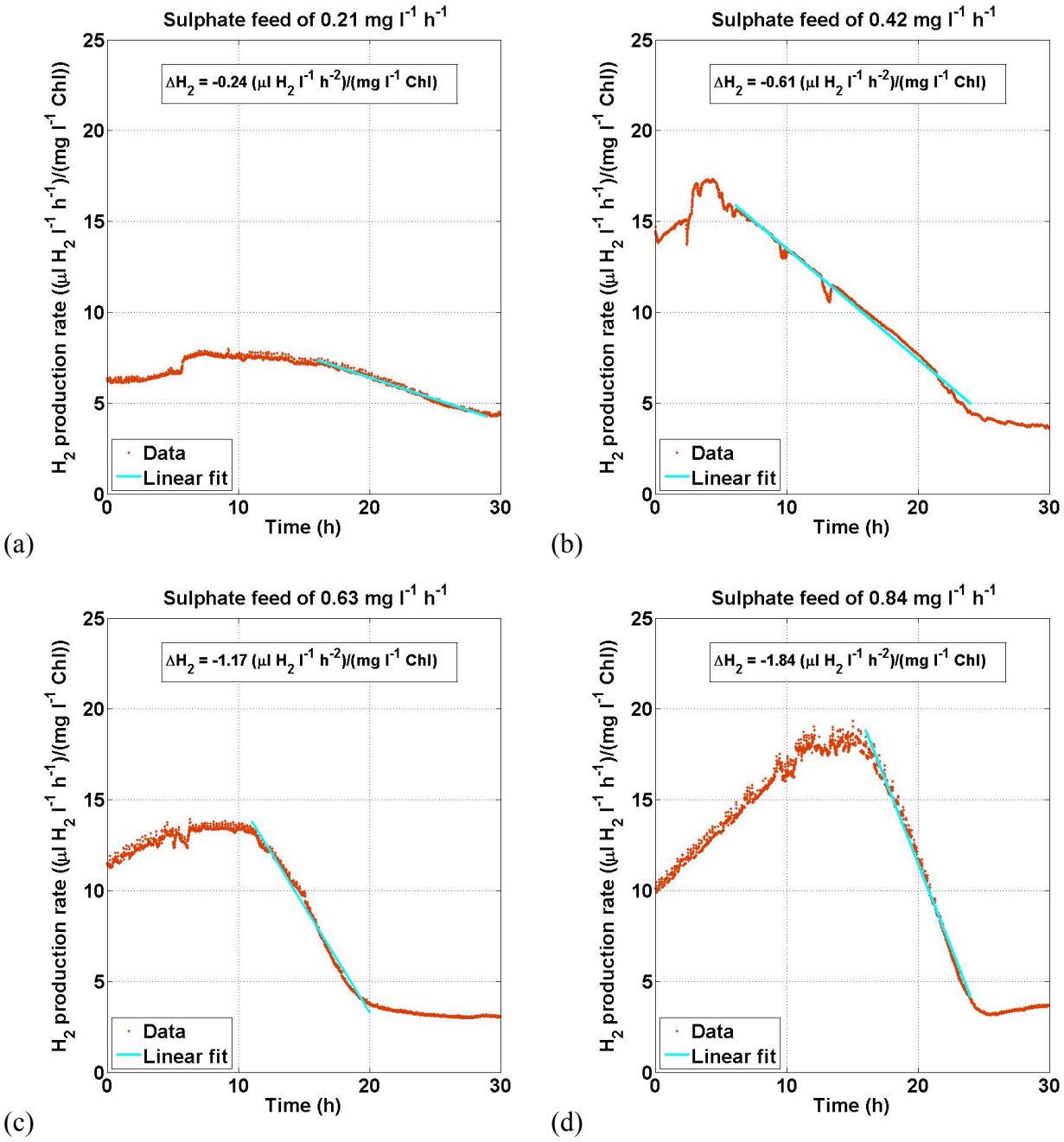


Figure IV.06: Assigning a linear fit to the reduction in H_2 production (ΔH_2) associated with the introduction of a sulphate feed

(a) ΔH_2 for a sulphur feed of 0.21 mg l^{-1} h^{-1}

(b) ΔH_2 for a sulphur feed of 0.42 mg l^{-1} h^{-1}

(c) ΔH_2 for a sulphur feed of 0.63 mg l^{-1} h^{-1}

(d) ΔH_2 for a sulphur feed of 0.84 mg l^{-1} h^{-1}

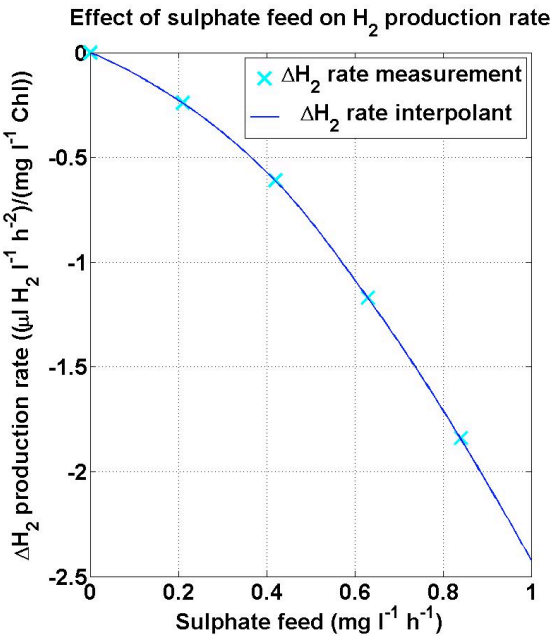


Figure IV.07: Relationship between the sulphate feed and the corresponding change in the H_2 production rate

IV.4. Summary

Extended H_2 production by sulphur re-addition was attempted using both sulphur dilution and sulphur feed techniques. Sulphur dilution with the TAP_{12} medium proved effective at encouraging cyclic H_2 production; it lead to alternating *C. reinhardtii* cell recovery and H_2 production stages. A 95% v/v dilution gave the best H_2 production results, with a maximum H_2 production rate of 1.13 $mlH_2 \cdot l^{-1} \cdot h^{-1}$ during the secondary H_2 production stage. The experimental results were extrapolated in order to understand the long-term implication of sulphur dilution. The important parameters turned out to be not only the H_2 production rate, but also the rates of biomass synthesis and consumption, as well as the nutrient consumption during the algal recovery stage. It was determined that a *C. reinhardtii* culture could produce H_2 at an average rate as high as 0.4 $mlH_2 \cdot l^{-1} \cdot h^{-1}$ under a series of consecutive 95% dilutions. The corresponding average dry biomass synthesis rate would be 6.0 $mg \cdot l^{-1} \cdot h^{-1}$. Although this dry biomass could serve as a useful by-product of biohydrogen production, the biomass synthesis does strongly depend on the sulphate and acetate concentrations supplied to the algal culture. A continuous batch PBR, which could facilitate long-term scaled-up H_2 production by sulphur dilution, was designed.

Extended H_2 production by sulphur feed was more difficult to implement. A micromolar source of sulphur was fed into a H_2-producing *C. reinhardtii* culture with the intention of initiating algal cell recovery without affecting the H_2 production rate. Although low sulphate feed rates of 0.21-0.84 $mg \cdot l^{-1} \cdot h^{-1}$ were attempted, all sulphur experiments resulted in a rapid decrease of the H_2 production rate. Since this decrease was linear, it was possible to quantify it in terms of a single variable, ΔH. ΔH was expressed as a function of the sulphur feed rate, resulting in a non-linear regression curve that passed through the origin. This implied that the only way not to reduce H_2 production with a sulphur feed is to feed no sulphur at all. The sulphur feed results suggest that algal H_2 production decreases as a direct response to the sulphur as opposed to a response to increased O_2 production by PSII. Additional sulphur feed experiments would be required to either prove this hypothesis, or to determine a way of achieving continuous H_2 production by sulphur feed.

7. Conclusion and Future Work

7.1. Conclusion

The aim of this thesis was to measure the growth and H_2 production kinetics of the green alga *C. reinhardtii* in order to develop a continuous, practical and scaleable biophotolytic H_2 production process. This aim was realised by addressing four key objectives: the design of a novel flat-plate PBR to facilitate green algal H_2 production (Chapter I), the measurement of *C. reinhardtii* growth kinetics (Chapter II), the development of a nutrient control technique to enable spontaneous H_2 production (Chapter III), and the development of a sulphur re-addition technique to extend the H_2 production process lifetime (Chapter IV).

Overall, the thesis aim and objectives were successfully accomplished. *C. reinhardtii* growth was measured under different light intensities, light regimes, phototrophic conditions and temperatures. Techniques for measuring the corresponding acetate and sulphate uptake were developed and used to optimise the nutrient concentrations in the algal growth medium. A Membrane Inlet Mass Spectrometry system was developed to measure H_2 production continuously, accurately and *in situ*. The practical measurement techniques and methodologies developed during this thesis may be used in the future to investigate the growth and H_2 production of various algal strains, in many different PBRs, and under different environmental conditions. In particular the novel ICL flat-plate PBR proved effective at facilitating *C. reinhardtii* growth and H_2 production at the laboratory scale. It enabled the development of a novel nutrient control technique that results in spontaneous H_2 production following algal growth, achieving the objective for a continuous growth and H_2 production cycle within a single PBR. H_2 production by nutrient control was not only more practical and scaleable than the alternative centrifugation and dilution processes, it also led to superior H_2 production rates and yields. The dilution technique of sulphur re-addition was used to develop a cyclic growth and H_2 production process. If operated as a semi-continuous system, this process would result in continuous H_2 and biomass production over a long time scale and could potentially be scaled up to pilot plant volume.

Objective I: Design novel flat-plate PBR (Chapter I)

A novel flat-plate PBR that facilitates algal growth and biophotolytic H_2 production at the laboratory scale was designed, constructed and commissioned (Tamburic *et al*., 2011b). This reactor featured an innovative dual-compartment design, where the primary compartment was designed to hold the *C. reinhardtii* culture and the key measuring instruments, while the secondary compartment was used to control the temperature and illumination conditions. Important environmental parameters, such as the light intensity, wavelength, temperature, mixing rate and nutrient feed rate were controlled using a fully-automated system. The key parameters of the H_2 production process, including the pO_2, pH, OD, temperature and the H_2 production rate were continuously measured and recorded. A novel MIMS system enabled *in situ* H_2 measurement and provided the opportunity for selective H_2 extraction. The ICL flat-plate PBR enabled the *C. reinhardtii* growth and H_2 production experiments, providing the baseline procedure that subsequently led to the development of H_2 production by nutrient control and sulphur re-addition by dilution. Its operational flexibility ensures that it will remain a valuable tool for future H_2 production process development.

Objective II: Evaluate algal growth kinetics (Chapter II)

Some of the key parameters that affect *C. reinhardtii* growth kinetics were investigated and optimised (Tamburic *et al*., 2011a). These included the algal strain, temperature, light regime, phototrophic condition and light intensity. The cc124 WT *C. reinhardtii* strain was shown to grow effectively at a temperature of 25°C. The algal culture grew faster under continuous illumination than under 12:12 hour light:dark cycles, indicating that the cells grow better under artificial illumination in the laboratory than they would otherwise do in nature when subjected to the diurnal cycle. This effect, when considered together with the variable temperatures inherent to an outdoor PBR, indicates that laboratory growth results need to be moderated accordingly when considering growth in a scaled-up outdoor reactor. Bubbling *C. reinhardtii* cultures with CO_2, an inexpensive carbon source, was shown to improve the final OD of algal culture grown under photomixotrophic conditions, providing that the CO_2 concentration was not high enough to cause overwhelming acidification of the culture. *C. reinhardtii* were also grown under photoautotrophic conditions, and

the optimum CO_2 feed concentration was determined to be circa 11%. This is an important result because economic large scale algal growth applications would probably need to rely on photoautotrophic growth (although the addition of inexpensive organic compounds such as carbonate is also feasible). The CO_2 partial pressure in flue gas resulting from the combustion of coal in 25% humid excess air is 11.6% (Jecht, 2012), which makes it a good candidate to supply the 11% CO_2 feed required by *C. reinhardtii* to grow optimally under photoautotrophic conditions. Increasing the light intensity gradually from 15 $W \cdot m^{-2}$ up to 60 $W \cdot m^{-2}$ consistently increased the *C. reinhardtii* specific growth rate but had little effect on the final OD of the culture. Complete photosaturation of *C. reinhardtii* WT cc124 cultures is believed to occur at 273 $W \cdot m^{-2}$ and clear evidence of photoinhibition is detectible at 600 $W \cdot m^{-2}$.

Objective III: Develop nutrient control technique (Chapter III)

A highly effective nutrient control technique was developed by optimising the sulphate and acetate concentrations in the algal growth medium (Tamburic *et al*., 2012). This was achieved by accurately measuring the sulphate and acetate uptake during algal growth using IC and HPLC techniques, respectively. Nutrient consumption was determined to be a function of the light intensity. High light intensities lead to higher photosynthesis rates, increasing the turnover of the PSII repair mechanism and hence increasing the demand for sulphur. At high light intensities, additional biomass is synthesised by CO_2 fixation processes, reducing the total quantity of acetate consumed, but increasing the rate of acetate consumption. These nutrient consumption rates were also shown to exhibit a linear, statistically significant and reactor-independent relationship with the algal specific growth rate. Using this relationship, it was possible to design an optimised algal growth medium to facilitate spontaneous H_2 production under a specific set of ambient conditions in any PBR.

This nutrient control approach was compared with two other methods of H_2 production by S-deprivation under identical ambient conditions in the ICL flat-plate PBR. The dilution method of S-deprivation, using a 10% v/v dilution of algal cells in TAP-S medium, resulted in a H_2 production rate of 0.18 $mlH_2 \cdot l^{-1} \cdot h^{-1}$ and a H_2 yield of 23.6 $mlH_2 \cdot l^{-1}$. The centrifugation method was more energy intensive overall, but the higher initial algal culture OD led to an improved H_2 production rate of 1.11 $mlH_2 \cdot l^{-1} \cdot h^{-1}$ and a H_2 yield of 102.7 $mlH_2 \cdot l^{-1}$. The nutrient control method combined the

high initial OD of the centrifugation method with the spontaneous H_2 production of the dilution method. The highest recorded OD of 35.9 $mg \cdot l^{-1}$ at the beginning of the H_2 production stage resulted in a subsequent H_2 production rate of 1.52 $ml H_2 \cdot l^{-1} \cdot h^{-1}$ and a H_2 yield of 119.8 $ml H_2 \cdot l^{-1}$. The nutrient control method of S-deprivation was easy to implement and it proved superior to its counterparts based on all the relevant H_2 production criteria, indicating that it should be the method of choice for future laboratory H_2 production experiments as well as for scaled-up applications of biophotolytic H_2 production. It creates the opportunity for effective, automated and spontaneous H_2 production using a single PBR. Nevertheless, H_2 production by nutrient control is not yet the basis for a commercial process because the relative H_2 production rates remain low and the process duration is only one week.

Objective IV: Extend H_2 production by sulphur re-addition (Chapter IV)

The insufficient duration of nutrient controlled H_2 production was addressed by attempting sulphur re-addition into the algal culture medium, which had been depleted of nutrients by the requirements of *C. reinhardtii* growth and H_2 production. Extended H_2 production by sulphur re-addition was attempted using sulphur dilution and sulphur feed techniques. Sulphur dilution proved effective at encouraging cyclic H_2 production, resulting in alternating *C. reinhardtii* cell recovery and H_2 production stages. A 95% v/v dilution gave the best H_2 production results, with a maximum H_2 production rate of 1.13 $ml H_2 \cdot l^{-1} \cdot h^{-1}$ during the secondary H_2 production stage. By extrapolating experimental results, it was determined that *C. reinhardtii* cultures could produce H_2 at an average rate as high as 0.4 $ml H_2 \cdot l^{-1} \cdot h^{-1}$ under a series of consecutive 95% dilutions. The corresponding average dry biomass synthesis rate was 6.0 $mg \cdot l^{-1} \cdot h^{-1}$. Biomass is a valuable by-product of *C. reinhardtii* H_2 production but biomass synthesis depended strongly on the quantity of nutrient supplied to the algal culture. The operating conditions for a scaled-up semi-continuous PBR were suggested; this PBR would facilitate long-term H_2 and biomass production by sulphur dilution. A more practical long-term H_2 production solution for achieving continuous H_2 production was explored by applying a steady micromolar sulphur feed to a H_2-producing *C. reinhardtii* culture. Although the sulphur feed experiments carried out in this thesis led to the eventual collapse of the H_2 production rate, it is possible that improved experimental design could result in successful

continuous H_2 production by sulphur feed in the future, since all of the possible parameter space associated with sulphur feed re-activation has not yet been explored.

7.2. Future Work

7.2.1. Scale-up

The experiments carried out during this thesis have contributed significantly towards an improved understanding of the growth and H_2 production processes of the green alga *C. reinhardtii.* The nutrient control technique of H_2 production and the dilution technique of sulphur re-addition were developed with the objective of enabling more effective and scaleable biophotolytic H_2 production. The next step is to construct and commission a scaled-up PBR in order to put these techniques into practice and investigate long-term spontaneous H_2 production by *C. reinhardtii* cultures under real-world conditions. This could be achieved by pursuing the concept of cyclic *C. reinhardtii* growth and H_2 production in an outdoor semi-continuous PBR (Figure IV.04).

The individual reactor units of this continuous batch PBR could be manufactured economically from high-density polyethylene in a process similar to the manufacture of commercial plastic bags. These plastic bag PBR units should have a working volume of the order of 10-20 litres, which represents scale-up by a factor of 10 from most laboratory PBR systems; nevertheless, it remains reasonable to expect that such PBR units could be maintained by a single vigilant operator. An important recommendation is to begin with a single plastic bag unit in order to investigate its applicability to H_2 production at this scale, before expanding operations to a complete semi-continuous PBR system involving multiple plastic bag units. It is critical to investigate *C. reinhardtii* culture adaptation to the plastic bag environment as well as the challenges associated with operating the semi-continuous PBR at this stage. In terms of culture adaptation, the main consideration involves the practicality of growing *C. reinhardtii* cultures in plastic bags, under natural illumination and ambient temperatures, and using an industrial CO_2 feed. Potential challenges could include leaks caused by structural instability of the plastic bags, the formation of algal films on surfaces and subsequent fouling of the system, difficulties in cleaning the system diligently enough to avoid contamination, the potential presence of toxic elements in the plastic or within the CO_2 feed, and poor algal growth rates and low cell densities when *C. reinhardtii* cultures are grown under ambient photoautotrophic conditions. A demonstration-scale plastic bag PBR system is currently under development by Dr Fessehaye Zemichael at Imperial College. The key

operational challenges will involve the development of H_2 and biomass extraction systems, the establishment of an *in situ* technique to measure, control and recycle nutrients effectively, and the automation of the system through the ability to control the timing of the nutrient feed and biomass drain valves.

Once these challenges have been overcome, the full continuous batch PBR can be commissioned. The PBR could feature a total of 10-20 plastic bags for a maximum working volume of 400 litres. Assuming the average H_2 production rate measured in this thesis of 0.4 $mlH_2 \cdot l^{-1} \cdot h^{-1}$, the continuous batch PBR could produce as much as 160 $mlH_2 \cdot h^{-1}$, which is enough H_2 to operate a small PEM fuel cell that could be used to power a little electric motor. If a sulphur feed technique could be developed to enable continuous H_2 production, the H_2 production rate could be significantly higher. In either case, the continuous batch PBR would showcase the biophotolytic H_2 production process at the demonstration scale. Alongside this, a detailed cradle-to-grave economic analysis of the potential process options is required. If economically viable, the project could then be taken up by industry, upgraded to pilot scale and eventually used in future commercial applications (provided that, should genetically-modified microorganisms be required, potential concerns about their use can be addressed and overcome).

7.2.2. Algal Biorefinery

At current biophotolytic H_2 production rates, it would be difficult to operate an industrial biohydrogen facility at a profit. This is because the cost of feedstock and process operation exceeds the potential revenue from H_2 and biomass at current market prices (Amos, 2004). It is therefore essential to extract multiple valuable by-products from *C. reinhardtii* biomass. The algal biorefinery approach aims to utilise all of the co-products associated with algal growth and H_2 production in order to minimise waste and maximise the revenue of the process. Along with biophotolytic H_2 production, this involves the production of bioethanol from the starch fraction of *C. reinhardtii*, biodiesel from the lipid fraction, the gasification of the protein fraction or its use as animal feed, and the extraction of various high-value products (HVPs). However, since many of these processes compete with each other for photosynthetic resources, the operation of the biorefinery would need to be orientated towards the synthesis of a specific set of primary products. In the short term, only

the production of lucrative HVPs could justify the construction of a commercial *C. reinhardtii* biorefinery. The HVP most commonly associated with *C. reinhardtii* is isoprene, a key pre-cursor chemical for synthetic rubbers (Kruse & Hankamer, 2010). Once the algal biorefinery is in operation, and successfully producing HVPs and H_2, the long-term aim would be to expand production in order to access the vast biofuels market. In addition to H_2, this would principally involve the production of biodiesel and jet fuel from *C. reinhardtii*.

7.2.3. Biological Integration

Large-scale industrial use of *C. reinhardtii* would soon encounter two major challenges: the quantum efficiency limitation of the process and a shortage of ammonium-based fertiliser. Green algae such as *C. reinhardtii* use only red light for photosynthesis. Quantum efficiency could be increased by growing purple cyanobacteria either underneath the *C. reinhardtii* culture or as a symbiotic co-culture within the same reactor. In nature, purple cyanobacteria normally live in deeper water than green algae, where they utilise regions of the solar spectrum that are inaccessible to the surface-dwelling phototrophs. The main nutrient requirements for *C. reinhardtii* growth are a source of carbon and a source of nitrogen. Any large-scale *C. reinhardtii* biorefinery would need to use CO_2 as the carbon source for photoautotrophic growth, perhaps by using the high salt medium (HSM) and a CO_2 partial pressure of circa 11%, as suggested in this thesis. The nitrogen requirements are more difficult to overcome because only fixed nitrogen in the form of ammonia is usable by algal cells. A potential solution would be to grow nitrogen-fixing cyanobacteria such as *Cyanothece* in symbiosis with *C. reinhardtii* cells. An alternative would be to move towards nitrogen-fixing cyanobacteria as the organism of choice for biophotolytic H_2 production. The PBRs and measuring techniques developed during this thesis would be equally applicable to a cyanobacterial culture. The principles of initiating spontaneous H_2 production and extending H_2 production duration would need to be confirmed and quantified for the cyanobacterium of choice. The advantage of using cyanobacteria is that they are simpler organisms than algae, so they would be easier to genetically modify for enhanced H_2 or HVP production. On the other hand, cyanobacterial biomass consists almost entirely of protein, which removes the potential of producing biodiesel or jet fuel as a co-product during H_2 production. The correct choice of microorganism and optimal choice of biofuel products remains uncertain. This situation calls for

even more basic research into the benefits and drawbacks of individual systems so that an informed decision can be made in the future.

7.3. Concluding Remarks

The green algae *C. reinhardtii* are capable of producing a clean, efficient and sustainable biofuel through the biophotolysis of water to H_2. Unfortunately, the H_2 production rate remains very low, with a photochemical efficiency of less than one percent. The success of genetic engineering approaches aimed at improving *C. reinhardtii* light-harvesting, electron transport and H_2 production efficiencies will eventually determine the commercial viability of the process. In the meantime, flexible engineering solutions, in the form of practical photobioreactors, measurement techniques and novel methodologies, are urgently required to facilitate present and future biophotolytic H_2 production processes. This thesis makes a small but important step towards providing these engineering solutions and achieving the goal of sustainable H_2 production, but a lot of work remains to be done.

References

Akkerman, I., Janssen, M., Rocha, J. & Wijffels, R.H. (2002) Photobiological hydrogen production: photochemical efficiency and bioreactor design. *International Journal of Hydrogen Energy*. 27 (11-12), 1195–1208.

Amos, W.A. (2004) Updated cost analysis of photobiological hydrogen production from *Chlamydomonas reinhardtii* green algae. *National Renewable Energy Laboratory (NREL) - Milestone Completion Report*.

Antal, T.K., Krendeleva, T.E., Laurinavichene, T.V., Makarova, V.V., Ghirardi, M.L., Rubin, A.B., Tsygankov, A.A. & Seibert, M. (2003) The dependence of algal H_2 production on Photosystem II and O_2 consumption activities in sulfur-deprived *Chlamydomonas reinhardtii* cells. *Biochimica et Biophysica Acta (BBA)*. 1607 (2-3), 153–160.

Antal, T.K., Volgusheva, A.A., Kukarskih, G.P., Krendeleva, T.E. & Rubin, A.B. (2009) Relationships between H_2 photoproduction and different electron transport pathways in sulfur-deprived *Chlamydomonas reinhardtii*. *International Journal of Hydrogen Energy*. 34 (22), 9087–9094.

Armstrong, F.A. (2004) Hydrogenases: active site puzzles and progress. *Current Opinion in Chemical Biology*. 8 (2), 133–140.

Armstrong, F.A. (2005) Recent developments in dynamic electrochemical studies of adsorbed enzymes and their active sites. *Current Opinion in Chemical Biology*. 9 (2), 110–117.

Arnon, D.I. (1949) Copper enzymes in isolated chloroplasts. Polyphenoloxidase in Beta Vulgaris. *Plant Physiology*. 24 (1), 1–15.

BBSRC (2010) Algal research in the UK. *Biotechnology and Biological Sciences Research Council (BBSRC) - A Scoping Study*.

Bamberger, E.S., King, D., Erbes, D.L. & Gibbs, M. (1982) H_2 and CO_2 evolution by anaerobically adapted *Chlamydomonas reinhardtii* F-60. *Plant Physiology*. 69 (6), 1268–1273.

Bandyopadhyay, A., Stöckel, J., Min, H., Sherman, L.A. & Pakrasi, H.B. (2010) High rates of photobiological H_2 production by a cyanobacterium under aerobic conditions. *Nature Communications*. 139 (1), 1–7.

Barbir, F. (2005) PEM electrolysis for production of hydrogen from renewable energy sources. *Solar Energy*. 78 (5), 661–669.

Barbosa, M.J., Rocha, J., Tramper, J. & Wijffels, R.H. (2001) Acetate as a carbon source for hydrogen production by photosynthetic bacteria. *Journal of Biotechnology*. 85 (1), 25–33.

Barbosa, M.J., Hoogakker, J. & Wijffels, R.H. (2003a) Optimisation of cultivation parameters in photobioreactors for microalgae cultivation using the A-stat technique. *Biomolecular Engineering*. 20 (4-6), 115–123.

Barbosa, M.J., Janssen, M., Ham, N., Tramper, J. Wijffels, R.H. (2003b) Microalgae cultivation in air-lift reactors: modeling biomass yield and growth rate as a function of mixing frequency. *Biotechnology and Bioengineering*. 82 (2), 170–179.

Barbosa, M.J., Hadiyanto & Wijffels, R.H. (2004) Overcoming shear stress of microalgae cultures in sparged photobioreactors. *Biotechnology and Bioengineering*. 85 (1), 78–85.

Bartels, J.R., Pate, M.B. & Olson, N.K. (2010) An economic survey of hydrogen production from conventional and alternative energy sources. *International Journal of Hydrogen Energy*. 35 (16), 8371–8384.

Bassham, J., Benson, A. & Calvin, M. (1950) The path of carbon in photosynthesis. *Journal of Biological Chemistry*. 185 (2), 781–787.

Beckmann, J., Lehr, F., Finazzi, G., Hankamer, B., Posten, C., Wobbe, L. & Kruse, O. (2009) Improvement of light to biomass conversion by de-regulation of light-harvesting protein translation in *Chlamydomonas reinhardtii*. *Journal of Biotechnology*. 142 (1), 70–77.

Beckmann, K., Messinger, J., Badger, M.R., Wydrzynski, T. & Hillier, W. (2009) On-line mass spectrometry: membrane inlet sampling. *Photosynthesis Research*. 102 (2-3), 511–522.

Beer, L.L., Boyd, E.S., Peters, J.W. & Posewitz, M.C. (2009) Engineering algae for biohydrogen and biofuel production. *Current Opinion in Biotechnology*. 20 (3), 264–271.

Ben-Amotz, A., Erbes, D.L., Riederer-Henderson, M.A., Peavey, D.G. & Gibbs, M. (1975) H_2 metabolism in photosynthetic organisms: I. Dark H_2 evolution and uptake by algae and mosses. *Plant Physiology*. 56 (1), 72.

Benemann, J.R. (1997) Feasibility analysis of photobiological hydrogen production. *International Journal of Hydrogen Energy*. 22 (10-11), 979–987.

Benemann, J.R. (1999) Process analysis and economics of biophotolosys of water. *International Energy Agency (IEA) - Agreement on the Production and Utilization of Hydrogen*.

Berberoglu, H., Yin, J. & Pilon, L. (2007) Light transfer in bubble sparged photobioreactors for H_2 production and CO_2 mitigation. *International Journal of Hydrogen Energy*. 32 (13), 2273–2285.

Blanchette, S. (2008) A hydrogen economy and its impact on the world as we know it. *Energy Policy*. 36 (2), 522–530.

Blankenship, R.E., Tiede, D.M., Barber, J., Brudvig, G.W., Fleming, G., Ghirardi, M.L., Gunner, M.R., Junge, W., Kramer, D.M., Melis, A., Moore, T.A., Moser, C.C., Nocera, D.G., Nozig, A.J., Ort, D.R., Parson, W.W., Prince, R.C. & Sayre, R.T. (2011) Comparing photosynthetic and photovoltaic efficiencies and recognizing the potential for improvement. *Science*. 332 (5), 805–809.

Borowitzka, M.A. (1999) Commercial production of microalgae: ponds, tanks, tubes and fermenters. *Journal of Biotechnology*. 70 (1), 313–321.

Bosma, R., Zessen, E.V., Reith, J.H., Tramper, J. & Wijffels, R.H. (2007) Prediction of volumetric productivity of an outdoor photobioreactor. *Biotechnology and Bioengineering*. 97 (5), 1108–1120.

Boyle, N.R. & Morgan, J.A. (2009) Flux balance analysis of primary metabolism in *Chlamydomonas reinhardtii*. *BMC Systems Biology*. 3 (4), 1–14.

Brand, J.J., Wright, J.N. & Lien, S. (1989) Hydrogen production by eukaryotic algae. *Biotechnology and Bioengineering*. 33 (1), 1482–1488.

Brenner, M.P. (2006) Engineering microorganisms for energy production. *The MITRE Corportion*.

Burgess, S.J., Tamburic, B., Zemichael, F.W., Hellgardt, K. & Nixon, P.J. (2011) Solar-driven hydrogen production in green algae. *Advances in Applied Microbiology*. 75 (1), 71–110.

Burgess, S.J., Tredwell, G., Molnàr, A., Bundy, J.G. & Nixon, P.J. (2012) Artificial microRNA-mediated knockdown of pyruvate formate lyase (PFL1) provides evidence for an active 3-hydroxybutyrate production pathway in the green alga *Chlamydomonas reinhardtii*. *Journal of Biotechnology*. In Press.

Carvalho, A.P., Meireles, L.A. & Malcata, F.X. (2006) Microalgal reactors: a review of enclosed system designs and performances. *Biotechnology Progress*. 22 (6), 1490–1506.

Cavallini, F. (1993) Fitting a logistic curve to data. *College Mathematics Journal*. 24 (3), 247–253.

Chen, C., Saratale, G., Lee, C., Chen, P. & Chang, J. (2008) Phototrophic hydrogen production in photobioreactors coupled with solar-energy-excited optical fibers. *International Journal of Hydrogen Energy*. 33 (23), 6886–6895.

Chen, F. & Johns, M.R. (1994) Substrate inhibition of *Chlamydomonas reinhardtii* by acetate in heterotrophic culture. *Process Biochemistry*. 29 (4), 245–252.

Chisti, Y. & Jauregui-Haza, U.J. (2002) Oxygen transfer and mixing in mechanically agitated airlift bioreactors. *Biochemical Engineering Journal*. 10 (2), 143–153.

Chisti, Y. (2007) Biodiesel from microalgae. *Biotechnology Advances*. 25 (3), 294–306.

Chisti, Y. (2008) Biodiesel from microalgae beats bioethanol. *Trends in Biotechnology*. 26 (3), 126–131.

Chochois, V., Dauvillée, D., Beyly, A., Tolleter, D., Cuiné, S., Timpano, H., Ball, S., Cournac, L. & Peltier, G. (2009) Hydrogen production in *Chlamydomonas*: photosystem II-dependent and -independent pathways differ in their requirement for starch metabolism. *Plant Physiology*. 151 (2), 631–640.

Chochois, V., Constans, L., Dauvillée, D., Beyly, A., Solivérès, M., Ball, S. Peltier, G. & Cornac, L. (2010) Relationships between PSII-independent hydrogen bioproduction and starch metabolism as evidenced from isolation of starch catabolism mutants in the green alga *Chlamydomonas reinhardtii*. *International Journal of Hydrogen Energy*. 35 (19), 10731–10740.

Cohen, J., Kim, K., Posewitz, M.C., Ghirardi, M.L., Schulten, K., Seibert, M. & King, P. (2005) Molecular dynamics and experimental investigation of H_2 and O_2 diffusion in [Fe]-hydrogenase. *Biochemical Society Transactions*. 33 (1), 80–82.

Cornet, J.F. & Dussap, C.G. (2009) A simple and reliable formula for assessment of maximum volumetric productivities in photobioreactors. *Biotechnology Progress*. 25 (2), 424–435.

Cournac, L., Mus, F., Bernard, L., Guedeney, G., Vignais, P. & Peltier, G. (2002) Limiting steps of hydrogen production in *Chlamydomonas reinhardtii* and Synechocystis PCC 6803 as analysed by light-induced gas exchange transients. *International Journal of Hydrogen Energy*. 27 (11-12), 1229–1237.

Cracknell, J.A., Vincent, K.A., Ludwig, M., Lenz, O., Friedrich, B. & Armstrong, F.A. (2008) Enzymatic oxidation of H_2 in atmospheric O_2: the electrochemistry of energy generation from trace H_2 by aerobic microorganisms. *Journal of the American Chemical Society*. 130 (2), 424–425.

DBERR (2007) Meeting the energy challenge: a White Paper on energy. *Department of Business, Enterprise and Regulatory Reform (DBERR)*.

Darzins, A., Pienkos, P. & Edye, L. (2010) Current status and potential for algal biofuels production. *National Renewable Energy Laboratory (NREL) - A Report to Bioenergy Task 39*.

Das, D. (2009) Advances in biohydrogen production processes: An approach towards commercialization. *International Journal of Hydrogen Energy*. 34 (17), 7349–7357.

Das, D. & Veziroglu, T.N. (2001) Hydrogen production by biological processes: a survey of literature. *International Journal of Hydrogen Energy*. 26 (1), 13–28.

Dasgupta, C.N., Jose Gilbert, J., Lindblad, P., Heidorn, T., Borgvang, S.A., Skjånes, K. & Das, D. (2010) Recent trends on the development of photobiological processes and photobioreactors for the improvement of hydrogen production. *International Journal of Hydrogen Energy*. 35 (19), 10218–10238.

Davies, J.P., Yildiz, F.H. & Grossman, A.R. (1994) Mutants of *Chlamydomonas* with aberrant responses to sulfur deprivation. *The Plant Cell*. 6 (1), 53–63.

Degrenne, B., Pruvost, J., Christophe, G., Cornet, J.F., Cogne, G. & Legrand, J. (2010) Investigation of the combined effects of acetate and photobioreactor illuminated fraction in the induction of anoxia for hydrogen production by *Chlamydomonas reinhardtii*. *International Journal of Hydrogen Energy*. 35 (19), 10741–10749.

Degrenne, B., Pruvost, J. & Legrand, J. (2011) Effect of prolonged hypoxia in autotrophic conditions in the hydrogen production by the green microalga *Chlamydomonas reinhardtii* in photobioreactor. *Bioresource Technology*. 102 (2), 1035–1043.

Demirbas, A. (2007) Progress and recent trends in biofuels. *Progress in Energy and Combustion Science*. 33 (1), 1–18.

Derrick, R.G. & McIntyre, R.L. (1974) Permeability of teflon polytetrafluoroethylene resin and buna-N butadine-nitrile rubber to deuterium. *Journal of Chemical and Engineering Data*. 19 (1), 48–51.

Ding, M.-Y., Koizumi, H. & Suzuki, Y. (1995) Comparison of three chromatographic systems for determination of organic acids in wine. *Analytical Sciences*. 11 (2), 239–243.

Doebbe, A., Rupprecht, J., Beckmann, J., Mussgnug, J.H., Hallman, A., Hankamer, B. & Kruse, O. (2007) Functional integration of the HUP1 hexose symporter gene into the genome of *C. reinhardtii*: Impacts on biological H_2 production. *Journal of Biotechnology*. 131 (1), 27–33.

Doebbe, A., Keck, M., La Russa, M., Mussgnug, J.H., Hankamer, B., Tekçe, E., Niehaus, K. & Kruse, O. (2010) The interplay of proton, electron, and metabolite supply for photosynthetic H_2 production in *Chlamydomonas reinhardtii*. *The Journal of Biological Chemistry*. 285 (39), 30247–30260.

Ducat, D.C., Way, J.C. & Silver, P.A. (2011a) Engineering cyanobacteria to generate high-value products. *Trends in Biotechnology*. 29 (2), 95–103.

Ducat, D.C., Sachdeva, G. & Silver, P. a (2011b) Rewiring hydrogenase-dependent redox circuits in cyanobacteria. *Proceedings of the National Academy of Sciences (PNAS)*. 108 (10), 3941–3946.

Eroglu, E. & Melis, A. (2011) Photobiological hydrogen production: Recent advances and state of the art. *Bioresource Technology*. 102 (18), 8403–8413.

Esper, B., Badura, A. & Rögner, M. (2006) Photosynthesis as a power supply for (bio-)hydrogen production. *Trends in Plant Science*. 11 (11), 543–549.

Esquivel, M.G., Amaro, H.M., Pinto, T.S., Fevereiro, P.S. & Malcata, F.X. (2011) Efficient H_2 production via *Chlamydomonas reinhardtii*. *Trends in Biotechnology*. 29 (12), 595-600.

Evans, G. (2007) Liquid transport biofuels - technology status report. *Internation Biofuels Strategy Project*.

Extrand, C.W. & Monson, L. (2006) Gas permeation resistance of a perfluoroalkoxy-tetrafluoroethylene copolymer. *Journal of Applied Polymer Science*. 100 (3), 2122–2125.

Faraloni, C., Ena, A., Pintucci, C. & Torzillo, G. (2011) Enhanced hydrogen production by means of sulfur-deprived *Chlamydomonas reinhardtii* cultures grown in pretreated olive mill wastewater. *International Journal of Hydrogen Energy*. 36 (10), 5920–5931.

Faraloni, C. & Torzillo, G. (2010) Phenotypic characterization and hydrogen production in *Chlamydomonas reinhardtii* QB-binding D1-protein mutants under sulphur starvation: Changes in Chl fluorescence and pigment composition. *Journal of Phycology*. 46 (4), 788–799.

Faunce, T. (2011) Artificial photosynthesis - feeding and fuelling the future. *Australian Science*. 32 (10), 20–22.

Ferreira, K.N., Iverson, T.M., Maghlaoui, K., Barber, J. & Iwata, S. (2004) Architecture of the photosynthetic oxygen-evolving center. *Science*. 303 (5665), 1831–1838.

Forestier, M., King, P., Zhang, L., Posewitz, M.C., Schwarzer, S., Happe, T., Ghirardi, M.L. & Seibert, M. (2003) Expression of two [Fe]-hydrogenases in *Chlamydomonas reinhardtii* under anaerobic conditions. *European Journal of Biochemistry*. 270 (13), 2750–2758.

Fouchard, S., Pruvost, J., Degrenne, B. & Legrand, J. (2008) Investigation of H_2 production using the green microalga *Chlamydomonas reinhardtii* in a fully controlled photobioreactor fitted with on-line gas analysis. *International Journal of Hydrogen Energy*. 33 (13), 3302–3310.

Gaffron, H. (1939) Reduction of CO_2 with H_2 in green plants. *Nature*. 143 (1), 204–205.

Gaffron, H. & Rubin, J. (1942) Fermentative and photochemical production of hydrogen in algae. *The Journal of General Physiology*. 219–240.

Ghirardi, M.L., Togasaki, R.K. & Seibert, M. (1997) Oxygen sensitivity of algal H_2-production. *Applied Biochemistry and Biotechnology*. 63 (65), 141–151.

Ghirardi, M.L., Zhang, L., Lee, J.W., Flynn, T., Seibert, M., Greenbaum, E., Melis, A. (2000) Microalgae: a green source of renewable H_2. *Trends in Biotechnology*. 18 (12), 506–511.

Ghirardi, M.L., Dubini, A., Yu, J. & Maness, P.-C. (2009) Photobiological hydrogen-producing systems. *Chemical Society Reviews*. 38 (1), 52–61.

Giannelli, L., Scoma, A. & Torzillo, G. (2009) Interplay between light intensity, chlorophyll concentration and culture mixing on the hydrogen production in sulfur-deprived *Chlamydomonas reinhardtii* cultures grown in laboratory photobioreactors. *Biotechnology and Bioengineering*. 104 (1), 76–90.

González-Ballester, D., Casero, D., Cokus, S., Pellegrini, M., Merchants, S.S. & Grossman, A.R. (2010) RNA-seq analysis of sulfur-deprived *Chlamydomonas cells* reveals aspects of acclimation critical for cell survival. *The Plant Cell*. 22 (6), 2058–2084.

Gorman, D.S. & Levine, R.P. (1966) Photosynthetic Electron Transport Chain of *Chlamydomonas reinhardi*. V. Purification and Properties of Cytochrome 553 and Ferredoxin. *Plant Physiology*. 41 (10), 1643–1647.

Greenbaum, E. (1988) Energetic efficiency of hydrogen photoevolution by algal water splitting. *Biophysical Journal*. 54 (8), 365–368.

Groom, M.J., Gray, E.M. & Townsend, P.A. (2008) Biofuels and biodiversity: principles for creating better policies for biofuel production. *Conservation Biology*. 22 (3), 602–609.

Grossman, A.R. (2000) *Chlamydomonas reinhardtii* and photosynthesis: genetics to genomics. *Current Opinion in Plant Biology*. 3 (2), 132–137.

Grossman, A.R. (2005) Paths toward algal genomics. *Plant Physiology*. 137 (2), 410–427.

Grossman, A.R., Croft, M.T., Gladyshev, V.N., Merchant, S.S., Posewitz, M.C., Prochnik, S.E. & Spalding, M.H. (2007) Novel metabolism in *Chlamydomonas* through the lens of genomics. *Current Opinion in Plant Biology*. 10 (2), 190–198.

Grossman, A.R., Catalanotti, C., Yang, W., Dubini, A., Magneschi, L., Subramanian, V., Posewitz, M.C. & Seibert, M. (2011) Multiple facets of anoxic metabolism and hydrogen production in the unicellular green alga *Chlamydomonas reinhardtii*. *New Phytologist*. 190 (2), 279–288.

Hahn, J.J., Ghirardi, M.L. & Jacoby, W.A. (2007) Immobilized algal cells used for hydrogen production. *Biochemical Engineering Journal*. 37 (1), 75–79.

Hallenbeck, P.C. & Benemann, J.R. (2002) Biological hydrogen production; fundamentals and limiting processes. *International Journal of Hydrogen Energy*. 27 (1), 1185–1193.

Hallenbeck, P.C. & Ghosh, D. (2009) Advances in fermentative biohydrogen production: the way forward? *Trends in Biotechnology*. 27 (5), 287–297.

Ham, M.-H., Choi, J.H., Boghossian, A.A., Jeng, E.S., Graff, R.A., Heller, D.A., Chang, A.C., Mattis, A., Bayburt, T.H., Grinkova, Y.V., Zeiger, A.S., Van Vliet, K.J., Hobbie, E.K., Sligar, S.G., Wraight, C.A. & Strano, M.S. (2010) Photoelectrochemical complexes for solar energy conversion that chemically and autonomously regenerate. *Nature Chemistry*. 2 (11), 929–936.

Hammarström, L., Winkler, J.R., Gray, H.B. & Styring, S. (2011) Shedding light on solar fuel efficiencies. *Science*. 333 (6040), 288.

Hankamer, B., Lehr, F., Rupprecht, J., Mussgnug, J.H., Posten, C. & Kruse, O. (2007) Photosynthetic biomass and H_2 production by green algae: from bioengineering to bioreactor scale-up. *Physiologia Plantarum*. 131 (1), 10–21.

Hansen, J., Sato, M., Kharecha, P., Russell, G., Lea, D.W. & Siddall, M. (2007) Climate change and trace gases. *Philosophical Transactions of the Royal Society. Series A, Mathematical, Physical, and Engineering Sciences*. 365 (1856), 1925–1954.

Happe, T. & Kaminski, A. (2002) Differential regulation of the Fe-hydrogenase during anaerobic adaptation in the green alga *Chlamydomonas reinhardtii*. *European Journal of Biochemistry*. 269 (3), 1022–1032.

Healey, F.P. (1970) Hydrogen evolution by several algae. *Planta*. 226 (1), 220–226.

Hejazi, M.A. & Wijffels, R.H. (2004) Milking of microalgae. *Trends in Biotechnology*. 22 (4), 189–194.

Hemmes, H., Driessen, A. & Griessen, R. (1986) Thermodynamic properties of hydrogen at pressures up to 1 Mbar and temperatures between 100 and 1000K. *Journal of Physics C: Solid State Physics*. 19 (1), 3571–3585.

Hemschemeier, A., Fouchard, S., Cournac, L., Peltier, G. & Happe, T. (2008) Hydrogen production by *Chlamydomonas reinhardtii*: an elaborate interplay of electron sources and sinks. *Planta*. 227 (2), 397–407.

Hemschemeier, A., Melis, A. & Happe, T. (2009) Analytical approaches to photobiological hydrogen production in unicellular green algae. *Photosynthesis Research*. 102 (2-3), 523–540.

Hemschemeier, A. & Happe, T. (2005) The exceptional photofermentative hydrogen metabolism of the green alga *Chlamydomonas reinhardtii*. *Biochemical Society Transactions*. 33 (1), 39–41.

Hemschemeier, A. & Happe, T. (2011) Alternative photosynthetic electron transport pathways during anaerobiosis in the green alga *Chlamydomonas reinhardtii*. *Biochimica et Biophysica Acta (BBA)*. 1807 (8), 919–926.

Holdich, R., Cumming, I. & Kosvintsev, S. (2004) Slotted pore microfilters for oil/water filtration, fractionation and aggressive filtration environments. *Membrane Technology*. 3 (1), 5–10.

Horner, J.K. & Wolinsky, M.A. (2002) A power-law sensitivity analysis of the hydrogen-producing metabolic pathway in *Chlamydomonas reinhardtii*. *International Journal of Hydrogen Energy*. 27 (1), 1251–1255.

IEA (2011) Key world energy statistics. *International Energy Agency (IEA)*.

IPCC (2007) Climate change 2007 - the physical science basis. *Climate Change 2007: The Physical Science Basis, Contribution of Working Group I to the Fourth Assessment Report of the Intergovernmental Panel on Climate Change (IPCC)*.

Iwai, M., Takizawa, K., Tokutsu, R., Okamuro, A., Takahashi, Y. & Minagawa, J. (2010) Isolation of the elusive supercomplex that drives cyclic electron flow in photosynthesis. *Nature*. 464 (7292), 1210–1213.

James, B.D., Baum, G.N., Julie, P. & Baum, K.N. (2009) Technoeconomic analysis of photoelectrochemical (PEC) hydrogen production. *Directed Technologies*.

Janssen, M., de Winter, M., Tramper, J., Mur, L.R., Snel, J. & Wijffels, R.H. (2000a) Efficiency of light utilization of *Chlamydomonas reinhardtii* under medium-duration light/dark cycles. *Journal of Biotechnology*. 78 (2), 123–137.

Janssen, M., de Bresser, L., Baijens, T., Tramper, J., Mur, L.R., Snel, J. & Wijffels, R.H. (2000b) Scale-up aspects of photobioreactors: effects of mixing-induced light/dark cycles. *Journal of Applied Phycology*. 12 (3), 225–237.

Janssen, M., Tramper, J., Mur, L.R. & Wijffels, R.H. (2003) Enclosed outdoor photobioreactors: light regime, photosynthetic efficiency, scale-up, and future prospects. *Biotechnology and Bioengineering*. 81 (2), 193–210.

Jech, U. (2012) Flue Gas Analysis in Industry. *Testo Practical guide for Emission and Process Measurements*.

Jo, J.H., Lee, D.S. & Park, J.M. (2006) Modeling and optimization of photosynthetic hydrogen gas production by green alga Chlamydomonas reinhardtii in sulfur-deprived circumstance. *Biotechnology Progress*. 22 (2), 431–437.

Jorquera, O., Kiperstok, A., Sales, E., Embirucu, M. & Ghirardi, M.L. (2008) S-systems sensitivity analysis of the factors that may influence hydrogen production by sulfur-deprived *Chlamydomonas reinhardtii*. *International Journal of Hydrogen Energy*. 33 (9), 2167–2177.

Kim, J.P., Kim, K.-R., Choi, S.P., Han, S.J., Kim, M.-S. & Sim, S.J. (2010) Repeated production of hydrogen by sulfate re-addition in sulfur deprived culture of *Chlamydomonas reinhardtii*. *International Journal of Hydrogen Energy*. 35 (24), 13387–13391.

Kim, M.-S., Baek, J., Yun, Y., Junsim, S., Park, S. & Kim, S.-C. (2006) Hydrogen production from *Chlamydomonas reinhardtii* biomass using a two-step conversion process: Anaerobic conversion and photosynthetic fermentation. *International Journal of Hydrogen Energy*. 31 (6), 812–816.

Kooijman, S., Hanstveit, A.O. & Oldersma, H. (1983) Parametric analyses of population growth in bio-assays. *Water Research*. 17 (5), 527–538.

Kosourov, S.N., Tsygankov, A.A., Seibert, M. & Ghirardi, M.L. (2002) Sustained hydrogen photoproduction by *Chlamydomonas reinhardtii*: Effects of culture parameters. *Biotechnology and Bioengineering*. 78 (7), 731–740.

Kosourov, S.N., Seibert, M. & Ghirardi, M.L. (2003) Effects of extracellular pH on the metabolic pathways in sulfur-deprived, H_2-producing *Chlamydomonas reinhardtii* cultures. *Plant & Cell Physiology*. 44 (2), 146–155.

Kosourov, S.N., Patrusheva, E., Ghirardi, M.L., Seibert, M. & Tsygankov, A.A. (2007) A comparison of hydrogen photoproduction by sulfur-deprived *Chlamydomonas reinhardtii* under different growth conditions. *Journal of Biotechnology*. 128 (4), 776–787.

Kosourov, S.N., Ghirardi, M.L. & Seibert, M. (2011) A truncated antenna mutant of *Chlamydomonas reinhardtii* can produce more hydrogen than the parental strain. *International Journal of Hydrogen Energy*. 36 (3), 2044–2048.

Kosourov, S.N. & Seibert, M. (2009) Hydrogen photoproduction by nutrient-deprived *Chlamydomonas reinhardtii* cells immobilized within thin alginate films under aerobic and anaerobic conditions. *Biotechnology and Bioengineering*. 102 (1), 50–58.

Krassen, H., Stripp, S., von Abendroth, G., Ataka, K., Happe, T. & Heberle, J. (2009) Immobilization of the [FeFe]-hydrogenase CrHydA1 on a gold electrode: design of a catalytic surface for the production of molecular hydrogen. *Journal of Biotechnology*. 142 (1), 3–9.

Kruse, O. & Hankamer, B. (2010) Microalgal hydrogen production. *Current Opinion in Biotechnology*. 21 (3), 238–243.

Kruse, O., Rupprecht, J., Mussgnug, J.H., Dismukes, G.C. & Hankamer, B. (2005a) Photosynthesis: a blueprint for solar energy capture and biohydrogen production technologies. *Photochemical & Photobiological Sciences*. 4 (12), 957–970.

Kruse, O., Rupprecht, J., Bader, K.-P., Thomas-Hall, S.R., Schenk, P.M., Finazzi, G. & Hankamer, B. (2005b) Improved photobiological H_2 production in engineered green algal cells. *The Journal of Biological Chemistry*. 280 (40), 34170–34177.

Kunjapur, A.M. & Eldridge, R.B. (2010) Photobioreactor design for commercial biofuel production from microalgae. *Industrial & Engineering Chemistry Research*. 49 (8), 3516–3526.

Lardans, A., Förster, B., Prásil, O., Falkowski, P.G., Sobolev, V., Edelman, M., Osmond, C.B., Gillham, M.W. & Boynton, J.E. (1998) Biophysical, biochemical, and physiological characterization of *Chlamydomonas reinhardtii* mutants with amino acid substitutions at the Ala251 residue in the D1 protein that result in varying levels of photosynthetic competence. *The Journal of Biological Chemistry*. 273 (18), 11082–11091.

Laurinavichene, T.V., Tolstygina, I.V., Galiulina, R.R., Ghirardi, M.L., Seibert, M. & Tsygankov, A.A. (2002) Dilution methods to deprive *Chlamydomonas reinhardtii* cultures of sulfur for subsequent hydrogen photoproduction. *International Journal of Hydrogen Energy*. 27 (1), 1245–1249.

Laurinavichene, T.V., Tolstygina, I.V. & Tsygankov, A.A. (2004) The effect of light intensity on hydrogen production by sulfur-deprived *Chlamydomonas reinhardtii*. *Journal of Biotechnology*. 114 (1-2), 143–151.

Laurinavichene, T.V., Fedorov, A.S., Ghirardi, M.L., Seibert, M. & Tsygankov, A.A. (2006) Demonstration of sustained hydrogen photoproduction by immobilized, sulfur-deprived *Chlamydomonas reinhardtii* cells. *International Journal of Hydrogen Energy*. 31 (1), 659–667.

Lee, J.W. & Greenbaum, E. (2003) A new oxygen sensitivity and its potential application in photosynthetic H_2 production. *Applied Biochemistry and Biotechnology*. 105 -108 (1), 303–313.

Lehr, F. & Posten, C. (2009) Closed photo-bioreactors as tools for biofuel production. *Current Opinion in Biotechnology*. 20 (3), 280–285.

Lemesle, V. & Mailleret, L. (2008) A mechanistic investigation of the algae growth "Droop" model. *Acta Biotheoretica*. 56 (1-2), 87–102.

Levin, D. (2004) Biohydrogen production: prospects and limitations to practical application. *International Journal of Hydrogen Energy*. 29 (2), 173–185.

Lewis, N.S. & Nocera, D.G. (2006) Powering the planet: chemical challenges in solar energy utilization. *Proceedings of the National Academy of Sciences (PNAS)*. 103 (43), 15729–15735.

Li, Z., Wakao, S., Fischer, B.B. & Niyogi, K.K. (2009) Sensing and responding to excess light. *Annual Review of Plant Biology*. 60 (1), 239–260.

Lloyd, D., Thomas, K.L., Cowie, G., Tammam, J.D. & Williams, A.G. (2002) Direct interface of chemistry to microbiological systems: membrane inlet mass spectrometry. *Journal of Microbiological Methods*. 48 (2-3), 289–302.

Lopes, F.A., Troshina, O. & Lindblad, P. (2002) A brief look at three decades of research on cyanobacterial hydrogen evolution. *International Journal of Hydrogen Energy*. 27 (1), 1209–1215.

Luiten, E., Akkerman, I., Koulman, A., Kamermans, P., Reith, H., Barbosa, M.J., Sipkema, D. & Wijffels, R.H. (2003) Realizing the promises of marine biotechnology. *Biomolecular Engineering*. 20 (4-6), 429–439.

Mahan, K., Odorn, O. & Herrin, D. (2005) Controlling fungal contamination in *Chlamydomonas reinhardtii* cultures. *BioTechniques*. 39 (4), 457–458.

Makarova, V.V., Kosourov, S.N., Krendeleva, T.E., Semin, B.K., Kukarshkin, G.P., Rubin, A.B., Sayre, R.T., Ghirardi, M.L. & Seibert, M. (2007) Photoproduction of hydrogen by sulfur-deprived *C. reinhardtii* mutants with impaired photosystem II photochemical activity. *Photosynthesis Research*. 94 (1), 79–89.

Manish, S. & Banerjee, R. (2008) Comparison of biohydrogen production processes. *International Journal of Hydrogen Energy*. 33 (1), 279–286.

Markov, S., Eivazova, E. & Greenwood, J. (2006) Photostimulation of H_2 production in the green alga *Chlamydomonas reinhardtii* upon photoinhibition of its O_2-evolving system. *International Journal of Hydrogen Energy*. 31 (10), 1314–1317.

Marín-Navarro, J., Esquivel, M.G. & Moreno, J. (2010) Hydrogen production by *Chlamydomonas reinhardtii* revisited: Rubisco as a biotechnological target. *World Journal of Microbiology and Biotechnology*. 26 (10), 1785–1793.

Meherkotay, S. & Das, D. (2008) Biohydrogen as a renewable energy resource - prospects and potentials. *International Journal of Hydrogen Energy*. 33 (1), 258–263.

Melis, A. (2002) Green alga hydrogen production: progress, challenges and prospects. *International Journal of Hydrogen Energy*. 27 (11-12), 1217–1228.

Melis, A. (2007) Photosynthetic H_2 metabolism in *Chlamydomonas reinhardtii* (unicellular green algae). *Planta*. 226 (5), 1075–1086.

Melis, A. (2009) Solar energy conversion efficiencies in photosynthesis: Minimizing the chlorophyll antennae to maximize efficiency. *Plant Science*. 177 (4), 272–280.

Melis, A. & Happe, T. (2004) Trails of green alga hydrogen research - from Hans Gaffron to new frontiers. *Photosynthesis Research*. 80 (1-3), 401–409.

Melis, A. & Melnicki, M. (2006) Integrated biological hydrogen production. *International Journal of Hydrogen Energy*. 31 (11), 1563–1573.

Melis, A., Zhang, L., Forestier, M., Ghirardi, M.L. & Seibert, M. (2000) Sustained photobiological hydrogen gas production upon reversible inactivation of oxygen evolution in the green alga *Chlamydomonas reinhardtii*. *Plant Physiology*. 122 (1), 127–136.

Merchant, S.S., Prochnik, S.E., Vallon, O., Harris, E.H., Karpowicz, S.J., Witman, J.B., Terry, A., Salamov, A., Fritz-Laylin, L.K., Maréchal-Drouard, L., Marshall, W.F., Qu, L.-H., Nelson,

D.R., Sandefoot, A.A., Spalding, M.H., Kapitonov, V.V., Ren, Q., Ferris, P., Lindquist, E., Shapiro, H., Lucas, S.M., Grimwood, J., Schmutz, J., Cardol, P., Cerutti, H., Chanfreau, G., Chen, C.-L., Cognat, V., Croft, M.T., Dent, R., Dutcher, S., Fernández, A., Fukuzawa, H., González-Ballester, D., González-Halphen, D., Hallman, A., Hanikenne, M., Hippler, M., Inwood, W., Jabbari, K., Kalanon, M., Kuras, R., Lefebvre, P.A., Lemaire, S.D., Lobanov, A.V., Lohr, M., Manuell, A., Meier, I., Mets, L., Mittag, M., Mittelmeier, T., Moroney, J.V., Moseley, J., Napoli, C., Nedelcu, A.M., Niyogi, K.K., Novoselov, S.V., Paulsen, I.T., Pazour, G., Purton, S., Ral, J.-P., Riaño-Pachón, D.M., Riekhof, W., Rymarquis, L., Schroda, M., Stern, D., Umen, J., Willows, R., Wilson, N., Zimmer, S.L., Allmer, J., Balk, J., Bisova, K., Chen, C.-J., Elias, M., Gendler, K., Hauser, C., Lamb, M.R., Ledford, H., Long, J.C., Minagawa, J., Page, M.D., Pan, J., Pootakham, W., Roje, S., Rose, A., Stahlberg, E., Terauchi, A.M., Yang, P., Ball, S., Bowler, C., Dieckmann, C.L., Gladyshev, V.N., Green, P., Jorgensen, R., Mayfield, S.P., Mueller-Roeber, B., Rajamani, S., Sayre, R.T., Brokstein, P., Dubchak, I., Goodstein, D., Hornick, L., Huang, Y.W., Jhaveri, J., Luo, Y., Martínez, D., Ngau, W.C.A., Otillar, B., Poliakov, A., Porter, A., Szajkowski, L., Werner, G., Zhou, K., Grigoriev, I.V., Rokhsar, D.S., & Grossman, A.R. (2007) The *Chlamydomonas* genome reveals the evolution of key animal and plant functions. *Science*. 318 (5848), 245–250.

Meuser, J.E., Ananyev, G., Wittig, L.E., Kosourov, S.N., Ghirardi, M.L., Seiber, M., Dismukes, G.C. & Posewitz, M.C. (2009) Phenotypic diversity of hydrogen production in chlorophycean algae reflects distinct anaerobic metabolisms. *Journal of Biotechnology*. 142 (1), 21–30.

Miron Sanchez, A., Garcia Camacho, F., Contreras Gomez, A., Molina Grima, E. & Chisti, Y. (2000) Bubble-column and airlift photobioreactors for algal culture. *AIChE*. 46 (9), 1872–1887.

Miyake, J., Miyake, M. & Asada, Y. (1999) Biotechnological hydrogen production: research for efficient light energy conversion. *Journal of Biotechnology*. 70 (1-3), 89–101.

Molina Grima, E., Acien Fernandez, F.G. & Chisti, Y. (1999) Photobioreactors: light regime, mass transfer and scaleup. *Journal of Biotechnology*. 70 (1), 231–247.

Molina Grima, E., Acien Fernandez, F.G., Garcia Camacho, F., Camacho Rubio, F. & Chisti, Y. (2000) Scale-up of tubular photobioreactors. *Journal of Applied Phycology*. 12 (1), 355–368.

Momirlan, M. & Veziroglu, T.N. (1999) Recent directions of world hydrogen production. *Renewable and Sustainable Energy Reviews*. 3 (2-3), 219–231.

Morineau-Thomas, O., Jaouen, P. & Legentilhomme, P. (2002) The role of exopolysaccharides in fouling phenomenon during ultrafiltration of microalgae (Chlorellasp. and Porphyridium purpureum): advantage of a swirling decaying flow. *Bioprocess and Biosystems Engineering*. 25 (1), 35–42.

Morweiser, M., Kruse, O., Hankamer, B. & Posten, C. (2010) Developments and perspectives of photobioreactors for biofuel production. *Applied Microbiology and Biotechnology*. 87 (4), 1291–1301.

Mus, F., Dubini, A., Seibert, M., Posewitz, M.C. & Grossman, A.R. (2007) Anaerobic acclimation in *Chlamydomonas reinhardtii*: anoxic gene expression, hydrogenase induction, and metabolic pathways. *The Journal of Biological Chemistry*. 282 (35), 25475–25486.

Mussgnug, J.H., Thomas-Hall, S.R., Rupprecht, J., Foo, A., Klassen, V., McDowall, A., Schenk, P.M., Kruse, O. & Hankamer, B. (2007) Engineering photosynthetic light capture: impacts on improved solar energy to biomass conversion. *Plant Biotechnology Journal*. 5 (6), 802–814.

Mussgnug, J.H., Klassen, V., Schluter, A. & Kruse, O. (2010) Microalgae as substrates for fermentative biogas production in a combined biorefinery concept. *Journal of Biotechnology*. 150 (1), 51–56.

Nath, K. & Das, D. (2004) Improvement of fermentative hydrogen production: various approaches. *Applied Microbiology and Biotechnology*. 65 (5), 520–529.

Nedbal, L., Trtílek, M., Cervený, J., Komárek, O. & Pakrasi, H.B. (2008) A photobioreactor system for precision cultivation of photoautotrophic microorganisms and for high-content analysis of suspension dynamics. *Biotechnology and Bioengineering*. 100 (5), 902–910.

Nguyen, A.V., Thomas-Hall, S.R., Malnoë, A., Timmins, M., Mussgnug, J.H., Rupprecht, J., Kruse, O., Hankamer, B. & Schenk, P.M. (2008) Transcriptome for photobiological hydrogen production induced by sulfur deprivation in the green alga *Chlamydomonas reinhardtii*. *Eukaryotic Cell*. 7 (11), 1965–1979.

Nixon, P.J., Michoux, F., Yu, J., Boehm, M., *et al*. (2010) Recent advances in understanding the assembly and repair of photosystem II. *Annals of Botany*. 106 (1), 1–16.

Norsker, N.-H., Barbosa, M.J., Vermuë, M.H. & Wijffels, R.H. (2011) Microalgal production - a close look at the economics. *Biotechnology Advances*. 29 (1), 24–27.

Oh, S.-E., Iyer, P., Bruns, M.A. & Logan, B.E. (2004) Biological hydrogen production using a membrane bioreactor. *Biotechnology and Bioengineering*. 87 (1), 119–127.

Oncel, S. & Vardar Sukan, F. (2009) Photo-bioproduction of hydrogen by *Chlamydomonas reinhardtii* using a semi-continuous process regime. *International Journal of Hydrogen Energy*. 34 (18), 7592–7602.

Oncel, S. & Vardar Sukan, F. (2011) Effect of light intensity and the light: dark cycles on the long term hydrogen production of *Chlamydomonas reinhardtii* by batch cultures. *Biomass and Bioenergy*. 35 (3), 1066–1074.

Park, W. & Moon, I. (2007) A discrete multi states model for the biological production of hydrogen by phototrophic microalga. *Biochemical Engineering Journal*. 36 (1), 19–27.

Peharz, G., Dimroth, F. & Wittstadt, U. (2007) Solar hydrogen production by water splitting with a conversion efficiency of 18%. *International Journal of Hydrogen Energy*. 32 (15), 3248–3252.

Peltier, G., Tolleter, D., Billon, E. & Cournac, L. (2010) Auxiliary electron transport pathways in chloroplasts of microalgae. *Photosynthesis Research*. 106 (1-2), 19–31.

Perner-Nochta, I. & Posten, C. (2007) Simulations of light intensity variation in photobioreactors. *Journal of Biotechnology*. 131 (3), 276–285.

Peters, J.W. (1999) Structure and mechanism of iron-only hydrogenases. *Current Opinion in Structural Biology*. 9 (6), 670–676.

Philipps, G., Happe, T. & Hemschemeier, A. (2011a) Nitrogen deprivation results in photosynthetic hydrogen production in *Chlamydomonas reinhardtii*. *Planta*. 235 (4), 729-745.

Philipps, G., Krawietz, D. & Hemschemeier, A. (2011b) A pyruvate formate lyase−deficient *Chlamydomonas reinhardtii* strain provides evidence for a link between fermentation and hydrogen production in green algae. *The Plant Journal*. 66 (2), 330–340.

Pimentel, D., Marklein, A., Toth, M.A., Karpoff, M.N., Paul, G.S., McCormack, R., Kyriazis, J., Krueger, T. (2009) Food versus biofuels: environmental and economic costs. *Human Ecology*. 37 (1), 1–12.

Pinnau, I. & He, Z. (2004) Pure- and mixed-gas permeation properties of polydimethylsiloxane for hydrocarbon/methane and hydrocarbon/hydrogen separation. *Journal of Membrane Science*. 244 (1-2), 227–233.

Pootakham, W., González-Ballester, D. & Grossman, A.R. (2010) Identification and regulation of plasma membrane sulfate transporters in *Chlamydomonas*. *Plant Physiology*. 153 (4), 1653–1668.

Posten, C. (2009) Design principles of photo-bioreactors for cultivation of microalgae. *Engineering in Life Sciences*. 9 (3), 165–177.

Posten, C. & Schaub, G. (2009) Microalgae and terrestrial biomass as source for fuels - a process view. *Journal of Biotechnology*. 142 (1), 64–69.

Pulz, O. (2001) Photobioreactors: production systems for phototrophic microorganisms. *Applied Microbiology and Biotechnology*. 57 (3), 287–293.

Putt, R. (2007) Algae as a biodiesel feedstock: A feasibility assessment. *Center for Microfibrous Materials Manufacturing (CM3)*.

Rasala, B.A., Muto, M., Lee, P.A., Jager, M., Cardoso, R.M.F., Behnke, C.A., Kirk, P., Hokanson, C.A., Crea, R., Mendez, M. & Mayfield, S.P. (2010) Production of therapeutic proteins in algae, analysis of expression of seven human proteins in the chloroplast of *Chlamydomonas reinhardtii*. *Plant Biotechnology Journal*. 8 (6), 719–733.

Redding, K., Cournac, L., Vassiliev, I.R., Golbeck, J.H., Peltier, G. & Rochaix, J.-D. (1999) Photosystem I is indispensable for photoautotrophic growth, CO_2 fixation, and H_2 photoproduction in *Chlamydomonas reinhardtii*. *The Journal of Biological Chemistry*. 274 (15), 10466–10473.

Ricci, M., Bellaby, P. & Flynn, R. (2008) What do we know about public perceptions and acceptance of hydrogen? A critical review and new case study evidence. *International Journal of Hydrogen Energy*. 33 (21), 5868–5880.

Ricci, M., Bellaby, P. & Flynn, R. (2010) Engaging the public on paths to sustainable energy: Who has to trust whom? *Energy Policy*. 38 (6), 2633–2640.

Rochaix, J.-D. (1995) *Chlamydomonas reinhardtii* as the photosynthetic yeast. *Annual Review of Genetics*. 29 (1), 209–230.

Rochaix, J.-D. (2011) Regulation of photosynthetic electron transport. *Biochimica et Biophysica Acta (BBA)*. 1807 (3), 375–383.

Rosello Sastre, R., Csögör, Z., Perner-Nochta, I., Fleck-Schneider, P. & Posten, C. (2007) Scale-down of microalgae cultivations in tubular photo-bioreactors - a conceptual approach. *Journal of Biotechnology*. 132 (2), 127–133.

Rossignol, N., Vandanjon, L., Jaouen, P. & Que, F. (1999) Membrane technology for the continuous separation microalgae / culture medium: compared performances of cross-flow microfiltration and ultrafiltration. *Aquacultural Engineering*. 20 (1), 191–208.

Rupprecht, J., Hankamer, B., Mussgnug, J.H., Ananyev, G., Dismukes, G.C. & Kruse, O. (2006) Perspectives and advances of biological H_2 production in microorganisms. *Applied Microbiology and Biotechnology*. 72 (3), 442–449.

Sander, R. (1999) Compilation of Henry's Law constants for inorganic and organic species of potential importance in environmental chemistry. *Max-Planck Institute of Chemistry*.

Schenk, P.M., Thomas-Hall, S.R., Stephens, E., Marx, U.C., Mussgnug, J.H., Posten, C., Kruse, O. & Hankamer, B. (2008) Second generation biofuels: High-efficiency microalgae for biodiesel production. *BioEnergy Research*. 1 (1), 20–43.

Schmollinger, S., Strenkert, D. & Schroda, M. (2010) An inducible artificial microRNA system for *Chlamydomonas reinhardtii* confirms a key role for heat shock factor 1 in regulating thermotolerance. *Current Genetics*. 56 (4), 383–389.

Scoma, A., Giannelli, L., Faraloni, C. & Torzillo, G. (2011) Outdoor H_2 production in a 50-L tubular photobioreactor by means of a sulfur-deprived culture of the microalga *Chlamydomonas reinhardtii*. *Journal of Biotechnology*. 157 (4), 620-627.

Scott, R.I., Norman Williams, T., Whitmore, T.N. & Lloyd, D. (1983) Direct measurement of methanogenesis in anaerobic digestors by membrane inlet mass spectrometry. *Applied Microbiology and Biotechnology*. 18 (4), 236–241.

Searchinger, T.D., Hamburg, S.P., Melillo, J., Chameides, W., Havlik, P., Kammen, D.M., Likens, G.E., Lubowski, R.N., Oppenheimer, M., Robertson, G.P., Schlesinger, W.H. & Tilman, G.D. (2009) Fixing a critical climate accounting error. *Science*. 326 (5952), 1–3.

Sheehan, J., Dunahay, T., Benemann, J.R. & Roessler, P. (1998) A look back at the US Department of Energy's Aquatic Species Program: Biodiesel from algae. *US Department of Energy (US DoE) Office of Fuels Development, Prepared by National Renewable Energy Laboratory (NREL)*.

Sialve, B., Bernet, N. & Bernard, O. (2009) Anaerobic digestion of microalgae as a necessary step to make microalgal biodiesel sustainable. *Biotechnology Advances*. 27 (4), 409–416.

Siaut, M., Cuiné, S., Cagnon, C., Fessler, B., Nguyen, M., Carrier, P., Beyly, A., Beisson, F., Triantaphylidès, C., Li-Beisson, Y. & Peltier, G. (2011) Oil accumulation in the model green alga *Chlamydomonas reinhardtii*: characterization, variability between common laboratory strains and relationship with starch reserves. *BMC Biotechnology*. 11 (1), 7.

Sierra, E., Acien Fernandez, F.G., Fernández, J.M., García, J.L., González, C. & Molina Grima, E. (2008) Characterization of a flat plate photobioreactor for the production of microalgae. *Chemical Engineering Journal*. 138 (1-3), 136–147.

Skjånes, K., Lindblad, P. & Muller, J. (2007) BioCO_2 - a multidisciplinary, biological approach using solar energy to capture CO_2 while producing H_2 and high value products. *Biomolecular Engineering*. 24 (4), 405–413.

Skjånes, K., Knutsen, G., Kallqvist, T. & Lindblad, P. (2008) H_2 production from marine and freshwater species of green algae during sulfur deprivation and considerations for bioreactor design. *International Journal of Hydrogen Energy*. 33 (2), 511–521.

Spalding, M.H. (2008) Microalgal carbon-dioxide-concentrating mechanisms: *Chlamydomonas* inorganic carbon transporters. *Journal of Experimental Botany*. 59 (7), 1463–1473.

Spolaore, P., Joannis-Cassan, C., Duran, E. & Isambert, A. (2006) Commercial applications of microalgae. *Journal of Bioscience and Bioengineering*. 101 (2), 87–96.

Stephens, E., Ross, I.L., Mussgnug, J.H., Wagner, L.D., Borowitzka, M.A., Posten, C., Kruse, O. & Hankamer, B. (2010a) Future prospects of microalgal biofuel production systems. *Trends in Plant Science*. 15 (10), 554–564.

Stephens, E., Ross, I.L., King, Z., Mussgnug, J.H., Kruse, O., Posten, C., Borowitzka, M.A. & Hankamer, B. (2010b) An economic and technical evaluation of microalgal biofuels. *Nature Biotechnology*. 28 (2), 126–128.

Stern, D. (2006) Stern review: the economics of climate change. *UK Treasury*.

Tamburic, B., Zemichael, F.W., Maitland, G.C. & Hellgardt, K. (2011a) Parameters affecting the growth and hydrogen production of the green alga *Chlamydomonas reinhardtii*. *International Journal of Hydrogen Energy*. 36 (13), 7872–7876.

Tamburic, B., Zemichael, F.W., Crudge, P., Maitland, G.C. & Hellgardt, K. (2011b) Design of a novel flat-plate photobioreactor system for green algal hydrogen production. *International Journal of Hydrogen Energy*. 36 (11), 6578–6591.

Tamburic, B., Zemichael, F.W., Maitland, G.C. & Hellgardt, K. (2012) A novel nutrient control method to deprive green algae of sulphur and initiate spontaneous hydrogen production. *International Journal of Hydrogen Energy*. 37 (11), 8988–9001.

Taylor, G. (2008) Biofuels and the biorefinery concept. *Energy Policy*. 36 (12), 4406–4409.

Teplyakov, V.V., Gassanova, L.G., Sostina, E.G., Slepova, E.V., Modigell, M. & Netrusov, A.I. (2002) Lab-scale bioreactor integrated with active membrane system for hydrogen production: experience and prospects. *International Journal of Hydrogen Energy*. 27 (11-12), 1149–1155.

Timmins, M., Zhou, W., Rupprecht, J., Lim, L., Thomas-Hall, S.R., Doebbe, A., Kruse, O., Hankamer, B., Marx, U.C., Smith, S.M. & Schenk, P.M. (2009a) The metabolome of *Chlamydomonas reinhardtii* following induction of anaerobic H2 production by sulfur depletion. *The Journal of Biological Chemistry*. 284 (35), 23415–23425.

Timmins, M., Thomas-Hall, S.R., Darling, A., Zhang, E., Hankamer, B., Marx, U.C. & Schenk, P.M. (2009b) Phylogenetic and molecular analysis of hydrogen-producing green algae. *Journal of Experimental Botany*. 60 (6), 1691–1702.

Tolstygina, I.V., Antal, T.K., Kosourov, S.N., Krendeleva, T.E., Rubin, A.B. & Tsygankov, A.A. (2009) Hydrogen production by photoautotrophic sulfur-deprived *Chlamydomonas reinhardtii* pre-grown and incubated under high light. *Biotechnology and Bioengineering*. 102 (4), 1055–1061.

Torri, C., Samorì, C., Adamiano, A., Fabbri, D., Faraloni, C. & Torzillo, G. (2011) Preliminary investigation on the production of fuels and bio-char from *Chlamydomonas reinhardtii* biomass residue after bio-hydrogen production. *Bioresource Technology*. 102 (18), 8707–8713.

Torzillo, G., Scoma, A., Faraloni, C., Ena, A. & Johanningmeier, U. (2009) Increased hydrogen photoproduction by means of a sulfur-deprived *Chlamydomonas reinhardtii* D1 protein mutant. *International Journal of Hydrogen Energy*. 34 (10), 4529–4536.

Tsygankov, A.A. (2001) Laboratory scale photobioreactors. *Applied Biochemistry and Microbiology*. 37 (4), 333–341.

Tsygankov, A.A., Kosourov, S.N., Seibert, M. & Ghirardi, M.L. (2002) Hydrogen photoproduction under continuous illumination by sulfur-deprived, synchronous *Chlamydomonas reinhardtii* cultures. *International Journal of Hydrogen Energy*. 27 (11-12), 1239–1244.

Tsygankov, A.A., Kosourov, S.N., Tolstygina, I.V., Ghirardi, M.L. & Seibert, M. (2006) Hydrogen production by sulfur-deprived *Chlamydomonas reinhardtii* under photoautotrophic conditions. *International Journal of Hydrogen Energy*. 31 (11), 1574–1584.

US DoE (2005) Basic research needs for solar energy utilization. *US Department of Energy (US DoE) - Report of the Basic Energy Sciences Workshop on Solar Energy Utilization*.

US DoE (2009) Current (2009) state-of-the-art hydrogen production cost estimate using water electrolysis. *US Department of Energy (US DoE) Hydrogen Program*.

US DoE (2008) Hydrogen & our energy future. *US Department of Energy (US DoE) Hydrogen Program*.

US DoE (2010) Own your power! A consumer guide to solar electricity for the home. *US Department of Energy (US DoE) Energy Efficiency & Renewable Energy*.

US EPA (2010) Light-duty automotive technology, carbon dioxide emissions and fuel economy trends: 1975 through 2010. *US Environmental Protection Agency (US EPA)*.

Ugwu, C.U., Aoyagi, H. & Uchiyama, H. (2008) Photobioreactors for mass cultivation of algae. *Bioresource Technology*. 99 (10), 4021–4028.

Uyar, B., Eroglu, I., Yucel, M., Gunduz, U. & Turker, L. (2007) Effect of light intensity, wavelength and illumination protocol on hydrogen production in photobioreactors. *International Journal of Hydrogen Energy*. 32 (18), 4670–4677.

Vijayaraghavan, K., Karthik, R. & Kamala Nalini, S.P. (2009) Hydrogen production by *Chlamydomonas reinhardtii* under light driven sulfur deprived condition. *International Journal of Hydrogen Energy*. 34 (19), 7964–7970.

Weaver, P.F., Lien, S. & Seibert, M. (1980) Photobiological production of hydrogen. *Solar Energy*. 24 (1), 3–45.

Weiss, M.A., Heywood, J.B., Drake, E.M., Schafer, A. & AuYeung, F.F. (2000) On the road in 2020- A life-cycle analysis of new automobile technologies. *Massachusetts Institute of Technology (MIT) - Energy Laboratory Report*.

Wijffels, R.H. & Barbosa, M.J. (2010) An outlook on microalgal biofuels. *Science*. 329 (5993), 796–799.

Winkler, M., Kuhlgert, S., Hippler, M. & Happe, T. (2009) Characterization of the key step for light-driven hydrogen evolution in green algae. *The Journal of Biological Chemistry*. 284 (52), 36620–36627.

Wykoff, D.D., Davies, J.P., Melis, A. & Grossman, A.R. (1998) The regulation of photosynthetic electron transport during nutrient deprivation in *Chlamydomonas reinhardtii*. *Plant Physiology*. 117 (1), 129–139.

Xu, Z., Dapeng, L., Yiping, Z., Xiaoyan, Z., Zhaoling, C., Wei, C. & Fan, O. (2002) Comparison of photobioreactors for cultivation of *Undaria pinnatifida* gametophytes. *Biotechnology Letters*. 24 (18), 1499–1503.

Yacoby, I., Pochekailov, S., Toporik, H., Ghirardi, M.L., King P.W. & Zhang, S. (2011) Photosynthetic electron partitioning between [FeFe]-hydrogenase and ferredoxin: NADP+-oxidoreductase (FNR) enzymes in vitro. *Proceedings of the National Academy of Sciences (PNAS)*. 108 (23), 9396.

Yildiz, F.H., Davies, J.P. & Grossman, A.R. (1994) Characterization of sulfate transport in *Chlamydomonas reinhardtii* during sulfur-limited and sulfur-sufficient growth. *Plant Physiology*. 104 (3), 981–987.

Zhang, L., Happe, T. & Melis, A. (2002) Biochemical and morphological characterization of sulfur-deprived and H2-producing *Chlamydomonas reinhardtii* (green alga). *Planta*. 214 (4), 552–561.

Zhang, L. & Melis, A. (2002) Probing green algal hydrogen production. *Philosophical Transactions of the Royal Society. Series B, Biological Sciences*. 357 (1426), 1499–1507.

Zhang, T. (2011) Interplay among culture parameters, light, mixing, and photobioreactor configuration during H_2 production by sulfur-deprived *Chlamydomonas reinhardtii*. *International Journal of Hydrogen Energy*. 36 (19), 12220–12230.

Zhang, X.W. & Chen, F. (1999) Kinetic models for heterotrophic growth of *Chlamydomonas reinhardtii* in batch and fed-batch cultures. *Process Biochemistry*. 35 (3-4), 385–389.

Zijffers, J.-W.F., Janssen, M., Tramper, J. & Wijffels, R.H. (2008) Design process of an area-efficient photobioreactor. *Marine Biotechnology*. 10 (4), 404–415.